Contention Techniques for Opportunistic Communication in Wireless Mesh Networks

A Cross-Layer Perspective on Opportunistic Routing and Opportunistic Scheduling under Carrier Sensing Multiple Access

D I S S E R T A T I O N

zur Erlangung des akademischen Grades

doctor rerum naturalium (Dr. rer. nat.)
im Fach Informatik

eingereicht an der
Mathematisch-Naturwissenschaftlichen Fakultät II
Humboldt-Universität zu Berlin

von
Dipl.-Inf. Mathias Kurth

Präsident der Humboldt-Universität zu Berlin:
Prof. Dr. Jan-Hendrik Olbertz

Dekan der Mathematisch-Naturwissenschaftlichen Fakultät II:
Prof. Dr. Elmar Kulke

Gutachter:
1. Prof. Dr. Jens-Peter Redlich
2. Prof. Dr. Adam Wolisz
3. Prof. Dr. Mesut Güneş

eingereicht am: 20.07.2011
Tag der mündlichen Prüfung: 16.12.2011

Abstract

In the field of wireless communication, a tremendous progress can be observed especially at the lower layers. Innovative physical layer (PHY) concepts and technologies can be rapidly assimilated in cellular networks. Wireless mesh networks (WMNs), on the other hand, cannot keep up with the speed of innovation at the PHY due to their flat and decentralized architecture. Many innovative PHY technologies rely on multi-user communication, so that the established abstraction of the network stack does not work well for WMNs.

The scheduling problem in WMNs is inherent complex. Surprisingly, carrier sense multiple access (CSMA) in WMNs is asymptotically utility-optimal even though it has a low computational complexity and does not involve message exchange. Hence, the question arises whether CSMA and the underlying concept of contention allows for the assimilation of advanced PHY technologies into WMNs.

In this thesis, we design and evaluate contention protocols based on CSMA for opportunistic communication in WMNs. Opportunistic communication is a technique that relies on multi-user diversity in order to exploit the inherent characteristics of the wireless channel. In particular, we consider opportunistic routing (OR) and opportunistic scheduling (OS) in memoryless and slow fading channels, respectively. We present models for congestion control, routing and contention-based opportunistic communication in WMNs in order to maximize both throughput and fairness of elastic unicast traffic flows. At the instance of IEEE 802.11, we illustrate how the cross-layer algorithms can be implemented within a network simulator prototype. Our evaluation results lead to the conclusion that contention-based opportunistic communication is feasible. Furthermore, the proposed protocols increase both throughput and fairness in comparison to state-of-the-art approaches like DCF, DSR, ExOR, RBAR and ETT.

Keywords:
wireless mesh network, utility-optimal carrier sense multiple access, opportunistic routing, opportunistic scheduling, network utility optimization, cross-layer design

Zusammenfassung

Auf dem Gebiet der drahtlosen Kommunikation und insbesondere auf den tieferen Netzwerkschichten sind gewaltige Fortschritte zu verzeichnen. Innovative Konzepte und Technologien auf der physikalischen Schicht (PHY) gehen dabei zeitnah in zelluläre Netze ein. Drahtlose Maschennetzwerke (WMNs) können mit diesem Innovationstempo nicht mithalten. Die Mehrnutzer-Kommunikation ist ein Grundpfeiler vieler angewandter PHY Technologien, die sich in WMNs nur ungenügend auf die etablierte Schichtenarchitektur abbilden lässt.

Insbesondere ist das Problem des Scheduling in WMNs inhärent komplex. Erstaunlicherweise ist der Mehrfachzugriff mit Trägerprüfung (CSMA) in WMNs asymptotisch optimal obwohl das Verfahren eine geringe Durchführungskomplexität aufweist. Daher stellt sich die Frage, in welcher Weise das dem CSMA zugrunde liegende Konzept des konkurrierenden Wettbewerbs (engl. Contention) für die Integration innovativer PHY Technologien verwendet werden kann.

Opportunistische Kommunikation ist eine Technik, die die inhärenten Besonderheiten des drahtlosen Kanals ausnutzt. In der vorliegenden Dissertation werden CSMA-basierte Protokolle für die opportunistische Kommunikation in WMNs entwickelt und evaluiert. Es werden dabei opportunistisches Routing (OR) im zustandslosen Kanal und opportunistisches Scheduling (OS) im zustandsbehafteten Kanal betrachtet. Ziel ist es, den Durchsatz von elastischen Paketflüssen gerecht zu maximieren. Es werden Modelle für Überlastkontrolle, Routing und konkurrenzbasierte opportunistische Kommunikation vorgestellt. Am Beispiel von IEEE 802.11 wird illustriert, wie der schichtübergreifende Entwurf in einem Netzwerksimulator prototypisch implementiert werden kann. Auf Grundlage der Evaluationsresultate kann der Schluss gezogen werden, dass die opportunistische Kommunikation konkurrenzbasiert realisierbar ist. Darüber hinaus steigern die vorgestellten Protokolle den Durchsatz im Vergleich zu etablierten Lösungen wie etwa DCF, DSR, ExOR, RBAR und ETT.

Schlagwörter:
drahtloses Maschennetzwerk, optimaler Mehrfachzugriff mit Trägerprüfung, opportunistisches Routing, opportunistisches Scheduling, Netzwerkoptimierung, schichtübergreifender Entwurf

Contents

1. Introduction

In the field of wireless communication, a tremendous progress can be observed in recent years especially at the lower layers. Among them, important concepts and technologies that have been developed are:

- Spatial diversity and multiple-input multiple-output spatial multiplexing, beamforming, space-time coding,
- Frequency diversity and orthogonal frequency-division multiple access,
- Cooperative diversity and cooperative relaying, superposition coding,
- Multi-user diversity and opportunistic communication.

The principle of layering is a well-established design paradigm for communication systems. Both the Internet protocol stack and the ISO/OSI reference model have a layered architecture. Layering is an engineering principle that reduces the complexity of a system through abstraction and modularization [34], and it has been applied to the Internet stack and the OSI model for that reason with great success [40, 311]. In wireless systems, however, the established abstraction of a network stack does not work well. In particular, most of the above mentioned techniques require multi-user communication and cooperation in order to release their full potential. Nevertheless, the wireless multi-user channel is generally more than the aggregation of multiple single-user channels, so that the traditional model of isolated network layers is taken to its limits.

The innovations at the lower layers have been driven by the demands of cellular networks in most cases and they have already found their way into cellular standards and systems. On the other hand, wireless mesh and ad-hoc networks *cannot keep up with the speed of innovation* at the physical layer. In particular, innovative technologies are often used from a point-to-point perspective only and the multi-user nature is ignored as it is the case with IEEE 802.11n [105]. What are the reasons for the observed disparity? The architecture of cellular networks is hierarchical and centralized, which allows for a joint resource allocation across network layers. Thus, innovative physical layer concepts and technologies can be assimilated rapidly. On the other hand, wireless mesh networks have a flat and decentralized architecture, which renders the scheduling problem more complex. The necessary information for scheduling is probably scattered within the network. Decisions have to be made in a distributed way without global knowledge and their outcomes have to be propagated accordingly in order to coordinate the cooperation between network nodes.

From the theoretical point of view, it is known that maximum-weight scheduling in wireless mesh networks is throughput-optimal across many environments and conditions [48, 49, 69, 192, 258]. However, maximum-weight scheduling is not scalable since

it is generally NP-hard. For distributed solutions, the complexity translates to excessive message passing that is prohibitively resource consuming. On the other hand, the complexity of contention-based protocols like carrier sense multiple access (CSMA) is much lower, which makes them well suited for wireless mesh networks. Recently, the properties of CSMA have been understood: It is asymptotically utility-optimal in wireless mesh networks [112] at the expense of delay [285]. Furthermore, the result is constructive in terms of a cross-layer design because it provides a network utility maximization framework for modeling and understanding CSMA. The cross-layer design offers a formal justification for layering that is essential to systematically understand and design wireless mesh networks. Using the words of Yi *et al.* [285], it "becomes a foundation to understand, in a conceptually simple way, the complexities of network architectures: 'who does what' and 'how to connect them' ."

According to the results above, the principle of contention is suitable for medium access in wireless mesh networks. However, the question arises whether CSMA and the underlying concept of contention allows for the assimilation of advanced physical layer (PHY) technologies into wireless mesh networks (WMNs). Of course, the question is too broad to be answered within a single thesis. We will focus on one of the above mentioned techniques instead. Our objective is to design and evaluate contention protocols based on CSMA for opportunistic communication in wireless mesh networks.

1.1. Thesis Statement

In this dissertation, we claim that:

Thesis Statement. *Contention techniques based on carrier sense multiple access are an effective and efficient means to utilize opportunistic communication in wireless mesh networks in order to enhance both throughput and fairness of elastic unicast traffic flows in relation to state-of-the-art approaches.*

1.2. Terminology

The thesis statement refers to several technical terms, which we are going to define in the following. In the context of this dissertation, we are addressing the domain of communication networks and, in particular, the domain of wireless mesh networks.

Definition (Wireless Mesh Network)**.** A WMN is a network of nodes that are equipped with wireless transceivers. The topology of a WMN is flat and decentralized. Adjacent nodes communicate with each other directly via wireless signals. Multi-hop forwarding enables the communication between non-adjacent network nodes.

Communication links are established via wireless signals, which are assumed to propagate according to established and well-defined models that have been empirically validated. In this dissertation, fading is the propagation effect of interest. We consider both block fading and slow fading according to the Rayleigh and the Rician distributions. The wireless nodes are equipped with half-duplex digital packet transceivers that possess omnidirectional antennas and carrier sensing capabilities.

Definition (Carrier Sensing)**.** Carrier sensing (CS) refers to the process of listening to the communication medium in order to detect the presence of a communication signal indicating that an adjacent node is currently transmitting.

The detection of a transmission can be accomplished by several techniques. For example, a CS threshold for the power of the received signal can be used. We assume that both the transmission power and the CS threshold are fixed, i.e. we do not address the problems of topology control and CS threshold adaption. Hence, the power budget at the receiver may vary depending, among other things, on the physical length of a wireless link. The communication system utilizes the power budget via a predefined set of modulation and coding schemes (MCSs), which are also called bit-rates in the following. All nodes are assumed to operate on the same radio frequency (RF) channel. The wireless transceivers employ the CSMA protocol.

Definition (Carrier Sense Multiple Access)**.** Carrier sense multiple access (CSMA) is a decentralized MAC protocol that relies on the CS capabilities of the transceivers in order to arbitrate the access to the shared communication channel. Each node is required to listen to the communication medium in order to check the availability of the shared communication resources. As long as the medium is sensed busy, the channel access has to be deferred.

Depending on the application domain, the observable communication patterns may vary greatly. In this dissertation, we address the following type of traffic flows.

Definition (Traffic Flow)**.** A traffic flow is a sequence of packets that are exchanged between a source and a destination node. A traffic flow is unidirectional and unicast with respect to the network layer, i.e. there is exactly one source and one destination network node. Every node of the WMN can become source or destination.

Note that our definition of traffic flow is more specific than RFC 3697 [226] since network-layer broadcast and multicast communication is not within our scope. We assume that traffic flows are elastic and saturated, i.e. the source generates packets from a potential infinite information supply and it does not impose delay or throughput constraints. Packets are forwarded from source to destination in a store and forward manner without any in-network modification of the application data like network coding, for example. Thereby, the packets may traverse multiple intermediate network nodes until they reach the destination, which we refer to as multi-hop forwarding. The term route refers to the sequence of network nodes that a packet traverses from source to destination. Multi-path routing is allowed, i.e. multiple routes can be used simultaneously. We assume that link state routing information is available, i.e. the topology is known to every network node. Protocols for neighbor and topology discovery are known in literature [60, 106, 124], whereas they are not in the scope of this thesis.

Using the term opportunistic communication, we refer to two different techniques that exploit the inherent characteristics of the wireless channel. Opportunistic routing (OR), the first one, is a technique to benefit from multi-user diversity (MUD) in WMNs. The building block of OR is the anycast transmission primitive.

Definition (Anycast)**.** An anycast is a wireless transmission that addresses multiple receivers at the MAC layer. Only one of them is required to receive the frame for

the anycast to be successful. At the PHY, the anycast transmission benefits from the broadcast nature of the wireless medium. The medium access control (MAC) protocol has to ensure that each receiver is free from destructive interference when it takes part in the anycast.

Our definition of anycast is more specific compared to related work [22, 315]. A receiver candidate is required to be free from interference in order to participate in the anycast transmission. This requirement is not enforced in related work, so that the reception may fail due to either channel errors or hidden node effects. Hence, the anycast transmission mitigates both PHY and MAC layer impairments. In contrast, we assume that a MAC protocol handles the hidden node problem, so that we can focus on the PHY aspects of anycasting.

Definition (Opportunistic Routing)**.** Opportunistic routing (OR) is a forwarding technique for WMNs that is based on anycast transmissions. It mitigates transmission errors using multiple candidate receivers within an anycast.

Transmission errors are common in wireless networks, so that the forwarding attempt of a relay node may fail. At the PHY, however, the wireless channel is generally a broadcast medium. The rationale of OR is to make the routing decision after the actual transmission based on the information which candidate(s) successfully received the frame.

The second technique we consider is opportunistic scheduling. It is a well known concept from the domain of cellular networks to increase the throughput efficiency of a wireless system.

Definition (Opportunistic Scheduling)**.** Opportunistic scheduling (OS) refers to the scheduling of transmissions that additionally takes the instantaneous channel conditions into account.

The rationale of OS is to "ride the peaks of the fading process", i.e. use the channel at good instances and refrain from transmission while the channel is in bad conditions [264]. Occasionally, the term opportunistic communication is used to refer to delay tolerant networks that are nevertheless not within the scope of this thesis.

Both OR and OS are complementary techniques. The latter exploits the knowledge about the instantaneous channel state whereas the former tries to mitigate the missing channel knowledge by using multiple candidate receivers. Thus, the question whether OR or OS is better suited for a given system depends on the channel characteristics and the capabilities of the radio hardware. Both approaches are opportunistic within different resource dimensions. OS seeks for opportunities in time whereas OR exploits the user dimension.

1.3. Methodology

The thesis statement is validated using the methodology shown in Figure 1.1. We develop models of opportunistic communication under CSMA in WMNs based on modeling assumptions, which include the so-called protocol exclusion model [282], for example. A comprehensive description of the assumptions is given in the respective sections. In order to find models of manageable complexity, it is necessary to make strong

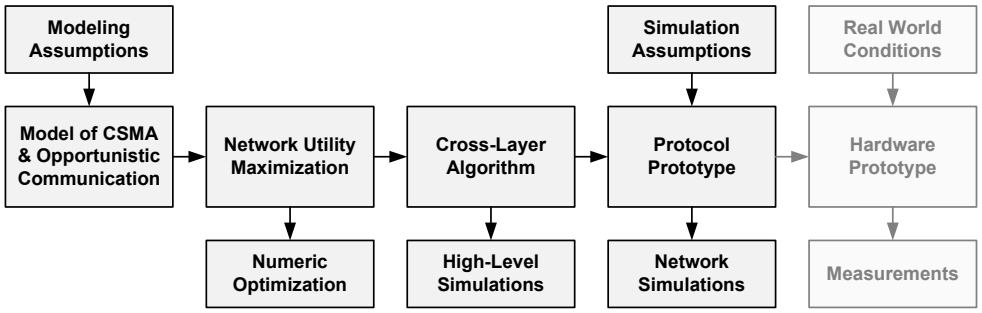

Figure 1.1.: Overview of our methodology.

modeling assumptions. They are relaxed in our network simulations, so that their impact can be assessed. Nevertheless, the question whether the modeling assumptions are "realistic" is not within the scope of this thesis.

Following our methodology, the models are plugged into a network utility maximization (NUM) framework that addresses congestion control and routing in WMNs in addition to opportunistic communication and CSMA. The congestion controller is responsible that the traffic flow makes use of the network resources in an efficient way. Multiple flows may coexist in the network and compete for resources. The congestion controller ensures fairness between them, i.e. it allocates the network resources to competing flows according to well-defined fairness objectives. On finishing this step, we are able to describe network scenarios in a declarative way by means of optimization problems. Although the size of these scenarios remains limited due to the involved descriptional complexity, the evaluation via numerical optimization is nevertheless illustrative since it reveals the potentials of opportunistic communication under CSMA.

Following our methodology in Figure 1.1 further, we derive technology-agnostic algorithms from the declarative optimization problems using the principle of layering as optimization decomposition (LAD). The cross-layer algorithms are evaluated in high-level simulations using the same set of modeling assumptions.

In the next step according to our methodology, we discuss how the algorithms can be implemented in a system using technologies similar to IEEE 802.11. We present protocol prototypes and evaluate them through network simulations. Our models rely on strong assumptions in order to keep the involved complexity manageable. In our network simulations, the assumptions are relaxed in way that is widely acknowledged in the research community and we refer to them as simulation assumptions, whereas their "realism" is not within the scope of our thesis. The relaxation provides an insight into the impact of the modeling limitations and the remaining potentials of opportunistic communication. For example, the simulation assumptions include the physical exclusion model [282] instead of the protocol model. Another example is the assumption about saturated queues at forwarding nodes, which is relaxed in the simulations. Due to the relaxed simulation assumptions, we are able to evaluate and compare the proposed protocols with state-of-the-art approaches based on the same premises.

According to our methodology shown in Figure 1.1, the last step would be the evaluation of a hardware prototype via measurements under real world conditions. However, both the available platforms and the scientific methods to evaluate MAC protocols on hardware prototypes are still in a preliminary stage. The main challenge for a

MAC prototyping platform is the requirement for high flexibility as well as stringent timing at the same time, which renders both hard-wired solutions and software defined radios unsuitable. The evaluation of protocol prototypes on hardware is left for future work although this step is non-replaceable and thus not less important. Nevertheless, we argue that our results provide sufficient evidence to support the thesis statement within the stated assumptions.

1.4. Contributions

We present a model of CSMA/CA with node-oriented carrier sensing that captures the characteristic tradeoff between multi-user gain and spatial reuse that arises with opportunistic routing (OR). Even under node-based carrier sensing, CSMA can be operated in a simple and distributed way if the receiver blocking problem is handled properly. Based on the idea of busy tones, we design a MAC protocol dedicated for WMNs called CSMA/HBT according to the presented model.

We propose a distributed algorithm for congestion control, opportunistic routing and CSMA in WMNs with unreliable and memoryless links. The objective of the algorithm is the maximization of the cumulated utility of elastic traffic flows that do not impose tight end-to-end delay constraints. We refine the algorithm to a cross-layer protocol. We design a method for the efficient adaptation of the CSMA parameters while preventing the breakdown of the system due to collisions. We illustrate how the throughput-delay tradeoff in CSMA can be controlled via upper bounds on the queues. In addition, we propose an approach to pre-select the routing paths according to a routing metric for WMNs.

We evaluate the proposed protocol through analysis and simulation. Based on our results, we conclude that contention techniques can handle the tradeoff between spatial reuse and multi-user gain efficiently. This observation becomes even more important since neither multi-user nor spatial diversity dominates in randomized WMN topologies according to our analytic characterization. The results suggest that the prototype is able to increase both throughput and fairness in comparison to state-of-the-art single-path and OR protocols. However, the optimality gap to the theoretical potentials is considerable for the chosen system parameters, and it increases with the utilized degree of multi-path and opportunism.

In addition, we propose a Markov model of CSMA in WMNs with slow fading channels that allow for opportunistic scheduling (OS). The problem possesses a favorable structure, so that it can be decomposed into simple and distributed subproblems under some assumptions. The model allows us to derive a NUM algorithm for congestion control, routing and CSMA in combination with OS. It is based on the so-called channel-differentiated contention. The rationale is to employ a large backoff when the channel is bad and increase the contention aggressiveness properly with better channel instances. We design a cross-layer protocol that addresses how channel knowledge is obtained in a WMN, how the sender maintains the window of packets that are in transit and how efficient backoff durations can be preserved in the contention process.

According to our evaluation results obtained from analysis and simulation, we conclude that distributed opportunistic scheduling (DOS) is feasibly in WMNs based on

the concept of contention. Our design relies on strong assumptions. When relaxing the assumptions about infinite buffers and non-hidden channel states, the system's performance becomes dependent on the memory of the channel and, fortunately, it degrades gracefully. When reducing the memory, the channel uncertainty becomes the limiting factor. In the opposite case, the limiting factor is the window size since it becomes more difficult to bridge over longer periods of bad channel conditions. However, achieving high OS gains takes a significant and non-negligible amount of end-to-end delay. Interestingly, multi-path forwarding is an alternative approach to increase the throughput in WMNs under DOS. Within typical use cases for WMNs, the potential of DOS is significant. However, the DOS gain remains moderate in our simulations for the chosen system parameters, which indicates that the optimality gap is considerable. Nevertheless, the benefits over state-of-the-art protocols are significant in terms of throughput and fairness especially with many flows.

1.5. Notation

The following list contains the symbols und units that we use throughout the thesis. Additional notation is introduced in the respective sections as necessary. As a convention, we use bold font to distinguish vectors from scalar values.

$\mathbb{R}$ ($\mathbb{R}_+$)	Real numbers (non-negative)
$\mathbb{C}$ ($\mathbb{C}_+$)	Complex numbers (non-negative)
$\mathcal{P}(.)$	Power set
$\mathcal{P}(.)_k$	Set of all k-subsets
$\langle .,. \rangle$	Dot product
$\lfloor . \rfloor$	Round down
$\lvert . \rvert$	Cardinality of a set (magnitude of a complex number)
$[.]_+$	Projection onto the nonnegative orthant
$(.)_k$	Selection the k-th component of the argument vector
$\mathbb{1}(.)$	Indicator function, 1 if the argument is true, 0 otherwise
$\delta^{\cdot}(.)$	Indicator function, $\delta^I(v) = \mathbb{1}(v \in I)$
$\mathrm{P}(.)$	Probability
$\mathrm{erfc}(.)$	Complementary error function
$\mathrm{Q}(.)$	Q-function, $\mathrm{Q}(x) = 0.5\,\mathrm{erfc}(x/\sqrt{2})$
$\mathrm{I}_0(.)$	Modified Bessel function of the first kind and zero-order
$\Gamma(.)$	Gamma function
$\mathrm{P}_{\mathrm{out}}$	Outage probability
t	Time
N	Set of nodes
N_i	Neighbors of node i

$N_{\mathrm{DS}}^{f}(i)$	Downstream neighbors of node i with respect to flow f
K	Number of links
F	Set of flows
$F(i)$	Flows traversing node i
$\sigma(f), \delta(f)$	Source and destination of flow $f \in F$
(i,j)	Link from node i to j, $i,j \in N$
(i,J)	Hyperlink from node $i \in N$ to nodes $J \subset N$
$r_{i,J}$	Transmission aggressiveness of (hyper-)link (i,J); average backoff $\exp(-r_{i,J})$
$p_{i,J}$	Packet error rate (PER) of (hyper-)link (i,J)
$p_{i,J}^{i,K}$	PER of (hyper-)link (i,J) when using the bit-rate $R_{i,K}$
$R_{i,J}$	Bit-rate of (hyper-)link (i,J) selected according to (3.12) (cf. p. 62)
B	Set of channel states per link
$P_{k,b}$	Probability that link k is in channel state b
$q_{i,J}$	Throughput of (hyper-)link (i,J) (optionally with superscript $f \in F$)
$x_{i,j}$	Goodput of link (i,j) (optionally with superscript $f \in F$)
y^{f}	Flow rate of flow f
λ	Input rate
$U(.)$	Increasing utility function
C	Credit
TC	Transmission credit
V	Positive parameter that controls the throughput-delay tradeoff within CSMA
W	Positive window size
f_{D}	Doppler frequency
. dB	Decibel
. s	Second
. m	Meter
. W	Watt
. dBm	Power ratio in decibels, relative to 1 mW
. Hz	Hertz
. bps	Bits per second
. pps	Packets per second

2. Background

In this chapter, we provide background information on applications and technologies for wireless mesh networks (WMNs). We discuss the properties of radio propagation at large and small scales. We briefly introduce IEEE 802.11, which is an example for a technology that enables the construction of WMNs. An overview of protocols and metrics for routing in WMNs is given and we conclude the chapter with a brief description of the simulation tool that we have used to conduct the network simulations. The related work concerning the research topics can be found at the beginning of the following chapters.

2.1. Applications of Wireless Mesh Networks

In comparison with other systems, the main differentiators of WMNs are the flat and decentralized architecture and the multi-hop communication. Nevertheless, our definition of WMNs is broad and it covers many applications that have vastly different requirements and constraints.

Two aspects that are common to WMNs are cooperation and self-organization. In particular, *cooperation* is necessary since there is no central controller. For example, the network nodes have to generate topology information and forward packets in a distributed and cooperative manner. On the other hand, the cooperation increases the robustness of the network since the architecture does not have a single point of failure. The breakdown of individual nodes may reduce the network performance, but the remaining network will eventually provide connectivity, if possible.

The aspect of *self-organization* is related to cooperation. A WMN has to cope with variability at both macroscopic and microscopic levels. Microscopic mobility may cause severe channel fluctuations. On the other hand, the deployment as well as the growth of WMNs is often spontaneous and unplanned. In either case, the planning as well as the maintenance of the network in a manual way is often infeasible.

Akyildiz *et al.* discuss several application scenarios for WMNs [5], which we summarize in the following. Note that the enumeration is non-exclusive.

Broadband Home Networks. The wireless Internet access in home networks has been one of the driving forces behind the success of IEEE 802.11. However, the existing technology cannot handle dead spots conveniently, since this often involves the extension of the wired infrastructure. On the other hand, the number of devices at home that are equipped with wireless transceivers continuously increases. The growth is not only limited to consumer electronics, but also household utensils become network-enabled due to the "smart grid" vision. Since the home networks become denser, the question arises in which way they can contribute to a meshed home network.

Community and Municipal Networks. The broad availability as well as the low cost of IEEE 802.11 hardware has lead to the emergence of many community network projects (cf. [315]). Community networks are operated by volunteers that provide the hardware and deploy it at their homes. On the other hand, municipal networks are an effort of the local administration or local companies. The Freifunk in Berlin[1] and the GoogleWiFi in Mountain View[2] [3] are examples for both categories. Nevertheless, their objectives are similar. They provide Internet connectivity in areas that do not have broadband access and they ensure a seamless outdoor coverage to residents, commuters and tourists. In addition, the costs per participant can be reduced due to shared Internet connections. Furthermore, information can be shared within the community in an autonomous manner without relying on external networks. Location based services can be incentives to participate for small businesses.

Enterprise Networks. The deployment and maintenance costs of wired networks and wireless hot spot solutions motivate the use of WMNs in the enterprise context. Due to the self-organization of WMNs, the network can easily grow as the enterprise expands. In the short term, however, the all-wireless office will probably remain a vision. On the one hand, modern office buildings provide an Ethernet deployment. Furthermore, the decision makers are often reluctant for security and availability reasons. For example, IEEE 802.11 operates in unlicensed spectrum that can be jammed at any time. In the short term, we suppose that WMNs will enhance the existing wired enterprise network instead of replacing it.

Carrier Grade Access Networks. Nowadays, the operators of mobile and fixed networks rely on a wired backhaul and well-planned point-to-point radio links to provide connectivity to their customers. A WMN is a compelling design alternative for their access network due to the higher flexibility and the reduced costs of deployment and operation. The growth of the wireless throughput over the past 50 years can be primarily attributed to smaller cells, whereas the contribution of larger bandwidths and better PHYs is surprisingly small [61]. Thus, WMNs may help to reduce the cell size further without the need to wire all additional base stations. For example, the MAN standard IEEE 802.16 defines multi-hop forwarding elements. In addition, the EU founded project CARMEN[3] has investigated in which way mesh networks can provide carrier grade services.

Transportation Systems. Although an external access to cellular systems is generally available in busses and trains, it may put a serious burden on them due to the high velocity and its impact on the channel, the frequent handovers and the large number of simultaneous users. Alternatively, a WMN that is deployed inside the vehicles would able to aggregate the outgoing traffic. The same applies to airplanes and ferries, as well, with the difference that an external cellular network is not available. In the context of airplanes, a further incentive for wireless systems is the weight reduction.

[1] `http://freifunk.net`
[2] `http://wifi.google.com`
[3] `http://www.ict-carmen.eu`

Sensor Networks. In contrast to the above-mentioned applications, sensor networks interact with the environment in the first place. They use sensors to monitor the environment. Optionally, the sensor data is aggregated within the network in order to detect events of interest or to control actors. Due to the varying application domains for sensor networks, their performance objectives are generally more diverse compared to access networks. In addition, the energy consumption is a limiting factor if the sensor nodes operate on battery power. Wireless sensor networks are used for environmental monitoring, building automation, precision agriculture, logistics, telematics and medicine and health care [130, chap. 1].

Emergency Early Warning, Response and Recovery. During and after a disaster, the communication infrastructure is important for the organization and coordination of response actions. The existing wired infrastructure, however, is prone to physical destruction as well as overloading. A WMN can provide a communication infrastructure that operates autonomously from existing networks, does not depend on the power grid and provides robustness against the failure of individual nodes. For example, the EU founded project SAFER[4] has investigated in which way an earthquake early warning can be accomplished using a large amount of inexpensive sensors that are connected by a WMN. The time between the first signs of an earthquake and the arrival of the destructive waves is in the order of seconds. If the earthquake can be reliably detected in time, large secondary damages can be prevented by turning off gas and water supplies, for example.

Meshed network architectures can be found on different scales. Both IEEE 802.16 WiMAX and IEEE 802.15.3 ZigBee offer meshed network elements at the WMAN and WPAN scale, respectively. Nevertheless, we will focus on WLANs based on IEEE 802.11 in the following since they are the most widespread instances of WMNs.

2.2. Radio Propagation

In the following, we give a brief overview of well-known propagation models for wireless signals that can be found in literature. If not stated otherwise, the primary sources that we refer to in this section are Goldsmith [84, chap. 2,3], Rappaport [228, chap. 4,5] and Sklar [246, chap. 15]. Wireless signals are transported by electromagnetic (EM) waves. Radio waves that are emitted by the transmitter propagate through space and may eventually arrive at the receiver. In the free space, the radio wave propagates along the line of sight (LOS) path only since there are no obstacles the radio wave can interact with. In urban and indoor environments, however, the LOS path may be obstructed and the arriving radio signals at the receiver have taken indirect paths only, which we refer to as non line of sight (NLOS) propagation.

The propagation of EM waves can generally be described by the physical effects of absorption, reflection, scattering, and diffraction. The absorption accounts for the attenuation of the energy of the wave by the matter it penetrates. Reflection refers to the change of the direction of a wave on impinging on a macroscopic object in relation to

[4] http://www.saferproject.net

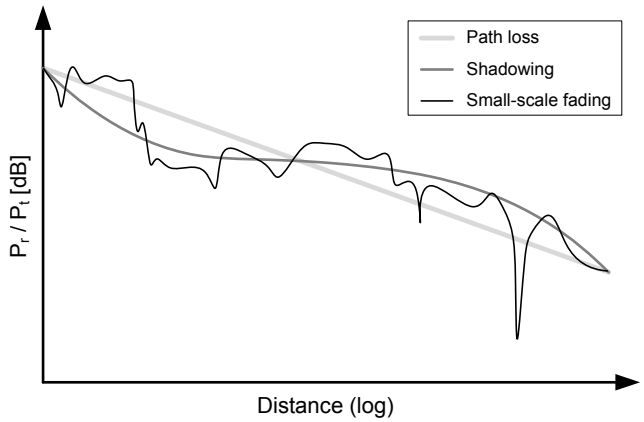

Figure 2.1.: Path loss, shadowing and small-scale fading (cf. [84, p. 25]).

its wave length. Scattering occurs as the radio wave interacts with a large number of objects that are small in terms of the wave length. A single scattering is perceived as random by an observer due to the strong dependence on the initial conditions. Nevertheless, multiple scatterings average out the randomness, so that the effect of these diffuse reflections can be described statistically. Diffraction refers to the effect that a small object in the order of a wave length causes secondary waves as the radio wave impinges on them. Depending on the geometry, the secondary waves may enter the shadow of the primary wave in a way that the radio wave bends around obstacles.

The physical effects of reflection, scattering, and diffraction change the direction of the wave front. Hence, the radio wave that arrives at the receiver may have travelled along different propagation paths of varying lengths, which we refer to as multipath propagation. The superposition of multiple signal copies at the receiver causes fluctuations of the resulting signal amplitude in both time and frequency. Although exact solutions according the physical laws can be obtained, they are often prohibitively complex or even impossible due to unknown geometries or material properties. Hence, stochastic models for the radio propagation have been developed that enable the evaluation and comparison of new approaches in a systematic and non-empirical way. They are available at varying granularities and level of details in order to reproduce the important properties of the real system. In the following, we briefly review models for both large and small-scale fading that are relevant in our context.

2.2.1. Large-Scale Fading

As shown in Figure 2.1, the wireless propagation can be differentiated according to their scale in space and time. In particular, the large-scale fading addresses macroscopic effects like the attenuation in terms of distance or due to obstacles within the propagation path. Small-scale fading refers to the microscopic effects due to multipath propagation. Despite their microscopic nature, however, the impact of small-scale fading on the received signal power can range up to 40 dB and thus, it is non-negligible with respect to the large-scale effects. Furthermore, mobility of both the transceivers as well as environmental objects affects the propagation properties over all scales.

Path Loss

Path loss models predict the average attenuation of the EM waves propagating through space. The averaging horizon typically covers between 5 and 40 wave lengths, so that both shadowing and small-scale fading effects are averaged out. In particular, the path loss L is defined as the ratio of the transmitted signal power P_t to the received signal power P_r.

$$L = \frac{P_\mathrm{t}}{P_\mathrm{r}}$$

As shown in Figure 2.1, the path loss generally increases with respect to the separation of transmitter and receiver, so that the received signal power diminishes. Several path loss models exist and they differ in whether they address LOS propagation or whether they consider additional reflections or NLOS environments.

Free Space Path Loss. The first model we are considering is the free space path loss. It assumes LOS propagation without any intermediate absorption or reflection of the radio energy. It is reported that the model can be applied to satellite communication. The free space path loss L depending on the distance d between transmitter and receiver is given by the Friis free space path loss.

$$L(d) = \left(\frac{G_\mathrm{t} G_\mathrm{r} \lambda^2}{(4\pi)^2 d^2 L_\mathrm{S}} \right)^{-1}$$

In the equation above, λ is the wave length and G_t and G_r refer to the gains of the transmit and receive antennas, respectively. Furthermore, L_S is the system loss due to the electrical equipment.

Log-Distance Path Loss. Empirical measurement results by Okumura and Hata suggest that the inverse-square relationship of the free space model describes the indoor and outdoor propagation in urban and sub-urban environments not satisfactorily. The log-distance model is an empirical model, in which the path loss L increases to a parameterized exponent γ.

$$L(d) = L(d_0) \cdot \left(\frac{d}{d_0} \right)^{\gamma}$$

In the equation above, d_0 is the reference distance and $L(d_0)$ is the path loss at d_0, which can be obtained from measurements or from a different path loss model. Typical values for the path loss exponent γ are given in Table 2.1.

Shadowing

Due to fixed and mobile obstacles in the propagation path like hills, houses and vehicles, the actual average path loss may vary vastly. Shadowing is a stochastic model

Environment	Range of γ
Free space	2
Urban macrocells	$3.7 - 6.5$
Urban microcells	$2.7 - 3.5$
Office Building (same floor)	$1.6 - 3.5$
Office Building (multiple floors)	$2 - 6$

Table 2.1.: Typical path loss exponents (cf. [84]).

that accounts for the deviations from the mean path loss due to obstacles at macroscopic scales of $5 - 40$ wave lengths. Measurement results suggest that shadowing can be modeled as a log-normally distributed random value. The joint path loss in combination with the log-distance path loss model is given as follows.

$$L(d) = L(d_0) \cdot \left(\frac{d}{d_0}\right)^{\gamma} \cdot 10^{X_\sigma/10}$$

In the equation above, $X_\sigma \sim \mathcal{N}(0, \sigma)$ is a Gaussian distributed random variable with zero mean and standard deviation σ. Typical values are given in Table 2.2.

Environment	Range of σ
Outdoor	$4 - 12$
Office, hard partition	7
Office, soft partition	9.6
Factory, LOS	$3 - 6$
Factory, NLOS	6.8

Table 2.2.: Typical shadowing deviations (cf. [315]).

2.2.2. Small-Scale Fading

Multiple versions of the same signal may arrive at the receiver due to reflections. Small-scale fading captures their impact on the received signal. The multipath copies of the signal may differ in power, time delay and frequency. In particular, propagation paths of unequal length cause multipath delays. Frequency offsets occur if the individual multipath signal copies undergo varying Doppler shifts. Based on the multipath delay and the Doppler spread, small-scale fading can be differentiated with respect to its impact on the received signal in the time and in the frequency domain.

Multipath Delay and Frequency Selective Fading. When multiple versions of the same signal arrive at the receiver, the *multipath delay spread* T_m measures the delay between the arrival of the first and the last (significant) signal copies. If the symbol time T_s is much larger than the multipath delay ($T_\mathrm{s} \gg T_\mathrm{m}$), the multipath copies overlap to a large extend causing either constructive or destructive interference. The channel is said to experience *flat fading*: Its effect on the signal is the same across the signal bandwidth $B_\mathrm{s} \propto 1/T_\mathrm{s}$. The coherence bandwidth $B_\mathrm{c} \propto 1/T_\mathrm{m}$ refers to the range of frequencies that exhibit a correlation of the amplitudes if a signal passes through them.

The coherence bandwidth of the flat fading channel is larger than the bandwidth of the signal ($B_c > B_s$).

In the case $B_s > B_c$, on the other hand, the signal bandwidth exceeds the coherence bandwidth. The channel becomes *frequency selective*, i.e. it affects frequency components of the transmitted signal that are spaced by more than the coherence bandwidth in different ways. In the time domain, the multipath delay is larger than the symbol time ($T_m > T_s$), resulting in inter-symbol interference. One way to mitigate frequency selective fading is orthogonal frequency-division multiplexing (OFDM). Instead of using a small symbol time across the whole signal bandwidth, the OFDM system partitions the spectrum into many orthogonal subcarriers. Each subcarrier occupies a smaller bandwidth, so that the symbol duration is prolonged. In this way, the frequency selective wideband channel is converted to many parallel flat fading subcarriers.

Doppler Spread and Time Selective Fading. A superposition of multiple signal copies at the receiver may cause either constructive or destructive interference. If the superposition constantly changes due to mobility, for example, then the received signal strength at the receiver will vary in time. In particular, transceiver and environmental mobility may result in different Doppler shifts across the multipath components. In that case, the frequency offset causes continuous variations in the interference relationship between the affected multipath components. In the worst case, the destructive interference results in an (almost perfect) cancelation, which is called *deep fade*. Small-scale fading may cause rapid and severe fluctuation of the received signal strength at microscopic scales of a wave length or a wave period.

Whether a channel experiences fast or slow fading depends on both the system and the channel. The channel coherence time T_c refers to the time duration, over which the channel is assumed to remain constant. The coherence time is inversely proportional to the frequency domain Doppler spread. It is commonly approximated in the following way.

$$T_c = \sqrt{\frac{9}{16\pi f_D^2}}$$

In the equation above, f_D refers to the maximum Doppler shift that is given by $f_D = v/\lambda$ with wave length λ and velocity v.

If the coherence time is smaller than the symbol duration ($T_c < T_s$), then the channel is *fast fading*. The channel changes at a higher rate compared to the signal. Statistically, all symbols are affected by the fading process in the same way, i.e. the correlation of the fading process between adjacent symbols is low. Fast fading distorts the signal and causes an irreducible error rate at the receiver.

On the other hand, *slow fading* refers to the case that the rate of change of the channel is lower compared to the signal, i.e. the channel coherence time is larger than the symbol duration ($T_c > T_s$). Slow fading may induce long-lasting deep fades resulting in *outages*. Different from the AWGN channel, reliable communication is not possible anymore during outages.

Rayleigh Fading

Rayleigh fading is a well-known fading model for NLOS propagation in flat fading channels. The model assumes that no dominant LOS path is present and the received signal consists of many reflected paths. Assuming that the central limit theorem applies, the amplitude of both the in-phase and the quadrature components of the received signal are Gaussian distributed whereas the phase is uniformly distributed. The signal amplitude is the root of the squared in-phase and quadrature components. The amplitude is Rayleigh distributed and thus, the instantaneous signal power p_W of the Rayleigh faded signal is exponentially distributed according to the probability density function (PDF) (2.1) with average signal power P_W.

$$f(p_W|P_W) = \frac{1}{P_W}\exp\left(-\frac{p_W}{P_W}\right) \tag{2.1}$$

In slow fading channels, the system performance is dominated by outages. The outage probability $\mathrm{P_{out}} = \mathrm{P}(p_W < P_\mathrm{t}|P_W)$ captures the probability that the instantaneous signal power drops below a threshold P_t, so that the performance becomes unacceptable. As shown in (2.2), the outage probability for Rayleigh fading can be given in closed form.

$$\mathrm{P_{out}}(P_\mathrm{t}|P_W) = \int_0^{P_\mathrm{t}} \frac{1}{P_W}\exp\left(-\frac{p_W}{P_W}\right)\mathrm{d}p_W = 1 - \exp\left(-\frac{P_\mathrm{t}}{P_W}\right) \tag{2.2}$$

Important statistical measures to describe the temporal correlation of a fading channel are the average fade duration (AFD) $\bar{t}_\rho$, the average non-fade duration (ANFD) t_ρ and the level crossing rate (LCR) L_ρ. The LCR L_ρ measures the number of (directional) crossings of the amplitude threshold ρ per second. The AFD $\bar{t}_\rho$ accounts for the average duration the fading process spends below the amplitude threshold ρ. Under the assumption of a uniform scattering environment, L_ρ and $\bar{t}_\rho$ for Rayleigh fading can be estimated as follows.

$$L_\rho = \sqrt{2\pi} f_\mathrm{D} \rho \exp(-\rho^2) \tag{2.3}$$

$$\bar{t}_\rho = \frac{\mathrm{P_{out}}(P_\mathrm{t}|P_W)}{L_\rho} = \frac{\exp(\rho^2) - 1}{\sqrt{2\pi} f_\mathrm{D} \rho} \tag{2.4}$$

In (2.3) and (2.4), f_D is the Doppler frequency and $\mathrm{P_{out}}$ is the outage probability. Let P_t be the target power level and P_W be the average power level of the signal, then the signal envelope threshold becomes $\rho = \sqrt{P_\mathrm{t}/P_W}$.

Rician Fading

The Rician fading model addresses flat fading channels that exhibit a dominant LOS component in addition to other reflected paths. The parameter K captures the power ratio between the LOS and the NLOS components. Hence, it determines how severe the Rician fading is. In the most severe case ($K = -\infty$ dB), it is similar to Rayleigh

fading. On increasing K, the LOS path becomes more dominant, which reduces the variability of the fading. In the extreme case $K = \infty$ dB, only the LOS path remains and the randomly faded NLOS paths have vanished. The outage probability under Rician fading can be estimated according to (2.5)

$$f(p_W|K, P_W) = \frac{1+K}{P_W}\exp(-K) \cdot \exp\left(-\frac{1+K}{P_W}p_W\right) \cdot \mathrm{I}_0\left(\sqrt{4K\frac{1+K}{P_W}p_W}\right)$$
$$\mathrm{P}_{\mathrm{out}}(P_\mathrm{t}|K, P_W) = \int_0^{P_\mathrm{t}} f(p_W|K, P_W)\ \mathrm{d}p_W \tag{2.5}$$

In the expressions above, I_0 is the modified Bessel function of the first kind and zero-order. The LCR for a Rician faded signal can be estimated as follows.

$$L(\rho) = \sqrt{2\pi(K+1)}f_\mathrm{D}\rho\exp\left(-K-(K+1)\rho^2\right)\mathrm{I}_0\left(2\rho\sqrt{K(K+1)}\right) \tag{2.6}$$

In (2.6), the Doppler frequency is denoted by f_D and the threshold ρ is defined as $\rho = \sqrt{P_\mathrm{t}/P_W}$ with target power threshold P_t and average received power P_W.

One question that arises is how to parameterize the above models in terms of Rician K and Doppler shift. Fortunately, measurement results and standardized channel models exist that may help to find reasonable parameters. For example, the IEEE 802.11n channel model specifies a Doppler shift between $3-6$ Hz for stationary devices [199]. In indoor environments, Doppler shifts in the range of $0.1-6.1$ Hz have been reported.[5] Francisco *et al.* have estimated the Rician K parameter in the 2.4 GHz ISM band for a hospital environment [59]. For a slowly moving client node, they have observed that the K parameter is typically larger than 0 dB under LOS conditions and within $-10-0$ dB in the NLOS case. In addition, Carroll *et al.* have measured the Rician K in the 5 GHz ISM band for an indoor campus environment [37]. Both transmitting and receiving antennas have been fixed, whereas environmental mobility was present due to moving people in the vicinity of the receiver. The authors report values of K in the range of $1.8-4.7$ dB and an LCR between $3-6\ \mathrm{s}^{-1}$ at the threshold $\rho = 1$. According to (2.6), the Doppler shift is within the range of $4-8$ Hz. In contrast, the Doppler shift in a vehicle-to-vehicle channel is expected to be higher. Doppler spreads between $0.5-1.5$ kHz have been measured in experiments, resulting in a coherence time below 1 ms [14, 51].

Nakagami Fading

Nakagami fading is a generalization of Rayleigh and Rician fading. It is often used to describe experimental results that do not fit well into other distributions. The PDF of the signal power p subject to the average received power P_W and Nakagami parameter m is given in (2.7).

[5] `http://www.wirelesscommunication.nl/reference/chaptr03/indoor.htm`

$$f(p|m, P_W) = \left(\frac{m}{P_W}\right)^m \cdot \frac{p^{m-1}}{\Gamma(m)} \cdot \exp\left(\frac{-mp}{P_W}\right) \tag{2.7}$$

In the equation above, $\Gamma(.)$ is the Gamma function. Rayleigh and Rician fading can be approximated by setting $m = 1$ and $m = (K+1)^2/(2K+1)$, respectively.

2.3. IEEE 802.11

In the following, we give a brief overview of state-of-the-art PHY and MAC layer technologies using the example of IEEE 802.11 and, in particular, the OFDM PHY and the CSMA MAC of IEEE 802.11a/g. If not stated otherwise, our primary sources in this section are Gast [76], Tanenbaum [256, chap. 4] and Goldsmith [84, chap. 4-6]. IEEE 802.11 belongs to the IEEE 802 family of standards that address local area networks (LANs). According to the ISO/OSI model, it specifies both the physical and the data link layers for wireless LANs. The data link layer of IEEE 802.11 is divided into an upper logical link control (LLC) sublayer based on IEEE 802.2 and a lower MAC sublayer. The LLC allows using different network protocols like the Internet protocol (IP) on top of IEEE 802.11. The original IEEE 802.11 standard emerged in the year 1997, and it has subsequently been extended by several amendments. A selection is shown in Table 2.3.

Originally, IEEE 802.11 has covered two network architectures. The infrastructure mode is a cellular network design that extends the wired LAN by an additional wireless hop. A wireless cell is established by an access point (AP) node that acts as a bridge between associated stations (STAs) and the wired backbone. On the other hand, STA nodes that are in communication range of each other may establish an independent network in an ad-hoc manner that does not rely on the presence of an AP. Further network architectures are considered in recent amendments. For example, the IEEE 802.11s amendment specifies routing protocols for a meshed network topology. We will cover IEEE 802.11s in section 2.4.2.

Amendment	Year	Description
IEEE 802.11a	1999	OFDM PHY for the 5 GHz ISM band
IEEE 802.11b	1999	High rate DSSS PHY
IEEE 802.11e	2004	QoS enhancements
IEEE 802.11g	2003	OFDM PHY for the 2.4 GHz ISM band
IEEE 802.11n	2009	Higher throughput (MIMO-OFDM)
IEEE 802.11p	2010	Vehicular communication
IEEE 802.11s	2011[1]	Mesh networking
IEEE 802.11ac	2012[1]	Very high throughput < 6 GHz
IEEE 802.11ad	2012[1]	Very high throughput 60 GHz

[1] Expected ratification.

Table 2.3.: Ratified and upcoming amendments to IEEE 802.11 (Selection).

2.3.1. Physical Layer

The original IEEE 802.11 standard defines three PHYs based on frequency-hopping spread spectrum (FHSS), infrared (IR) and direct-sequence spread spectrum (DSSS). Later amendments have introduced new technologies like OFDM (IEEE 802.11a/g), MIMO multiplexing (IEEE 802.11n) and MIMO beamforming (IEEE 802.11ad), for example. In addition, both the available carrier frequencies as well as the signal bandwidth have been adjusted in several amendments. In the following, we will cover the OFDM PHY only, which is probably the most prominent technology to date. OFDM has been introduced in IEEE 802.11a and IEEE 802.11g. Both amendments are very similar in terms of technology with only minor differences in some parameters. The former specifies the operation in the unused 5 GHz frequencies, whereas the latter addresses the 2.4 GHz spectrum and thus, it has to consider backward compatibility and coexistence with legacy IEEE 802.11 devices.

PHY Parameter	IEEE 802.11a (g)
Symbol time	4 µs incl. 0.8 µs cyclic prefix
Subcarrier spacing	312.5 kHz
Channel bandwidth	20 MHz
No. subcarriers	48 data + 4 pilot
Frequency band	5 GHz (2.4 GHz)
Transmit power	30 dBm (20 dBm)
Preamble duration	16 µs
PLCP header	4 µs
CCA time	4 µs @ 90% (15 µs @ 99%)

Table 2.4.: PHY parameters.

One way to increase the throughput capacity of a wireless system is the extension of the signal bandwidth. However, if the signal bandwidth exceeds the coherence bandwidth, the system will experience frequency selective fading. In other words, the larger signal bandwidth reduces the symbol time, which may result in inter-symbol interference if it falls below the multipath delay spread. The rationale of OFDM is to occupy higher signal bandwidths without having to reduce the symbol time, which is achieved by using multiple orthogonal *subcarriers* in parallel. In contrast to traditional frequency-division multiplexing (FDM), the OFDM subcarriers are spaced more efficiently in the frequency domain without any guard bands. Their orthogonality is preserved by spacing the subcarriers in a way that the spectral peak of a carrier coincides with the spectral zero-crossing of adjacent carriers. However, multipath delay spread may compromise the orthogonality of the subcarriers due to leakage of frequency components into successive symbols, which results in inter-carrier interference. Hence, an OFDM system has to account for multipath delay spread by extending the symbol time by a guard interval that is also called *cyclic prefix*. As long as the (significant) multipath components arrive within the duration of the cyclic prefix, the orthogonality is preserved. The parameters of IEEE 802.11a are summarized in Table 2.4. The transmit power may vary depending on the RF channel and the regulatory domain.

According to IEEE 802.11a/g, an OFDM frame starts with a preamble and the physical layer convergence protocol (PLCP) header. The preamble consists of 12 short sym-

PHY Bit-Rate	Modulation	Coding	Bit/Symbol	Min. Sensitivity
6 Mbps	BPSK	1/2	24	−82 dBm
9 Mbps	BPSK	3/4	36	−81 dBm
12 Mbps	QPSK	1/2	48	−79 dBm
18 Mbps	QPSK	3/4	72	−77 dBm
24 Mbps	16-QAM	1/2	96	−74 dBm
36 Mbps	16-QAM	3/4	144	−70 dBm
48 Mbps	64-QAM	2/3	192	−66 dBm
54 Mbps	64-QAM	3/4	216	−65 dBm

Table 2.5.: IEEE 802.11a bit-rates and sensitivity requirements.

bols with a total duration of 16 µs. Among others, the preamble is important for the signal detection and the timing acquisition at the receiver. The PLCP header in the next symbol contains information about the bit-rate and the length of the MAC frame that follows. The MCS of the PLCP header is binary phase shift keying (BPSK) 1/2. IEEE 802.11a specifies 8 MCSs for the following MAC frame, which are listed in Table 2.5. In particular, a convolutional code with a constraint length 7 is used for forward error correction (FEC). The overhead of both the preamble and the PLCP header is fixed and independent from the actual bit-rate of the MAC frame.

According to IEEE 802.11a, the clear channel assessment (CCA) should indicate that the medium is busy if the signal power is above −82 dBm and the preamble has been observed. More precisely, the CCA should respond correctly in 90% of all cases within a detection time of 4 µs. If the preamble has been missed, the medium should be considered busy if the signal power exceeds −62 dBm. The CCA procedure of IEEE 802.11g is very similar. The main difference is that both energy and preamble detection become mandatory. Furthermore, the energy detection threshold is lowered to −76 dBm.

Performance

Noise imposes a fundamental limit on capacity and throughput of communication systems. The causes of noise are manifold. One of them is the thermal noise that is present in electrical equipment. Let k_B and T be the Boltzmann constant and the absolute temperature, respectively. The thermal noise P_{th} over the bandwidth Δf can be estimated via $P_{th} = k_B T \Delta f$. For example, the thermal noise in the 20 MHz channel of IEEE 802.11a/g at room temperature is approximately $P_{th} = -101$ dBm.

The well-known additive white Gaussian noise (AWGN) channel model addresses the communication under noise. Let $x[i] \in \mathbb{C}$ be the channel input at time i. The channel output $y[i] \in \mathbb{C}$ is the sum of both input and noise $n[i] \in \mathbb{C}$.

$$y[i] = x[i] + n[i]$$

In particular, the noise $n \sim \mathcal{CN}(0, \sqrt{N_0})$ is an i.i.d. zero-mean complex Gaussian distributed random variable with variance N_0, which is the noise power spectral density.

The signal to noise ratio (SNR) γ of the received signal y is defined as follows.

$$\gamma = \frac{P}{BN_0} = \frac{R_\mathrm{b}}{B}\frac{E_\mathrm{b}}{N_0} \tag{2.8}$$

In (2.8), P denotes the power of the input signal x, B refers to the signal bandwidth, E_b is the energy per bit and R_b is the data rate of the signal. The product $N = BN_0$ is known as noise floor. The thermal noise is included in the noise floor. However, the radio hardware generally introduces additional noise, which is covered in the noise figure. The 802.11g standard assumes a noise figure of 10 dB. For Atheros hardware, noise figures between $4.5 - 8$ dB have been reported [182, 293, 294]. Under some assumptions, the sum power of interfering signals P_I can be added to the noise, which leads to the following signal to interference and noise ratio (SINR).

$$\gamma = \frac{P}{N + P_\mathrm{I}} \tag{2.9}$$

The Shannon-Hartley theorem gives an upper bound on the capacity of the AWGN. According to the theorem, the capacity C is determined by the bandwidth B and the SNR γ in the following way.

$$C = B\log_2(1+\gamma)$$

Thus, the channel capacity increases continuously in the SNR. On the other hand, communication systems generally provide only a limited set of MCSs. Lacage *et al.* have proposed a performance model for IEEE 802.11a that can be used in packet level simulations [152, 212]. It consists of three steps. At first, the bit error rate (BER) $\mathrm{P_b}$ for the uncoded transmission over the AWGN channel is derived. The resulting expressions for BPSK and quadrature amplitude modulation (QAM) are shown in (2.10) and (2.11), respectively. The parameter M determines the order of the QAM modulation. The quadrature phase-shift keying (QPSK) modulation is interpreted as 4-QAM.

$$\mathrm{P_b} = \mathrm{Q}\left(\sqrt{\frac{2E_\mathrm{b}}{N_0}}\right) = \frac{1}{2}\mathrm{erfc}\left(\frac{E_\mathrm{b}}{N_0}\right) \tag{2.10}$$

$$\mathrm{P_b} = 1 - \left[1 - \left(1 - \frac{1}{\sqrt{M}}\right)\mathrm{erfc}\left(\sqrt{\frac{1.5\log_2 M}{M-1}\frac{E_\mathrm{b}}{N_0}}\right)\right]^2 \tag{2.11}$$

In the next step, the BER $\mathrm{P_{bc}}$ for the coded transmission is derived. For convolutional coding and Viterbi hard decision decoding, equation (2.12) gives an upper bound.

$$\mathrm{P_{bc}} \leq \sum_{d=d_f}^{\infty} a_d \begin{cases} \displaystyle\sum_{i=(d+1)/2}^{d} \binom{d}{i} {\mathrm{P_b}}^i (1-\mathrm{P_b})^{d-i} & d \text{ odd} \\ \displaystyle\frac{1}{2}\binom{d}{d/2} \sum_{i=d/2+1}^{d} \binom{d}{i} {\mathrm{P_b}}^i (1-\mathrm{P_b})^{d-i} & \text{otherwise} \end{cases} \tag{2.12}$$

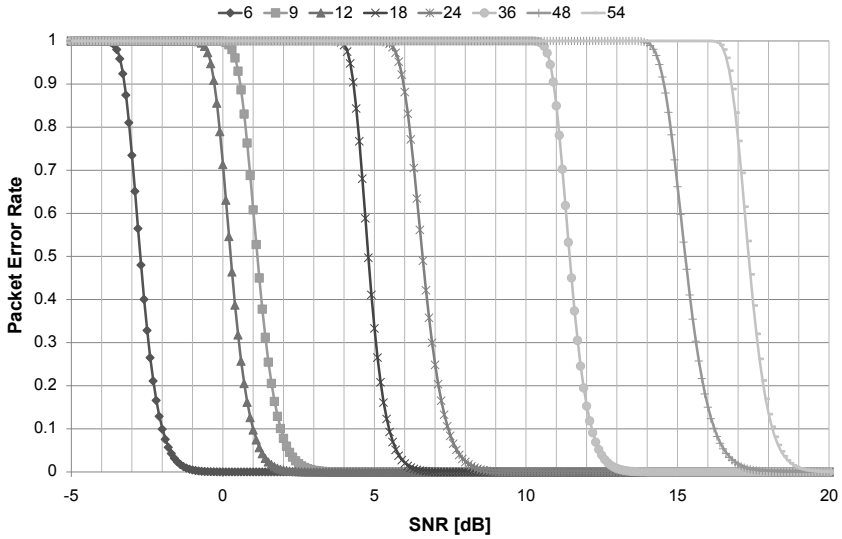

Figure 2.2.: Packet error rate for a frame of 1530 bytes according to Equation 2.13 for the IEEE 802.11a bit-rates (in Mbps) using the parameters given in section A.1.

In the following, we consider only the term d_f with BPSK and two terms d_f and $d_f + 1$ with QAM. The associated parameters a_d are listed in section A.1. The final step is the estimation of the packet error rate (PER) $\mathrm{P_{per}}$ in (2.13), which is straightforward since the bit error process is i.i.d. in the AWGN channel.

$$\mathrm{P_{per}} = 1 - (1 - \mathrm{P_{bc}})^n \tag{2.13}$$

In the equation above, n refers to the number of bits. The packet success rate (PSR) $\mathrm{P_{psr}}$ is the complement of the PER, i.e. $\mathrm{P_{psr}} = 1 - \mathrm{P_{per}}$. Figure 2.2 shows the resulting SNR-PER curves for all IEEE 802.11a bit-rates.

The imperfectness of actual receiver hardware causes a so-called implementation loss, so that the theoretical derived performance becomes a lower bound in terms of SNR. The IEEE 802.11 standard assumes a noise figure of 10 dB and an implementation loss of 5 dB, which are both considered in the sensitivity values shown in Table 2.5. For Atheros hardware, a PER performance of 10% is achieved at the SNR thresholds $\{5.4, 5.8, 7.0, 9.5, 11.3, 14.9, 18.6, 20.6\}$ dB for the IEEE 802.11a bit-rates in increasing order [261].

In slow and flat fading channels, the fading realization $h[j] \in \mathbb{C}$ has to be taken into account in addition to the additive noise term. The fading realization h is a random variable. In the case of Rayleigh fading, for example, $h \sim \mathcal{CN}$ has a circular-symmetric complex Gaussian distribution.

$$y[i] = h[j] \cdot x[i] + n[i]$$

In slow fading channel, the fading realization $h[j]$ changes slower compared to the symbol time. The block fading model is reasonable if the coherence time of the channel is sufficiently large. In this case, the same fading realization $h[j]$ applies to a block of

symbols as large as a frame or a TXOP. Assuming that the receiver is able to compensate the potential phase shift using receiver channel state information (CSI), the AWGN reception model can be applied if the fading magnitude $|h|$ is considered in the SNR estimation.

Link Adaptation

The IEEE 802.11 standard does not specify an adaptive modulation and coding (AMC) protocol, i.e. it is left to the manufacturers to decide how the MCSs should be adapted. At a coarse level, the existing AMC can be distinguished into loss and SNR triggered approaches.

The *loss triggered* AMC relies on active or passive link probing in order to estimate the PER. For example, auto rate fallback (ARF), adaptive auto rate fallback (AARF) and SampleRate vary the bit-rate of the actual data transmission [21, 128, 153], whereas the routing metric ETT employs active link probing [62]. Nevertheless, combinations of active and passive link probing are possible [135]. The time scale of the AMC operation may vary. Protocols like AARF try to adapt the bit-rate on a per-packet basis, whereas SampleRate and ETT average over several packets. However, the loss triggered approach will probably become unsuited for further evolutionary stages of IEEE 802.11. For example, 76 different MCSs are available in IEEE 802.11n [105]. Such a large amount of bit-rates cannot be probed individually without sacrificing medium resources or timeliness and accuracy. Thus, it becomes necessary to look for indicators the AMC can be based on.

The *SNR triggered* AMC relies on the indicator received signal strength (RSS). Husted *et al.* explain how the received signal strength indication (RSSI) is estimated on Atheros hardware [99]. However, RSSI is different from SINR in two ways. The power of interfering signals P_{I} cannot be distinguished from the intended signal, so that the term P_{I} occurs in the numerator instead of the denominator of (2.9). Furthermore, an accurate estimation of the instantaneous noise floor is technically challenging and may cause unexpected results. For example, the OFDM performance severely degrades due to the Atheros ambient noise immunity [19, 238, 253, 262].

Two well-known AMC proposals that rely on RSS indicators are receiver-based auto-rate (RBAR) by Holland *et al.* and opportunistic auto-rate (OAR) by Sadeghi *et al.* [95, 235]. However, measurement results suggest that the correlation between PER and RSSI is low [4, 279]. In recent years, the observations have been further analyzed in order to identify the causes. It turns out that one important cause is interference. As mentioned above, any interference power renders the estimation of both signal and noise power difficult. In isolation, the PER-RSSI of an IEEE 802.11 link is close to theory, whereas interference significantly distorts the relationship [47, 83, 144, 145, 298]. Furthermore, the RSSI is generally not calibrated and its relationship to the PER additionally depends on characteristics of the fading process. Thus, it may become necessary to dynamically learn the PER-RSSI curve [36, 298].

Recently, Halperin *et al.* have reported that frequency selectivity is another cause for the low correlation between PER and RSSI [93]. In particular, they show that a highly accurate channel prediction is possible when considering the complete CSI of the wideband OFDM channel. The RSSI is an aggregated value across all subcarriers,

whereas the performance of IEEE 802.11 is limited by a small number of subcarriers that experience the highest channel attenuation. Note that a coherence bandwidth of 20 MHz would require multipath delay spreads below 50 ns, which corresponds to a path length difference of 15 m only. By taking the frequency selectivity into account, the SNR is able to predict both BER and PER within $1 - 2$ dB, which is close to the theoretical bound. In the same line, Rahul *et al.* propose a bit-rate selection protocol for IEEE 802.11-like systems with sub-channel AMC [222]. They have empirically validated that the SNR per (frequency-flat) sub-channel is able to accurately predict the performance of the sub-channel if it is continuously estimated using pilot tones.

Other indicators are also available. For example, Vutukuru *et al.* have recently proposed the *SoftRate* protocol. Under SoftRate, the AMC relies on soft information from the PHY, i.e. the confidence values associated with a decoding decision are used within the bit-rate selection process [270]. Compared to RSSI based approaches that estimate the channel quality only from a short preamble, the BER estimate can take the whole packet transmission into account in order to assess the interference conditions and temporal coherence of the channel.

2.3.2. Medium Access Control

The wireless medium is a shared resource in a WMN. The medium access control (MAC) is responsible for the allocation of wireless resources to nodes that have data to transmit. MAC protocols can be coarsely classified into two categories. The *circuit-switched* protocols like time-division multiple access (TDMA), code-division multiple access (CDMA) and frequency-division multiple access (FDMA) allocate a fixed amount of resources over a longer period of time in an exclusive manner. This type of MAC is well suited for applications with fixed or predictable throughput requirements like voice. On the other hand, data traffic is often bursty and thus not predictable. The efficiency of circuit-switching for data traffic is generally low since the only way to account for the unknown demands is over-provisioning. The second category of MAC protocols relies on *packet switching*. Since the available resources are allocated on demand, packet switching handles data traffic more efficiently. Multiple users and connections can share a resource while the packet oriented MAC allows for high resource utilization due to the statistical multiplexing gain.

MAC protocols based on packet switching can further be classified into *centralized* and *distributed*. The former rely on a single controller that performs the resource allocation. This category includes all WMN scheduling protocols that are based on dynamic TDMA. In contrast, a distributed MAC does not possess a central controller. Instead, the distributed MAC instances have to allocate resources in a cooperative manner. Examples are ALOHA, CSMA and binary countdown protocols. A border case is a MAC that operates in a distributed way, but depends on centralized resources like time synchronization.

In addition, the MAC provides an addressing mechanism. Similar to Ethernet, the realization in IEEE 802.11 is straightforward. A predetermined and globally unique MAC address is assigned to every network interface controller (NIC). The IEEE 802.11 standard specifies transmission primitives for the MAC addressing schemes unicast, broadcast and multicast.

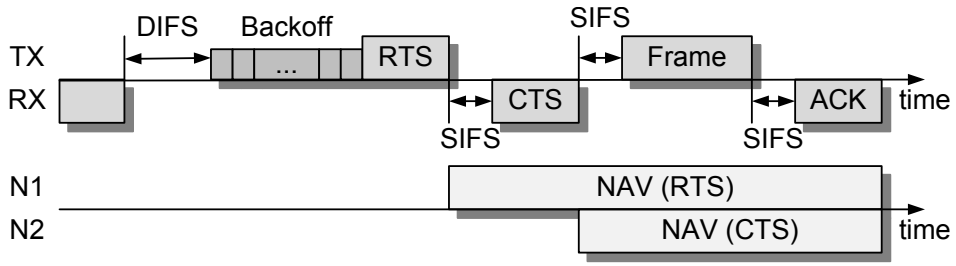

Figure 2.3.: DCF unicast transmission between transmitter *TX* and receiver *RX* including the NAV at neighbors *N1* and *N2* (cf. [76]).

The standard IEEE 802.11-2007 defines the following 3 coordination functions.

Distributed Coordination Function. Contention-based access using CSMA and collision avoidance (CA).

Point Coordination Function. A centralized MAC, in which a point coordinator provides contention-free access.

Hybrid Coordination Function. Adaption of both the distributed coordination function (DCF) and the point coordination function (PCF) for quality of service (QoS) and prioritized channel access. Available as contention-based and contention-free version called enhanced distributed channel access (EDCA) and HCF controlled channel access (HCCA), respectively.

In the following, we will cover DCF only. IEEE 802.11 addresses several further issues like association, authentication and other management functions, encryption, energy saving, etc. The interested reader may refer to the book [76] for a comprehensive description.

Distributed Coordination Function

The IEEE 802.11 DCF is a distributed MAC protocol based on CSMA. A node has a single interface queue and arriving packets are processed in first in, first out (FIFO) order. The procedure of a unicast transmission is sketched in Figure 2.3. Each transmitter has to perform carrier sensing before accessing the medium. The DCF uses both physical and virtual carrier sensing simultaneously. For now, we will focus on the former and explain virtual carrier sensing in the following section. If the medium is occupied, the medium access has to be deferred until the medium becomes idle again and remains idle for a time period of a distributed interframe space (DIFS). Afterwards, the transmitter should process a randomized backoff. It draws a uniformly distributed random number from its so-called *contention window* and waits the given number of slots while it continuously senses the medium. If the medium becomes occupied during the backoff, the transmitter should suspend its backoff until the medium becomes idle again. If the backoff expires, the transmitter accesses the medium. The usage of the RTS/CTS is optional according to the DCF. We will consider this issue in the next section. If RTS/CTS in not employed, the transmitter starts with the transmission of

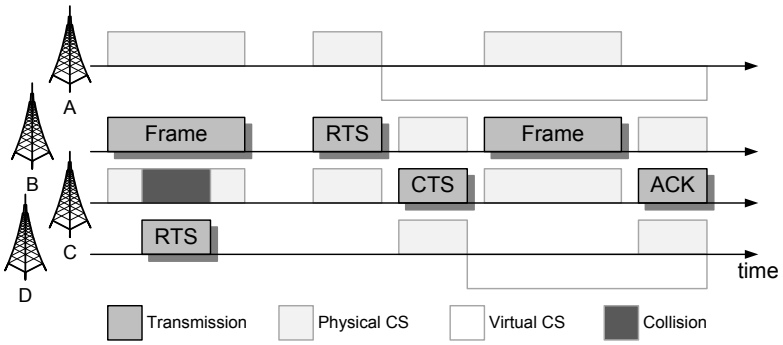

Figure 2.4.: The hidden node problem and the RTS/CTS solution.

the data frame after the backoff has expired. Both the RTS and the CTS frames that are shown in Figure 2.3 are omitted in that case.

For a broadcast or a multicast transmission, the MAC transaction is finished after the data frame has been transmitted. Nevertheless, transmission errors may arise due to channel noise or fading, or multiple nodes may have selected the same backoff slot resulting in a so-called CSMA collision. A stop-and-wait automatic repeat request (ARQ) protocol at the MAC layer protects unicast transmissions. In particular, if the data frame has arrived without errors, the receiver transmits an acknowledgement (ACK) frame after a time period of a short interframe space (SIFS). The absence of the ACK is interpreted as a transmission error. In this case, the transmitter initiates retransmissions for a limited number of times in the above described way. In order to prevent a further CSMA collision, it employs the so-called binary exponential backoff (BEB): It doubles its contention window with each retry. Either one of the retransmissions is successful or the data frame is discarded. The contention window is reset to its initial value for the next frame. The slot time, the SIFS, the DIFS and the contention window limits are design parameters. The values for IEEE 802.11a/g are shown in Table 2.6.

MAC Parameter	**IEEE 802.11a (g)**
Max. frame length	4095 bytes
Slot time	9 µs (20 µs)
SIFS time	16 µs (10 µs)
DIFS time	34 µs (50 µs)
Contention window	$15(31) - 1023$ slots

Table 2.6.: MAC parameters (cf. [76]).

The IEEE 802.11e amendment has introduced the concept of transmission opportunities (TXOPs) within EDCA. The rationale thereof is that a transmitter does not have to contend for the transmission of a frame but for a fixed amount of medium time instead. The contention per frame corresponds to the max-min fairness objective, which has lead to the IEEE 802.11 performance anomaly due to the solidarity property [215]. The contention for TXOPs changes the objective to medium time.

The Hidden Node Problem

The hidden node problem is depicted in Figure 2.4. Due to the overlapping collision domains in WMNs, node *D* is hidden from the transmitter *B* but within the interference range of the receiver *C*. Hence, it may cause a collision at node *C* since it is not aware of any potential transmissions between *B* and *C*. According to Kosek *et al.* [143], the approaches to mitigate the hidden node problem can be classified into out-of-band and directional antenna solutions, virtual CS and hidden node free design.

The *virtual CS* approach relies on additional in-band signaling to agree upon and exchange of the future allocation of the channel. However, the in-band signaling is itself prone to the hidden node problem. However, the rationale is to minimize collisions of data packets, which wastes a larger amount of resources than collided signaling packets. Examples are multiple access with collision avoidance (MACA) [131], MACAW [17], floor acquisition multiple access (FAMA) [73] and the IEEE 802.11 DCF. In particular, the DCF employs an RTS/CTS prologue. As shown in Figure 2.3, the medium access begins with the request to send (RTS) that additionally contains the duration of the upcoming data transmission including the ACK. In return, the receiver sends a clear to send (CTS) that also contains the transmission duration. The embedded duration is extracted by neighboring nodes in order to update the network allocation vector (NAV) accordingly. In this way, the hidden node *D* shown in Figure 2.4 becomes aware of the ongoing transmission from *B* to *D*. Note that it is straightforward to construct scenarios, in which the virtual CS is ineffective to prevent the hidden node problem.

The *out-of-band solutions* can be coarsely classified into busy tone and multi-channel approaches. The former separate the CS from the actual data transmission into dedicated busy tone channel(s). For example, Tobagi and Kleinrock have proposed the busy-tone multiple-access (BTMA) protocol [263]. BTMA divides the bandwidth into a data and a busy tone channel. On sensing a carrier signal on the data channel, a receiver emits a busy tone to indicate its CS state to neighboring nodes. Another example is dual busy tone multiple access (DBTMA) proposed by Haas *et al.* [90]. DBTMA uses a second busy tone emitted by the transmitter to protect the bidirectional operation of the MAC protocol.

The rationale of multi-channel approaches is the separation of the contention from the actual data transmission. The contention takes place in a control channel, which is also used to exchange and distribute the information about the data channel usage similar to virtual CS. Neighboring nodes will listen to the control channel, so that they become aware of the utilization of the data channel(s). Examples are MAC-SCC [203], C^2M [151], DUCHA [297], MCMAC [303] and DSMA [283].

The *hidden node free design (HFD)* takes a different direction [122]. The cause of the hidden node problem is an inherent coordination handicap because a designated transmitter is unable to determine the CS state of its receiver(s). The rationale of the HFD is the adaption of the CS area in a way that it covers all hidden nodes. As discussed above, however, physical and technological constraints impose a lower limit on the CS threshold. Thus, the HFD has to introduce large SNR margins of up to 20 dB. The margins guarantee that the CS state at the transmitter is sufficient to determine the interference situation at all potential receivers. Nevertheless, the large margins waste a huge amount of spatial resources.

2.4. Routing in Wireless Mesh Networks

In packet switched networks, routing addresses the question which path a packet should take in order to reach the destination(s). In the following, we give a brief overview of unicast routing protocols and metrics that have been proposed for WMNs. If not stated otherwise, our primary sources in this section are Zhang *et al.* [301, chap. 4], Misra *et al.* [184, chap. 8] and Akyildiz *et al.* [5, chap. 4, 10]. In a narrow sense, routing only refers to the decision about potential network paths, whereas forwarding denotes the actual process of packet relaying. Nevertheless, we will use the term routing in its broad sense only.

A prerequisite for routing is an addressing scheme. According to the network stack architecture, routing typically resides at the network layer, where the Internet protocol (IP) and IP addressing is predominating. An alternative is routing on the MAC layer using the MAC addressing scheme. The advantage of the latter architecture is that the meshed topology of the WMN is not revealed to network layer protocols. From the point of view of the Internet protocol, the WMN looks like a large layer 2 switch. Thus, modifications are restricted to the NIC driver software, whereas the host operating system remains unaffected.

The routing in small wired networks is often static, i.e. the routing information is manually configured during the network deployment. However, mobile ad-hoc networks (MANETs) and WMNs have to cope with mobility of client and core network nodes, link quality variations and a spontaneous as well as continuous network growth, which renders the static routing approach infeasible. Thus, the routing should be dynamic and self-organizing. Several classification criteria exist for dynamic routing protocols addressing wireless mesh and (mobile) ad-hoc network. One of them is the addressing method. We will consider unicast routing only in the following, i.e. the destination is a single network node. Network traffic directed to multiple nodes (multicast, broadcast) or to a geographic region (geocast) is out of scope. Unicast routing protocols may use the logical topology of the network or the position of the nodes.

Position-Based Routing. As the name suggests, the routing decision is based on the position of network nodes with respect to a coordinate system. A widely used coordinate system is the geographical position of nodes in either two or three space dimensions, which can be obtained via GPS. Examples are greedy perimeter stateless routing (GPSR) by Karp *et al.* [132] and geographic random forwarding (GeRaF) by Zorzi *et al.* [312, 313]. If the geographical positions are not available, the nodes can be organized within a virtual coordinate system. The virtual coordinate assignment protocol by Caruso *et al.* falls within this category [38].

Topology-Based Routing. The problem with position-based routing is that the relationship between position and link quality is generally not determined by distance only (cf. section 2.2). The rationale of topology-based approaches is to make routing decisions based on the actual observed link state.

Routing Overlays. Similar to the overlay routing protocols known from the peer-to-peer networking domain, overlay structures can be placed over (virtual or geographical) positions as well as topologies. For example, the dynamic address

routing (DART) protocol by Eriksson *et al.* is organized as a binary tree [67]. In the same line, Fuhrmann *et al.* have proposed the scalable source routing (SSR) protocol [72], which is based on a virtual ring similar to Chord.

The generation of topology information consists of the discovery of neighboring nodes and the distribution of topology information within the network. The neighbor discovery is generally straightforward. For example, optimized link state routing (OLSR) relies on the MANET neighborhood discovery protocol (NHDP) [55], which specifies how nodes exchange so-called HELLO packets. Similar to intra-domain routing in wired networks, the topology-based approaches can be further categorized according to the dynamic distribution of the topology information.

Distance Vector Routing. Every node maintains a distance vector that contains the shortest path distance to every destination along with the associated next hop. The distance vectors are initially empty. On startup, entries for the local node and its neighbors are added. The distributed Bellman-Ford algorithm is used to generate the final distance vectors as follows. Neighboring nodes regularly exchange their distance vectors and update the entries, for which shorter paths become available. Well-known protocols belonging to this category are destination-sequenced distance-vector routing (DSDV) [202] and ad-hoc on-demand distance vector (AODV) routing [200, 201].

Link State Routing. Instead of storing the distances only, a network node maintains an internal representation of the whole topology or parts thereof. In order to generate the complete topology, the local information of *every* network node about its neighbors has to be distributed to *all other* nodes. The process of distributing the routing information is called flooding. The next-hop forwarders can be estimated from the internal topology representation using a shortest path algorithm like Dijkstra's algorithm. Examples are OLSR [54, 106] and dynamic source routing (DSR) [123, 124].

A further criterion is the generation and maintenance of routing information.

Proactive Routing. With proactive or table-driven routing, the network continuously maintains and updates the routing information using a periodic message exchange. Thus, the routing information of every network node is always up-to-date, which comes at the expense of throughput. Especially in combination with link state routing, the scalability of the network in terms of nodes may be limited. Both DSDV [202] and OLSR [106] are proactive protocols.

Reactive Routing. The rationale of reactive routing is to postpone the generation of routes until traffic for the associated destination has actually arrived. In this case, the source node triggers a route discovery operation, which generally consists of a network-wide broadcast in order to find a route to the destination. Thus, reactive routing is also called on-demand routing, since it does not allocate resources to the maintenance of unused routes. Nevertheless, the first packet(s) of a traffic flow will experience larger delays. Examples are DSR [124] and AODV [200].

The number of proposed MANET and WMN routing protocols is large. Different application domains and requirements have lead to a vast variety of protocols that differ in their objectives and constraints [91, 271, 301]. Aspects that have been discussed are multi-path, multi-channel and multi-radio routing, link quality estimation, traffic load awareness, usage of multiple bit-rates, mobility, security and advanced PHY techniques like directional antennas and opportunistic routing. In many cases, the objective has been the network performance in terms of throughput and fairness. Further well-known objectives are latency, jitter and other QoS parameters, energy consumption, reliability, robustness and fault tolerance.

2.4.1. Routing Metrics

In essence, the routing metric is a cost function that allows us to assess and compare links and paths of the network in terms of the routing objective. Under some assumptions, the routing metric defines a weighted topology graph and shortest-path algorithms can be used to find the minimum cost routes. A recent survey about routing metrics can be found in the article [29]. Routing metrics generally operate at a coarse time scale from seconds to minutes due to the network-wide scale of the problem. In particular, low-latency metrics that trigger frequent changes may cause routing instability. Furthermore, the routing metric should support loop-free forwarding.

The hop count metric has been one of the first routing metrics used in WMNs. The design is straightforward. Every link is assumed to consume one cost unit per packet transmission. However, the design neglects the time-variable nature of the wireless channel as well as the advanced PHY capabilities of state-of-the-art radio hardware. It is based on the engineering principle of layering. The lower layers should hide the characteristics of the channel from the network layer in order to provide the bit-pipe abstraction that is used in wired networks. In many cases, the abstraction cannot be provided due to hardware and regulatory constraints, which has lead to a turning away from hop count towards routing metrics based on PHY and MAC layer measures.

Two widely used metrics for high throughput routing are ETX and ETT. Based on measurement results, DeCouto *et al.* have proposed the expected transmission count (ETX) routing metric [58]. The rationale is to use active probing in order to estimate the quality of a link in terms of the average number of transmissions that are necessary to successfully deliver a packet. Every node regularly broadcasts so-called link probe packets. On receiving them, the neighbor nodes estimate the directional packet delivery ratio (PDR). The ETX of a link is the product of the inversed PDRs of both directions. The ETX of a path is the sum of the individual ETX values of the considered links.

The main benefit of ETX is probably the consideration of the actual observable packet loss performance. ETX accounts for asymmetric links and it is independent from the instantaneous traffic load. However, the latter argument should be taken with caution since hidden node problems become more pronounced under high traffic loads. ETX assumes that all transmissions occur within the same collision domain, so that it cannot account for spatial diversity. The method of active link probing has several drawbacks. The ETX values should be accurate and up-to-date, whereas the probing overhead should be low. Thus, the parameterization of the probing interval and the

averaging horizon is difficult especially under varying node densities. In addition, the objective of broadcast probing is the estimation of a priori PDRs. In reciprocal channels with memory, however, the conditional PDR of an ACK is generally higher if it is sent shortly after a data frame has been successfully received. Furthermore, the probing packets have to compete with data traffic in terms of MAC service. If a transmitter processes excessive backoffs due to repeated packet loss during a channel outage, the probing traffic has to wait until the currently considered data packet is eventually discarded or an ACK is received due to better channel conditions. In either case, the observed PDR of link probe packets is increased.

The expected transmission time (ETT) is an extension of ETX for networks with support for multiple bit-rates [62]. It considers both the PDR of the underlying link as well as the size and the bit-rate of packets to transmit. Thus, the ETT value per link corresponds to the expected amount of medium time it takes to transmit one packet. A commonly used variant of ETT additionally includes the expected backoff similar to SampleRate [21]. Due to the BEB of IEEE 802.11, the relationship between ETX and backoff time becomes non-linear. High ETX values will result in considerable backoff durations. The link probing overhead of ETT is generally larger compared to ETX. In order to generate PDR statistics, link probe packets have to be transmitted at every bit-rate. In addition to hop count, ETX and ETT, many other routing metrics have been proposed that differ in the objectives and constraints mentioned in the previous section.

2.4.2. IEEE 802.11s

The upcoming amendment IEEE 802.11s addresses meshed WLANs. According to the standard, the client STAs remain unaware of the WMN. The mesh access point looks like an ordinary AP to the client, whereas it is part of the WMN backhaul that is used to relay traffic. Furthermore, mesh points are relays without AP capabilities and the so-called mesh portals act as gateways to other networks. Due to the scope of IEEE 802.11, the routing operates at layer 2. The amendment addresses various aspects like security, RF channel selection, beaconing, neighbor and topology discovery, multi-channel operation, congestion control and bridging with other IEEE 802 networks. In the following, we will consider the routing protocol and the routing metric only.

Extensibility in terms of routing is one design objective of IEEE 802.11s. In order to ensure a basic operation, the support of the airtime routing metric and the hybrid wireless mesh protocol (HWMP) is mandatory. In essence, the definition of the airtime metric is similar to ETT. The HWMP is derived from AODV, but combines reactive and proactive elements. A reactive route discovery is used to find routes between network nodes. Nevertheless, the mesh portal can regularly flood the network with announcements in a proactive manner. In this way, a tree topology with the mesh portal at its root is constructed and maintained. Furthermore, IEEE 802.11s specifies a radio-aware variant of OLSR, which can optionally be implemented and used as an alternative to HWMP.

2.5. Simulation of Wireless Mesh Networks

According to our methodology presented in section 1.3, we intend to evaluate a prototype of the proposed protocol through network simulation. For that purpose, we have chosen the JiST/SWANS simulator [15, 16]. The Java in Simulation Time (JiST) system is a kernel and a library for discrete event simulations. It introduces simulation semantics and the concept of simulation time into the Java virtual machine. The Scalable Wireless Ad hoc Network Simulator (SWANS) is a simulator for wireless networks that has been built on JiST. The component based architecture of SWANS is shown in Figure 2.5.

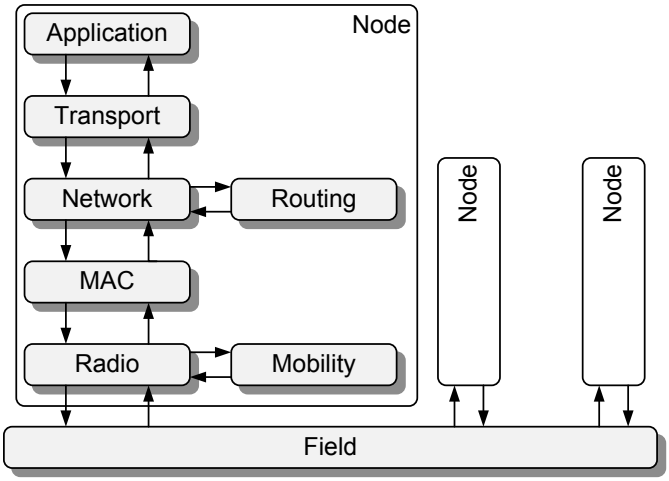

Figure 2.5.: Component architecture of SWANS (cf. [15]).

SWANS includes the path loss models free space and two ray ground as well as uncorrelated Rayleigh and Rician fading. We have added models for the log-distance path loss, log-normal shadowing and temporal correlated Rician fading according to Punnoose *et al.* [210]. The Rician fading is realized as a block fading process, i.e. a single fading value is generated per packet. The PHY and MAC models of SWANS correspond to IEEE 802.11b and the DSSS PHY. The SNR threshold-based radio supports cumulative interference, but it cannot use multiple bit-rates at the same time. We have added a BER-based PHY and MAC model for IEEE 802.11a/g according to the proposal of Lacage *et al.* [152]. The underlying relationship between SNR and BER has been explained in section 2.3.1.

At the network layer, SWANS provides the Internet protocol (IP) in version 4 [205] and the routing protocols DSR [123, 124], AODV [200, 201] and the zone routing protocol (ZRP) [89]. We have extended SWANS in order to support the routing metrics ETX [58] and ETT [62] and a reactive link state routing similar to OLSR [54, 106]. Both the transmission control protocol (TCP) [7, 206] and the user datagram protocol (UDP) [204] are available at the transport layer of SWANS. Since JiST/SWANS redirects the network API calls, generally all networking applications written in Java can be executed during the simulations. Throughout this thesis, we will consider the unicast transfer of bulk data similar to the FTP application.

3. Opportunistic Routing under Utility-Optimal CSMA

Transmission errors are common in wireless networks. Empirical results suggest that the majority of links in a WMN are of intermediate quality in terms of packet loss [4]. Diversity is a well-known concept to mitigate the inherent impairments of the wireless channel. An instance thereof is multi-user diversity (MUD) [141]. The rationale is to use the channel while its quality is good or, in other words, select the user with the instantaneous best channel. In this way, the users of a wireless system become an additional network resource similar to, for example, time or frequency. In contrast to the classical instances of diversity, MUD does not intend to average the channel quality. Instead, it is able to increase the observed capacity significantly in comparison to the equivalent non-fading channels [264].

Opportunistic routing (OR) is a technique to benefit from MUD in WMNs. OR mitigates transmission errors using multiple candidate receivers. Due to the broadcast nature of the wireless medium, the transmitter does not have to specify the relay on the next hop a priori. Instead, the routing decision is made a posteriori based on the information which candidate actually received the frame. For this purpose, the extremely opportunistic routing (ExOR) protocol introduces the slotted acknowledgement at the MAC layer [22]. If the packet loss is uncorrelated on different links, then OR can increase the throughput capacity since the probability that at least one candidate has received the packet is non-decreasing in the number of candidates. On the other hand, OR incurs additional costs at the MAC layer that will eventually outweigh the MUD benefits with increasing number of candidates. For example, the slotted acknowledgement introduces additional control traffic. Furthermore, there is the risk of duplicate transmissions due to coordination errors in the forwarder selection process.

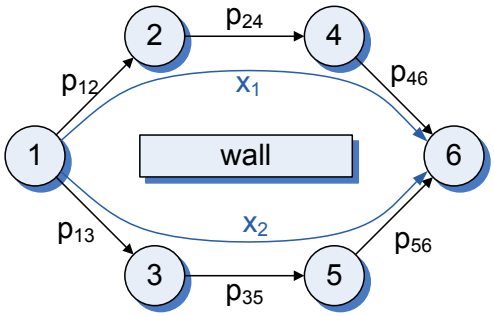

Figure 3.1.: A network with 6 nodes and a traffic flow from 1 to 6.

However, the costs of OR at higher layers are less well understood. Let us consider the network in Figure 3.1. The traffic from node 1 to node 6 flows along two disjoint paths. Let us assume that the links are subject to packet loss and p denotes the packet error rate (PER). The PER determines the relationship between *throughput* and *good-*

put: The former refers to the consumed medium time whereas the latter denotes the amount of information that is transmitted without errors. Due to the flow conservation constraint, all links on the upper (lower) route have to support the goodput x_1 (x_2). For a transmission to be successful, it is necessary that the receiver is free from interference. For ease of exposition, let us apply the two-hop interference model [125]: If node 1 transmits to node 2, for example, then none of their neighbors are allowed to take part in a transmission. Hence, node 3 and 4 must remain silent whereas the link $(5, 6)$ may operate concurrently. For every unicast link, there is exactly one unicast link that can operate concurrently in the considered topology. On the other hand, node 1 may decide to use the candidate nodes 2 and 3 simultaneously using an anycast transmission along a so-called hyperlink $(1, \{2, 3\})$. In this case, however, no other link is permitted to transmit concurrently. In other words, OR causes costs in terms of spatial reuse. The question that arises is whether the OR benefits in terms of PER at the first hop outweigh the costs with respect to lower spatial reuse at the last hop.

In this chapter, we address the question of how OR should be used in WMNs based on CSMA in order to efficiently utilize multi-user and spatial diversity. Our objective is to design a cross-layer protocol and to evaluate its properties using a prototype for a network level simulator. Our primary performance metric is utility, i.e. throughput subject to fairness constraints. We are targeting at applications that support elastic traffic and do not impose (tight) end-to-end delay or jitter constraints like FTP. As a first step in understanding OR, our target environment is a WMN with stationary, memoryless and unreliable links. The frame error process is assumed to be i.i.d. in time. This assumption covers several well-known channel models like the AWGN channel, the frequency-selective wideband fading channel, which arises from delayed multipath components at the receiver, and the fast fading channel, where the fading process evolves faster than the symbol duration [228]. Note that the slow fading channel and the Gilbert-Elliot model are not covered [84, 228]. In particular, the temporal uncorrelated channel is the best case for OR, since the transmitter cannot use any past information to deduce the instantaneous channel conditions. The more reliable the channel can be predicted beforehand, the lower the benefits of OR become in relation to OS [264].

Our contributions are as follows. We present a Markov model for CSMA/CA, in which CS is processed *per node* (cf. section 3.2). In contrast to state-of-the-art approaches that assume a link-based CS [111], our model captures the capabilities of available CS hardware more closely [145] and allows for a better spatial reuse. In addition, we show that CSMA with node-based CS can be operated in a simple and distributed way if the receiver blocking problem is handled properly.

According to the presented model, we design a CSMA/CA protocol for WMNs based on the idea of dual busy tone multiple access [90] (cf. section 3.3). The throughput-optimality of CSMA relies on the requirement that every transmitter can increase its service rate at any time through a more aggressive contention. We show how this requirement can be ensured within an IEEE 802.11-like protocol for WMNs without excessively sacrificing spatial resources.

We present a cross-layer algorithm for congestion control, opportunistic routing and CSMA for WMNs (cf. section 3.4). The algorithm is completely distributed and relies on local and neighboring information only. It furthermore handles transmission errors and selects bit-rates.

Based on the algorithm, we propose a cross-layer protocol that can readily be implemented in a wireless network simulator (cf. section 3.5). The protocol design addresses the following three aspects. We define a working point for CSMA in terms of contention aggressiveness that ensures a high efficiency while avoiding the breakdown of CSMA due to collisions. The working point is approached via an intra-flow feedback loop, whereas an inter-flow feedback loop considers the fairness among competing flows. Furthermore, we present an approach to control the throughput-delay tradeoff in utility-optimal CSMA (UO-CSMA) via upper queue limits and virtual transmissions. In this way, we are able to reduce the convergence time and control the end-to-end delay at a level of practical relevance, although the costs in terms of throughput are lower compared to state-of-the-art delay reduction approaches [111]. In addition, we design a path pre-selection according to a WMN routing metric. For CSMA, every additional relay incurs costs in terms of throughput. Using the pre-selection, it is possible to pre-exclude relays that are supposed to have only a marginal contribution to the overall performance.

We evaluate the proposed protocol through analysis and simulation (cf. section 3.6 and section 3.7). According to our analytic results, randomized WMN topologies offer a high potential for both multi-user and spatial diversity. Since neither of them dominates, both forms of diversity should be exploited in a systematic and dynamical way. We illustrate how the proposed protocol handles the tradeoff between spatial reuse and multi-user gain. In particular, it is crucial that a transmitter does not decide for a single anycast link in advance. Instead, both anycast and unicast links should contend for medium access and the topology "decides" on the links to activate according to the CS relationship. Based on our simulation results, we conclude that the prototype is able to increase both throughput and fairness in relation to state-of-the-art single-path and OR protocols. On the other hand, multi-path and opportunistic routing increases the optimality gap with respect to the analytic potentials. The gain of spatial and multi-user diversity increases with additional relays. Nevertheless, the returns of diversity are diminishing whereas the optimality gap increases linearly in the number of relays.

3.1. Background and Related Work

This chapter builds upon a broad foundation of related work that includes both OR and CSMA, of course. Furthermore, network utility maximization (NUM) allows us to understand the cross-layer interaction between both concepts and provides us hints how to design a practical cross-layer protocol. In the following, we will briefly introduce NUM, CSMA and OR.

3.1.1. Network Utility Maximization and Maximum-Weight Scheduling

The characteristic property of WMNs is the coupling of link capacities at the lower layers of the network stack. In order to achieve objectives like throughput maximization, it is necessary to understand and control the cooperation between different layers. Network utility maximization (NUM) provides us the necessary tools to understand and design the cross-layer interaction of layered protocol stacks. The concept of NUM is

derived from a new perspective on the network that goes back to Kelly *et al.*: They think of the network itself and its operation as an optimizer for a particular optimization problem [134]. Following the theory of optimization decomposition, NUM gives us a formal justification for the layering of protocol stacks. In particular, the concept of layering as optimization decomposition (LAD) interprets the modularization process of network architectures as the decomposition of the optimization problem into smaller subproblems. The inter-connection between them determines the cross-layer interaction. In this way, the layers of the network stack are integrated into a single and coherent theory. They carry out local decisions in order to cooperatively solve a global optimization problem. The framework of NUM can be used in two different ways. On the one hand, we may ask which optimization problem an existing system solves. Through reverse-engineering, this question has been answered for several protocols like TCP [52]. On the other hand, we can specify the objectives and constraints of a system and use LAD to derive a network architecture. Note that the same NUM problem can lead to several alternative designs depending on how the problem is decomposed. Further information on NUM and LAD can be found in the articles [52, 78, 244, 285]. The concept of NUM is possibly best described by Yi *et al.* [285] as follows.

> The theory of decomposition of NUM thus becomes a foundation to understand, in a conceptually simple way, the complexities of network architectures: "who does what" and "how to connect them".

In this chapter, we are particularly interested in cross-layer designs for WMNs that maximize both throughput and fairness of elastic traffic flows. In this case, the optimization objective is accumulated utility subject to congestion control, flow conservation and scheduling (and possibly further) constraints [48, 68, 170]. The utility function handles the tradeoff between throughput and fairness that arises with competing flows. A logarithmic utility function results in proportional fairness (PF), which is regarded as a suitable form of fairness for WMNs [215, 216]. The optimization problem naturally decomposes vertically. Congestion control is situated at the transport layer and controls the packet ingress according to the queue length at the source. The differential queue back-pressure between neighboring nodes determines the routing decision as well as the MAC layer scheduling. The maximum-weight scheduling algorithm is throughput-optimal across many environments and conditions [258]. A schedule is a set of links that can be activated simultaneously within the same timeslot. Each link is weighted by the differential queue back-pressure. The max-weight scheduler is a collision-free dynamic TDMA scheduler that selects (one of) the schedule(s) with the highest accumulated weight in each time slot. However, maximum-weight scheduling (MWS) is a NP-hard problem [125, 285]. Thus, the scheduling becomes the bottleneck for a distributed realization of a cross-layer protocol.

Considering the complexity of MWS, the research took two different directions from here on [285]. On the one hand, the max-weight scheduler is approximated using heuristics with reduced complexity. However, even the approximation problem is complex, so that these approaches achieve a fraction of the MWS performance only [285]. In addition, they generally rely on message passing and require synchronization to ensure collision-free schedules.

On the other hand, a direction in research has started from existing random access protocols and considers the question whether and to which extent these protocols achieve optimality. For ALOHA networks, the scheduling problem consists of the adaptation of the access probabilities. Slotted ALOHA has been reverse-engineered using the LAD approach [52]. The problem has a desirable structure that allows for a distributed and greedy solution. The ALOHA capacity region is convex in the logarithmic domain of access probabilities, which is an important prerequisite for the NUM approach. Based on this result, several cross-layer protocols for single-hop and multi-hop communication have been proposed [88, 162, 172]. However, ALOHA scheduling is generally sub-optimal, i.e. it is not possible to achieve the MWS capacity region [285]. We do not go into details with this type of scheduling, since we focus on CSMA throughout this thesis. Nonetheless, further information can be found in [285].

3.1.2. Utility-Optimal CSMA

Recently, it has been shown that the so-called *utility-optimal CSMA (UO-CSMA)* [1] is able to approximate the MWS arbitrarily close even without message passing. The research directions on UO-CSMA can be categorized as follows.

- Distributed CSMA in WMNs as Markov random field (MRF); properties of non-adaptive CSMA [65, 133, 166, 166, 167, 207, 225, 268, 275].
- Utility-optimality in continuous time [111, 112, 115, 118, 180, 225, 280].
- Utility-optimality in slotted time with CSMA collisions and delayed CS [70, 111, 113, 114, 116, 117, 119, 121, 137, 138, 174, 175, 195, 196, 208, 242] or imperfect CS [136, 139].
- Characterization of the delay performance and the short-time fairness; delay-aware scheduling policies [65, 115, 120, 127, 159, 175, 177, 178, 225, 243, 285].
- Different weight functions [79, 225].
- CSMA with hidden nodes [97, 98].
- Alternative contention procedures [46, 126].
- Extension to multiple RF channels [28, 168, 208], multiple MCSs [126], multiple-input multiple-output (MIMO) [211], superposition coding [245], flow level dynamics [27, 28] and optical networks [224, 241].
- Design of protocols and evaluation through simulation and prototypes [6, 10, 11, 146–148, 160, 179, 250, 276, 288].

Except for the last point, the work is generally theoretical in nature. In the following, we will go through the most important contributions.

The breakthrough that has led to the development of UO-CSMA is the observation that *distributed CSMA* in WMNs can be described as Markov random field (MRF)

[1] Also called *adaptive CSMA*. We use both terms interchangeably.

[65, 133, 166, 167, 225, 275]: Each link of the WMN is represented as a node in the link conflict graph (LCG). Its state is either transmitting or idle. The state of the network is determined by the joint state of all links, and it forms a Markov chain, the so-called CSMA Markov chain. However, not all possible network states are valid, since the CS prevents the activation of conflicting links according to the LCG. The idle and active durations of a link, i.e. the backoff and transmission periods, are exponentially distributed with rate parameters λ and μ, which are either fixed with non-adaptive CSMA or traffic-adaptive with $CSMA(\lambda, \mu)$. The CSMA Markov chain $CSMA(\lambda, \mu)$ is a time-reversible spatial process and its stationary distribution is a MRF [111]. Spatial processes extend the Markov property from time to space, i.e. the state of every link is conditionally independent from all other links it is not in conflict with [111, 133]. It is an *idealized CSMA* model since the CSMA backoff periods, i.e. the idle durations, are continuous in time and instantaneous propagation is assumed, so that no CSMA collisions occur. Non-adaptive CSMA protocols like IEEE 802.11 try to push the system into states that are the maximal independent sets (MISs) of the LCG, so that the sum-throughput of the network is maximized. However, the network and user objectives are generally different from sum-throughput resulting in unfairness [74, 75].

UO-CSMA tries to harmonize the network operation and the objectives of the network and the user. The canonical form of UO-CSMA for congestion controlled single-hop flows is as follows [285]:

UO-CSMA: The transmitter of link l runs $CSMA(\lambda[t], \mu)$ using

$$q_l[t+1] = \left[q_l[t] + \frac{b[t]}{W'(q_l[t])} \left(U'^{-1} \left(\frac{W(q_l[t])}{V} \right) - S_l[t] \right) \right]_{q^{\min}}^{q^{\max}} \tag{3.1}$$

$$\lambda_l[t+1] = \mu^{-1} \exp\left(W(q_l[t+1])\right) \tag{3.2}$$

where W is an increasing *weight function*, V is a positive parameter that controls the throughput-delay tradeoff, U is an increasing *utility function* that controls the throughput-fairness tradeoff and $S_l[t]$ is the throughput on link l during slot t. The variable q_l corresponds to the queue length when using a constant *step size* $b[t]$.

The rationale of the algorithm is as follows. We can think of the U'^{-1} term in (3.1) as the congestion-controlled arrival rate on link l. Thus, q increases if the arrival rate exceeds the service rate S and declines in the opposite case. In other words, it captures the queueing process on link l. The medium access rate λ on link l is adjusted in relation to q in (3.2), i.e. the scheduler contends for the medium more aggressively if it cannot realize the anticipated flow rate, and it becomes less aggressive if it consumes more resources as requested by the congestion controller. The algorithm does not assume slot-synchronization, it does not need to know the arrival rates in advance and it is furthermore completely distributed, i.e. each transmitter uses local information only.

The UO-CSMA algorithm is asymptotically utility-optimal in continuous time where no collisions occur due to identical backoff counters or propagation delays [111, 112, 115, 180, 225]. A further assumption is a time scale separation, i.e. the underlying CSMA Markov chain is assumed to converge quickly in-between the parameter up-

dates in (3.2). The optimization problem that belongs to the solution in (3.1) and (3.2) is the following [175].

$$\begin{aligned} \max_{\gamma,\pi} \; & V \sum_{l \in \mathcal{L}} U(\gamma_l) - \sum_{m \in \mathcal{N}} \pi_m \log(\pi_m) \\ \text{s.t.} \; & \gamma_l \leq \sum_{m \in \mathcal{N}: m_l = 1} \pi_m, \quad \sum_{m \in \mathcal{N}} \pi_m = 1 \end{aligned} \tag{3.3}$$

In the formulation above, γ_l denotes the long-term throughput on link l, $\mathcal{L}$ is the set of links, $\mathcal{N}$ is the set of schedules and π is the distribution of the CSMA Markov chain over all schedules $m \in \mathcal{N}$. The notation m_l refers to the state of link l within schedule m, which is either transmitting (1) or inactive (0). Surprisingly, the objective (3.3) contains the entropy of the CSMA Markov chain, in addition, and we will consider the consequences within the next paragraphs.

The utility-optimality of UO-CSMA has been extended to slotted time without the time scale separation [70, 111, 113, 114, 116, 121, 137, 174, 175, 195, 196, 242]. In particular, Jiang *et al.* and Liu *et al.* use a very intuitive idea to establish the result [111, 175]. The average backoff λ^{-1} in (3.2) can be traded off against the average channel holding time μ^{-1} within $CSMA(\lambda, \mu)$. Thus, instead of decreasing the backoffs, which would result in severe collisions in slotted time, the idea is to hold the channel longer and thus transmit more frames per successful contention attempt. In addition, the RTS/CTS signaling keeps potential collision durations short. In this way, the impact of collisions remains arbitrarily small while the utility-optimality is preserved. However, the short-term fairness seriously suffers in the proposed approach. In contrast, Ni *et al.* use a slightly different approach [195, 196]. They assume that the time is slotted into superframes consisting of a signaling and a data sub-frame. Collisions occur only within the signaling frame using a CA technique based on RTS/CTS. Interestingly, the modeling approach leads to the same product form distribution and thus to the same optimality results.

Proutière *et al.* have shown that a time scale separation between the discrete update process of the CSMA parameters and the continuous evolution of the network dynamics is not necessary [208]. In particular, if the network dynamics can be modeled as a continuous-time Markov process, then UO-CSMA achieves asymptotical optimality with properly diminishing step sizes even in the case that the control parameters are updated at the same time scale. Furthermore, constant but small step sizes achieve a weak convergence in the sense that the system converges into a small neighborhood of the optimum. A remarkable point in the work of Proutière and Liu is the assumption that the queue length at the optimum must be within the specified limits $q^{\min}$ and $q^{\max}$ in (3.1) [175, 208]. In section 3.5.2, we will consider this issue in detail and present an algorithm that dynamically adapts the system parameters accordingly.

The results on UO-CSMA are promising. However, we should take a look at the other side of the coin and ask about the price we have to pay. In particular, the MWS problem is NP-hard and does not allow for polynomial time approximations [125, 285, 287]. How is it possible that UO-CSMA solves the problem asymptotically optimal at a significant low level of complexity? The reason lies within a three-dimensional tradeoff between throughput, complexity and delay shown in Figure 3.2. We can think

of it as follows. If we increase the parameter V in (3.1), the queue length as well as the medium access rates increase and we approach a more efficient working point in terms of throughput and utility. According to [111, 112, 175], the optimality gap of the problem (3.3) is bounded as follows.

$$\left| \sum_{l \in \mathcal{L}} \left(U(\gamma_l[\infty]) - U(\gamma_l^\star) \right) \right| \leq \frac{\log |\mathcal{M}|}{V} \leq \frac{|\mathcal{L}| \log(2)}{V} \tag{3.4}$$

In the expression above, $\gamma_l^\star$ is the optimal throughput under MWS and $\gamma_l[\infty]$ denotes the solution to (3.3) with diminishing step sizes. The utility gap, i.e. the right-hand side (RHS) of (3.4), is determined by the number of active links $|\mathcal{L}|$ and the parameter V. The derivation of the RHS relies on the fact that the entropy of the distribution of the CSMA Markov chain in (3.3) is bounded above. Thus, the algorithm converges into a small neighborhood of the MWS solution that depends on both $|\mathcal{L}|$ and V.

Nevertheless, we have to pay for a small utility gap in terms of short-term MAC fairness and end-to-end delay [65, 115, 120, 159, 175, 178, 225, 285]. The intuition behind this result is as follows. Let us consider an even number of nodes that are placed on a circle with equal distances. Single-hop traffic flows exist in counterclockwise direction and the primary interference model is used. In that case, the MISs consist of two schedules that contain the even and the odd links, respectively. Increasing the parameter V leads to longer queues and shorter backoffs. Thus, it takes longer to switch from one MIS to another [65], i.e. the system "locks into" a particular schedule [178]. The consequences are interesting: The throughput increases since the system spends more time in the MIS. Remember that throughput is an asymptotic concept that averages over a long period of time. On the other hand, the short-term fairness declines since the inactive links have to wait longer to regain medium access. The end-to-end delay suffers as well from larger queues according to Little's law [18].

The derivation of exact expressions for the delay performance is challenging due to the coupling of queues due to multi-hop routing. The interested reader may refer to [196] for an overview of delay approximation and bounding approaches. However, a very general result from collision-free MWS is the three-dimensional tradeoff between throughput, delay and complexity [285, 287]. As shown in Figure 3.2, greedy schedulers have a lower complexity, but they achieve only a fraction of the capacity region of MWS. Interestingly, we can trade complexity off for delay with a scheduling policy called randomized pick-and-compare (RPC) [285]. Instead of calculating the MWS for each time slot anew, the idea of RPC is to persist within "good" schedules, so that the costs of finding them amortize over time. Hence, RPC sacrifices delay, while the throughput remains unaffected since it is an asymptotic concept. It is assumed that UO-CSMA operates within a throughput-delay plane that has a low complexity [173, 175, 178, 285].

Thus, delay cannot be eliminated, but unnecessary latency can be removed and the throughput-delay tradeoff can be controlled according to the user requirements. For the latter goal, two approaches have been presented in recent literature. According to Jiang *et al.*, the congestion controller of (3.1) should inject slightly more (virtual) qs than (physical) packets [111]. In this way, the actual arrival rate of physical packets in (3.1)

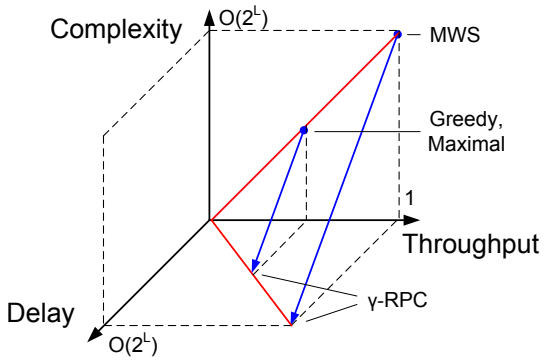

Figure 3.2.: Three-dimensional tradeoff between throughput, delay and complexity (According to [285, 287]).

becomes less than the (physical) service rate of the link, so that the (physical) queues tend to zero. The price to pay is throughput, since we have to emit *dummy packets* if the physical queue runs empty. Lotfinezhad *et al.* presents another interesting approach to control the tradeoff that does not rely on dummy packets [178]. In particular, they propose to regularly "reset" the state of the CSMA Markov chain to zero, which prevents an excessive locking of the system within a schedule. Further approaches exist also for the former goal of removing unnecessary delays. One observation with back-pressure routing is that many packets get stuck within intermediate queues only to provide differential back-log. However, these physical packets can readily be substituted by virtual packets that are nothing more than counters [33, 186, 218]. Ni *et al.* propose a dual scheduler with two different policies [195, 196]. If the back-pressure of the considered link exceeds a threshold, the throughput-optimal policy is used. In the remaining case, the authors propose to use a heuristic policy that has a better delay performance. Furthermore, Moeller *et al.* report delay improvements from changing the queueing discipline to last in, first out (LIFO) [186].

The influence of the weight function W in (3.1) is less well understood [160]. Rajagopalan *et al.* propose to weight the queues with the very slow increasing function $W(q) = \log\log q$. They argue that the shallow slope is necessary for unsaturated sessions [225]. With saturated sessions, on the other hand, the requirements on the weight function can be relaxed since the network dynamics is sufficiently slow in order to average out the noise [285]. However, the shallow slope leads to longer queues and delays. Ghaderi *et al.* present another weight function that is able to reduce the end-to-end delays and the convergence time of the system [79].

Hung *et al.* propose an interesting approach to deal with hidden nodes in the downlink of an IEEE 802.11 infrastructure network [98]. They assume that a wired backbone connects all APs. Each client STA is associated with one AP. Long-lasting traffic flows exist from the APs to the STAs. An AP b becomes a hidden node for the transmission from the AP a to an associated STA if a and b cannot sense each other's activity whereas the STA is able to detect both of them. The authors employ the CSMA Markov model and quantify the throughput loss due to hidden nodes. Since the resulting optimization problem is non-convex, they apply geometric programming and successive convex approximations. The authors present a distributed algorithm that relies on the

knowledge about hidden nodes. Each AP has to construct (parts of) the state space of the CSMA Markov chain. The problem is solved by numerical optimization that requires the exchange of intermediate results between APs. A convergence speed in the order of hundreds of milliseconds is reported.

There are also some initial results addressing the feasibility of UO-CSMA on state-of-the-art hardware [6, 11, 160, 179, 250, 276, 288]. The shortcoming of commodity IEEE 802.11 hardware is that only marginal parts of the MAC operation are accessible. For example, the hardware constraints render it difficult to dynamically adapt the backoffs on a per-packet basis. Interestingly, wireless sensor network (WSN) hardware is more flexible on the MAC layer [250]. The perspective of the early papers is different from UO-CSMA [6, 11, 250, 276]. In particular, the authors intend to find heuristic and empirical solutions that approximate the collision-free MWS with IEEE 802.11 as good as possible. On the other hand, Lee *et al.* present a prototype and some initial results for UO-CSMA using simulation and a real world test-bed [160, 288].

3.1.3. Opportunistic Routing

Opportunistic routing (OR) is a technique to benefit from multi-user diversity (MUD) in WMNs. The wireless communication is prone to transmission errors. Empirical results suggest that the majority of links in a WMN are of intermediate quality in terms of packet loss [4]. The rationale of OR is to mitigate transmission errors via the simultaneous usage of multiple candidate receivers. Due to the broadcast nature of the wireless medium, the transmitter does not have to specify the relay on the next hop a priori. Instead, the routing decision is made a posteriori based on the information which candidate actually received the frame. The additional process of determining the next-hop relay within the MAC transaction is called *forwarder selection* or alternatively *relay (self)-selection*.

Most of the recent literature considers OR from a MAC centric perspective and focuses on the forwarder selection. A detailed review can be found in [315]. In the following, we highlight the most important contributions only. Selection diversity forwarding (SDF) as proposed by Larsson *et al.* uses a four-way handshake for forwarder selection [155]. The approach is refined to a two-way handshake by Valenti *et al.* [266] and by Biswas *et al.* [23]. The latter authors propose a technique called *slotted ACK* in order to orthogonalize the ACKs of all candidates in time. Alternative designs that estimate the instantaneous channel conditions and select the bit-rates accordingly have been proposed by Larsson *et al.* [156], Zubow *et al.* [319], Wang *et al.* [273, 274], Ji *et al.* [110] and Bletsas *et al.* [24]. Assuming that the wireless channel evolves on a slower time scale compared to the frame duration, an additional probing stage is able to determine the instantaneous channel quality to all candidates, so that the best bit-rate for the data transmission can be estimated. The overhead of the slotted ACK can be further reduced by compression [317], which relies on the CS capabilities of the transceiver to detect missing ACK frames. Bletsas *et al.* propose an alternative to the slotting of the probe replies: The candidates have to contend among each other according to their instantaneous channel conditions [24]. The actual data exchange is a unicast transmission to the selected candidate. Yang *et al.* propose a similar contention approach for the ACK stage of the MAC transaction [284]. Furthermore, the overhead of relay

self-selection can be significantly reduced via logarithmic splitting algorithms [13, 274].

In recent literature, two categories of forwarder selection policies can be found. With relay *self*-selection, we refer to a distributed agreement among all candidates. The objective is that the best candidate should be selected according to a metric like ETX [23, 232], geographical distance [312, 313] or instantaneous channel conditions [24]. Self-selection has to handle the inherent risk of coordination failures due to communication errors that may cause duplication of data frames. On the other hand, *transmitter-based relay selection* centralizes the selection responsibility to a single entity, e.g. to the transmitter [155, 189, 309]. In this way, the problem of duplicates can be mitigated at the expense of a four-way handshake [155, 189]. The overhead can be further reduced using robust acknowledgements as proposed by Zhong *et al.* [309]. Similar to passive acknowledgements, the additional handshake is integrated into the following transmission. In addition, the complexity of the signaling schemes can be reduced by network coding [41, 82, 150, 217, 220, 300]. In this way, OR becomes more robust against coordination errors, so that the overall efficiency increases.

Srinivasan *et al.* propose a new metric called κ, which measures the packet loss correlation between two wireless links [251]. Measurement results from IEEE 802.11b and 802.15.4 networks suggest that a fraction of the wireless links experience high loss correlations, which reduce the expected gains of OR. The authors suppose that especially the low-power IEEE 802.15.4 links are subject to cross-correlation due to high-power IEEE 802.11 interferers, whereas IEEE 802.11b networks are affected less seriously.

On the one hand, the identity of a candidate receiver is not important for the transmitter of a data frame. What matters is that at least one of them has successfully received the frame. On the other hand, the data frame is generally present at several relays of the same routing stage, and a downstream receiver does not care about the actual origin of a frame. Advanced PHY techniques enable the cooperative transmission of both data and signaling frames, in which multiple transmitters can take part in. We have proposed an OR protocol for WMNs based on MISO and STC as enabling technology for cooperation on the PHY [149].

From the MAC centric point of view, the objective of the forwarder selection is the selection of the *best* relay according to a given metric. The underlying assumption is that the local decision is also beneficial from the global point of view. The metrics used consider geographic locations [312, 313], instantaneous channel conditions [24], opportunistic gain [32] or topology and link quality information [35, 63, 64, 157, 309]. However, these approaches split the flow onto the outgoing links without considering the interference relationship between transmitters, so that spatial diversity due to multi-path routing cannot be exploited systematically. Furthermore, they split the flow unaware of their own and foreign traffic. As we will see in section 3.7, the traffic-unawareness may result in congestion on paths that do not perform as well as the metric suggested. Thus, the end-to-end congestion controller will limit the flow rate on *all* paths regardless that some of them might support even more traffic.

In conclusion, the area of forwarder selection strategies is well explored, and we have highlighted the most important contributions. However, considering OR from the MAC perspective only is not sufficient in order to achieve desirable end-to-end properties. In particular, it is crucial to consider the question "What are the *best* relays?" from a cross-layer perspective.

The network and cross-layer aspects of OR have been less well explored. Neely *et al.* use control theory to derive a back-pressure routing algorithm for OR with perfect TDMA-like scheduling [189, 194]. In special cases, the algorithm supports decentralized and channel-blind operation. Zeng *et al.* cast OR as a linear program and analytically explore bounds on the performance assuming perfect MAC scheduling [295, 296]. In the same line, Zhang *et al.* formulate a convex optimization problem for network-encoded OR and derive a distributed online algorithm using decomposition and duality [300]. In particular, they use an approximation of the OR capacity region within their optimization and assume perfect MAC scheduling as well. The closest to our work is the optimization framework for network-encoded OR by Radunović *et al.* [217, 220]. Similar to the approaches above, they assume perfect MAC scheduling, but they use exact expressions for the OR capacity region. In addition, they design a protocol called multi-path code casting [82] that addresses the scheduling, opportunistic routing and congestion control problem.

The bottleneck in the contributions above is the attempt to solve the MAC scheduling problem directly. MWS is the optimal strategy [258], which is known to be NP-hard and thus hard to solve even in centralized settings [125, 285]. Thus, most of the approaches above rely on heuristics for random access in order to enable a distributed operation. It is to note that Jiang *et al.* present an extension of UO-CSMA to anycast [111, chap. 9.7.4]. However, they use the term *anycast* to address multi-path routing. In particular, they do not consider the OR capacity region resulting from lossy links and the MUD gain.

3.2. A Node-Oriented Model of CSMA in WMNs

Recent modeling approaches of CSMA in WMNs employ a link-based CS, i.e. they characterize interference by links (cf. section 3.1). The contention is processed by the link as a whole, which requires that transmitter and receiver have the same view on the channel [160]. However, this model is inadequate for state-of-the-art technologies. As we have shown in [144, 145], the CS range of IEEE 802.11b hardware does not significantly extend beyond the receiving range, which gives rise to the well-known *hidden node* problem (cf. section 2.3.2). Hidden interference is likely the most important source of packet loss in today's WMNs [83]. It renders the network capacity region non-convex [43] and causes severe performance degradation [96, 116]. Thus, it is essential to address the hidden node problem before any optimization can be applied.

In section 2.3.2, we have surveyed the approaches to mitigate the hidden node problem. The hidden node free design (HFD) is the justification for the link-oriented CS in the idealized CSMA model [122]. It eliminates hidden nodes by lowering the CS power threshold. However, physical and technological constraints impose a lower limit on the CS threshold, so that large SNR margins of up to 20 dB have to be introduced. The large margins waste a huge amount of spatial resources. According to Ven *et al.*, the optimal CS range for a CSMA network is just large enough to preclude all hidden collisions [267]. Increasing the CS range further consumes spatial resources only without any benefits in return.

In the following, our objective is to derive a MAC model for OR in WMNs based on

the continuous-time CSMA Markov model [112]. The HFD approach does not meet the requirements for OR. Due to the large SNR margins, HFD allocates spatial resources unnecessarily leading to a low spatial reuse. Furthermore, the wireless links will most likely be lossless due to the large SNR margins, so that the anycast does not have any multi-user gain. Furthermore, HFD silences *all possible* receivers, so that additional receivers can be included in the MAC transaction at no extra cost in terms of spatial resources. Thus, HFD does not capture the characteristic tradeoff between opportunistic gain and spatial reuse that arises with OR. Based on our observations about CS in WMNs [144, 145], we develop a *node-oriented* CS model that reconsiders the operation of CA with respect to the characteristics of wireless mesh networks. Furthermore, it supports OR via anycast transmissions and allows for a higher spatial reuse through a selective allocation of spatial resources on demand. In section 3.3, we design a MAC protocol according to the presented model.

3.2.1. Node-Oriented CSMA/CA as a Markov Random Field

During the anycast transmission, the transmitter tries to send a frame to at least one receiver. We assume that the MAC protocol operates bidirectional, so that transmitter and receiver(s) can exchange signaling information. Furthermore, we assume that the MAC transaction is opaque in terms of interference, i.e. identical interference constraints apply to all involved nodes. For example, we do not allow that another transmission takes place even if it would interfere with the transmitter of an ongoing transmission only, which is the well-known exposed node situation [122]. In this way, an actual MAC protocol remains flexible in the realization of signaling schemes, since there are no temporal dependencies involving the role assignment.

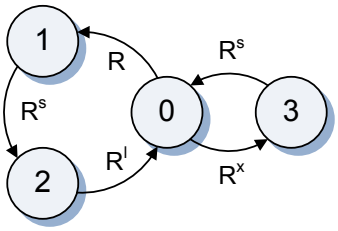

Figure 3.3.: Markov chain model of the internal CSMA operation of a wireless link.

A wireless link can be in one of the following four states: In the *contending state* (denoted 0), the link is idle and tries to get access to the medium. If it wins the contention, it enters one of the *probing states* (1 or 3). Both states are technically equivalent, however, we associate two different values to emphasize the outcome of the probe. If the probe is successful (state 1), the link enters the *data transmission* state (2), otherwise it proceeds from state 3 to state 0. The reader might associate the RTS of IEEE 802.11 [102] with the probing states. As shown in Figure 3.3, the operation of link k can be modeled as a Markov chain when assigning the medium access rate $R = R_k$, signaling rate R^s and transmission length R^l to the edges. The synchronization rate R^x captures the extent of failed probes that might arise, which we consider in detail in one of the next sections. Let v be the state of the link. The stationary distribution P of the internal CSMA Markov chain is given in (3.5). The constant C normalizes P to a probability distribution.

$$P(v) = \frac{1}{C} \begin{cases} 1 & v = 0 \\ R/R^s & v = 1 \\ R/R^l & v = 2 \\ R^x/R^s & v = 3 \end{cases} \tag{3.5}$$

The link conflict graph (LCG) captures the interference between any two links. Each wireless link of the network is represented as a site in the LCG $G = (\mathcal{V}, \mathcal{E})$. The set $\mathcal{V}$ contains K sites, which are both unicast and anycast links. We assign a value $v_k \in \{0, 1, 2, 3\}$ to each link k in $\mathcal{V}$ corresponding to the state of the link. The K-dimensional vector $\boldsymbol{v} = (v_1, v_2 \dots v_K)$ captures the state of all links in the LCG. In the following, we assume that the state space $V \ni \boldsymbol{v}$ is indexed by j: Hence, the notation $\boldsymbol{v}^j$ refers to the j-th vector of V, and v_k^j selects the k-th element of it.

Due to the CS constraints, the space $\{0, 1, 2, 3\}^K$ generally contains infeasible states. For example, two neighboring transmitters k and l are not allowed to access the medium simultaneously, i.e. if $v_k \neq 0$ then $v_l = 0$ and vice versa. The LCG contains a weighted edge $e_{k,l} \in \mathcal{E}$ between site k and l if the links are in conflict. The weight determines the type of conflict. By exhaustive search over all topologies, we have identified 5 structurally different conflict types, which are depicted in Figure 3.4. In particular, if both transmitters are separated by more than 3 hops, they can operate simultaneously without any conflicts (cf. Figure 3.4a-c). Otherwise the transmitters are within each other's (3-hop) *contention neighborhood*, so that they are in conflict with each other. With type 1 conflicts (cf. Figure 3.4d-f), only the probes must be serialized. The joint probing state 11 does not exist, whereas concurrent data transmission is possible. A type 5 conflict results from a topology in which both transmitters are neighbors, for example. In this case, every transmitter has perfect knowledge about the state of the medium at the other node, which prevents them from accessing the medium simultaneously (cf. Figure 3.4m-o).

The conflict types 2, 3 and 4, which is opposite symmetric to type 3, exhibit an *information deficit* at either one or both transmitters. Ongoing data transmissions may exist that are hidden from the transmitter but within the vicinity of the receiver. In that case, if the transmitter experiences an unsuccessful probe, we will *block* the link until it is *re-synchronized*. Since the unsuccessful probe indicates that the intended receiver is occupied, the blocking prevents further excessive probing without success. Unsuccessful probes cannot be prevented, but they should be limited while ensuring a fair competition between links. However, the blocked sender needs to know when the receiver becomes available again, so that the competition with hidden nodes remains fair in the next contention period. Note that the IEEE 802.11 CA does not meet this requirement. The transition rate into the state of an unsuccessful probe R^x depends on how often the link is re-synchronized, which in turn depends on the data frame length and the number of active data transmissions in the contention neighborhood of the transmitter. In the following, we make the simplifying assumption that R^x is independent from R. The assumption might not be fulfilled in real systems. However, the model remains accurate, as we will point out in the evaluation.

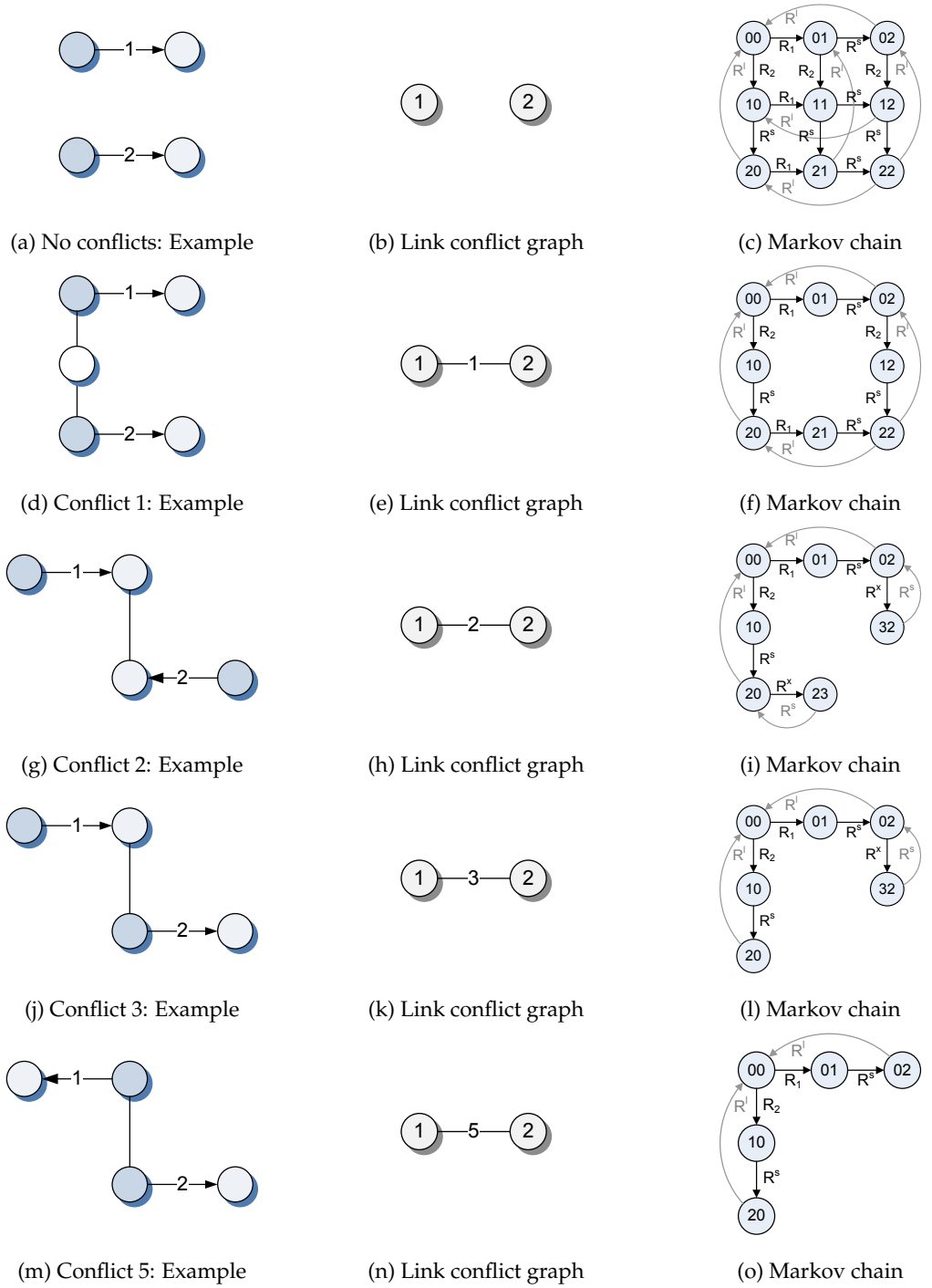

(a) No conflicts: Example (b) Link conflict graph (c) Markov chain

(d) Conflict 1: Example (e) Link conflict graph (f) Markov chain

(g) Conflict 2: Example (h) Link conflict graph (i) Markov chain

(j) Conflict 3: Example (k) Link conflict graph (l) Markov chain

(m) Conflict 5: Example (n) Link conflict graph (o) Markov chain

Figure 3.4.: Each row illustrates a type of link conflict using a topology example, the LCG and the Markov chain. The arrows in the leftmost figures point from transmitter to receiver and lines denote interfering links. In the CSMA Markov chain, the first and second digits correspond to the states of the first and second link, respectively, and arrows mark transitions.

The spatial dependencies of CSMA in WMNs can be captured by a Markov random field [65, 112, 167]. Spatial processes generalize the Markov property of limited dependency from time to space [133]. The extended CSMA Markov chain presented above is a MRF, and we give an intuition for this result in section A.2. In the following, we substitute $R = \exp(r)$ and we refer to r as transmission aggressiveness (TA). Furthermore, the indicator function $\delta^I(v_k^j) = \delta_{j,k}^I$ classifies the state j: It is evaluated to 1 if $v_k^j \in I$ (or $v_k^j = I$) and to 0, otherwise. The stationary distribution p of the CSMA Markov chain has product form since it is a MRF and is given by

$$p(\boldsymbol{v}^j;\boldsymbol{r}) = \frac{\prod_{k=1}^K P(v_k^j)}{C(\boldsymbol{r})} = \frac{\exp\left(\sum_{k=1}^K \delta_{j,k}^1(r_k - r^s) + \delta_{j,k}^2(r_k - r^l) + \delta_{j,k}^3(r^x - r^s)\right)}{C(\boldsymbol{r})} \tag{3.6}$$

$$C(\boldsymbol{r}) = \sum_j \exp\left(\sum_{k=1}^K \delta_{j,k}^1(r_k - r^s) + \delta_{j,k}^2(r_k - r^l) + \delta_{j,k}^3(r^x - r^s)\right)$$

The model operates at two spatial levels. For data transmissions, it considers the *necessary* receivers only and generates a 1-hop exclusion region around transmitter and receiver(s), which is set up during the probing state. However, to protect the probing frames from hidden interference, the transmitter has to establish a larger exclusion region comparable to HFD, which we call (3-hop) *contention neighborhood*. The contention neighborhood is silenced for a short probing duration only. After the probe, the allocated spatial resources are reduced in any case: Either the probe has failed and the exclusion is completely removed, or the probe has been successful and the exclusion is reduced to the (1-hop) neighborhood around transmitter and receiver(s). In this way, the spatial reuse is increased compared to HFD, and the model captures the characteristic tradeoff between multi-user gain and spatial reuse.

For unicast transmissions, the probing policy is straightforward: Only if the CTS has been returned, the sender proceeds with the transmission of the data frame. However, it becomes more involved with anycast. The model demands an *all-or-nothing policy*: The sender transmits the data frame only if *all* CTS frames have been returned. This approach seems cumbersome on first sight, and one might be tempted to address the data frame to the subset of candidates that have transmitted a CTS. However, the stationary distribution of the CSMA Markov chain would lose its product form this way. On the other hand, if we would ignore missing CTSs and use all receivers in any case, it would be hardly possible to reason about the link quality for data transmissions since channel errors and occupied receivers cannot be distinguished anymore.

Using the abbreviation $p_j(\boldsymbol{r}) = p(\boldsymbol{v}^j;\boldsymbol{r})$, we define the throughput q_k of a link k as

$$q_k(\boldsymbol{r}) = \sum_j \delta^2(v_k^j) p(\boldsymbol{v}^j;\boldsymbol{r}) = \sum_j \delta_{j,k}^2 p_j(\boldsymbol{r}).$$

The summation proceeds over the complete state space V. Furthermore, we introduce the superscript i on q_k^i that refers to the state, in which the throughput was generated. For example, $q_k^2 = q_k$ is the data throughput, and q_k^1 and q_k^3 refer to the throughput of successful and unsuccessful probing.

3.2.2. Operating CSMA/CA in WMNs

In the same line as [112], the TAs $\boldsymbol{r}$ that stabilize the network within a particular steady state $\bar{\boldsymbol{p}}$ of the extended CSMA Markov chain can be found via maximum likelihood (ML) estimation, assuming that the input rates per link $\lambda_k = \sum_j \delta^2_{j,k} \bar{p}_j$ are feasible. Note that the objective of the MAC is not the maximization of the link throughput. Instead, the maximal feasible flow and link rates are determined by the congestion controller and the routing layer (cf. section 3.4), and the objective of the MAC is to adapt its parameters to achieve the predetermined rates. The ML estimate [30, p. 361] of $\boldsymbol{r}$ is found by maximizing the log-likelihood function $F(\boldsymbol{r})$ with respect to $\boldsymbol{r}$. By plugging (3.6) into $F(\boldsymbol{r}) = \sum_j \bar{p}_j \log(p_j(\boldsymbol{r}))$ as follows

$$F(\boldsymbol{r}) = \sum_{k=1}^{K} \Big(\lambda_k (r_k - r^l) + \lambda^1_k (r_k - r^s) + \lambda^3_k (r^x - r^s) \Big) - \log(C(\boldsymbol{r}))$$

and maximizing $F(\boldsymbol{r})$ with respect to $\boldsymbol{r}$, we get

$$\begin{aligned} \frac{\partial F(\boldsymbol{r})}{\partial r_k} &= \lambda_k + \lambda^1_k - \sum_j \delta^{1,2}_{j,k} \frac{\exp\left[\sum_{i=1}^{K} \delta^1_{j,i}(r_i - r^s) + \delta^2_{j,i}(r_i - r^l) + \delta^3_{j,i}(r^x - r^s)\right]}{C(\boldsymbol{r})} \\ &= \lambda_k + \lambda^1_k - \sum_j \delta^{1,2}_{j,k} p_j(\boldsymbol{r}) = \lambda_k + \lambda^1_k - q_k - q^1_k \end{aligned}$$

where λ^1_k and q^1_k are the target and observed signaling costs for successful probing. Due to our assumption about the independence of r^x from any other r_i, the costs for unsuccessful probing are not considered in the estimation of $\boldsymbol{r}$. By construction, the overhead for successful probing is a constant fraction of the data throughput, i.e. q^1_k and q_k differ only by the constant factor R^l / R^s. Hence, we can update the TAs via the sub-gradient $r_k \leftarrow [r_k + \alpha(\lambda_k - q_k)]_+$ with positive step size α. In other words, the queue backlog can be used for CSMA scheduling.

In the derivation, we have assumed that every transmitter is *saturated*, i.e. the queues are non-empty at all times. This assumption is reasonable for the source of the flow since the arrival process provides sufficient packets. However, especially at the intermediate relays the queues have to be filled via the upstream. Similar to [112], we may transmit dummy packets if the queue runs empty in order to fulfill the assumption. In section 3.5.3, we will present an alternative approach to deal with empty queues.

3.3. CSMA/CA with Hierarchical Busy Tones

In the following, we illustrate how to modify the well-known IEEE 802.11 protocol [102] to conform to the extended CSMA model that we have introduced in the previous section. We refer to the refined protocol as CSMA/CA with hierarchical busy tones (CSMA/HBT). The extended CSMA model is based on the rationale that every link can increase its service rate by using higher TAs, so that it can resolve any unfairness locally. Even with adaptive backoffs, the DCF of IEEE 802.11 cannot ensure this requirement. For example, consider the scenario in Figure 3.5. Three transmitters

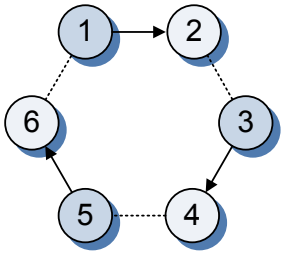

Figure 3.5.: Scenario: 3 links in a circular dependency.

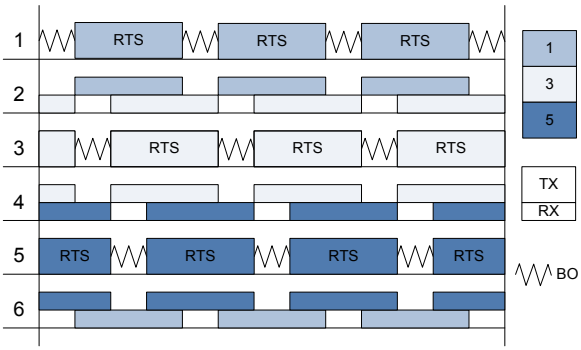

Figure 3.6.: Temporal dimension of DCF: Small backoff durations cause a livelock.

are connected to their respective receivers and to one receiver of another link, in addition. If the transmitters 1, 3 and 5 increase their TAs, so that the average backoffs become significantly smaller than the RTS duration, then a livelock occurs under DCF. As shown in Figure 3.6, every sender constantly probes the channel only to find out that its intended receiver is silenced by an ongoing transmission. At the same time, its probe silences the receiver of another link in a circular fashion, so that no link is able to transmit data.

The model in section 3.2 acquires resources in two stages. The rationale is to use a large exclusion region, the so-called contention neighborhood, during the short probing stage in order to protect the RTS frames from hidden interference. In the following data transmission stage, the exclusion region is reduced to the necessary level in order to allow for higher spatial reuse. In particular, CSMA/HBT relies on physical CS only, whereas virtual CS is not used. Similar to dual busy tone multiple access (DBTMA) [90], we conceptually separate carrier sensing from the data transmissions using out-of-band busy tones (BTs), although we use *three BT channels* instead of only one. We assume that the receiver is able to detect activity in each BT channel with a high probability even if multiple BT signals are superimposed. Interestingly, approaches similar to DBTMA find their way into cellular systems, as well [80].

There are three types of BTs: The *contention busy tone (BTC)* accompanies the RTS (state 1). It covers the contention neighborhood around the transmitter as shown in Figure 3.7. It indicates that the medium is busy, i.e. every receiver of the BTC should suspend its contention. As shown in Figure 3.8, the BTC has a high consumption of spatial resources, whereas the holding time is short. On entering state 2, the transmitter turns the BTC off and activates the *data busy tone (BTD)*, which covers and silences its (1-hop) neighborhood. If an addressed receiver is not silenced by ongoing transmissions, it also activates its BTD and sends a CTS. All returning CTS packets are properly orthogonalized, e.g. in time, space or frequency. In the case that all CTS frames have returned, the transmitter initiates the actual data delivery. Otherwise, it goes back to contention (state 0) and marks the link as blocked. It does not contend on the blocked link until it is re-synchronized. The rationale is to reduce the consumption of spatial resources to the necessary level in order to allow for a higher reuse during the data transmission (cf. Figure 3.8).

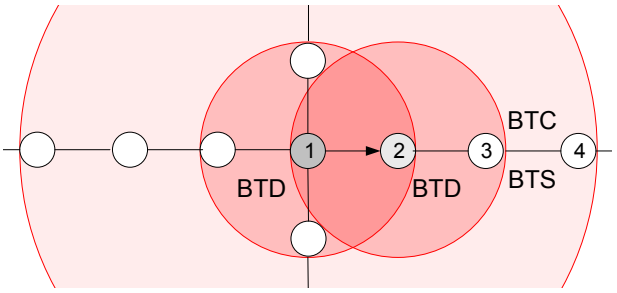

Figure 3.7.: Spatial dimensions of CSMA/HBT.

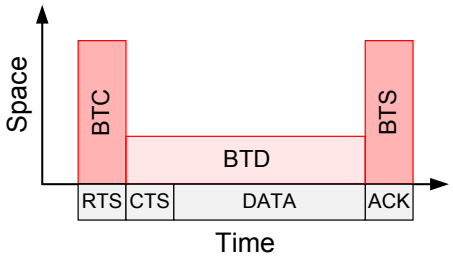

Figure 3.8.: Temporal and spatial dimensions of CSMA/HBT.

Every receiver acknowledges the successful reception of a data frame using an ACK frame. At this time, the transmitter has to re-synchronize all blocked links in its contention neighborhood. In this way, nodes with blocked links become aware of the start of the next contention period, so that the competition among all transmitters remains fair. In particular, the transmitter actives the *synchronization busy tone (BTS)* to announce the end of its TXOP. The BTS covers the (3-hop) contention neighborhood of the transmitter similar to the BTC (cf. Figure 3.7). On finishing the MAC transaction, the transmitter deactivates the BTS, which releases all blocked links and synchronizes all nodes in the contention neighborhood, so that they start to contend for medium access again.

If multiple frames are transmitted within the TXOP, the synchronization occurs for the last ACK only. The synchronization should take place even if the TXOP is prematurely terminated due to missing ACKs. If the probe has not been successful due to missing CTSs, the transmitter cannot distinguish whether the affected receiver(s) are silenced, the RTS frames have collided or the fading channel is in outage. If this knowledge would be available, the transmitter could differentiate its reaction: For example, it could schedule the next probing attempt according to the channel coherence time in the latter case. Since we cannot rely on this knowledge, an *unblock timeout* in the order of a TXOP ensures that fading outages, CSMA collisions as well as missing and overheard BTSs do not block a link infinitely.

Note that the outcome of the probing stage is already determined at the beginning of the probe. However, the transmitter is not aware of it until the end of the probe. If the outcome is positive, the access to the medium is granted and no other link may interrupt the ongoing communication. All BTs prevent receiving nodes from contending for medium access, i.e. they suspend their backoff on receiving a BT. However, there is an important difference: On sensing the BTD, the node should be completely silent. In particular, it should not answer any incoming RTS, since a data transmission is in progress in its neighborhood.

There are multiple alternatives for the realization of the BTs. For example, they can be allocated in the white spaces of the wireless spectrum. The three-hop coverage can be ensured through higher transmission power, smaller signal bandwidth or lower carrier frequencies. Furthermore, advanced concepts like relaying and multi-carrier technologies like orthogonal frequency-division multiple access (OFDMA) may assist

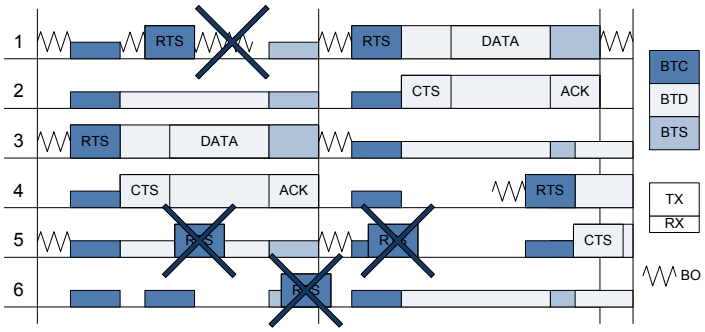

Figure 3.9.: Temporal dimension of CSMA/HBT. Actions that are not allowed are marked with crosses.

in the realization of the BTs. In addition, the costs for an additional BT transceiver should be reasonable in relation to the hardware for time synchronization that would be necessary for collision-free MWS.

Referring back to the topology in Figure 3.5, CSMA/HBT prevents the livelock since it removes the circular dependency using a larger contention neighborhood. For example, if transmitter 3 sends an RTS as shown in Figure 3.9, all other transmitters are silenced by the BTC. After the probing stage, only node 2 and node 5 remain in the reduced exclusion region as determined by the BTD. On the other hand, transmitter 1 is not silenced and may send an RTS as shown in the figure. Since the intended receiver is silenced, node 1 will block its link to node 2 until it is re-synchronized by the BTS, or a timeout occurs. However, it will suspend its contention on that link in order to prevent excessive probing. Similar to the BTC, the BTS should cover the (3-hop) contention neighborhood, so that all contenders are synchronized to the start of the next contention period. Note that an interleaved operation as shown with transmitter 4 in Figure 3.5 is possible.

As long as one link is in a probing state (1 or 3), all links within the contention neighborhood should not change their state (which can only be 0 and 2) in order to comply with the proposed model in section 3.2. To prevent collisions between probing frames, the model has no joint probing state 11 for conflicting links (cf. Figure 3.4). However, allowing a transmitting link (state 2) to become idle (state 0) while a conflicting link sends a probe introduces a non-reversible transition in the Markov chain, since the link cannot become transmitting again (state 2) as long as the conflicting link remains in the probing state. The product form distribution would be lost this way (cf. section A.2). Hence, the transmission of a link should be prolonged by the time the respective contenders spend in probing in order to comply with the model. From the practical point of view, this is difficult to achieve. Fortunately, through simulations we have gained evidence that the discrepancy to the model is acceptable even when this issue is ignored.

3.3.1. Link Level Evaluation

In this section, we evaluate the CSMA/HBT protocol analytically and through simulation in order to derive characteristic properties. Our intention is three-fold. At first, we have not discussed the synchronization rate yet, which determines the amount of probing failures. In the following, we will establish bounds on the synchronization

rate for CSMA/HBT and illustrate the probing overhead in typical cases. Secondly, we evaluate CSMA/HBT in non-idealized settings, in which collisions occur. We estimate the amount of collisions and formulate the tradeoff between collisions and efficiency that arises with UO-CSMA. Thirdly, we have used the protocol model in the design of CSMA/HBT. However, the signal propagation is more sophisticated in physical environments. We illustrate the degree to which CSMA/HBT orthogonalizes the medium access and discuss arising risks for the following optimization problem in section 3.4.

Synchronization Rate and Probing Overhead

The probing overhead consists of both successful and unsuccessful probes. The former are a fraction of the achieved data throughput. The latter are determined by the synchronization rate r^x in the extended CSMA model in section 3.2. In the following, we characterize CSMA/HBT in terms of the synchronization rate. From a technological point of view, the amount of unsuccessful probes under CSMA/HBT depends on how often an unblocked link experiences probing timeouts (*a priori failure*), and on how often false unblocking occurs, i.e. a previously blocked link unnecessarily probes the channel due to an unblocking signal from another node in the contention neighborhood (*unblocking failure*). Remember that the BTs and particularly the BTSs do not carry any additional information like sender addresses.

An exact expression for the *a priori failures* is hard to obtain: It depends among others on the frame sizes, the number of active transmitters in the contention neighborhood and the joint distribution of link states, and it may furthermore vary in time. Nevertheless, we can upper bound the a priori failures in the following way. Consider a system with two links, which experience an information deficit as shown in Figure 3.4g. In the scenario, unblocking failures cannot occur since there are only two links. At the time the primary link decides to probe the channel, the secondary link can be either idle or active, but the actual state is hidden from the primary link due to the information deficit. The probing succeeds if the secondary link is idle, and the probing overhead is a constant fraction of the transmission duration. If the secondary link is active, on the other hand, the probing attempt is not successful. Thus, the primary link remains blocked for the rest of the data transmission on the secondary link. The secondary link synchronizes the other link at the end of its data frame, which enables a fair competition between them. In the worst case, the secondary links always wins the medium contention. In this case, the primary link sends exactly one probe packet within each TXOP of the secondary link. In summary, the probing overhead of a priori failures is bounded by the overhead of successful probes on the competing link in the considered scenario, i.e. we have $r^x \leq r^l$.

In the same way, we can argue about bounds on *unblocking failures*. If there are multiple transmitters within the contention neighborhood, the primary link may experience unblocking failures. In particular, let n be the number of additional links within the contention neighborhood, which can be activated concurrently. In the worst case, the secondary link is transmitting a data frame, and all n remaining links trigger an unblocking failure within the transmission duration (assuming equal frame sizes). In the worst case, the probing overhead increases by a factor of n due to unblocking failures, i.e. we have $r^x = r^l + \log(n)$. Fortunately, the number of links within the contention

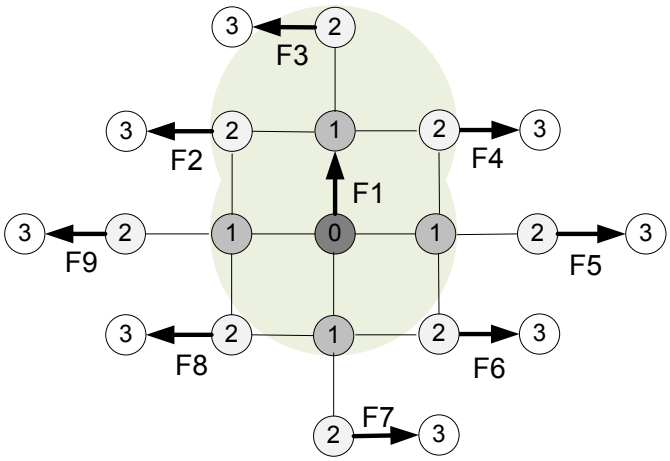

Figure 3.10.: Scenario: The flow $F1$ competes with 8 flows in its contention neighborhood, and it competes with $F2 - F4$ for data transmissions.

neighborhood that might cause an unblocking failure is limited due to the propagation properties of the wireless signal.

When transmitting a 1480 Byte data frame at 6 Mbps using the PHY parameters of IEEE 802.11g, the duration of the BTC covers 2.8% of the MAC transaction. We have conducted MATLAB simulations to estimate the effect of probe failures in typical settings. For example, consider the star topology in Figure 3.10. The primary flow $F1$ competes with 8 one-hop flows within its contention neighborhood. In particular, the sender and receiver of the other flows are 2-hop and 3-hop neighbors, respectively, of the primary transmitter. All competing flows can concurrently transmit data. They only have to serialize their probes, if necessary (cf. Figure 3.4d-f). On the other hand, the primary flow competes with the flows $F2 - F4$ about resources for data transmissions. Each sender transmits 1480 Byte frames at 6 Mbps at a target flow rate of 0.18, 0.64 and 0.82 for $F1$, $F2 - F4$ and $F5 - F9$, respectively. We have observed a probing overhead of 0.114 at the primary sender, whereas the overhead for (successful) probing is about 0.018 and 0.022 for the remaining three and five flows, respectively. Thus, the surrounding flows consume at most 16% of the available medium around the primary transmitter via their BTCs. The primary flow uses only 0.5% of the medium for successful probing, and unsuccessful probing accounts for the remaining 10.9% of the probing overhead. Nevertheless, the primary flow is able to realize its flow rate even in the presence of multiple hidden transmitters.

Collisions in CSMA/HBT

In the idealized CSMA model [112], collisions cannot occur due to the assumption about instantaneous propagation and arbitrarily small backoffs. However, these assumptions do not hold in general, so that the transmitters do not have a consistent view on the channel and CSMA-inherent collisions may arise. In particular, the CSMA collision problem boils down to the probability that an interferer accesses the channel during the *vulnerable period* [140].

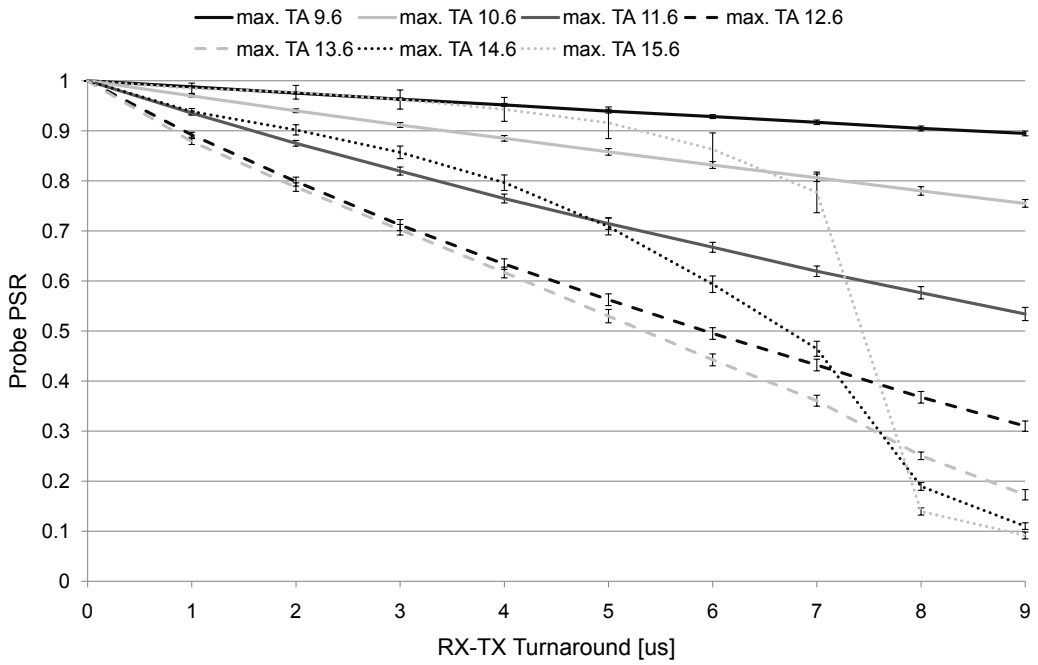

Figure 3.11.: Two links within the same collision domain: Probe success rate in relation to the radio turnaround and the per-link target TA ($\pm std.dev.$).

A recently started transmission is vulnerable for physical and technological reasons. The propagation speed of wireless signals is physically limited by the speed of light. A node separation of 300 m leads to a propagation delay of no less than 1 µs, for example. The imperfectness of today's technology causes additional delays like the CCA delay or the turnaround time to switch the radio from receiving to transmitting. On the other hand, the probability to start a concurrent transmission during the vulnerable period depends on the average backoff per contender and their number within the collision domain. In the following, we illustrate how the performance of CSMA/HBT is affected by both the length of the vulnerable period and the average backoff duration.

The simulation topology consists of two single-hop flows in the same collision domain. Each flow consists of 1480 Byte data frames that are transmitted at 6 Mbps using the PHY parameters of IEEE 802.11g. The channel is modeled as AWGN without fading. The receiver uses the SINR-BER relationship to derive the PERs and supports cumulative interference. Further details about the network simulator can be found in section 2.5. We have varied the average backoff via the target TAs and the radio turnaround latency, which accounts for the vulnerable period. Note that the radio turnaround has the same effect on the vulnerable period as the propagation delays and the CCA duration. Each parameter setting is averaged over 100 random seeds.

The probe success rate is defined as the PSR of the RTS probe and the following CTS frame. The data transmissions are almost error-free in our simulations, so that the achieved goodput is proportional to the shown probe success rate. Since the vulnerable period is fixed and the backoffs are exponential distributed, we expect to see the CCDF

of the exponential distribution

$$F_c(x) = P(X > x) = \exp(-rx) \tag{3.7}$$

with vulnerable period $x \geq 0$ and target TA r.

The probe success rate is shown in Figure 3.11. In addition, Table 3.1 lists the TAs r that we have estimated from the empirical results according to (3.7) for a vulnerable period of 9 µs. The results for lower target TAs are in good match with our expectation. The deviation with higher TA targets is most likely caused by the following implementation detail. Remember that a link is blocked after a failed probe for the rest of the TXOP. Thus, both links involved in the probe failure would be unblocked with a separation of the vulnerable period at most, since they have started their probes therein. If both vulnerable period and target TA are large, then subsequent probe failures are likely. However, timers on real hardware have a limited precision only. Hence, we have randomly jittered the unblocking time by ±5 µs. Note that $-\log(10 \cdot 10^{-6}) \approx 11.5$. We suppose that the deviation from the exponential CCDF is mainly due to the jittering, since it becomes dominant for the contention round after a failed probe under high target TAs and large radio turnarounds.

Target TA	Estimated TA r
9.6	9.42
10.6	10.35
11.6	11.15
12.6	11.78
13.6	12.18
14.6	12.41
15.6	12.49

Table 3.1.: Estimated TA r according to (3.7) for a vulnerable period of 9 µs.

The results for two links cannot be directly extended to multiple contenders. The backoff is exponentially distributed and thus memoryless, but the blocking of links introduces memory. In particular, the two-link topology is a pessimistic estimate for the multi-link case, since both links are blocked after a failed probe. While they are blocked, none of them can generate throughput and the medium time is wasted. With additional contenders, there is a probability that some of them do not take part in the collision. Hence, they remain unblocked and might use the medium time for transmitting, while the links involved in the collision are blocked.

In conclusion, we have confirmed that both physical and technological constraints have to be considered in the design of a CSMA protocol. The most important factors that influence CSMA collisions are the length of the vulnerable period and the conditional probability that an interferer meanwhile accesses the medium. The former factor is of physical and technological nature, whereas the latter mainly depends on the protocol design. With UO-CSMA [112], a more efficient working point can be approached by increasing the per-link TA. As we have seen, however, this comes at the expense of collisions in a non-idealized model. A tradeoff between the efficiency of the CSMA scheduling and the collision losses arises. We design an algorithm to control this tradeoff in section 3.5.2.

Parameter	Value
Radio frequency	2.4 GHz
Path loss	Log-distance, exponent 3, ref. dist. 1 m
Channel	AWGN & Rayleigh fading
Reception	Physical model (SINR-based)
PHY	IEEE 802.11a/g
Signal bandwidth B	20 MHz
Bit-rate	6 Mbps
SINR threshold γ_t^{dB}	5.4 dB
TX power	19 dBm
Noise floor N	-92.965 dBm
Frame size	1500 bytes

Table 3.2.: System parameters for the analytic evaluation

Mutual Exclusion under Physical Interference

We have used the protocol model [282] in the derivation of the extended CSMA model and the CSMA/HBT protocol. In contrast, the physical model is considered to have a higher predictive value for the performance that can be encountered in the real world [282]. In this section, we are going to illustrate to which extent the proposed protocol achieves mutual exclusion under a SINR based reception model within both AWGN and fading channels.

In our analytic evaluation in Maple, we consider a topology of interfering links. We are interested in the performance of the *primary* link in relation to the *secondary* link, which acts as an interferer in our case. Our performance metric is the PSR of the primary link. We evaluate the system with varying separation between the primary receiver and the secondary transmitter. The parameters of our evaluation are summarized in Table 3.2. Most importantly, we compare the system within two different channels models, which are the AWGN channel and the Rayleigh fading channel.

In AWGN channels, the PSR of a link is determined by the BER. According to [84, 152], the BER P_b of uncoded BPSK can be estimated as

$$P_b(\gamma) = Q\left(\sqrt{\frac{2E_b}{N_0}}\right) = Q\left(\sqrt{\gamma\frac{2B}{R}}\right) = \frac{1}{2}\mathrm{erfc}\left(\sqrt{\gamma\frac{B}{R}}\right)$$

with energy per bit E_b, noise power spectral density N_0, signal bandwidth B, data rate R and SINR γ. In particular, we have set $B = 20$ MHz and $R = 6$ Mbps. We assume uncoded operation. Thus, a frame is received correctly only if all bits are free from errors. Due to the i.i.d. nature of the BER in the AWGN channel, the PSR P_{psr} becomes

$$P_{psr}(\gamma) = (1 - P_b(\gamma))^n, \tag{3.8}$$

where n is the number of bits per frame. Furthermore, we add the constant term $(4.4\ \mathrm{dB} - \gamma_t^{dB})$ to the SINR γ^{dB} in logarithmic scale in order to shift the SINR-PSR curve in a way that the PSR at the reception threshold γ_t^{dB} for a 1500 Byte frame is about 90%.

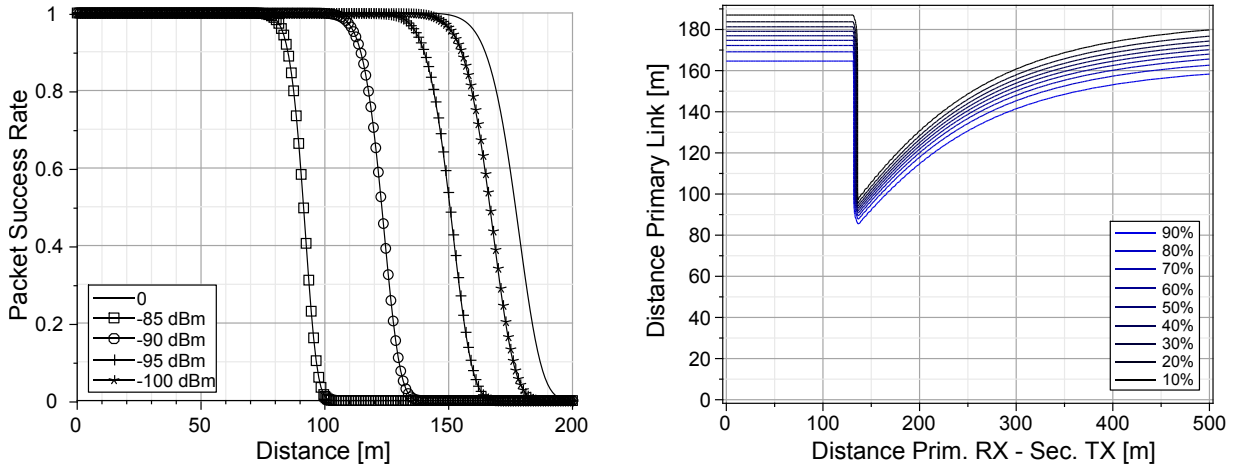

(a) Without CCA: PSR versus distance according to (3.8).

(b) With CCA: PSR versus distance according to (3.9) with CCA power threshold $C = -85$ dBm.

Figure 3.12.: Analytic PSR in the AWGN channel under interference.

The resulting PSR is shown in Figure 3.12a for different levels of interference. On first sight, one might wonder why an interfering signal with a power of -100 dBm, which is far below the noise floor, causes such a degradation of the receiver performance. When the reception process is already noise-limited, however, even small amounts of additional interference lead to further SINR losses. Remember that the SINR-PSR curve is rather steep for the AWGN.

If the interferer is within carrier sensing range of the primary receiver, it will be silenced by the BTs. Otherwise, we have to consider the contribution of the secondary transmitter within the SINR. Thus, the combined PSR P can be written as the piecewise function (3.9).

$$\mathrm{P} = \mathrm{P}_{\mathrm{psr}}\left(\frac{P_{W1}}{N + P_{W2} \cdot \mathbb{1}(P_{W2} < C)}\right) \tag{3.9}$$

In the equation above, P_W denotes the received power according to the log-distance path loss model. N is the noise power and C is the CCA power threshold. Furthermore, the indicator function $\mathbb{1}(z)$ evaluates to 1 if z is true and is 0, otherwise. Figure 3.12b shows the resulting PSR for a CCA threshold of $C = -85$ dBm. If the interferer is sufficiently close to the primary receiver, then the CCA procedure is able to orthogonalize the transmissions. However, if the distance to the interferer is increased, the CCA will eventually become ineffective. With a CCA threshold of $C = -85$ dBm as in the figure, this point is reached at about 135 m. By lowering the CCA threshold, we can move the critical distance farther away. For example, the CCA threshold distance becomes 199 m (292 m, 428 m) with $C = -90$ dBm (-95 dBm, -100 dBm). We observe a severe PSR degradation especially for distances immediately beyond the CCA threshold, which can be mitigated to some extent by lowering the CCA threshold. Nevertheless, the protocol model has a limited reliability when additionally considering the physical impairments.

In slow fading channels, the instantaneous signal power becomes a random variable. It evolves slowly in comparison to the symbol duration, so that deep fades may corrupt multiple consecutive symbols. An *outage* occurs if the system is not able to recover from these error bursts, so that no reliable communication is possible during that time. In slow fading channels, the system performance is dominated by outages. The outage probability $\mathrm{P}_{\mathrm{out}}$ captures the probability that the instantaneous signal power drops below a threshold, so that the performance becomes unacceptable [84].

In the following, the outage probability is our performance metric. Thus, we use the terms non-outage probability and packet success rate (PSR) interchangeably. In particular, we assume that the channel is reciprocal and slowly Rayleigh block-fading. In this case, the instantaneous signal power p_W is exponentially distributed according to the PDF (3.10) with average signal power P_W. Furthermore, the instantaneous fading realization captures the whole frame and it is i.i.d. between frames.

$$f(p_W; P_W) = \frac{1}{P_W} \exp\left(-\frac{p_W}{P_W}\right) \tag{3.10}$$

At the primary receiver, the instantaneous signal strength of both the primary signal as well as the interfering signal is random. In order to keep the analysis tractable, we assume independence between both random processes. Hence, the joint PDF is the product of the individual PDFs, i.e. $f(p_{W1}, p_{W2}; P_{W1}, P_{W2}) = f(p_{W1}; P_{W1}) \cdot f(p_{W2}; P_{W2})$. If the interference channel from the primary receiver to the secondary transmitter is above the CCA threshold, i.e. the instantaneous fading realization is in a way that the received signal strength is above the threshold, the CCA procedure is effective and we have to consider the outage probability of the primary link only. Otherwise, the additional interference power raises the required power level in the outage calculation of the primary link. In summary, we get the following outage probability for a Rayleigh fading channel with CCA and Rayleigh faded interference.

$$\begin{aligned} \mathrm{P}_{\mathrm{out}} = &\int_0^C \int_0^{(N+p_{W2})\gamma_{\mathrm{t}}} f(p_{W1}, p_{W2}; P_{W1}, P_{W2})\, \mathrm{d}p_{W1}\, \mathrm{d}p_{W2} \\ &+ \int_C^\infty \int_0^{N\gamma_{\mathrm{t}}} f(p_{W1}, p_{W2}; P_{W1}, P_{W2})\, \mathrm{d}p_{W1}\, \mathrm{d}p_{W2} \end{aligned} \tag{3.11}$$

Note that (3.11) contains perfect and absent CCA as special cases with $C = 0$ and $C = \infty$, respectively. The latter special case is shown in Figure 3.13a. Figure 3.13 shows the resulting PSR for different CCA thresholds. Interestingly, the degradation of the PSRs is slightly less severe with Rayleigh fading, if we compare Figure 3.13c and Figure 3.12b, for example. Nevertheless, a degradation of the PSR cannot be prevented for some link constellations with reasonable CCA thresholds.

In conclusion, we have illustrated the limitations of CSMA/HBT under the physical model. The accumulative nature of the interference power gives rise to hidden nodes to a certain extent. However, other physical effects like shadowing or multi-slope propagation, which has been empirically observed, may render the degradation less severe

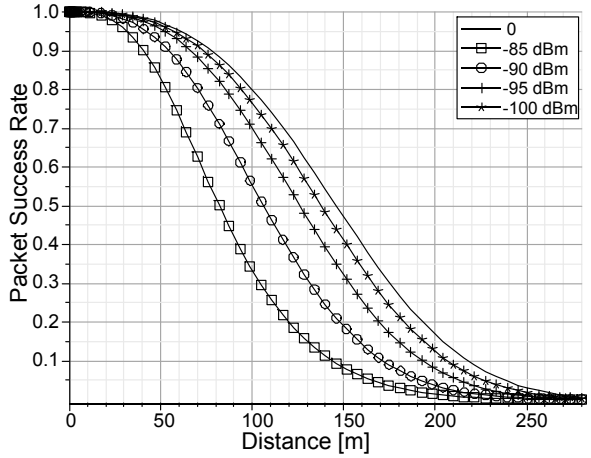

(a) Without CCA: $C = \infty$

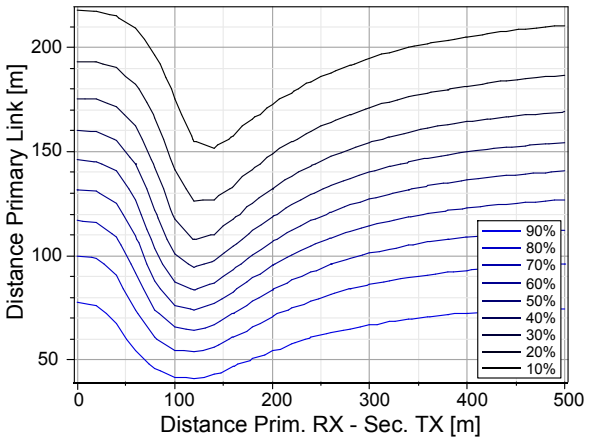

(b) With CCA: $C = -80$ dBm.

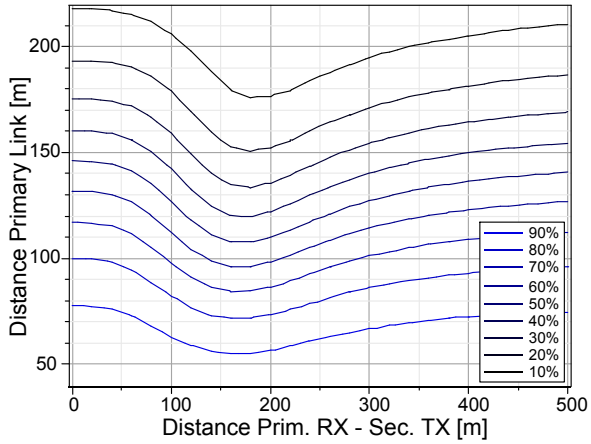

(c) With CCA: $C = -85$ dBm.

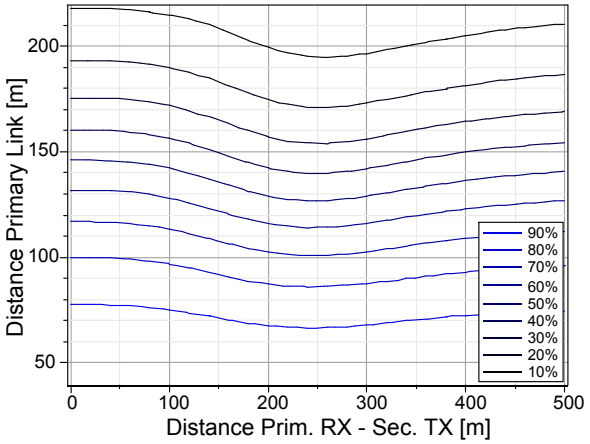

(d) With CCA: $C = -90$ dBm.

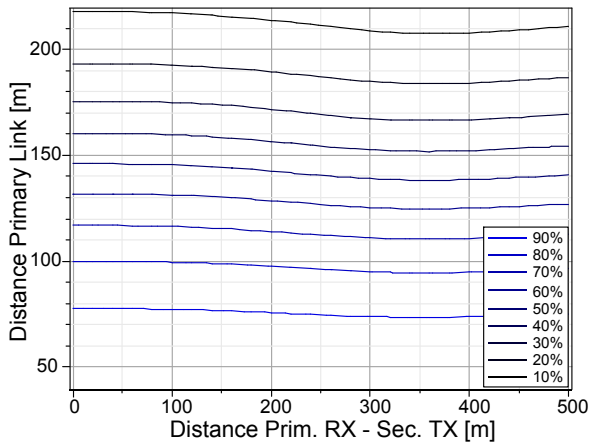

(e) With CCA: $C = -95$ dBm.

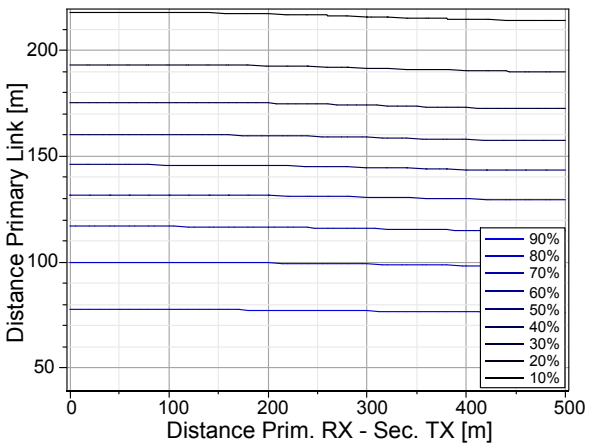

(f) With CCA: $C = -100$ dBm.

Figure 3.13.: Analytic PSR in the Rayleigh fading channel under interference according to (3.11).

[84, 271]. The problem can be mitigated using larger exclusion regions via a higher transmission power for the BTs, which comes at the expense of lower spatial reuse.

In the following, we assume that the PSR is constant and independent from hidden nodes. As we have illustrated above, the assumption does not hold in some cases, and the PSR will degrade. Nevertheless, the nodes conduct PSR measurements, which will capture the effect of hidden nodes, so that they can react to severe degradations. However, we have to face the risk that the system does not approach the most efficient working point or even worse, that the system is not stable. Looking ahead to our evaluation in section 3.6 and section 3.7, we have observed that the risk is low when using a reasonable CCA threshold.

3.4. Optimization Framework

In this section, we derive a cross-layer algorithm for opportunistic routing (OR) in WMNs based on utility-optimal CSMA (UO-CSMA). Before we go into details about the optimization problem, we introduce the concepts of the multi-user gain and the anycast goodput capacity region first.

To start with, let us introduce the notation of *hyperlinks*[2]. A hyperlink is an ordered pair (i, J) of a transmitter $i \in N$ and a non-empty receiver set $J \subset N$ containing receivers $j \in J$. In order to model the anycast transmission, we introduce hyperlinks into the CSMA Markov chain. For example, consider the topology in Figure 3.14a on page 63. In addition to the unicast links $(0, 1)$ and $(0, 2)$, node 0 can select the hyperlink $(0, \{1, 2\})$ for transmission. Hence, the LCG in Figure 3.14b contains another node for the newly introduced hyperlink. However, the properties of a hyperlink are generally different compared to the underlying unicast links in terms of spatial resource consumption and PSR.

In typical WMNs, *unreliable* links of intermediate quality are common [4] and the frame errors are *conditionally independent* across different wireless links [318]. Thus, the anycast transmission can achieve a *multi-user gain*: The probability that the packet transmission succeeds for at least one out of a set of wireless links from the transmitter to multiple candidate receivers is not less than the maximum PSR of the individual unicast links. In particular, let $p_{i,j}$ denote the PSR of the unicast link (i, j), $i, j \in N$. The PSR of the hyperlink (i, J), $i \in N, J \in \mathcal{P}(N)$[3] is defined as follows.

$$p_{i,J} = 1 - \prod_{j \in J} (1 - p_{i,j})$$

In particular, we assume that the frame error process is stationary and i.i.d. in time, which results in a memoryless channel. The memoryless channel is the best case for OR since it has the highest uncertainty about the transmission success. The better the channel can be predicted in advance, the lower the benefits of OR become in comparison to opportunistic scheduling. In the following, we assume that the frame sizes are equal, so that they do not affect the PSRs. If the assumption does not hold for a partic-

[2] We use the terms hyperlink and *anycast link* synonymously.
[3] The notation $\mathcal{P}(.)$ refers to the power set.

ular system, then there are two options: Either the buffered frames are aggregated or reassembled to match the anticipated frame size, or the PSRs have to be estimated per frame size, in addition.

We distinguish between *throughput* q and *goodput* x. The former captures the consumed medium time resources of a hyperlink whereas the latter refers to the rate, at which the data is transported between two neighboring nodes. Hence, the goodput additionally accounts for bit-rates and channel errors. For the anycast link (i, J), we select the bit-rate $R_{i,J}$ that offers the highest goodput according to the estimated PSRs. In particular, we assume that the communication system provides a finite and fixed set of bit-rates. The PSR per link and per bit-rate can be obtained via link probing [62]. We use the qualification $p_{i,J}(R)$ to refer to the PSR of link (i, J) when using bit-rate R. The bit-rate $R_{i,J}$ of link (i, J) is selected as follows, breaking ties arbitrarily.

$$R_{i,J} = \arg\max_{R} p_{i,J}(R) \cdot R \tag{3.12}$$

In addition, we use the shorthand notation $p_{i,J}^{i,K} = p_{i,J}(R_{i,K})$ to refer to the PSR of link (i, J) when using the selected bit-rate of link (i, K). On first sight, it seems counterintuitive to use a bit-rate that has been selected for a different link. As we will see later, a hyperlink needs to be decomposed in order to specify the capacity region.

In a multi-user system, the capacity region is the union of achievable rate vectors under all multi-user transmission strategies [84]. The *capacity region of anycast goodput* or in short, the anycast goodput region, has to consider all multi-user transmission strategies. The goodput $x_{i,j}$ between node i and j can be realized via any hyperlink $q_{i,J}$ with transmitter i and receiver set $J \ni j$ containing node j, which leads to the inner summation in (3.13). Furthermore, the anycast goodput region has to account for *non-innovative* throughput. If multiple candidates have successfully received a packet, then it is innovative for the further forwarder only. It is non-innovative and thus does not generate goodput for all other receivers, since relaying the packet would result in duplication and, hence, it would waste wireless resources. Thus, we have to introduce one constraint for every receiver set J or, in other words, for every anycast link (i, J) in (3.13).

$$\sum_{j \in J} x_{i,j} \leq \sum_{L \in \mathcal{P}(J)} \sum_{K \in \mathcal{P}(N \setminus J)} p_{i,L}^{i,L \cup K} \cdot R_{i,L \cup K} \cdot q_{i,L \cup K}, \quad \forall i \in N, \forall J \in \mathcal{P}(N) \tag{3.13}$$

In general, the number of constraints that are necessary to describe the anycast capacity region is exponential in the number of network nodes. However, we can reduce the amount of constraints to a polynomial number if we apply an upper bound on the maximum number of (simultaneous usable) candidates (cf. section A.4). Furthermore, an upper bound for the number of active constraints[4] is the number of candidates (cf. section A.5). Due to the multi-user gain, the anycast goodput region is a superset of the unicast capacity region.

[4] An inequality constraint is called *active* if it holds with equality at a point [30].

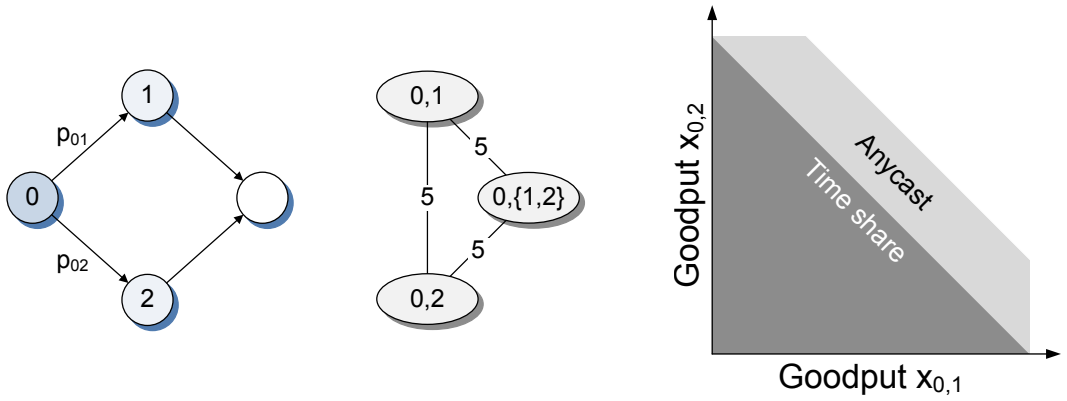

(a) Topology (b) Link conflict graph (c) Goodput region

Figure 3.14.: Scenario: Transmitter 0 with two candidate receivers 1 and 2.

For example, consider the topology in Figure 3.14a. Transmitter 0 may use any non-empty subset of the node set $\{1,2\}$ as candidates. The following constraints describe the anycast goodput region.

$$\begin{aligned} x_{0,1} &\leq p_{0,1}^{0,1} \cdot R_{0,1} \cdot q_{0,1} && + p_{0,1}^{0,\{1,2\}} \cdot R_{0,\{1,2\}} \cdot q_{0,\{1,2\}} \\ x_{0,2} &\leq && p_{0,2}^{0,2} \cdot R_{0,2} \cdot q_{0,2} + p_{0,2}^{0,\{1,2\}} \cdot R_{0,\{1,2\}} \cdot q_{0,\{1,2\}} \\ x_{0,1} + x_{0,2} &\leq p_{0,1}^{0,1} \cdot R_{0,1} \cdot q_{0,1} && + p_{0,2}^{0,2} \cdot R_{0,2} \cdot q_{0,2} + p_{0,\{1,2\}}^{0,\{1,2\}} \cdot R_{0,\{1,2\}} \cdot q_{0,\{1,2\}} \end{aligned}$$

Since the throughput is bounded, it holds $q_{0,1} + q_{0,2} + q_{0,\{1,2\}} \leq 1$. The example illustrates why a second bit-rate index is necessary for the PSRs: The anycast link operates with bit-rate $R_{0,\{1,2\}}$ and thus, the PSR at this bit-rate has to be considered in the second term of the first constraint. Figure 3.14c shows the capacity region for time sharing (dark shade) and anycast (both shades). The anycast link is not used under time sharing ($q_{0,\{1,2\}} = 0$), so that one link can be traded for the other in terms of goodput. With error-prone links, the anycast goodput region is a proper superset of the time share region. However, the multi-user gain changes the shape of the region. Even if the goodput of one link is at its maximum, the other link can achieve goodput. Compared to time sharing, the additional goodput is for free since the first link does not have to make sacrifices. If the system operates at the bound of the anycast capacity region, either one or two constraints are active, depending on whether the working point lies on the intersection of the bounding lines.

3.4.1. Optimization Problem

Given the set of nodes N, the link conflict graph (LCG), the distribution $\boldsymbol{u}$ of the CSMA Markov chain, the PSRs p, the set of flows $f \in F$ and the concave and increasing utility function U, the optimization problem of congestion control, opportunistic routing and CSMA in WMNs is as follows.

$$\max_{\boldsymbol{y},\boldsymbol{x},\boldsymbol{q},\boldsymbol{u}} -\sum_l u_l \log(u_l) + V \sum_f U(y^f) \tag{3.14}$$

$$\text{s.t.} \sum_j x^f_{j,i} + y^f \, \mathbb{1}(\sigma(f) = i) \leq \sum_j x^f_{i,j}, \quad \forall f, i \in N \backslash \delta(f) \tag{3.15}$$

$$\sum_{j \in J} x^f_{i,j} \leq \sum_{L \in \mathcal{P}(J)} \sum_{K \in \mathcal{P}(N \backslash J)} p^{i,L \cup K}_{i,L} \cdot R_{i,L \cup K} \cdot q^f_{i,L \cup K}, \quad \forall f, i, J \tag{3.16}$$

$$0 \leq x^f_{i,j} \quad \forall f, i, j \tag{3.17}$$

$$0 \leq q^f_{i,J} \quad \forall f, i, J \tag{3.18}$$

$$\sum_f q^f_{i,J} \leq \sum_l \delta^2_{l,(i,J)} u_l, \quad \forall i, J \tag{3.19}$$

$$\sum_l u_l = 1, \quad 0 \leq u_l \; \forall l \tag{3.20}$$

The notation $\sigma(f)$ and $\delta(f)$ denotes the source and the destination of flow f, respectively. The indicator function $\mathbb{1}(z)$ evaluates to 1 if z is true and it is 0, otherwise. Our objective is to maximize the sum-utility of all flows. The flow rates are constrained by the flow conservation, anycast goodput region and non-negativity constraints (3.15), (3.16), (3.17) and (3.18). As shown in section A.3, UO-CSMA introduces the constraints (3.19), (3.20) and an entropy term into the objective function (3.14).

Based on the optimization problem (3.14), we have derived Algorithm 1 in the following way. At first, let us relax the constraints (3.15), (3.16) and (3.17) and get the Lagrangian (3.21). The problem separates vertically in its primal variables, and the Lagrangian will get separated into $\mathcal{L} = \mathcal{L}_y + \mathcal{L}_x + \mathcal{L}_{q,u}$ in the following.

$$\begin{aligned} \mathcal{L}(\boldsymbol{y}, \boldsymbol{x}, \boldsymbol{q}, \boldsymbol{u}; \boldsymbol{\alpha}, \boldsymbol{\beta}, \boldsymbol{\gamma}) = & -\sum_l u_l \log(u_l) + V \sum_f U(y^f) \\ & + \sum_{f,i} \alpha^f_i \left(\sum_j x^f_{i,j} - \sum_j x^f_{j,i} - y^f \, \mathbb{1}(\sigma(f) = i) \right) + \sum_{f,i,j} \gamma^f_{i,j} x^f_{i,j} \\ & + \sum_{f,i,J} \beta^f_{i,J} \left(\sum_{L \in \mathcal{P}(J)} \sum_{K \in \mathcal{P}(N \backslash J)} p^{i,L \cup K}_{i,L} \cdot R_{i,L \cup K} \cdot q^f_{i,L \cup K} - \sum_{j \in J} x^f_{i,j} \right) \end{aligned} \tag{3.21}$$

The newly introduced $\boldsymbol{\alpha}$, $\boldsymbol{\beta}$ and $\boldsymbol{\gamma}$ are dual variables for the constraints (3.15), (3.16) and (3.17). Intuitively, a physical meaning may be assigned to $\boldsymbol{\alpha}$ and $\boldsymbol{\beta}$. For incoming traffic, routing is the operation of allocating the packets to outgoing links. Forwarding eventually transports traffic to the next hop(s). Neglecting the superscript f that denotes the flow, a gradient algorithm to solve for $\arg\min_\alpha \mathcal{L}$ is

$$\alpha_i(t+1) = \left[\alpha_i(t) - s_\alpha(t) \left(\sum_j (x'_{i,j}(t) - x'_{j,i}(t)) - y'(t) \, \mathbb{1}(\sigma(f) = i) \right) \right]_+ \tag{3.22}$$

where $s_\alpha(t)$ is a small positive step size, $[.]_+$ denotes the projection onto the nonnegative orthant, and x', y' are the average arrival and service rates, respectively. The

Algorithm 1 Cross-Layer Opportunistic CSMA.

Require: $t_{\text{up}} > 0$ ▷ Update interval
Require: $s > 0$ ▷ Fixed step size

procedure UPDATETA(Link (i, J))
  $f_{i,J} \leftarrow \arg\max_f V^f \sum_{L \in \mathcal{P}(J)} p_{i,L}^{i,J} \sum_{K \in \mathcal{P}(N_i \setminus J)} \beta_{i,L \cup K}^{f}$
  $r_{i,J} \leftarrow R_{i,J} V^{f_{i,J}} \sum_{L \in \mathcal{P}(J)} p_{i,L}^{i,J} \sum_{K \in \mathcal{P}(N_i \setminus J)} \beta_{i,L \cup K}^{f_{i,J}}$
  SETAVGBACKOFF($\exp(-r_{i,J})$) ▷ Adapt CSMA
  SLEEP(t_{up})
  UPDATETA(i, J)
end procedure

procedure UPDATEC(Node i, Flow f)
  $\beta_{i,J}^{f} \leftarrow 0, \forall J$ ▷ Zero otherwise
  $J = [1, \ldots, j] \leftarrow \text{SORT}(C_{N_i}^{f})$ ▷ Least cost neighbors
  $C_i^f \leftarrow \min_{j \in J} C_j^f + TC_i^f$
  for all $j \in J : C_j^f < C_i^f$ **do** ▷ Allocate transmission credits
    $TC_{i,j}^f = \beta_{i,\{1,\ldots,j\}}^{f} \leftarrow \min(C_i^f, C_{j+1}^f) - C_j^f$
  end for
  SLEEP(t_{up})
  UPDATEC(i)
end procedure

procedure UPDATEY(Flow f) ▷ At source of f
  $y^f \leftarrow 1/C_{\sigma(f)}^{f}$
  SLEEP(t_{up})
  UPDATEY(f)
end procedure

Require: $L \subseteq J$ ▷ Receiver set
procedure PACKETFORWARDED(Link (i, J), L)
  $f \leftarrow f_{i,J}, j = \arg\min_{j \in L} C_j^f$
  $TC_i^f \leftarrow TC_i^f - s$
  $TC_j^f \leftarrow TC_j^f + s$
end procedure

procedure PACKETARRIVED(Flow f) ▷ Exogenous arrival
  $TC_{\sigma(f)}^{f} \leftarrow TC_{\sigma(f)}^{f} + s$
  $t \leftarrow \text{EXPRND}(1/y^f)$
  SLEEP(t)
  PACKETARRIVED(f)
end procedure

dynamics of α_i and the queue evolution at node i are very similar [112]. If the start conditions for the queue length and α_i are set to 0, then α_i is proportional to the packet queue. The value of a queued packet with respect to α_i is determined by the step size $s_\alpha(t)$. Similar to Radunović *et al.* [217], we associate one unit of α_i with a *node credit (C)*. Thus, α_i can be regarded as a virtual queue of node credits.

Using similar argumentation, the dynamics of β is given by

$$\beta_{i,J}(t+1) = \left[\beta_{i,J}(t) - s_\beta(t)\left(\sum_{L\in\mathcal{P}(J)}\sum_{K\in\mathcal{P}(N\setminus J)} p_{i,L}^{i,L\cup K} R_{i,L\cup K} q'_{i,L\cup K}(t) - \sum_{j\in J} x'_{i,j}(t)\right)\right]_+ \quad (3.23)$$

In particular, β is the difference between supply and demand of link capacity. Intuitively, if the supply exceeds the demand, it will decrease to zero. In the opposite case, the capacity demand cannot be satisfied and β increases. Thus, it can be interpreted as differential back-pressure, i.e. the number of credits that wait to be served on the considered link. In the following, we use the term *transmission credit (TC)* with β according to the terminology of Radunović *et al.* [217].

In Algorithm 1, both node credits (Cs) and transmission credits (TCs) are used relative to the V parameter in (3.14). In section 3.5, we will highlight the benefits of the relative notation. The dynamics of the TCs can be found on line 23 et seq. of Algorithm 1 and the dynamics of the Cs is derived from the TCs as we will describe in section 3.4.1.

Congestion Control

Separating the flow variables $\boldsymbol{y}$ in the Lagrangian (3.21), we get

$$\mathcal{L}_y(\boldsymbol{y};\boldsymbol{\alpha}) = \sum_f \left(VU(y^f) - \alpha^f_{\sigma(f)} y^f\right).$$

The congestion control problem is to find the flow variables $\boldsymbol{y} = \arg\max \mathcal{L}_y$ that maximize the Lagrangian. For proportional fairness, in particular, the utility function $U(y) = \log(y)$ applies. Solving $\partial\mathcal{L}_y/\partial y^f = 0$ provides us the following solution.

$$y^f = \frac{V}{\alpha^f_{\sigma(f)}} \quad (3.24)$$

Hence, knowing its credits α, each source is able to solve the congestion control problem locally. Remember that C is used relative to V on line 19 of Algorithm 1.

Opportunistic Routing

After some rearranging, we get the partial routing Lagrangian (3.25).

$$\mathcal{L}_x(\boldsymbol{x};\boldsymbol{\alpha},\boldsymbol{\beta},\boldsymbol{\gamma}) = \sum_{f,i,j} x^f_{i,j}\left(\alpha^f_i - \alpha^f_j - \sum_{J\ni j}\beta^f_{i,J} + \gamma^f_{i,j}\right) \quad (3.25)$$

The goodput $x_{i,j}^f$ can be regarded as a dual variable for the Lagrange dual problem (3.26). In particular, we have used the relation $0 \leq \gamma_{i,j}^f$ to derive the lower inequality constraints of the feasibility problem (3.26).

$$\begin{aligned} &\max 0 \\ &\text{s.t. } 0 \leq \alpha_i^f,\ 0 \leq \beta_{i,J}^f \ \ \forall f, i, J \\ &\qquad 0 \geq \alpha_i^f - \alpha_j^f - \sum_{J \ni j} \beta_{i,J}^f \ \ \forall f, i, j \end{aligned} \tag{3.26}$$

At the Karush-Kuhn-Tucker (KKT) points, it holds $\alpha_i^f - \alpha_j^f = \sum_{J \ni j} \beta_{i,J}^f$ if $x_{i,j}^f > 0$ due to complementary slackness [30]. In other words, the credit difference between neighboring nodes can be interpreted as back-pressure. In the next paragraph, we describe how the opportunistic routing layer determines the back-pressure and thus solves the arising system of linear equations.

Let the cumulated transmission credits TC_i^f be the number of *queued packets* of flow f at node i. Routing solves the problem of how the queued packets (or equivalently, the cumulated transmission credits) are allocated to the outgoing links in a way that it holds $TC_i^f = \sum_j TC_{i,j}^f$, where $TC_{i,j}^f$ is the number of queued packets per flow f and link (i, j). Furthermore, let the node credits C_j^f be the *accumulated costs* to route traffic from node j to the destination of flow f, which is zero at the destination itself. Let N_i be the set of neighbors of node i. Knowing TC_i^f, node i solves the routing problem and determines its costs in terms of node credits as follows.

$$TC_{i,j}^f = \begin{cases} C_{j+1}^f - C_j^f, & C_0 \leq \ldots \leq C_j^f \leq C_{j+1}^f \leq \ldots < C_i^f \\ 0, & C_j^f \geq C_i^f \end{cases} \tag{3.27}$$

$$C_i^f = \min_j C_j^f + TC_i^f = \min_j C_j^f + \sum_{j \in N_i} TC_{i,j} \tag{3.28}$$

The approach is straightforward, as shown on line 8 et seq. of Algorithm 1. For flow f, node i sorts its neighbors according to ascending node credits, so that it holds $C_0^f \leq \ldots \leq C_j^f$ WLOG. Node i starts with allocating transmission credits to the least cost neighbor 0 according to (3.27) until the cumulated credits $C_0^f + TC_{i,0}^f$ reach the costs of the neighbor having the next higher credits C_1^f. The sender proceeds in the same way with node 1 and afterwards with the following neighbors. The allocation process terminates when all transmission credits have been allocated, i.e. it holds $TC_i^f = \sum_j TC_{i,j}^f$. The sender determines its costs C_i^f according to (3.28).

After the routing decision, the costs of the transmitter C_i^f in terms of node credits are higher than the costs of any neighbor with transmission credits assigned. Furthermore, all neighbors that will not relay traffic coming from node i do not have lower costs. However, if two neighbors j and k have equal costs and node i assigns transmission credits to them, then only one queue will receive transmission credits, say $TC_{i,j} > 0$,

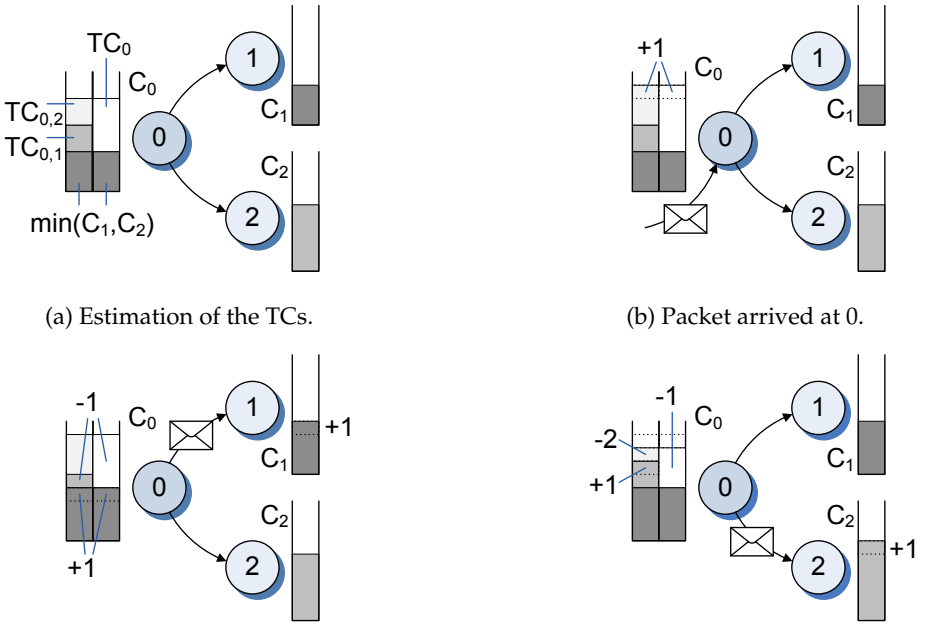

(a) Estimation of the TCs.

(b) Packet arrived at 0.

(c) Packet forwarded from 0 to 1.

(d) Packet forwarded from 0 to 2.

Figure 3.15.: Estimation and evolution of the Cs and the TCs (Step size $s = 1$).

and the other remains empty by design ($TC_{i,k} = 0$). Note that the proposed approach is completely distributed since it involves information from neighboring nodes only. The information can be obtained via periodic link probing or via piggy-backing during the MAC transaction.

The presented approach is based on the idea to reduce the queueing efforts from squared to linear complexity [33, 218], which is also called *floating queues* [186]. A formal justification can be found in section A.6. In the following, we will illustrate the routing decisions using the topology in Figure 3.15. The transmitter 0 starts to allocate TCs to the least cost neighbor, which is node 1 in Figure 3.15a. According to (3.28), the resulting credits of node 0 are $C_0 = C_1 + TC_0$, as shown in the picture. In this example, node 2 is included in the routing decision since it has lower costs ($C_2 < C_0$). Node 0 assigns TCs to both neighbors according to (3.27). We have $TC_{0,1} = \beta_{0,1} = C_2 - C_1$ and $TC_{0,2} = \beta_{0,\{1,2\}} = C_0 - C_2$ and all other βs are zero.

When a packet arrives at node 0 either exogenously or from upstream nodes as shown in Figure 3.15b, we increase the cumulated transmission credits TC_0 at node 0. In this way, the credits C_0 of node 0 increase as well as $TC_{0,2}$, i.e. the transmitter allocates the newly arrived credit to neighbor 2. After a packet has been forwarded to a receiver set J, we determine the receiver with the least costs $j = \arg\min_{j \in J} C_j^f$ from J and transfer one credit from node 0 to j. In particular, the credit is transferred from TC_0 to TC_j, so that C_j increases (cf. line 23 et seq. of Algorithm 1). If the receiver j is the least cost neighbor as shown in Figure 3.15c, then the node credits of the transmitter C_0 remain unchanged since C_1 increases in the same way as TC_0 decreases. Furthermore, the transmitter allocates fewer TCs to neighbor 1 due to its higher costs

($TC_{0,1} = C_2 - C_1$). On the other hand, if the receiver j is not the least cost candidate, the credit dynamics is slightly different as shown in Figure 3.15d. In this case, the node credits of the receiver C_2 increase as before. Nevertheless, the node credits of the transmitter C_0 are reduced at the same time. This means that $TC_{0,1}$ increases, whereas the transmission credits $TC_{0,2}$ of the receiver decrease by two units.

From the practical point of view, it is preferable to upper limit the size of the candidate set. The returns for additional candidates are generally diminishing whereas the costs increase linearly due to the slotted ACK [22]. If the candidate set size is limited to m nodes, then the least cost neighbors are considered up to a number of m only in the routing decision (3.27) and (3.28). All remaining neighbors j having $C_j^f < C_i^f$ are ignored.

CSMA Scheduling

Separating the variables $\boldsymbol{u}$ and $\boldsymbol{q}$ in the Lagrangian (3.21), we get

$$\mathcal{L}_{q,u}(\boldsymbol{q},\boldsymbol{u};\boldsymbol{\beta}) = -\sum_l u_l \log(u_l) + \sum_{f,i,J} R_{i,J} \cdot q_{i,J}^f \left(\sum_{L\in\mathcal{P}(J)} p_{i,L}^{i,J} \sum_{K\in\mathcal{P}(N\setminus J)} \beta_{i,L\cup K}^f \right)$$

subject to constraint (3.18), (3.19) and (3.20). We fix $\boldsymbol{u}$ and $\boldsymbol{\beta}$ in $\mathcal{L}_{q,u}$ and solve for $\boldsymbol{q}$, which corresponds to the following optimization problem.

$$\begin{aligned} &\max_q \sum_{f,i,J} R_{i,J} q_{i,J}^f \left(\sum_{L\in\mathcal{P}(J)} p_{i,L}^{i,J} \sum_{K\in\mathcal{P}(N\setminus J)} \beta_{i,L\cup K}^f \right) \\ &s.t.\ \ 0 \le q_{i,J}^f \quad \forall f,i,J \\ &\qquad \sum_f q_{i,J}^f \le \sum_l \delta_{l,(i,J)}^2 u_l, \quad \forall i,J \end{aligned}$$

The solution to the given problem is to schedule the flow $f_{i,J}$ on the hyperlink (i,J) that maximizes

$$r_{i,J} = R_{i,J} \max_f \left(\sum_{L\in\mathcal{P}(J)} p_{i,L}^{i,J} \sum_{K\in\mathcal{P}(N\setminus J)} \beta_{i,L\cup K}^f \right) \tag{3.29}$$

The throughput $q_{i,J}^f$ of the remaining flows is set to zero. Thus, $\mathcal{L}_{q,u}$ simplifies to

$$\mathcal{L}_{q,u}(\boldsymbol{u}) = -\sum_l u_l \log(u_l) + \sum_{i,J} r_{i,J} \left(\sum_l \delta_{l,(i,J)}^2 u_l \right),$$

subject to the constraint (3.20), i.e. that $\boldsymbol{u}$ is a distribution. The maximum is achieved if $\boldsymbol{u}$ is the stationary distribution of the CSMA Markov chain with TA $r_{i,J}$. Note that node i is able to solve the medium access problem for each of its outgoing links with local information only, as shown on line 1 et seq. of Algorithm 1.

3.5. Design of a Cross-Layer Protocol

In a straightforward realization, the derived cross-layer algorithm on page 65 has several drawbacks. The V parameter in the optimization problem (3.14) determines the working point of the system in terms of throughput efficiency. A higher CSMA efficiency can be approached via larger Vs at the expense of larger TAs and smaller backoffs. As we have illustrated in section 3.3.1, the backoff cannot be arbitrarily decreased for physical and technological reasons. In the following, we design an adaptation mechanism for V that maximizes the CSMA efficiency while operating the TAs in a feasible regime and maintaining proportional fairness among competing flows.

The optimization problem (3.14) considers neither convergence nor end-to-end delay. Theoretical results suggest that UO-CSMA sacrifices delay in order to achieve high throughput with low complexity [285]. From the practical point of view, the tradeoff between throughput and delay should be controlled in order to provide a satisfactory service to the user. A newly started flow should get end-to-end service as soon as possible, whereas a less efficient working point is acceptable. While the flow persists, the system should incrementally increase the throughput efficiency until a working point is reached that offers an appropriate tradeoff between throughput and delay.

The vanilla approach to back-pressure routing is topology-blind. It considers neighboring information only, so that all possible paths have to be taken into account, even if they carry marginal or no traffic at all. On the other hand, each additional path increases the optimality gap with UO-CSMA (cf. section 3.1.2). From the practical point of view, the traffic should be concentrated to the important paths only. In the following, we illustrate how routes can be pre-selected based on topology information.

Throughout this section, we use the following notation in addition to section 1.5.

S	Packet sequence number
C_i^f	Credits of flow f and node i
$TC_{i,j}^f$	Transmission credits of flow f and link (i,j)
V^f	Tradeoff parameter V of flow f
$V_i^{\min}$	Minimum V as overheard by node i
V_i^f	V feedback of flow f at node i
$r_{i,J}^f$	TA of hyperlink (i,J) if flow f would be selected in (3.29)
$r_{\text{opt}}, r_{\min}$	Target and minimum TA
s^f, s_0, s_∞	Step size of flow f; initial and target step size
λ_i^f	Average arrival rate for flow f and node i
$Q_i^f, \hat{Q}_i^f$	Number of packets of flow f queued at node i; upper limit thereof according to the hop-wise delay limit $t_{\max}$
$\hat{Q}_{\min}$	Minimum queue limit
δ	Hysteresis factor
$t_{\text{up}}, t_{\text{hl}}$	Update interval, half-life of the step size adaptation
$f_{\text{r}}, f_{\text{h}}$	Routing and relay count stretch limit

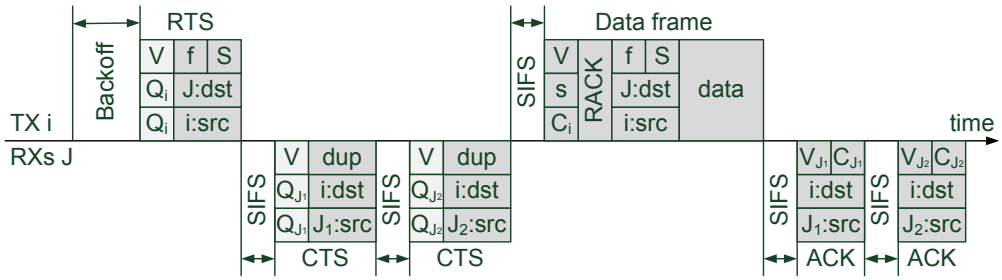

Figure 3.16.: MAC frame format and MAC operation on link (i, J) with two candidates. Lighter shaded fields are intended to be overheard by neighboring nodes and may not have an immediate impact on the MAC operation.

3.5.1. Packet Transition and Forwarder Selection

The field of forwarder selection policies on the MAC layer is well explored (cf. section 3.1.3). We do not intent to design another selection procedure. Instead, we will select an existing one based on the requirements of the presented cross-layer algorithm. According to Algorithm 1, the forwarder having the fewest credits should be selected. The influence of the forwarder selection procedure on the performance results should be as low as possible. Thus, reliability and robustness against coordination errors are the main requirements in our design. On the other hand, the delay of the selection policy is not a primary issue as long as the back-pressure related delays dominate.

According to our cross-layer algorithm, the transmitter should be aware of the selected forwarder. The successful transmission of a packet causes credit transitions as illustrated in section 3.4.1. Without the knowledge of the actual forwarder at the transmitter, the routing decision has to be delayed until new credit information from the downstream nodes arrives. Delayed feedback does not necessarily result in instability. Nevertheless, it may slow down the convergence or raise the variability.

According to Algorithm 1, it is not necessary that the transmitter gets feedback from all candidates that have successfully received the data frame. However, the perceived link qualities for forwarding data traffic may differ from the link probe results due to the hidden node problem, for example. Although it cannot prevent the hidden node problem under physical exclusion, CSMA/HBT reduces the occurrence probability (cf. section 3.3.1). Thus, the forwarder selection procedure should provide reception feedback from all candidates to improve the PSR estimation at the transmitter.

The robust ACK policy according to Zhong *et al.* complies with the specified requirements [309]. The resulting MAC frame format as well as the MAC operation is sketched in Figure 3.16. In particular, the MAC transaction starts with an RTS/CTS exchange according to CSMA/HBT, which is necessary to allocate the spatial resources around transmitter and receiver(s). Only if all CTS frames have been returned and no duplicate would be created, the transmitter initiates transmission of the data frame. The candidate(s) acknowledge the successful reception of the data via ACK frames. Both the CTS and the ACK frames are orthogonalized in time. Thus, the slotted ACK provides the source node with the necessary PSR feedback. The robust ACK works in a way that the transmitter selects the forwarder on the next hop after the slotted

ACK phase. It communicates its decision using the RACK field in a subsequent transmission. Hence, the robust ACK is more robust against communication errors and duplication than the vanilla slotted ACK since it relies on transmitter-based forwarder selection instead of self-selection (cf. section 3.1.3). The additional delay that incurs with the robust ACK approach is acceptable in our case: It coarsely corresponds to an increase of the queue length by one.

3.5.2. Adaption of the Tradeoff Factor V

The throughput efficiency of Algorithm 1 depends on the selection of the tradeoff parameter V in the objective function (3.14). Using a larger V, the source of the flow pumps more aggressively packets into the network resulting in longer queues and higher TAs. Thus, the cross-layer algorithm increases the throughput efficiency at the expense of longer credit queues $\boldsymbol{\alpha}$. With multi-hop routing, there are packet queues on all intermediate nodes. From section 3.4 we know that the back-pressure is expressed in terms of TCs. Hence, reducing V at the source results in smaller node credit queues, so that there are fewer TCs available along the route and the TAs decrease. However, this means that the system approaches a less efficient working point in terms of the flow rate. To verify our intuitions, we have solved the optimization problem (3.14) for the idealized CSMA model and a logarithmic utility function using an optimizer in Maple for a chain of 3 and 7 links.[5] The resulting flow rates and queue lengths are plotted in Figure 3.17. The optimal flow rate of 0.333 is approached in both cases with increasing V. However, the 7-hop flow is less efficient at lower Vs, e.g. at $V = 4$ the flow rates is 0.306 and 0.203 for the 3-hop and the 7-hop flow, respectively. Thus, a fixed V will not meet our design requirements. If it is too high, then the TA of a short flow may exceed the technological limits. On the other hand, the throughput and efficiency of long flows will be low with small Vs.

The tradeoff is also present in the utility gap (cf. section 3.1.2). Let us consider a large network with a (single-path) multi-hop flow of n hops. Since all nodes that are not on the route do not participate in the forwarding process, we can ignore them and focus on the remaining n nodes on the route. The final destination can also be ignored, since it is not involved in the forwarding process. The difference of the achievable and the optimal utility is bounded by $n \log(2)/V$ [112]. The bound on the optimality gap increases linearly in the length of the route.

From the practical point of view, real systems impose upper bounds on the TAs (cf. section 3.3.1). On the one hand, there are physical and technological reasons like the speed of light and the duration of the CCA procedure, which lead to inconsistencies within the channel state between different nodes at the affected time scale. On the other hand, the collision probability of CSMA crucially depends on the number of contenders within the same collision domain. Hence, an upper limit for the TA on each link should be established to accommodate for the above mentioned impairments. In addition, an advanced approach may try to adapt to the instantaneous conditions within the collision domains in order to prevent a collision breakdown in dense networks.

[5] More precisely, we added the term $-3\sum q$ to the objective function in order to realize a minimal TA below zero.

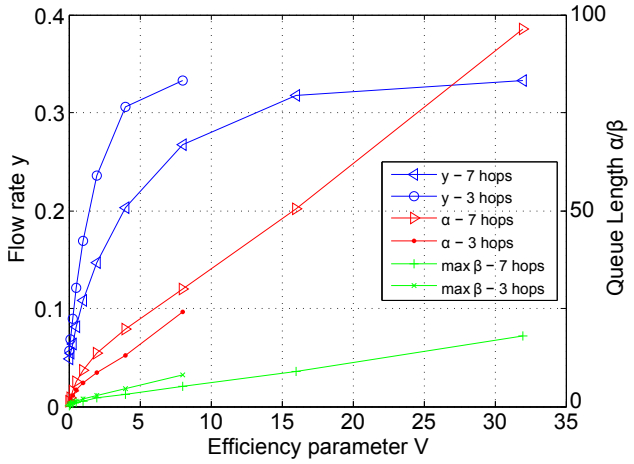

Figure 3.17.: Flow rate and queue length versus the efficiency parameter V for a chain of 3 and 7 links. The results are obtained from numerically solving (3.14) under the idealized CSMA model with error-free links and a minimal TA of -3 per link.

In related work, it is assumed that the requested input rates are supported within the reduced capacity region of the TA-limited UO-CSMA [115, 175]. In particular, if the requested input rates are outside of the TA-limited UO-CSMA capacity region, then we have observed in our simulations that the back-pressure that is not supported accumulates at the bottleneck links. In other words, the bottleneck links become unable to control their queue length via UO-CSMA.

The determination of a working point for the considered tradeoff is a matter of design, of course. However, we argue that fixing the V parameter leads to unexpected working points, which do not efficiently utilize precious resources in scenarios with long routes and few users. A more intuitive working point would be to provide proportional fairness and the highest throughput efficiency while ensuring that the TAs do not exceed their technological limits. Both objectives can be achieved using a combination of *intra-flow* and *inter-flow adaptation* of the V parameter, as we will illustrate in the following.

Achieving High Throughput Efficiency with Limited TAs

The so-called *intra-flow adaptation* of the parameter V ensures that the TAs per link remain feasible while maintaining a high throughput efficiency. In particular, we embed an end-to-end feedback loop into the forwarding process. Our objective is to *upper limit the aggregated TA per flow and node*. The intra-flow adaptation works as follows. Each node determines its aggregated TA per flow across all outgoing links and estimates its preferred value of V_i^f. It feeds back the estimate V_i^f in the upstream direction, e.g. via the ACK or piggy-backed via data packets. During the upstream feedback, the minimum is estimated, which eventually arrives at the source of the flow. The source takes the feedback as input, and adapts the efficiency parameter V^f of the flow accordingly. As shown in Figure 3.16, both the feedback V_i^f and the adapted value V^f can be propagated during the MAC transaction. The intra-flow adaptation is summarized in Algorithm 2.

Algorithm 2 Intra-Flow Efficiency Adaptation.

procedure FEEDBACKUPSTREAM(Flow f, Node i)
  $r_{\text{sum}} \leftarrow \log \sum_J \exp r_{i,J}^f$ ▷ Aggregated TA per flow
  $V_i^f \leftarrow V^f \dfrac{r_{\text{opt}} - r_{\min}}{r_{\text{sum}} - r_{\min}}$ ▷ Estimate feedback
  for all $j \in N_{\text{DS}}^f(i)$ **do** ▷ Downstream neighbors
    $V_i^f \leftarrow \min(V_i^f, \text{FEEDBACKUPSTREAM}(f, j))$
  end for
  return V_i^f
end procedure

Require: $\gamma \in (0, 1)$ ▷ EWMA smoothing factor
procedure ADAPTEFFICIENCY(Flow f) ▷ At the source node $\sigma(f)$ of f
  $V^f \leftarrow (1-\gamma)V^f + \gamma\text{FEEDBACKUPSTREAM}(f, \sigma(f))$
  PROPAGATEDOWNSTREAM$(f, \sigma(f), V^f)$
end procedure

procedure PROPAGATEDOWNSTREAM(Flow f, Node i, V)
  $C_i^f \leftarrow C_i^f \cdot V / V^f$ ▷ Adapt credits
  for all j **do**
    $TC_{i,j}^f \leftarrow TC_{i,j}^f \cdot V / V^f$ ▷ Adapt transmission credits
  end for
  for all $j \in N_{\text{DS}}^f(i)$ **do** ▷ Downstream neighbors
    PROPAGATEDOWNSTREAM(f, j, V)
  end for
  $V^f \leftarrow V$
end procedure

We are using a model predictive approach for the estimation of the preferred feedback value V_i^f. As shown in Figure 3.17, the queue length at the source increases with V. In the regime of small Vs, the increase in the queue length is steep. As an interpretation, it can be seen as overcoming the entropy of the CSMA Markov chain. Afterwards, the slope decreases and becomes almost constant in the high efficiency regime. In other words, the queue becomes proportional to V. Considering the congestion control (3.24) on page 66, we observe that the relation between V and C approaches proportionality the closer the flow rate gets to its optimum. As a simplification, we assume that the flow already operates in the high efficiency regime and proportionality between the credit queue C and the parameter V holds. At each node, we estimate the feedback value V_i^f that meets the aggregated TA target r_{opt}. During the upstream feedback, the minimum across all feedback values is estimated. Hence, the feedback value $V_{\sigma(f)}^f$ that arrives at the source of flow f characterizes the bottleneck link(s), i.e. the links exposing the highest TA along the route. During the update process, we filter our estimate of V using an EWMA to smooth the convergence.

For proportional fairness, the estimation of the optimal V is as follows. In the high efficiency regime, the flow rate y is (near) maximal and (almost) fixed so that V is proportional to the queue length C at the source. As shown in Figure 3.17, any additional packet ingress will accumulate at the bottleneck links, thereby increasing their TAs approximately proportional to V. Thus, our new estimate for the efficiency parameter is $V_i^f(t+1) = (r_{\text{opt}} - r_{\min})/(r_{\text{sum}} - r_{\min})V^f(t)$ as shown on line 3 of Algorithm 2, where r_{opt} is the target TA and r_{sum} is the aggregated TA per node and flow.

On adapting V, the packet influx into the system is regulated, which will be reflected in the credit queues. However, the convergence of the credits will take some time. Furthermore, the response time may vary with the length of the routes and the number of involved nodes. In order to minimize the response time, we adapt the credit queues along all paths according to V as shown on line 14 et seq. of Algorithm 2. In this way, the association between packets and credits becomes weakened, as we will point out in the next section.

For both the 3-hop and the 7-hop scenario, we have conducted high level simulations using MATLAB in order to demonstrate the effectiveness of our approach. The results are shown in Figure 3.18. We observe that the system converges into a small neighborhood of the optimum, for which the TAs are at the technological limit. Solving the optimization numerically yields slightly larger Vs of 4.7 and 7.9 for the short and long flow, respectively. We have observed that this loss of efficiency is related to the step size of the TA updates. In particular, the burstiness of the packet dynamics is independent of the step size. On the other hand, smaller step sizes lead to longer queues, since more packets have to be enqueued to achieve the same TA level. Hence, the overall variability of the C and TC queues decreases with smaller step sizes, so that the accuracy of the estimated V increases. We consider the step size in more detail in section 3.5.3.

Furthermore, we observe that the credit queues do not fill evenly across the transmitters along the route. With 7 links, for example, the queue of the first link is filled first, and only afterwards the downstream queues fill one by one. As shown in Figure 3.18f, it takes about 5 s until the throughput on the seventh link reaches its operation point. The convergence time depends among others on the step size, and we will consider this point in more detail in the section section 3.5.3.

Enforcing Proportional Fairness

In the vanilla UO-CSMA [112], each link is able to increase its TA at any time in order to take its fair share of the wireless resources. Thus, if a transmitter experiences unfairness, it can resolve this situation locally by taking the appropriate actions itself. However, the effectiveness of this approach is limited in our case due to the technologically limited TAs. Hence, instead of increasing the TA on the affected links, the TAs of the competing links have to be decreased, which requires cooperation between all involved flows. In the following, we propose an *inter-flow adaptation* approach in order to meet the specified objective.

In the previous section, we have shown how to adapt the parameter V in order to find a working point where the TAs at the bottleneck are at the technological limit. If flows that compete with each other use different V parameters, however, they achieve

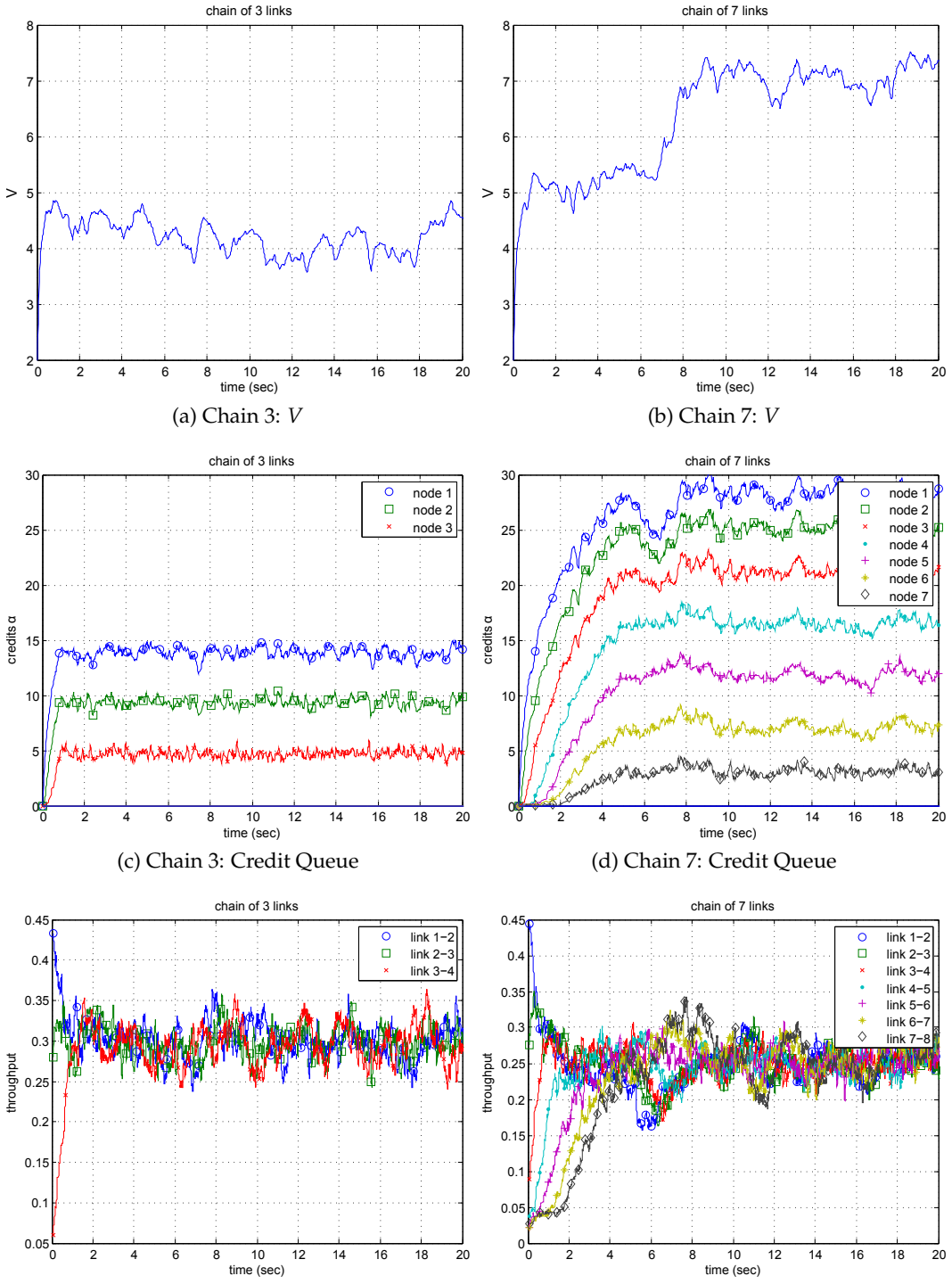

(a) Chain 3: V (b) Chain 7: V

(c) Chain 3: Credit Queue (d) Chain 7: Credit Queue

(e) Chain 3: Throughput (1 s moving average) (f) Chain 7: Throughput (1 s moving average)

Figure 3.18.: Simulation results for a chain of 3 and 7 error-free link under the extended CSMA model. The PHY and MAC layer properties are chosen according to IEEE 802.11g operating at 6 Mbps. ($r_{\text{opt}} = 2$, $r_{\min} = -3$, $s = 20$ packets/credit, EWMA $\gamma = 0.1$, $t_{\text{up}} = 20$ ms).

the so-called weighted instead of unweighted proportional fairness [134]. We conclude that the V parameters of different flows should be equal if the flows share resources in the WMN. Competing flows can be identified by monitoring the wireless medium. In particular, if a network node carries traffic for the flow f_1, either as transmitter, relay or receiver, and it observes data or signaling frames belonging to a different flow f_2, then it identifies f_2 as a competitor to f_1. It is to note that there is a tradeoff between accuracy and efficiency in a multi bit-rate environment. With using AMC for data and signaling frames, the MAC transaction becomes more efficient. However, the competition between flows may not be recognized due to the higher SNR requirements, which may render the decoding of overheard signaling frames impossible.

Algorithm 3 Inter-Flow Fairness Adaptation.

1: **procedure** PROMICRECEIVED(Packet p, Node i)
2: $V_i^{\min} \leftarrow \min(V_i^{\min}, p.V)$ ▷ +Timeout for aged entries
3: **end procedure**

Require: $\delta > 1$ ▷ Hysteresis factor
4: **procedure** FEEDBACKUPSTREAM(Flow f, Node i)
5: ... ▷ As in Algorithm 2
6: **return** $\min(V_i^f, \delta \cdot V_i^{\min})$
7: **end procedure**

On overhearing one of the signaling or data frames depicted in Figure 3.16 on page 71, a network node i extracts and stores the V parameter of competing flows. It determines the minimum among them $V_i^{\min}$ as shown on line 2 of Algorithm 3. In turn, it determines whether its local flow(s) $f \in F(i)$ are *technologically* or *fairness limited*. In the former case, it proceeds as lined out in the previous section. Otherwise, its anticipated feedback V_i^f exceeds the minimal V of the competing flows $V_i^{\min}$, so that it would unfairly take wireless resources away from its competitors. Hence, node i adapts its feedback V_i^f according to $V_i^{\min}$ as shown on line 6 of Algorithm 3, so that proportional fairness is enforced between the involved flows.

The proposed approach introduces a form of global coupling between competing flows due to the transitivity. In particular, a problem arises that is similar to starvation in scheduling problems. For example, let us consider two competing flows. The first one is technologically and the other is fairness limited. The system will adapt the V parameter of the second flow according to the first one's V. After the convergence, however, the technologically limited flow will become fairness limited as soon as it increases its V parameter. Hence, it will become impossible for both flows to increase their V parameters regardless whether the throughput efficiency is unnecessarily low.

We address this problem in the following way. A flow is considered fairness limited only if it exceeds the V parameter of competing flows by more than a fixed hysteresis factor $\delta > 1$. In the example above, both flows are now allowed to increase their Vs up to a ratio of δ over the other one's V, so that one of them will eventually reach its technological limit. The downside is that the other flow may still increase its V over the now technological limited flow by the given factor δ, so that the resulting flow rates are

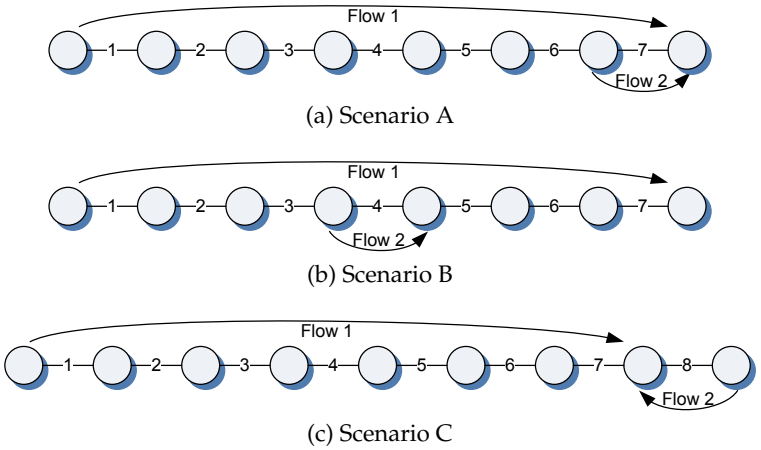

Figure 3.19.: Scenarios A-C. All links are considered error-free.

generally not proportional fair. The deviation from proportional fairness increases with δ. For reasonable small δs, we have observed that the inter-flow adaptation remains effective while the deviation from proportional fairness is small.

For the scenarios in Figure 3.19, we have conducted high level simulations in MATLAB to demonstrate the effectiveness of the inter-flow adaptation. The setup is identical to the simulations presented in Figure 3.18 except that we have given the system 30 s to settle. The results in Table 3.4 are averages over the following 30 s. All scenarios consist of two flows having seven hops and a single hop, respectively. However, they differ in the way the flows interact with each other. In scenario A and B, they share a wireless link at different positions. In scenario C, there is no shared link. Instead, certain links of both flows are within the same collision domains and compete for wireless resources. For comparison, the PF rates achievable with MWS are $(y_1, y_2) = (0.166, 0.5)$ in scenario A and B and $(0.25, 0.5)$ in scenario C. In the idealized CSMA model, we have analytically estimated the parameters V, for which the bottleneck TA matches the target value. The simulated flow rates match the analytical results within reasonable accuracy. Without inter-flow adaptation, the resulting rates deviate from proportional fairness (PF), which can be seen in Table 3.4 in the rows *WPF*. We have observed that the longer flow benefits in this situation, in particular, due to its longer response time of the feedback loop.

3.5.3. Convergence Period and Queueing Delays

In the previous sections, we have focused on the operating point of the system and its properties. Now, we will consider the convergence process to reach the operating point. With convergence period, we refer to the duration from the start of the flow until it reaches its operating point within a small proximity. We have already mentioned the problem of the *delayed start* (cf. Figure 3.18). During the convergence period, the incoming packets are used to fill the queues first, so that the associated TAs are raised to the target level. The queues do not fill evenly but one after another. Thus, the system cannot achieve end-to-end throughput until a queue on the last hop has sufficiently

Scenario	Method	Fairness	V^1	y_1	V^2	y_2
A	Analytic		2.58	0.133	2.58	0.515
	Simulation	PF	2.5	0.136	2.5	0.519
	Simulation	WPF	4.9	0.200	1.8	0.375
B	Analytic		2.26	0.118	2.26	0.451
	Simulation	PF	2.3	0.122	2.3	0.462
	Simulation	WPF	5.0	0.205	1.0	0.198
C	Analytic		3.01	0.158	3.01	0.602
	Simulation	PF	3.0	0.163	3.0	0.611
	Simulation	WPF	5.0	0.205	2.6	0.528

Table 3.4.: Inter-flow fairness adaptation in the scenarios A-C in Figure 3.19. In contrast to the fairness model *PF*, we turned off the inter-flow adaptation with *WPF*. The methods *Analytic* and *Simulation* refer to analytical results in Maple (for the idealized CSMA model) and simulations in MATLAB, respectively.

filled. For example, it takes 5 s for the flow in Figure 3.18f to approximately achieve its target service level. On the other hand, *queueing delay* is an inherent problem in back-pressure routing. In the scenario of Figure 3.18, for example, we have assigned one credit to 20 packets. Thus, the system enqueues about 300 (600) packets at its operating point in the 3 (7) link scenario, which leads to excessive queueing delays.

In this section, we address the delayed start problem and the queueing delay from the practical point of view. As our first objective, the system should provide service in terms of end-to-end throughput as soon as possible, whereas the throughput efficiency may be lower at the initial starting point. During the convergence period, the system should incrementally improve its efficiency until it approaches its final operating point. The rationale is as follows. Traffic flows can be coarsely divided into short and long-lived flows that originate, for example, from interactive web browsing and FTP file download, respectively. From a user's point of view, the reactivity becomes more important for short-lived flows whereas the lower throughput efficiency is more likely to be tolerated. However, the classification of newly arriving flows into short and long-living is generally not possible. Thus, an adaptive strategy that classifies and treats flows according to their age should offer an acceptable tradeoff between reactivity and efficiency. Furthermore, the system should avoid excessive queueing that results in large end-to-end delays. In Figure 3.18, we have observed that the temporal variability of the credit queues is small after convergence. The system builds up queues mainly to generate back-pressure, and the risk of draining the queues below a certain level is small. Hence, our objective is to reduce the queueing efforts to a level of practical relevance.

We address both problems by decoupling the physical packet queues from the credit queues as suggested by Jiang *et al.* [111]. We propose an algorithm that handles the above-mentioned problems and reduces the end-to-end delays to a level of practical relevance. With a constant step size s, one credit can be associated with a fixed number of packets according to Algorithm 1. In other words, the packet and credit queues are proportional. With an adaptive step size, the physical and the credit queues gener-

ally evolve differently. When starting with a large step size, a coarse neighborhood of the target operating point is located in shorter time, and the system incrementally improves it by reducing the step size. Furthermore, the queueing delay can be reduced by limiting the amount of in-flight packets in the network. In the following, we consider both approaches in detail.

Providing Service during Convergence

The step size s in (3.22) and (3.23) on page 64 expresses the value of a packet in terms of credits. The step size controls the tradeoff between convergence speed and variability at the operating point. With a smaller step size, the convergence is slower but the credit queues vary less. We use the *interquartile range (IQR)* to measure the variation of the credit queues after convergence. Furthermore, we define the *convergence time* t_c as the duration from the start of the flow until the credit queue $C^f_{\sigma(f)}$ at the source of the flow exceeds the first quartile of the credit queue distribution in steady state. For the 7 link chain considered in Figure 3.18, we have determined the variability and convergence time for several step sizes s in Table 3.5 through high level simulations.

Step size s	V	y	C_1	IQR C_1	t_c [s]
0.50	5.05	0.215	23.6	4.11	0.45
0.10	6.77	0.247	27.4	1.55	1.95
0.05	7.07	0.253	27.9	1.10	5.40
0.01	7.46	0.256	29.1	0.55	25.9

Table 3.5.: Convergence time t_c and variability (interquartile range) of the credit queue C_1 for a chain of 7 links for several step sizes s, as observed in MATLAB simulations. The presented values of the V parameter, the flow rate y and the credits C_1 are 30 s averages taken after convergence.

In the design of an algorithm for the adaptation of the step size s^f per flow, we have to consider the initial and the target step size, the adaptation rate and the way the changes are propagated through the network. The algorithm is summarized in Algorithm 4, and we will discuss the details in the following. For the initial step size s_0, we have to take two observations into account. At first, the TAs grow in relation to the bit-rate of the underlying links according to (3.29) on page 69. An initial value that is designed for a low bit-rate may not be appropriate for higher bit-rates. Thus, the initial step size should depend on the bit-rate of the involved links. Since multiple different bit-rates may be involved, the initial step size should be node dependent. On first sight, a link dependent initial value may seem more natural, since bit-rates are associated with links instead of nodes. However, the step size is used to update the credit queues when a packet arrives, whereas the association to outgoing links is done afterwards within the routing decision (cf. Algorithm 1 on page 65).

The V parameter may vary rapidly during convergence, and these changes quickly propagate. In simulations with long flows, for example, we have observed that the convergence slows down with the distance from the source of the flow. The relative step size of downstream nodes that are involved by the flow a little later may be dif-

Algorithm 4 Step Size Adaptation.

Require: $R_{\text{base}} > 0$ ▷ Technologically lowest bit-rate
Require: $s^f = s_0 > 0$ ▷ Initial step size w.r.t. R_{base}
Require: $s_\infty > 0$ ▷ Target step size relative to 1 credit
Require: $t_{\text{up}} > 0$ ▷ Update interval
Require: $t_{\text{hl}} > 0$ ▷ Half-life of the step size

1: **procedure** UPDATESTEPSIZE(Flow f) ▷ At the source $\sigma(f)$ of f
2: $s^f_\infty \leftarrow C^f_{\sigma(f)} \cdot s_\infty$
3: $s^f \leftarrow s^f_\infty + (s^f - s^f_\infty) \cdot 2^{-t_{\text{up}}/t_{\text{hl}}}$
4: SLEEP(t_{up})
5: UPDATESTEPSIZE(f)
6: **end procedure**

7: **procedure** PACKETARRIVAL(Flow f, Packet p) ▷ At the source $\sigma(f)$ of f
8: $p.s \leftarrow s^f$
9: PACKETRECEIVED($f, p, \sigma(f)$)
10: **end procedure**

11: **procedure** PACKETRECEIVED(Flow f, Packet p, Receiver j)
12: $R \leftarrow \max(R_{j,k}), \forall k \in N^f_{\text{DS}}(j)$ ▷ Downstream neighbors
13: $C^f_j \leftarrow C^f_j + p.s \cdot R_{\text{base}}/R$
14: $TC^f_j \leftarrow TC^f_j + p.s \cdot R_{\text{base}}/R$
15: **end procedure**

16: **procedure** PACKETTRANSMITTED(Flow f, Packet p, Transmitter i)
17: $R \leftarrow \max(R_{i,k}), \forall k \in N^f_{\text{DS}}(i)$ ▷ Downstream neighbors
18: $C^f_i \leftarrow C^f_i - p.s \cdot R_{\text{base}}/R$
19: $TC^f_i \leftarrow TC^f_i - p.s \cdot R_{\text{base}}/R$
20: **end procedure**

ferent from upstream nodes because the credit queues C are scaled according to V in the intra-flow efficiency adaptation (cf. section 3.5.2). As shown in Figure 3.18b, the parameter V quickly increases at the source in the scenario with long flows, so that the initial step size for the transmitter on the last hop is smaller compared to its upstream nodes, which explains the slowdown of the convergence. Thus, the initial step size should be used relative to V.

In consideration of the specified design goals above, the source node of a flow f maintains the *current step size* s^f, which is initialized with an empirical value s_0 that has been determined for the technologically lowest bit-rate R_{base}. When a packet arrives exogenously, the source node embeds its current step size s^f into the packet as shown in Figure 3.16 on page 71. Thus, the value of a packet in terms of credits is readily available whenever a packet enters or leaves a node. In either case, the node and

transmission credits are updated according to the embedded step size that is down-scaled according to the maximal bit-rate among its downstream links as shown on line 13 et seq. and line 18 et seq. of Algorithm 4. Furthermore, the credit update is independent from the current parameter V, since the node and transmission credit queues are independent from V.

The *target step size* s_∞^f determines the operating point after convergence in terms of step size. Thus, it affects both the reactivity and the variability after convergence. Environmental changes like newly arriving flows or node and link breakdowns may alter the operating point for the considered flow. The duration of the necessary re-convergence process mainly depends on the number of packets necessary to drive the credit queues to their new value. In that case, a high reactivity is desirable. However, it comes at the expense of higher variability at the operating point. An advanced approach may solve this tradeoff by detecting and reacting on changes, e.g. it enlarges the step size if another operating point should be approached. However, our intention is to verify the effectiveness of the step size adaptation in the initial convergence period. Using an appropriate means of change detection, it is straightforward to extend our approach to the re-convergence case.

Nevertheless, it is not sufficient to use a common target step size for all flows across the network. For example, let us consider two competing flows. The first flow achieves significantly higher throughput than the second, because it uses higher bit-rates, for example. Hence, the credit queue $C^1_{\sigma(1)}$ of the first flow is smaller compared to $C^2_{\sigma(2)}$ according to (3.24) on page 66 under the assumption of equal Vs. A common target step size for both flows would result in a higher variability for the first flow. Thus, a common target step size is not able to provide equal variability across all flows. We introduce a flow rate dependent target step size s_∞^f. As shown on line 2 of Algorithm 4, it is determined as product of an empirical determined relative target step size s_∞ and the credits at the flow source $C^f_{\sigma(f)}$. In the update the current step size s^f on line 3 of Algorithm 4, we are using an exponential decay determined by a given half-live t_{hl}. The step size adaptation proceeds in fixed update intervals t_{up}.

Back-Pressure with Reduced End-To-End Delays

So far, our focus has been throughput efficiency, and it remains our main objective throughout this chapter. However, an inherent problem in back-pressure based routing is the end-to-end delay. In this section, we illustrate how the delays can be reduced to a level of practical relevance at the expense of throughput efficiency.

The causes of end-to-end delay are manifold. The actual radio transmission as well as the acknowledgement and forwarder selection process consumes medium time. On the other hand, the back-pressure routing introduces further delay. The links have to generate back-pressure for scheduling purposes, which results in queueing delay for the involved packets. In addition, the objective of UO-CSMA is utility maximization. The minimization of resource usage or delay is not considered. For example, in the local perspective of back-pressure routing, two different paths that offer the same throughput are considered equal regardless whether one of them is substantially longer and has higher resource consumptions. In the following, we will focus on the

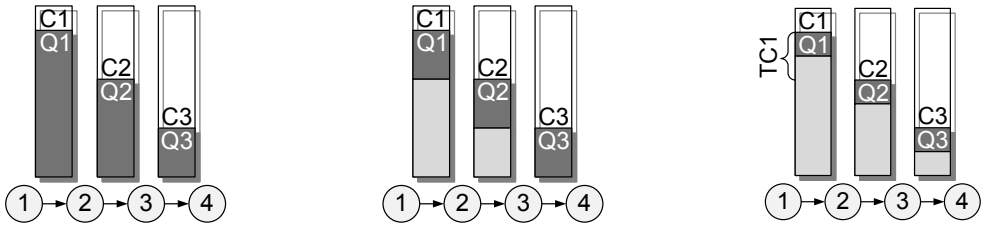

(a) Vanilla back-pressure. (b) According to Horizon [218]. (c) Proposed approach.

Figure 3.20.: Physical queues (in dark gray) and virtual queues (also called shadow queues, in light gray) for a chain topology with 3 link and a single flow.

delays caused by back-pressure scheduling and discuss routing related issues in section 3.5.5. Note that the robust ACK scheme presented in section 3.5.1 can be seen as an enlargement of the link queues by one hidden space. Thus, its contribution to the end-to-end delay is covered within the following discussion.

Related Work. In section 3.4.1, we have already introduced the *Horizon* queue design that reduces the scheduling delays [218]. In back-pressure routing, the differential back-log between two nodes is used for scheduling purposes. In order to provide positive back-log, the queues have to grow with increasing distance from the destination. (cf. Figure 3.20a). In general, a node has to generate a sufficient amount of back-pressure before it is allowed to generate throughput, and the associated threshold increases with the distance from the destination. The amount of queued packets per flow in the network can be reduced if the physical queue is replaced up to the threshold by shadow queues, which are counters only (cf. Figure 3.20b). In particular, the growth of the queues is reduced from squared to linear efforts in the number of hops [33].

In section 3.1.2, we have already discussed the characteristic throughput-delay-complexity tradeoff of MWS. In order to limit the end-to-end delay of UO-CSMA, we have to sacrifice throughput. Nevertheless, the precise delay characterization of MWS in wireless multi-hop networks with general interference constraints is still an open problem [85, 86, 285]. Neely *et al.* characterize the tradeoff between utility and end-to-end delay for NUM problems [78, 190, 192]. Given the control parameter V[6], they present an algorithm that achieves a total network utility within $O(1/V)$ of the optimum while the average network delay is within $O(\log V)$, which is the best possible tradeoff [190]. However, the stochastic upper bounds are order results, and they may be of limited value in characterizing real systems. Large-deviations analysis is an alternative approach, which tries to estimate the probability of queue overflows. Interestingly, Venkataramanan *et al.* have observed that a modified back-log that favors links closer to the destination may lead to lower end-to-end delays [269]. Furthermore, Gupta *et al.* propose to analyze a reduced system capturing the bottlenecks only [85, 86]. They derive a lower bound on the end-to-end delay and propose a modification of the back-log definition similar to Venkataramanan *et al.*. The heavy traffic approximation is another

[6]Our parameter V from section 3.5.2 is comparable to Neely's V. However, it is important to remember that CSMA imposes technological limits on V in our case.

approach to address network delay. Using this approach, Yi *et al.* provide an exact characterization of the average delay [289].

As lined out in [189, 192], Little's law is useful in deriving bounds on the network delay. For a stable system, Little's law can be stated as

$$L = \lambda \cdot W,$$

where L, λ and W are the average queue length, arrival rate and delay, respectively [18].

Bounded End-To-End Delay. According to Little's law, the average delay for each path from source to destination can be bounded above by controlling the number of in-flight packets in relation to the achieved rate on the path. In a straightforward realization, the source may keep track of the number of in-flight packets and limit the packet ingress accordingly. However, the actual aggregated queue length across all nodes is volatile in relation the time necessary for the feedback. Furthermore, the approach will be unable to control the delays across different routing paths if the source is involved only.

We favor a distributed solution, in which *each* transmitter dynamically determines an *upper limit* $\hat{Q}$ *for its queue* Q. As shown on line 2 of Algorithm 5, the queue limit $\hat{Q}$ is estimated using the average arrival rate λ_i^f and a predetermined upper limit for the per-hop delay $t_{\max}$. Thus, the physical queues Q_i^f per flow and node have a lower and an upper limit $0 \dots \hat{Q}_i^f$, so that the amount of physical packets per hop remains small (cf. Figure 3.20c). We estimate the arrival rate λ_i^f using an EWMA rate estimator. Furthermore, we have introduced a lower limit for the per-hop queues $\hat{Q}_{\min}$ in Algorithm 5 to ensure that the node remains operational.

The relay nodes exchange the queue size information Q and limits $\hat{Q}$ within their neighborhood, so that upstream transmitters are aware of the queue utilization of potential relays. As shown in Figure 3.16 on page 71, we put this information into the RTS and the CTS frames. Neighboring nodes can extract the necessary information on overhearing them. Furthermore, a timeout mechanism takes care that this information is periodically propagated even if the considered node has not accessed the medium for a longer period of time, so that possible stalls are resolved. In the best case, the backpressure should primarily be generated in the virtual queues C_i^f, and the remaining physical queue space Q_i^f should account for all variations due to the underlying network dynamics. However, we have to sacrifice throughput efficiency if the network dynamics cannot be outweighed via the remaining physical queue.

Dummy and Virtual Transmissions. According to Jiang *et al.*, the delays can be reduced by injecting slightly more (virtual) credits than (physical) packets [111]. In this way, the actual arrival rate of physical packets becomes smaller than the (physical) service rate of the link, so that the (physical) queues tend to zero. However, the saturation assumption is violated due to the decoupling of the packet and credit queues. If the queue is empty when a TXOP is started, it is suggested to sends *dummy packets* that alter the credits C only while the packet queues Q remain unchanged [33, 111, 189].

Algorithm 5 Delay Limiting.

Require: $t_{\max} > 0$ ▷ Hop-wise delay limit
Require: $\hat{Q}_{\min} > 0$ ▷ Min. queue limit

procedure UPDATEQUEUELIMIT(Flow f, Node i, Arrival rate λ_i^f)
  $\hat{Q}_i^f \leftarrow \max(\hat{Q}_{\min}, \lambda_i^f \cdot t_{\max})$ ▷ According to Little's law
end procedure

procedure PACKETARRIVAL(Flow f, Packet p) ▷ At the source $\sigma(f)$ of f
  if $Q_{\sigma(f)}^f >= \hat{Q}_{\sigma(f)}^f$ **then**
    $p \leftarrow \emptyset$ ▷ Drop incoming packet
  end if
  PACKETRECEIVED$(f, p, \sigma(f))$
end procedure

procedure BACKOFFEXPIRED(Flow f, Node i, Link l)
  if $0 = Q_i^f$ **or** $\exists Q_j^f >= \hat{Q}_j^f, \forall j \in l$.dst **then** ▷ Receiver set l.dst
    VIRTUALTRANSMIT(f, i, l) ▷ Physical queue length Q
  else
    TRANSMIT(f, i, l)
  end if
end procedure

The credit transition within dummy packets is important for the convergence of the CSMA Markov chain because it conserves the relationship between the TAs and the consumed medium time. If the transmitter would remain idle instead until its queue gets non-empty again, the TAs become unable to control the node's throughput. The dimensioning of the injection rate of additional credits is difficult. If it is small, the delays still remain substantial. On the other hand, the throughput seriously suffers if it is large. Our delay limiting algorithm mitigates the dimensioning problem. The queue limits are adapted according to the specified delay targets, and the injection rate of additional credits is calculated implicitly.

Empirically, we have observed that *virtual transmissions* are able to mitigate dummy packets to a large extend while preserving the stability as well as enhancing the throughput efficiency. In contrast to dummy packets, a virtual transmission is not a physical radio transmission that consumes wireless resources. Instead, the sender simulates the transmission: After contention for a TXOP, it enters the transmission state without actually accessing the wireless medium and remains there for the (anticipated) transmission duration. In contrast, neighboring nodes are not affected by the virtual transmission, so that precious resources are preserved. On the other hand, a virtual transmission includes a credit transition, although the actual credit delivery is postponed to the next physical packet exchange.

Virtual transmissions can be used in both cases, either if the transmitter queue is empty, or if the receiver queue is full. For an anycast link with multiple destinations,

Scenario	$t_{\max}$	t_{E2E}	y	$\sum_j x_{0,j}$	$\sum_j x_{0,j}^{\text{virt}}$	$\sum_i Q_i$	$\sum_i \hat{Q}_i$
A	400 ms	921 ms	0.265	0.264	0	0.225	0.728
	200 ms	835 ms	0.275	0.261	0.003	0.200	0.363
	100 ms	420 ms	0.291	0.259	0.035	0.092	0.179
	50 ms	216 ms	0.349	0.248	0.097	0.037	0.086
B	400 ms	1820 ms	0.276	0.252	0.019	0.422	0.714
	200 ms	825 ms	0.336	0.256	0.070	0.171	0.353
	100 ms	449 ms	0.432	0.247	0.189	0.072	0.172
	50 ms	354 ms	0.478	0.241	0.239	0.046	0.121

Table 3.6.: End-to-end delay t_{E2E} and flow rate y results obtained from network simulations for a 7-hop chain (A) and a 7 hop double chain (B). The results are 20 s averages excluding a 5 s warm-up phase. The last two columns show the amount of in-flight packets across all nodes and their respective upper limit. The two columns to the left refer to the physical and virtual goodput at the source 0. For a better comparability, the rate and queue values are given as fraction of the maximal link throughput of 442 pps.

a virtual transmission is initiated whenever there is at least one queue overflow. In addition, the congestion controller has to consider the queue limits. It injects packets only if the queue at the source can accommodate it. Otherwise, it injects the associated credit only and the packet is dropped.

Example. Table 3.6 shows simulation results for a 7 hop chain (Scenario A) and a 7 hop double chain (Scenario B, shown in Figure 3.21) for different per-hop delay limits. Considering scenario A, we observe that smaller per-hop delay limits are able to decrease the amount of in-flight packets $\sum_i Q_i$ and the end-to-end delays t_{E2E}. At the same time, the risk of queue under- and overflows increases. Transmissions are more often virtual, which can be observed at the virtual goodput at the source $\sum_j x_{0,j}^{\text{virt}}$. Furthermore, the flow rate y deviates from the actual goodput $\sum_j x_{0,j}$ at the source. In addition, the limited amount of in-flight packets leads to less efficient schedules and the goodput slightly decreases.

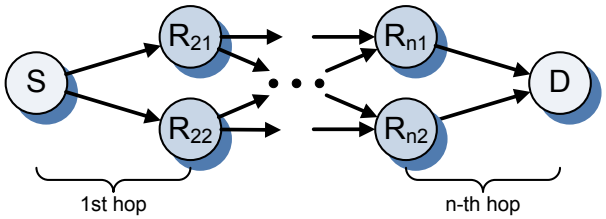

Figure 3.21.: Double chain with n hops and a flow from S and D.

The same observations apply to scenario B, as well. In addition, it demonstrates the effect of multi-path routing on the end-to-end delays. Although additional relays have been added, the achievable physical goodput $\sum_j x_{0,j}$ is almost unchanged. The traffic flow is split up between both chains. Hence, the per-hop queue limits $\hat{Q}$ at the relay nodes are halved, so that the aggregated queue limit $\sum_i \hat{Q}_i$ remains comparable to

scenario A. With smaller per-hop limits, the risk of virtual transmissions increases. Furthermore, we make two interesting observations in scenario B. Under $t_{\max} = 400$ ms, the amount of in-flight packets $\sum_i Q_i$ and the end-to-end delays t_{E2E} substantially increase in scenario B. We argue that the per-hop queue limits are rather conservative in this case and do not play a significant role in the queueing process. With $t_{\max} = 50$ ms on the other hand, the aggregated queue limit is higher than in scenario A, which causes a higher end-to-end delay. We argue that the reason is the lower queue limit of 4 packets, which corresponds to $\hat{Q}_{\min} = 0.009$ in the given notation. In summary, multi-path routing introduces additional relay nodes that may split up the traffic flow, so that the individual per-hop queue limits decrease. Thus, the risk of queue under- and overflows grows and virtual transmissions become more likely. In addition, the end-to-end delay increases if the per-hop limits reach the lower bound $\hat{Q}_{\min}$ and cannot be decreased further.

Discussion. Virtual transmissions do not compete with neighboring links in the collision domain, which may negatively affect the convergence of the CSMA Markov chain. With increasing virtual throughput in the example above, the physical goodput $\sum_j x_{0,j}$ has slightly decreased and the system converges to a less efficient operating point. On the other hand, the virtual goodput contributes to the traffic rate y of the flow. The higher flow rate y negatively affects the fairness between competing flows, since the congestion controller provides PF to the joint flow rate y of virtual and physical goodput. Thus, the hop-delay parameter should be chosen in order to keep the virtual flow sufficiently small, so that the above mentioned issues do not become critical. However, a tradeoff arises with multi-path routing. Additional paths and relays split the flow further. Our delay limiting approach becomes ineffective if the arrival rate λ_i^f of a sub-flow becomes too small and the lower bounds for the per-hop queue limits $\hat{Q}_{\min}$ apply. In these cases, concentrating the traffic flow while dropping low-throughput paths may reduce the end-to-end delay.

With UO-CSMA, the queueing behavior differs from TCP. The intention of TCP is to fully utilize all intermediate links in order to maximize the end-to-end throughput. In particular, TCP tries to adapt its window size, so that the maximum number of simultaneous transmitters can be activated at each time instance. Due to the overlapping collision domains in WMNs, the optimal window size is generally smaller than the number of relay nodes. Increasing the window size further does not change the throughput but affects the end-to-end delay according to Little's law. However, it may even reduce the throughput due to hidden nodes [71]. On the other hand, UO-CSMA relies on back-pressure and thus queueing information to adapt the MAC persistency in order to converge to an efficient operating point of the CSMA Markov chain. In particular, each link is assumed to be saturated. In the vanilla approach, this assumption is justified since back-pressure is expressed in terms of queued packets. The saturation assumption allows for an independent operation of CSMA and the queueing process. The presented approach to limit the end-to-end delay violates the saturation assumption to varying degrees, and the resulting tradeoff can be controlled via the per-hop delay limit parameter $t_{\max}$. An integrated approach that considers both CSMA and queueing in non-saturated conditions seems to be promising. However, the required theoretic foundations still have to be developed.

3.5.4. Compensation for Candidate Set Dynamics

The intra- and inter-flow adaptation presented in section 3.5.2 try to find a working point in terms of TA that offers the highest throughput efficiency while maintaining the physical and technological constraints. However, the characteristics of anycast links may cause oscillations in the feedback loop. For example, consider the scenario in Figure 3.22 that consists of the transmitter i and its neighbors and next hop candidates 1,2 and 3. Let us suppose that nodes 2 and 3 have longer credit queues than the transmitter i and only node 1 has fewer credits, i.e. it holds $C_3 > C_2 > C_i > C_1$. Thus, the transmitter assigns TCs to neighbor 1 only. According to the CSMA scheduling in section 3.4.1, the transmitter increases the TA on *all* hyperlinks containing neighbor 1. In particular, the transmitter should also activate the hyperlinks to node 1 and combinations of neighbor 2 and 3, although it does not intend to transmit a packet to neighbor 2 or 3.

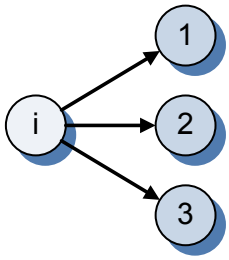

Figure 3.22.: Scenario: Transmitter i and three next hop candidates 1, 2 and 3.

On the one hand, the unnecessary receivers cause additional MAC overhead, since the number of signaling frames and the frame size increases. On the other hand, the aggregated TA r_{sum} increases with the number of activated hyperlinks, since *all* of them have to be taken into account at all times. The TAs sum up in the exponential domain as shown on line 2 of Algorithm 2 on page 74. Coming back to our example, if the minimal TA is 0 for a single link, then the aggregated TA r_{sum} cannot be smaller than $\log(7) \approx 2$ for 3 neighbors, as shown in Figure 3.23a. The increase of the aggregated TA r_{sum} is a problem because it leaves less room for the per-link TA adaptation in the presence of technological upper limits, so that the differentiation capabilities suffer.

The straightforward solution would be not to activate a hyperlink if it contains unnecessary receivers. However, this leads to oscillations. For example, if the system evolves and the credit queue at the transmitter C_i grows, then neighbor 2 might have a lower credit queue ($C_i > C_2$) , so that it is included in the routing decision and the transmitter assigns TCs to it. In addition to the link $(i,1)$, transmitter i now activates the link $(i,2)$ *and* the hyperlink $(i,\{1,2\})$. The TA of the hyperlink $r_{i,\{1,2\}}$ is equal or larger than the TA $r_{i,1}$ of the link to neighbor 1 by construction (cf. section 3.4.1). Thus, the aggregated TA r_{sum} at the transmitter abruptly changes, as shown in Figure 3.23b. The intra-flow efficiency adaptation uses the aggregated TAs r_{sum} to determine the working point in terms of V, so that the system may converge to a different working point after neighbor 2 has been included. Furthermore, the system may start to oscillate if the credit dynamics causes regular crossings of the credit levels of both the transmitter i and node 2.

We address the problem of abrupt changes of the aggregated TA in the following way. Let us reconsider the example above: Only neighbor 1 is included in the routing decision of node i, i.e. $C_1 < C_i \leq C_j \; \forall j > 1$. Since all other receivers are unnecessary in

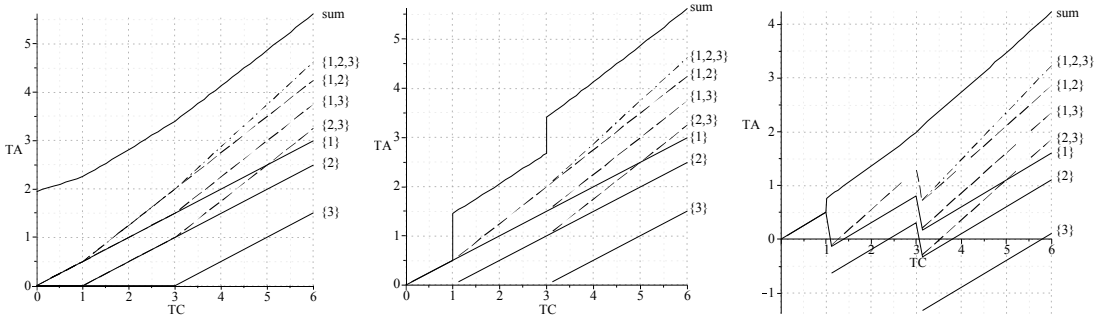

(a) According to (3.29). (b) Selective activation of links without compensation. (c) According to (3.30).

Figure 3.23.: TA versus TC for three candidate receivers having $C_1 = C_2 - 1 = C_3 - 3$. The PSR of an anycast link with one (two, three) receiver(s) is 0.50 (0.75, 0.875). All links use the same bit-rate.

this case, node i activates link $(i, 1)$ only using the TA $r_{i,1}$ similar to the straightforward approach. Let us assume the system evolves in a way that receiver 2 is included in the routing decision ($C_1 \leq C_2 < C_i$). Now, node i additionally activates the links $(i, \{1, 2\})$ and $(i, 2)$. Note that the former link would already have been activated according to the traditional approach. Thus, on activating link $(i, \{1, 2\})$, we split the TA $r_{i,1}$, which link $(i, 1)$ has had in isolation, into the TAs of link $(i, 1)$ and $(i, \{1, 2\})$ in a way that the aggregated TA is preserved. Since the aggregation is done in the exponential domain, we can accomplish this task by subtracting a compensation term $e_{i,\{1,2\}}$ from both TAs. In particular, if both links operate with equal bit-rates, the compensation term is $e_{i,\{1,2\}} = \log(2)$, i.e. we subtract $\log(2)$ from $r_{i,1}$ and $r_{i,\{1,2\}}$.

In the following, the uncompensated TAs have a subscript only (e.g. $r_{i,M}$), whereas TAs with an additional superscript are compensated according to the superscript (e.g. $r^J_{i,M}$). In general, let $J' = \{1, \ldots, j-1\}$ be the set of neighbors of node i that the routing decision has currently chosen ($C_1 \leq \ldots \leq C_{j-1} < C_i$). Thus, node i has used the TAs $r^{J'}_{i,M'}$ compensated according to J' for all $M' \in \mathcal{P}(J')\backslash\emptyset$. Now, node i chooses the additional receiver j having $C_{j-1} \leq C_j < C_i$. For link (i, M'), we adapt the TA as $r^J_{i,M'} = r^{J'}_{i,M'} - e_M$ with $J = J' \cup \{j\}$, $M = M' \cup \{j\}$, $m = \max(M')$ and e is defined as

$$e_M = \log\left(1 + \exp\left[(R_{i,M} - R_{i,M'}) \sum_{K \in \mathcal{P}(M')} p_{i,K} \sum_{L \in \mathcal{P}(\{1,\ldots,m-1\}\backslash M')} \beta_{i,K\cup L}\right]\right) \quad (3.30)$$

In addition, the link (i, M) is activated using the compensation terms of link (i, M'), i.e. $r^J_{i,M} = r_{i,M} - (r_{i,M'} - r^J_{i,M'})$. In this way, all links except (i, j) have been compensated so far. As a heuristics for the newly activated link (i, j), we use the lowest compensation term that any other link has experienced so far, i.e. $r^J_{i,j} = r_{i,j} - \min_J(r_{i,M'} - r^J_{i,M'})$. With multiple flows per link, we first apply the compensation to the TAs, and afterwards we select the flow per link as discussed in section 3.4.1.

The resulting aggregated TA r_{sum} of node i will still be discontinuous due to the

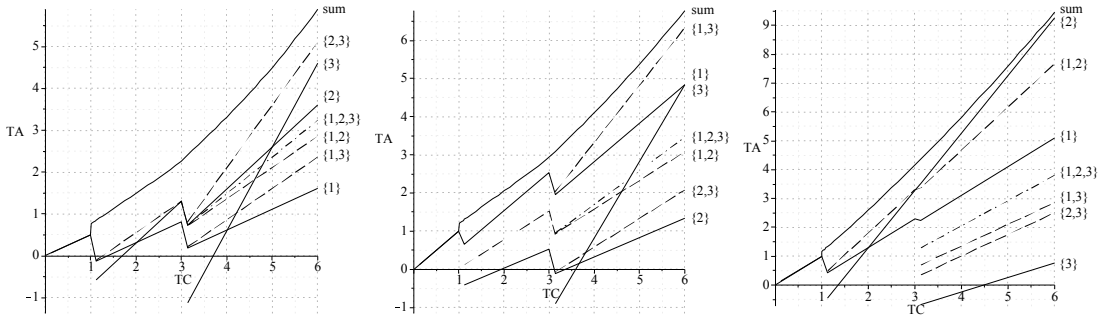

(a) Rate vector $R = (1, 2, 4)$. (b) Rate vector $R = (2, 1, 4)$. (c) Rate vector $R = (2, 4, 1)$.

Figure 3.24.: TA versus TC for three candidate receivers having $C_1 = C_2 - 1 = C_3 - 3$. The PSR of an anycast link with one (two, three) receiver(s) is 0.50 (0.75, 0.875). The bit-rate of the single receiver links is given in the rate vectors. The bit-rate of multi-receiver links is the minimum of the involved single-receiver links.

heuristics for the newly introduced TAs. Fortunately, the jumps in the aggregated TA will vanish in the high TA regime. Note that the aggregated TA is calculated via a log-sum-exp expression, which is an approximation of the max function [30]. The influence of the newly introduced term vanishes as the difference to the already contained TAs increases. As shown in Figure 3.23c, our heuristics mitigates the discontinuity at $TC_i = 1$ to some extend and the discontinuity at $TC_i = 3$ is not noticeable anymore. Let us consider the example in Figure 3.23 in detail. In the case $C_1 < C_i$ and the routing decision chooses neighbor 1 only, then the transmitter activates link $(i, 1)$ only using $r_{i,1} = R_{i,1} p_{i,1} \beta_{i,1}$. If the credits of the transmitter increase in a way that $C_1 \leq C_2 < C_i$ and receiver 2 is included in the routing decision, then we have the following.

$$
\begin{aligned}
e_{\{1,2\}} &= \log\left(1 + \exp\left[(R_{i,\{1,2\}} - R_{i,1}) p_{i,1} \beta_{i,1}\right]\right) \\
r_{i,1}^{\{1,2\}} &= r_{i,1} - e_{\{1,2\}} = R_{i,1} p_{i,1} (\beta_{i,1} + \beta_{i,\{1,2\}}) - e_{\{1,2\}} \\
r_{i,\{1,2\}}^{\{1,2\}} &= r_{i,\{1,2\}} - e_{\{1,2\}} = R_{i,\{1,2\}} (p_{i,1} \beta_{i,1} + p_{i,\{1,2\}} \beta_{i,\{1,2\}}) - e_{\{1,2\}} \\
r_{i,2}^{\{1,2\}} &= r_{i,2} - e_{\{1,2\}} = R_{i,2} p_{i,2} \beta_{i,\{1,2\}} - e_{\{1,2\}}
\end{aligned}
$$

Expressions for three and more receivers can be derived in the same way.

Note that the sum expression in the calculation of the compensation terms (3.30) looks very similar to the estimation of the TAs in section 3.4.1. However, an important difference can be found in the second summation, where we do not consider the whole complement of M, but only the subset having lower costs. Hence, the above compensation term $e_{\{1,2\}}$ does not contain any other TCs except $\beta_{i,1}$, so that it vanishes as the difference between the costs C_1 and C_2 decreases. Furthermore, $e_{\{1,2\}}$ stays the same regardless whether we include further candidate receivers, since it is independent from all TCs except $\beta_{i,1}$.

We have already presented the resulting TAs for equal bit-rates in Figure 3.23c. The results for different bit-rate combinations are plotted in Figure 3.24. By using different bit-rates across the candidate receivers, the compensation terms change slightly. In

Figure 3.24c, for example, receiver 3 has the lowest bit-rate so that the compensation terms are generally smaller then $\log 2$. In particular, they are almost not noticeable for the links $(i, 2)$ and $(i, \{1, 2\})$.

3.5.5. Route Pre-Selection via Routing Metrics

Back-pressure routing finds the throughput-optimal path(s) without relying on topology information. It is agnostic to network delay and resource usage. Individual packets may experience excessive delays. Furthermore, the system does not favor shorter routes (in terms of resource usage), which may increase the end-to-end delay and energy consumption.

The described problem has been addressed in related work. Neely *et al.* address the mentioned issues using a shortest path bias in the routing decision. They include the routing metric of the associated paths in the calculation of the back-pressure, so that shorter paths are favored [78, 191]. Gupta *et al.* consider bounds on the expected delay [87]. Similar to Naghshvar *et al.*, they define a back-pressure and a forwarder selection policy that is provable throughput-optimal [187, 188]. The basic idea is to dynamically determine the expected delay for all neighbor relays, and select the neighbor with the lowest delay as forwarder. The draining time based scheduling as proposed by Subramanian *et al.* uses a similar approach to address the delay performance in back-pressure routing [252].

Bui *et al.* include the resource consumption in the objective function. They introduce a tradeoff term into the routing decision, which controls the extent to which additional resources can be utilized [9, 33]. Ying *et al.* introduce the shortest path information directly into the optimization problem. In particular, they define a factor, for which back-pressure is traded off against the routing metric. In low traffic scenarios the nodes are encouraged to select short routes. With increasing traffic intensity, the allowed deviation from the shorted path increases in the same way as the intermediate queues grow [291]. Moeller *et al.* presents a similar approach that introduces the ETX routing metric as penalty function into the objective function [186].

In the following, our objective is the exploitation of MUD while ensuring an acceptable end-to-end delay. The system may use topology information obtained from state-of-the-art protocols for link quality estimation. In this way, we can eliminate all paths that lead to dead ends and focus on feasible routes. We differentiate between flows with short and long routes, i.e. whether the shortest path contains few or many relays.[7] In the former case, spatial (multi-path) diversity is generally not available since the transmitters compete for the same radio resources. On the other hand, MUD can be obtained if the involved links are unreliable. For long routes, both MUD and spatial diversity are available. In order to limit the resource usage and the end-to-end delay, only the most promising paths should be taken and the number of involved relays should be kept reasonable small. A broad diversification of the traffic within the network should be prevented, so that the traffic flow per link remains sufficiently high. Otherwise, the arising virtual transmissions may have detrimental effects on the end-to-end delay, throughput and fairness as described in section 3.5.3.

[7] Note that a numerical differentiator, e.g. in terms of hop count, has to consider the actual propagation

Algorithm 6 Route Pre-Selection.

procedure DIJKSTRA(Source n)
    ...
    return (H, D) ▷ Shortest path hop count and metric
end procedure

Require: $f_\mathrm{r} \geq 1, f_\mathrm{h} \geq 1$ ▷ Routing and relay count stretch limit
procedure SELECTCANDIDATES(Packet p) ▷ At node i
    $(H_d, D_d) \leftarrow \text{DIJKSTRA}(p.\text{dst})$
    $m^\mathrm{r} \leftarrow f_\mathrm{r} \cdot D_d(p.\text{src})$ ▷ Max. E2E metric
    $h \leftarrow f_\mathrm{h} \cdot H_d(p.\text{src})$ ▷ Max. relay count
    $(H_i, D_i) \leftarrow \text{DIJKSTRA}(i)$
    for all k **do**
        $D(k) \leftarrow D_i(k) + D_d(k)$
    end for
    $I \leftarrow \text{SORTASC}(D)$ ▷ Sorted index array
    $m^\mathrm{h} \leftarrow 0$
    for $l \leftarrow n$ **downto** 1 **do**
        if $l = n$ **or** $D(I(l)) \neq D(I(l+1))$ **then**
            $k \leftarrow l$ ▷ Handle nodes with identical metric
        end if
        if $k \leq h$ **or** $l = 1$ **then**
            $m^\mathrm{h} \leftarrow \max(m^\mathrm{h}, D(I(l)))$
        end if
    end for
    $C \leftarrow \emptyset$,
    for all k **do** ▷ Match against routing and relay count stretch
        if $k \in N_i$ **and** $D(k) \leq m^\mathrm{r}$ **and** $D(k) \leq m^\mathrm{h}$ **then**
            $C \leftarrow C \cup \{l\}$
        end if
    end for
    return C
end procedure

The route pre-selection heuristics should support back-pressure routing using a proactive and traffic-independent routing metric in a way comparable to Yuan *et al.* [292]. Routing paths are pruned according to their anticipated efficiency, expressed in terms of a cumulative metric like ETX or ETT [58, 62]. Before continuing with the presentation of our approach, we introduce the concept of routing stretch and relay count stretch. The routing metric stretch factor, or simply *routing stretch*, is defined as the ratio of the maximum end-to-end metric of all considered paths with respect to the shortest path. The *relay count stretch* is analogously defined in terms of the number of relay nodes.

Algorithm 6 summarizes the proposed routing heuristics. In the route pre-selection,

environment and the bit-rates used.

we prune the network topology according to the upper limits f_{r} and f_{h} for both routing and relay count stretch. Thus, the route pre-selection considers the network topology only similar to state-of-the-art WMN routing protocols like OLSR [106] and it is not traffic-adaptive. In particular, for every network node i, we estimate the shortest path between source and destination of the packet that includes node i, which can be obtained from two passes of the Dijkstra algorithm (cf. line 6 et seq. of Algorithm 6). The resulting route metric is denoted m_i, and the shortest path among them has the metric m^{s}. Given a maximum routing stretch of f_{r}, the largest admissible metric for a relay is $m^{\mathrm{r}} = f_{\mathrm{r}} m^{\mathrm{s}}$. In addition, we determine the largest shortest path metric m^{h}, for which the limit of the relay count stretch is still satisfied. A neighbor i will not become a relay if its shortest path metric m_i exceeds the given routing or relay count stretch limits, i.e. it holds $m_i > m^{\mathrm{h}}$ or $m_i > m^{\mathrm{r}} = f_{\mathrm{r}} m^{\mathrm{s}}$ (cf. line 25 of Algorithm 6).

3.6. Evaluation in Illustrative Scenarios

In this section, we evaluate the proposed cross-layer protocol within small and synthesized scenarios in order to illustrate the operation of the system. Our objective is to validate the effectiveness of the algorithm (cf. section 3.4) and our design decisions (cf. section 3.5) using a network simulator based on JiST/SWANS (cf. section 2.5). Thereby, we evaluate several facets of the protocol, one at a time, in isolated scenarios and characterize the static and dynamic properties of the system. Our models rely on strong assumptions in order to keep the involved complexity manageable. In the simulations, the modeling assumptions are relaxed in way that is widely acknowledged in the research community and we refer to them as simulation assumptions. Due to the limited scope of the scenarios, we are able to solve the underlying optimization problem numerically. The relaxation provides an insight into the impact of the modeling limitations and the remaining potentials of OR in WMNs. Furthermore, we are able to compare the proposed protocols with state-of-the-art approaches based on the same premises.

3.6.1. Efficiency Adaptation with Limited TAs

To start with, we illustrate the convergence of the V parameter to the predetermined tradeoff point. Similar to section 3.5.2, we consider an equispaced chain of nodes consisting of 3 and 7 links. Direct neighbors in the chain can exchange packets. Non-neighboring nodes are not able to carrier-sense each other, so that a hidden node situation might emerge depending on the protocol.

The simulation parameters are summarized in Table 3.7. The wireless links are almost error-free since no fading is applied. Furthermore, we use the log-distance path loss model. To generate the LCGs of interest, we have parameterized the model with a high path loss exponent throughout section 3.6. The bit-rate is fixed and we disable both the propagation and the radio turnaround delays. The per-hop delay limit and the step size are sufficiently large in order to minimize their influence on the results, so that virtual transmissions should not occur often (cf. section 3.5.3). In addition, we vary the target TA the system should converge to. Note that the transmission rate is

Parameter	Value
Path loss	Log-distance, exponent 6
Channel	AWGN
Fading	None
Receiver	BER & cumulated interference
PHY	IEEE 802.11a/g, 6 Mbps
PSR	100%
Propagation delay	0 ms
Radio turnaround	0 ms
TA limits	$4 \ldots \{8.8, 10.8, 12.8\}$
Inter-flow hysteresis	1.1
Step size (initial/target)	$0.1 \cdot V^{-1}$ / $0.002 \cdot V^{-1} \cdot C^{-1}$
Step size update interval	200 ms
Per-hop delay limit	0.4 s
Flow duration	20 s (excl. warm-up)
Packet size	1500 Byte
Seeds	20

Table 3.7.: Simulation parameters

approximately $R^l \approx 440$ pps ($r^l \approx 6.1$).

In Figure 3.25a, we have plotted the resulting goodput along with the standard deviation across all repetitions. For comparison, we have additionally plotted the results for TCP and genie-aided saturating UDP flows using the DSR [124] protocol, either with or without using the RTS/CTS prologue. As supposed according to Figure 3.17 on page 73, the results show that higher target TAs result in higher goodput. Furthermore, it is remarkable that the proposed protocol (OPT) performs better than UDP-DSR. The simulation scenario does not offer multi-user diversity, since the wireless links are free from errors. On the other hand, the proposed protocol relies on CSMA/HBT, so that the RTS/CTS exchange is mandatory. Using IEEE 802.11, the problem is that the upstream nodes are unable to determine their transmission opportunities. They probe the channel while their intended receivers are silenced and the medium access fails. Due to the missing CTS or ACK, the transmitters excessively back off. The RTS/CTS exchange does not solve this problem, but introduces additional overhead instead. The TCP performance suffers from the additional transport layer ACKs and from the specific problems of TCP in wireless networks [71], i.e. the implicit assumption of TCP that segment losses are due to congestion instead of channel impairments.

In Figure 3.25b, we have plotted the value of V, the bottleneck TA and the flow rate y, which are all estimated during the simulations. As the results suggest, the system is able to operate the TAs near the anticipated working point specified by the target TAs. In particular, the achieved TA at the bottleneck node becomes slightly smaller and more variable when increasing the length of the chain. Using the achieved Vs, we have calculated the flow rate in Maple using the idealized CSMA model without probing. The analytical flow rates closely match the simulation outcomes. Thus, we conclude that even the idealized model has a high predictive value.

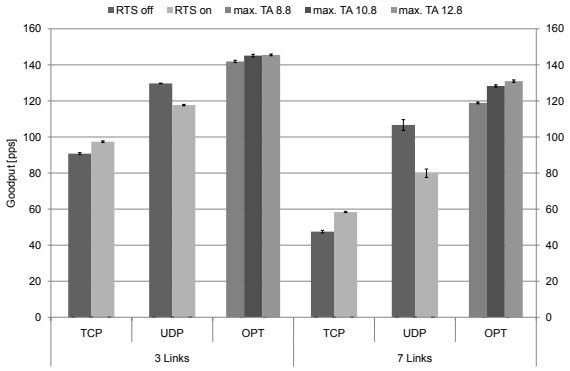

(a) Goodput of the proposed protocol in relation to DSR-UDP and DSR-TCP ($\pm std.dev.$).

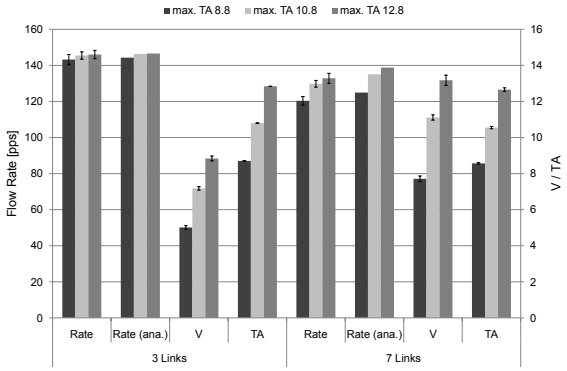

(b) Flow rate, efficiency parameter V and TA at the bottleneck ($\pm std.dev.$).

Figure 3.25.: Simulation results for a chain topology of 3 and 7 link.

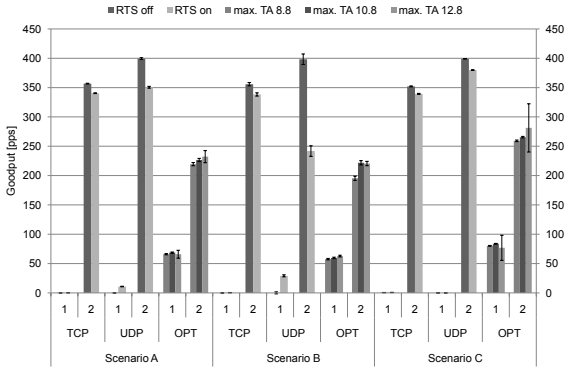

(a) Goodput of the proposed protocol in relation to DSR/TCP and DSR/UDP for both flows ($\pm std.dev.$).

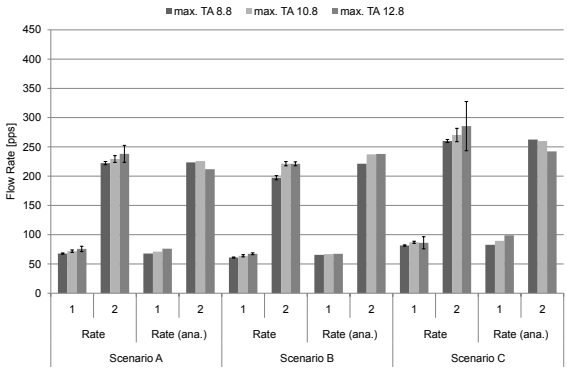

(b) Flow rate of both flows in relation to the analytical flow rate ($\pm std.dev.$).

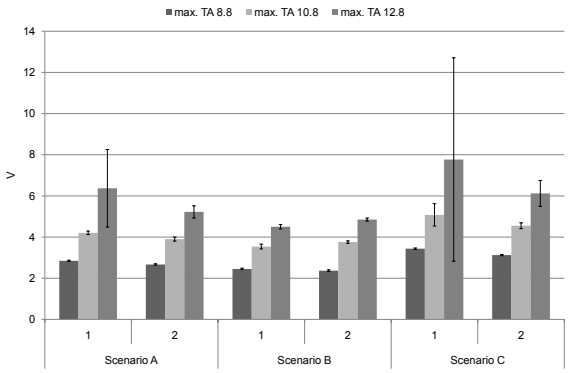

(c) Estimated V parameter ($\pm std.dev.$).

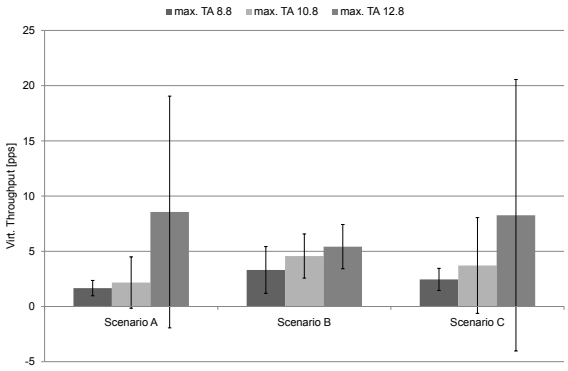

(d) Virtual throughput at the source of the longer flow ($\pm std.dev.$).

Figure 3.26.: Simulation results for the scenarios in Figure 3.19 on page 78 with 2 flows each.

3.6.2. Fairness with Limited TAs

In this section, we illustrate the effectiveness of the inter-flow adaptation in a network simulator. The inter-flow adaptation is designed to ensure that the throughput between flows is proportional fair. In particular, we have simulated the two flow scenarios in Figure 3.19 on page 75 using the simulation parameters from the previous section (cf. Table 3.7).

The goodput results are shown in Figure 3.26a. We observe that the longer flow starves in most cases under DSR/UDP and DSR/TCP. On the other hand, the proposed protocol converges to PF. In Figure 3.26c, the efficiency parameters V of both flows match each other closely. Remember that we have used a hysteresis factor in Algorithm 3 to prevent livelock situations, so that small imbalances between the Vs of both flows are inevitable. In addition, the analytic results under the idealized CSMA model for the dynamically estimated Vs are close to the achieved flow rates (cf. Figure 3.26b).

The variability in the results grows when increasing the target TA to approach more efficient working points. This problem can be observed in scenario C for V and the goodput, for example, which exhibit a considerable standard deviation for a target TA of 12.8. We suppose that the reason for this observation is the tradeoff between efficiency and short-time fairness [174]. When requesting higher efficiency, the short-time fairness decreases and the links have to wait longer to access the medium. Due to the delay and queue limits, however, the link may not hold the channel sufficiently long to be able to achieve the requested throughput burst. The system compensates for the limited queue sizes by transmitting virtual packets (cf. section 3.5.3). Figure 3.26d illustrates the growing virtual throughput in relation to the requested efficiency.

3.6.3. Step Size Adaption during and after Convergence

In the following, we evaluate the dynamic step size adaptation and its impact on the system during and after convergence. In particular, we illustrate the dynamics of the system during convergence using network simulations. Furthermore, we consider the convergence time and illustrate the impact of the step size adaptation in terms of variability and throughput efficiency after the system has converged. The simulation setup is similar to the previous sections, and we highlight the differences only. The simulation topology is a chain of nodes with 2 and 7 links, respectively, which is traversed by a single flow for about 70 s. In the evaluation, we assume that the system converges within the first 40 s, and we use the remaining 30 s for the calculation of the steady state values ("after convergence"). The target TA remains fixed at $r_{\text{opt}} = 8.8$ and we used an additional bit-rate of 12 Mbps.

Fixed Step Size

To start with, we investigate the dynamics of the system using fixed step sizes. The credits C and the step size s are reported relative to the efficiency parameter V in the following. The *relative credits* C/V can be directly compared across different step sizes. They are reciprocal to the flow rates. Furthermore, they are directly proportional to the

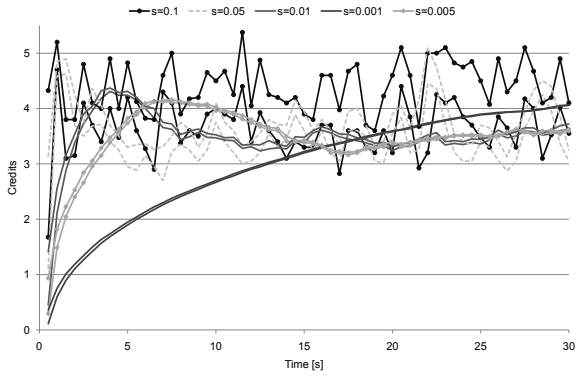

(a) Evolution of the relative credits C/V at the source of the flow depending on the step size s (5 individual simulations, 7 links, 6 Mbps). The values are grouped into 0.5 s slices with about 50 values each. The lines show the 25th and 75th percentile.

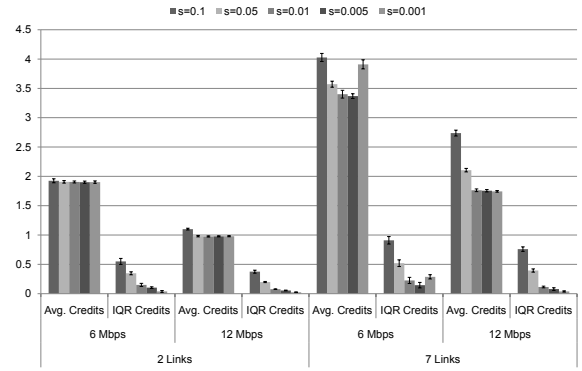

(b) Credits at the source of the flow (Average and IQR of C/V, after convergence, $\pm std.dev.$). Remember that the flow rate is reciprocal to the credits at the source.

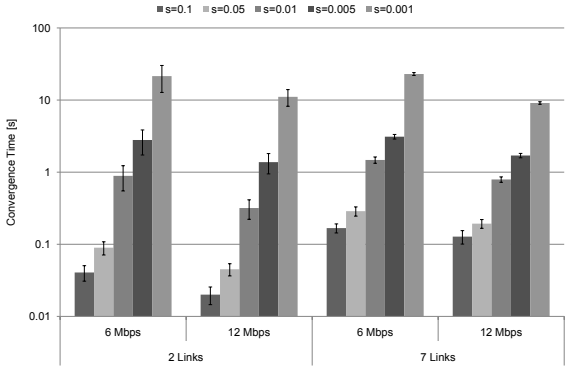

(c) Convergence time ($\pm std.dev.$).

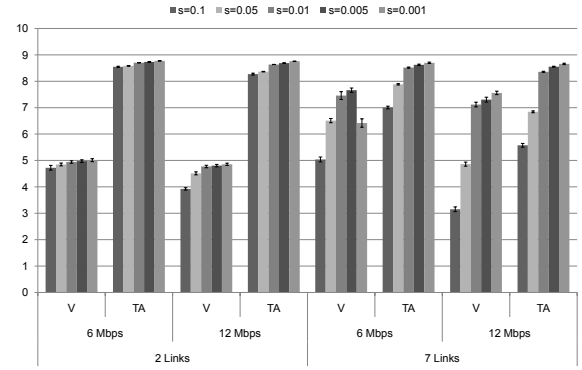

(d) Estimated V and max. TA at the bottleneck (after convergence, $\pm std.dev.$).

Figure 3.27.: Fixed step size: Simulation results for a chain of 2 and 7 hops and one flow.

queue lengths and the step size is the proportionality constant. In Figure 3.27a, we have plotted the evolution of the credit queues at the source for five individual simulations. The values are grouped into 0.5 s bins with about 50 entries each. The diagram shows the first and third quartile of each bin. As supposed, the speed at which the credit queues are filled heavily depends on the step size. For example, it takes more than 10 s for the credit queue to reach the working point with the smallest step size $s = 0.001$. On the other hand, the working point is reached within tens of milliseconds using the largest step size at the expense of a higher variability of the credits queues at the working point in terms of the IQR.

In Figure 3.27b, we observe that the relative credits after convergence decrease with smaller step sizes. Thus, the flow rate tends to grow since it is reciprocal to the credits at the source. At the same time, the variability declines in terms of credit IQR. We argue that it becomes more difficult for the intra-flow adaptation to meet the target TA at the bottleneck due to the higher variability in the credit queues. As shown in Figure 3.27d,

the achieved TA slightly decreases with larger step sizes. Using the largest step size on the 7-hop chain, for example, the average TA after convergence is about 7 for 6 Mbps and even lower for 12 Mbps. The target TA of 8.8 is almost exactly achieved with smaller step sizes. In the same line, the achieved V parameters in Figure 3.27d tend to increase with smaller step sizes. One exception to the observation above is the smallest step size $s = 0.001$ with 7 links. The problem is, however, that the convergence time exceeds the 70 s simulation time in this case.

Similar to section 3.5.3, the *convergence time* is the time from the start of the flow until the credit queue at the source breaks through the first quartile of the steady state distribution for the first time. As shown in Figure 3.27c, the convergence time increases with smaller step sizes. The results suggest that there is an inverse relationship between them. Furthermore, the impact of the bit-rate can be observed. Since the TAs are weighted by the bit-rate according to (3.29) on page 69, fewer credits are necessary to reach the efficiency working point with higher bit-rates (cf. Figure 3.27b). Hence, the convergence time is reduced (cf. Figure 3.27c). On the other hand, more credits are associated with a single packet at higher bit-rates. Thus, the effects of variability are more pronounced (cf. Figure 3.27d).

Dynamic Step Size Adaptation

Let us consider the dynamic step size adaption in the following. According to Algorithm 4, the step size adaptation is controlled by three parameters: the initial step size s_0, the target step size s_∞ and the half-life t_{hl} Note that the target step size is denoted relative to V and relative to C. A target step size of $s_\infty = 0.01$ means that a packet is worth 1% of the amount of (relative) credits at the source. The initial step size, on the other hand, is given in relation to V only. It is worth a fixed amount of (relative) credits not depending on the number of credits at the source.

We can think of the adaptation as a transition of the system from one step size configuration to another. In particular, the properties of the system after convergence are solely determined by the target step size. Both Figure 3.28b and Figure 3.28d illustrate the characteristic tradeoff between efficiency and variability at the working point that we have already encountered with fixed step sizes. On the other hand, we did not find a significant influence of the half-life on the system after convergence.

The initial step size and the half-life determine the dynamics of the system during convergence. For illustration purposes, we have plotted the credit queue dynamics of four simulation instances in Figure 3.28a. The convergence time depends on the selection of s_0. The higher the initial step size, the faster the credit queues fill. Thereafter, the dynamics of all simulation instances becomes essentially equal, since it is dominated by an identical target step size and the influence of the initial step size vanishes. However, the system may overshoot the working point during convergence for certain initial values. The system will outweigh this overshooting by reducing the V parameter in a way that the aggregated TA on each hop does not exceed the technological limits. After the overshooting has dissolved, the system raises V again to approach the requested efficiency. The convergence time for different initial step sizes shown in Figure 3.28c is similar to the results with fixed step sizes (cf. Figure 3.27c).

The influence of the half-life is harder to quantify. Using the indicators presented

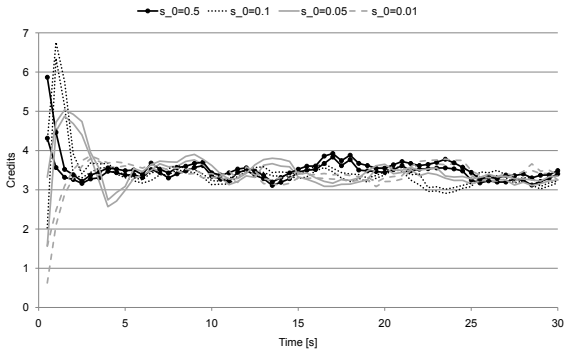

(a) Evolution of the credits C/V at the source of the flow depending on the initial step size s_0 (7 links, 6 Mbps, $s_\infty = 0.005$, $t_{\text{hl}} = 0.2$ s). The values are grouped into 0.5 s slices. The lines show the 25th and 75th percentile.

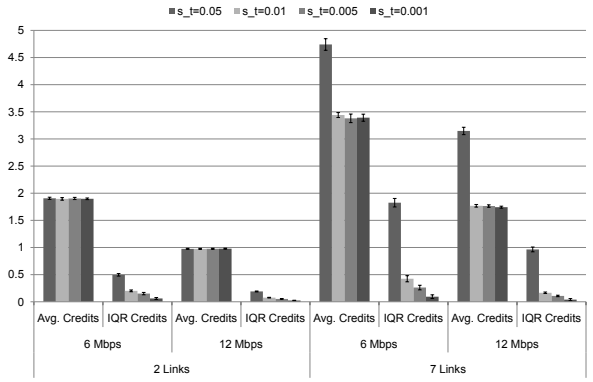

(b) Credits at the source of the flow in relation to the target step size s_∞ (Average and IQR of C/V, after convergence, $s_0 = 0.1$, $t_{\text{hl}} = 0.2$ s, $\pm std.dev.$).

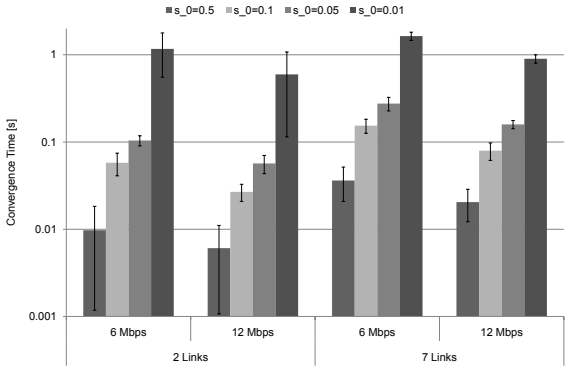

(c) Convergence time in relation the initial step size s_0 ($s_\infty = 0.005$, $t_{\text{hl}} = 0.2$ s, $\pm std.dev.$).

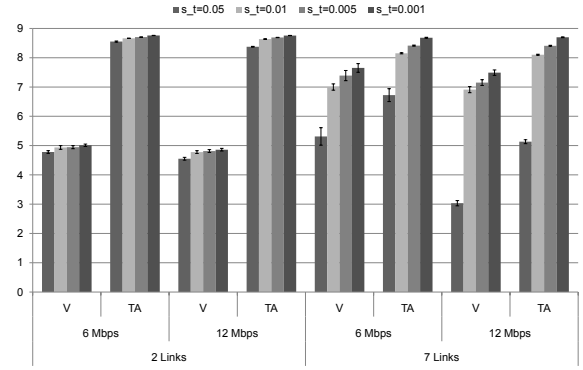

(d) Estimated V and max. TA at the bottleneck in relation to the target step size s_∞ (Average after convergence, $s_0 = 0.1$, $t_{\text{hl}} = 0.2$ s, $\pm std.dev.$).

Figure 3.28.: Adaptive step size: Simulation results for a chain of 2 and 7 hops and one flow.

above, the half-life does not have a significant impact. However, we have observed that a small half-life may lead to an uneven filling of the credit queues. The queues close to the source fill quickly, but the step size is reduced too fast so that the queues close to the destination need substantially more time to converge. Empirically, we found that a half-life $t_{\text{hl}} = 0.2$ s leads to an acceptable dynamics across all queues in the scenarios of interest.

In summary, the dynamic step size adaptation combines the advantages of both small and large step sizes. The convergence time is considerably reduced and the variability at the working point is low and controllable. We have investigated the impact of the individual parameters during and after the initial convergence. On the other hand, re-adaptation was out of scope for our investigation. Under real-world conditions, however, the re-adaptation may be necessary in case of arriving and departing flows or significant environmental changes.

3.6.4. End-To-End Delay and Short Time Fairness

In the following, we evaluate the delay properties and the short time fairness of the proposed system. In particular, we illustrate the fundamental tradeoff between throughput efficiency and short time fairness [173, 174]. We show the extent to which virtual transmissions are able to mediate between delay and throughput efficiency. Furthermore, we take a closer look at the relationship between multi-path routing and end-to-end delay.

In our network simulations, we explore the scenarios introduced in section 3.5.3 in detail: Scenario A and B consists of a 7-link chain and a double chain of 2x7 links (cf. Figure 3.21 on page 86), respectively. The links between direct neighbors are almost error-free, whereas two-hop neighbors do not interact with each other. We have set the lower queue limit to $\hat{Q}_{\min} = 4$ packets and we have varied the per-hop delay limits $t_{\max}$ introduced in Algorithm 5 on page 85. In addition, we have repeated the simulations with dummy packets [112] instead of virtual transmissions. The remaining simulation parameters are similar to the previous sections (cf. Table 3.7).

The results are shown in Figure 3.29. To start with, let us consider the influence of the per-hop delay limits $t_{\max}$. As supposed, a reduction of the delay limits leads to a smaller amount of in-flight packets (cf. Figure 3.29d), and the related end-to-end delays are reduced (cf. Figure 3.29c). Remember that Algorithm 5 calculates the queue limits $\hat{Q}$ in order to meet an average per-hop queueing delay. Thus, for the same per-hop delay, the queue limits for 12 Mbps are generally twice the limits for 6 Mbps in terms of packets. In Figure 3.29b, we notice that the goodput efficiency increases with higher delay limits, whereas the end-to-end delays rise at the same time (cf. Figure 3.29c). For comparison purposes, we have plotted the goodput results for DSR/UDP and DSR/TCP in Figure 3.29b. However, their delay results are meaningful to a limited extent only. In the simulations, we have set the maximum window size for TCP to 10 packets. The resulting delays are 70.7 ms (73.5 ms) in scenario A and 48.7 ms (44.8 ms) in scenario B, respectively, without (and with) the RTS/CTS exchange. For UDP, we have limited the number of in-flight packets to 600. The average delays are 540 ms (3800 ms) and 370 ms (3200 ms) in the above ordering.

Let us consider the influence of virtual and dummy transmissions. Figure 3.29a and Figure 3.29b illustrate the estimated flow rate and the achieved goodput. The difference between flow rate and goodput is the amount of virtual (or dummy) traffic. According to the figures, the goodput increases with higher per-hop delay limits, and the amount of virtual and dummy traffic is reduced at the same time. Under large per-hop delay limits, the behavior of the system is essentially equal for both virtual and dummy transmissions, since the risk of queue under- and overflows is low. With virtual transmissions, however, the system achieves higher goodput results even under small per-hop delays, which comes at the expense of a higher deviation from the proportional fair working point in terms of flow rate. With dummy transmissions, on the other hand, the system accurately maintains the working point of the flow rate at the expense of severe goodput degradations under small per-hop delay limits.

At first sight, the effect of virtual and dummy transmission on the end-to-end delay seems contradictory. With high per-hop delay limits, the number of in-flight packets is lower under dummy transmissions (cf. Figure 3.29d). The delay is also reduced

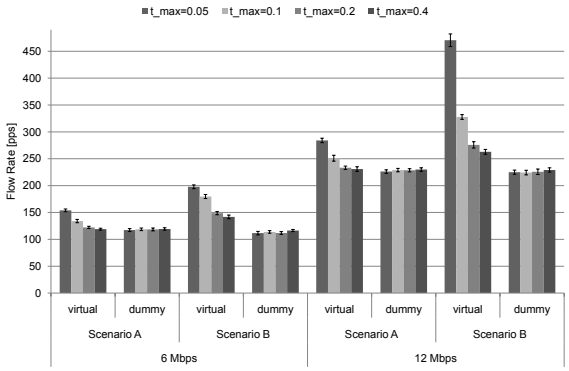

(a) Flow rate for different bit-rates and both virtual and dummy transmissions ($\pm std.dev.$).

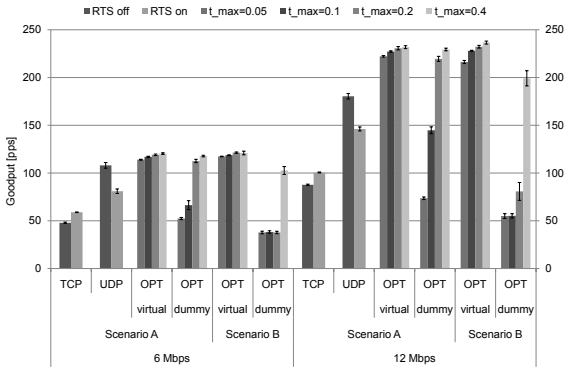

(b) Goodput in relation to DSR/TCP and DSR/UDP ($\pm std.dev.$).

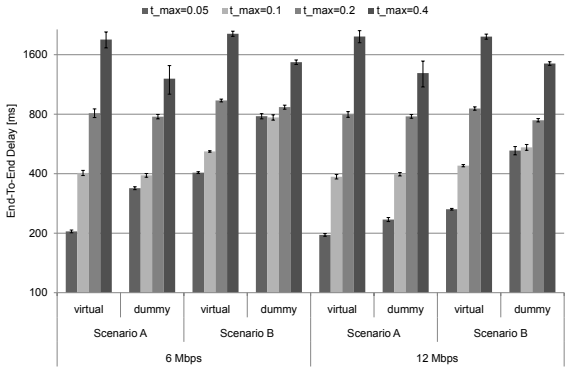

(c) End-to-end delay ($\pm std.dev.$).

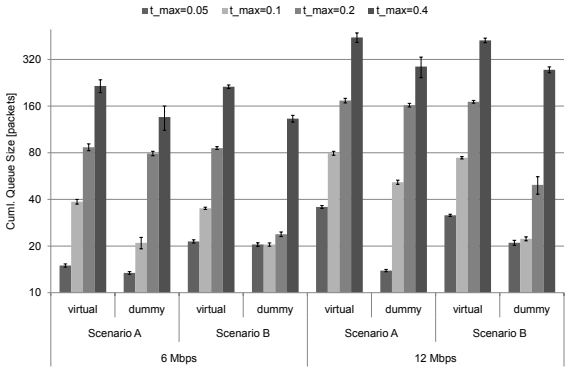

(d) Average queue size, cumulated across all nodes (corresponds to the number of in-flight packets, $\pm std.dev.$).

Figure 3.29.: Simulation results for a single flow (6 Mbps, $r_{\text{opt}} = 8.8$) in scenario A (7-hop chain) and B (7-hop double chain, see Figure 3.21 on page 86).

according to Little's law (cf. Figure 3.29c). With small per-hop delays, however, virtual transmissions achieve a lower end-to-end delay with no less or even more in-flight packets. We argue that the observation is caused by the tradeoff between throughput efficiency and short-term fairness [65, 173, 174]: The more efficient the working point of UO-CSMA is, the longer the nodes have to wait to gain access to the channel and the longer they have to hold the channel or, in other words, the higher the burstiness of the inter-access times.

For (one of) the last hop(s), we have estimated the distribution of the inter-transmission times and plotted the excess kurtosis in Figure 3.30. Remember that the higher the kurtosis, the more weight the tail of the distribution has in relation to the normal distribution. In particular, the normal and the exponential distributions have an excess kurtosis of 0 and 6, respectively. With dummy packets, the kurtosis in Figure 3.30a increases with the target TA and the traffic gets more bursty. On the other hand, it is virtually independent from the per-hop delay limits. The per-hop delay imposes

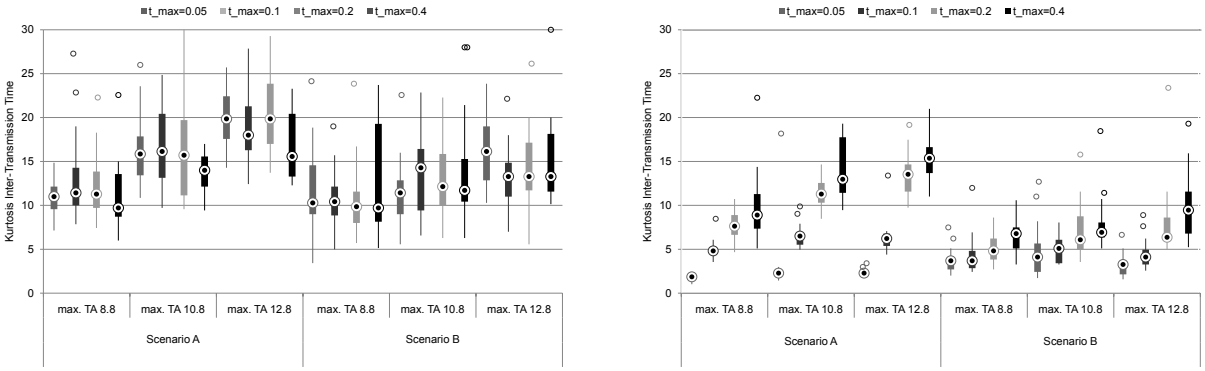

(a) Dummy transmissions (Box plot across all seeds).

(b) Virtual transmissions (Box plot across all seeds).

Figure 3.30.: Kurtosis of the inter-transmit time distribution on (one of) the last hop(s) for a single flow using 6 Mbps in scenario A (7-hop chain) and B (7-hop double chain, see Figure 3.21).

limits on each queue, and if the queue cannot sustain the required burst length, the node has to emit dummy packets. With virtual transmissions, on the other hand, the kurtosis in Figure 3.30b decreases with smaller per-hop delay limits. If the queue cannot sustain the required burst length due to the imposed hop-delay limits, a virtual transmission is initiated instead and the node releases the channel. Thus, the per-hop delay limit controls the burstiness and the short-term fairness, which comes at the expense of throughput efficiency according to Figure 3.29b. In this way, the contradiction above can be resolved: With virtual transmissions, the smaller per-hop delay limits increase the short-term fairness. Hence, the length of the packet bursts as well as the waiting time for the medium access is reduced, so that the individual packet traverses the network faster.

In summary, we have illustrated how the per-hop delay limits are able to control the amount of in-flight packets and the related end-to-end delay. However, the resulting queue limits may not be sufficient to sustain the required burstiness. In this case, throughput has to be sacrificed using either dummy or virtual packets. Using dummy packets, the flow rate and the short-term fairness is *maintained*, and the system excessively emits dummy packets in the case its queues cannot sustain the requested burst lengths. With virtual transmissions, on the other hand, the system *controls* the short-term fairness in order to reduce the burstiness to a sustainable level for the imposed per-hop delay limits. Based on our simulation results, we conclude that virtual transmissions cope better with small per-hop delay limits. In particular, the loss in goodput due to the reduced delay limits is gradually. Compared to dummy packets, the goodput loss is significantly smaller although the delay performance is even better. On the other hand, virtual traffic introduces a bias in the estimation of proportional fair flow rates, which may be detrimental to the fairness between flows (cf. section 3.5.3).

In order to illustrate the effect of multi-path routing, let us consider the difference between scenario A and B under virtual transmissions. Both scenarios offer the same spatial diversity. Although the number of nodes and links differs, the collision domains are identical. Figure 3.29b shows that the difference in goodput is marginal between

both scenarios. On the other hand, the flow rates in Figure 3.29a show a larger bias in scenario B especially for small delay limits. Furthermore, the end-to-end delays for small delay limits are generally higher under multi-path routing (cf. Figure 3.29c). Due to the additional chain of links in scenario B, the flow splits up between them evenly and halves the rate of incoming traffic. According to Algorithm 5, the maximum queue size per relay is also halved or the minimum of 4 packets applies. Thus, the risk of virtual transmissions increases, so that the flow rate in Figure 3.29a deviates from the goodput in Figure 3.29b under multi-path routing with smaller delay limits. In addition, the delay limiting approach becomes ineffective if the lower limit on the maximum queue size applies. We suppose that this is case with the per-hop delay limit of 50 ms under the bit-rate 6 Mbps in scenario B, since the number of in-flight packets is considerable smaller in scenario A (cf. Figure 3.29d).

To summarize, we have observed a tradeoff between multi-path usage and throughput and delay. By using multiple paths, the system may achieve additional spatial or multi-user diversity. On the other hand, the traffic has to split up for additional routing paths. Thus, the per-hop queue limits decrease, so that the risk of queue under- and overflows grows and virtual transmissions become more likely. Furthermore, if the rate of a sub-flow becomes too small and the lower bounds for the per-hop queue limits apply, our delay limiting approach becomes ineffective and the delay on that path cannot be controlled anymore. In section 3.5.5, we have presented a heuristics that limits the multi-path usage based on routing and relay count stretches.

3.6.5. Candidate Set Dynamics

In this section, we illustrate the oscillation problems within the intra-flow adaptation of the V parameter that arise with candidate set dynamics. We demonstrate our solution to that problem, in which we compensate the TAs for the dynamics in the candidate set as described in section 3.5.4. Figure 3.31 shows a network topology, in which oscillations may arise under OR if the PSR on link $(4, 2)$ is small. In particular, we vary $p_{4,2}$ from $0.1 \ldots 0.3$, whereas the PSRs of the remaining links are 1. A traffic flow is set up between node 1 and 2. The flow persists for 200 s, and we present results from the latter 100 s only in the following. The remaining simulation parameters are similar to the previous sections (cf. Table 3.7). Since all nodes are within the same collision domain, we can trade retransmissions on link $(4, 2)$ against transmissions on link $(3, 2)$ that are successful in any case. Thus, only the upper route involving node 3 should be used at the optimum.

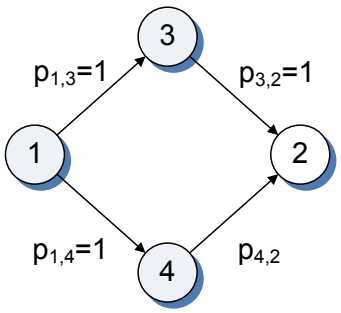

Figure 3.31.: Diamond topology with 4 nodes and a traffic flow from 1 to 2. The PSR $p_{4,2}$ is varied between $0.1 \ldots 0.3$.

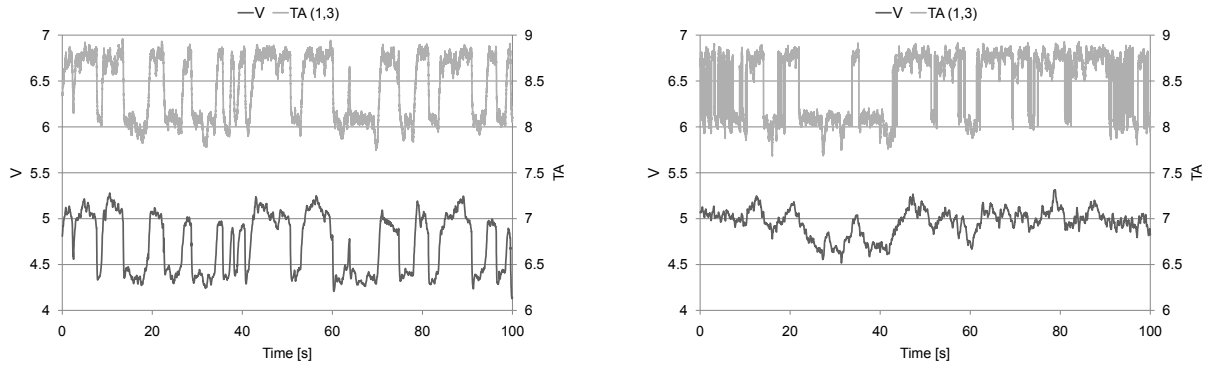

(a) Without compensation.

(b) With compensation.

Figure 3.32.: V and TA of link $(1,3)$ over time for one particular simulation ($p_{4,2} = 0.1$, $r_{\text{opt}} = 8.8$).

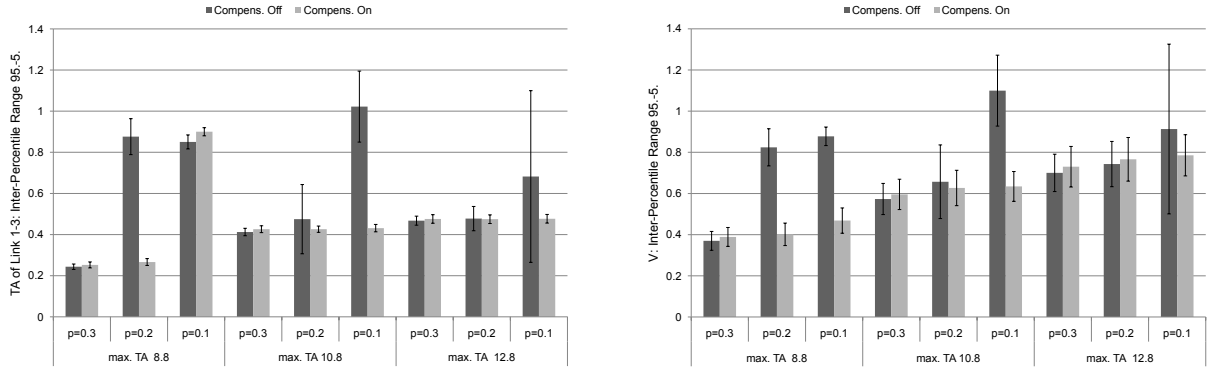

(a) Inter-Percentile Range (95th - 5th) of the TA of link $(1,3)$ ($\pm std.dev.$).

(b) Inter-Percentile Range (95th - 5th) of the V parameter ($\pm std.dev.$).

Figure 3.33.: Variability of TA and V for the diamond topology in Figure 3.31.

The results for one particular simulation run are plotted in Figure 3.32. In the left diagram, the compensation is turned off. As supposed, the credits of node 4 and node 1 almost equal, so that node 1 alternates between inclusion and exclusion of node 4 in its routing decision. On including node 4, it additionally activates the links $(1,4)$ and $(1,\{3,4\})$. The latter hyperlink and link $(1,3)$ have almost equal TAs by construction, so that the aggregated TA significantly exceeds the specified limit. Thus, the intra-flow adaptation has to decrease V in order to drive the aggregated TA of node 1 to its target value. In the same line, the parameter V has to be re-raised to its former level when node 4 is excluded from the routing decision, which leads to the oscillation of V in Figure 3.32a. The rationale of the compensation heuristics is to distribute the already available TA among the affected hyperlinks, so that the intra-flow adaptation remains almost unaffected. Thus, the TA of the compensated link $(1,3)$ in Figure 3.32b oscillates similar to the uncompensated link. However, the variability of V in the diagram is significantly reduced.

In the following, we measure the variability using the difference between the 95th and the 5th percentile of the underlying distributions of V and TA over time. The inter-percentile ranges of the V parameter and the TA of link $(1,3)$ across all simulation runs are shown in Figure 3.33. The results indicate that the example above is characteristic for the given parameters. However, the variability of the TA of link $(1,3)$ is considerably reduced when increasing the target sum-TA or when increasing the PSR on link $(4,2)$. We have observed that the routing decision of node 1 becomes more stable in both cases, i.e. the TCs assigned to node 4 run empty less often and the oscillation problem is less severe.

Nevertheless, there is a further difference between the compensated and uncompensated versions. As shown in Figure 3.32, the intra-flow efficiency adaptation ensures that the compensated and the uncompensated TAs of the link $(1,3)$ (and $(1,\{3,4\})$, of course) are approximately equal in average. However, we apply the compensation to link $(1,4)$ in addition, which increases the TC of node 4 and thus makes the routing decision with compensation more stable. In consequence, the routing decision in the compensated version alternates only for the parameter set $p_{4,2} = 0.1$ and maximum sum-TA 8.8, as shown in Figure 3.33a. In summary, the compensation approach significantly reduces the oscillation within the intra-flow adaptation, as indicated by the lower variability of the Vs in Figure 3.33b.

3.6.6. Multi-User Diversity

In this section, we illustrate how the system detects and utilizes MUD via anycast transmissions in order to enhance the end-to-end goodput in fading environments. We are using a block-fading channel model, in which the signal undergoes a parameterized Rician fading (cf. section 2.2.2). A single fading realization affects the data frame as a whole, and it varies i.i.d. between frames. For the ease of illustration, signaling traffic is not affected by fading, so that the underlying LCGs are stable in time. Due to the missing temporal correlations of the channel, an informed scheduler that relies on the memory of the channel has no advantages over channel-blind strategies considering statistical channel knowledge only. The considered channel model can be encountered in systems with short channel coherence times, for example.

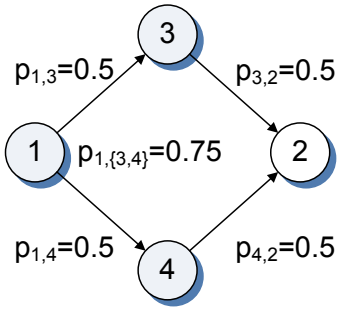

Figure 3.34.: Diamond topology with a flow from 1 to 2. The PSR is 50% (75%) for unicast (anycast) links.

The simulation topology is shown in Figure 3.34. It consists of 4 nodes and a two-hop flow between node 1 and node 2. The topology offers MUD but no spatial diversity, since at most one link can be activated at each time instance. The PSR is about 50% (75%) for unicast (anycast) links. The target step size and the per-hop delay limit are

$s_\infty = 0.001V^{-1}C^{-1}$ and $t_{\max} = 0.6$ s, respectively. The remaining parameters can be found in Table 3.7.

Figure 3.36 illustrates the evolution of the system for a particular simulation instance. The credits converge quickly according to Figure 3.36b. Since both routes offer the same throughput, the credits C_3 and C_4 of both relays are almost equal. Thus, the TC for both receivers $TC_{1,\{3,4\}} = C_1 - \max(C_3, C_4)$ is nonzero, whereas the TCs of the individual receivers $TC_{1,3} = [C_4 - C_3]_+$ and $TC_{1,4}$ are close to zero. The system weights the TCs with the PSR according to (3.29) on page 69 to get the TA in Figure 3.36c. Remember that the PSRs have to be determined from measurements and thus, they are subject to measurement noise. The system prefers the anycast link $(1, \{3, 4\})$, since it has the highest TA. Furthermore, the anycast link achieves substantially more throughput on the first hop compared to the unicast links (cf. Figure 3.36a).

In fact, the best solution according to the analytical model is to use the anycast link only on the first hop. However, the system approaches the optimum only asymptotically. In the finite regime, however, the usage of unicast links on the first hop cannot be completely prevented. We have solved the optimization problem for the idealized CSMA model in Maple using the given system parameters and $V = 4.5$ as estimated in the simulation. The average throughput on the anycast and unicast link is $q_{1,\{3,4\}} = 131$ pps and $q_{1,3} = q_{1,4} = 26.5$ pps, respectively, and the resulting flow rate is $f = 125$ pps. Hence, the local decision of the system to prefer the anycast link has turned out right in the end.

The scenario illustrates how the system detects opportunities to benefit from MUD. From the point of view of the network layer, there is no difference in using the anycast link or the unicast links, since the credits of both downstream nodes are equal. While determining the TAs, however, the MAC layer locally adjusts its preferences according to the PSR of the considered links (cf. Figure 3.36c). In particular, the MAC does not specify the best (hyper)-links in advance, since this would involve global knowledge. Instead, *all links* on the first hop have to *compete against each other* for medium access. The structure of the underlying optimization problem ensures that the resulting solution degrades gracefully. The optimum can be approached by increasing the V parameter. In this way, the TAs are linearly scales, so that the absolute difference between anycast and unicast TA increases. Hence, the preference of the system for the anycast link becomes more pronounced[8] and throughput is reallocated from the unicast links to the anycast link. Let us increase the efficiency parameter to $V = 6.2$, for example, so that the aggregated TA on the first hop becomes $r_{\text{sum}} = 10.8$ according to the analytic model. In this case, the analytic throughput changes to $q_{1,\{3,4\}} = 149$ pps and $q_{1,3} = q_{1,4} = 17.2$ pps. In the simulations, the throughput is $q_{1,\{3,4\}} = 138$ pps and $q_{1,3} = q_{1,4} = 21$ pps. Fortunately, the *local* decision coincides with the *global* solution in the diamond topology. In the next section, we will illustrate what happens if there is a disagreement between the local and the global view.

Let us generalize our view from a particular instance to a set of simulations. We have varied the target TA r_{opt} for the intra-flow efficiency adaptation. We have disabled the anycast operation for a subset of the simulations. Furthermore, we compare the performance against UDP and TCP on top of DSR and ExOR [23, 317]. In Figure 3.35a, we

[8] Remember that the TAs are the transition rates of the CSMA Markov chain in *exponential* scale.

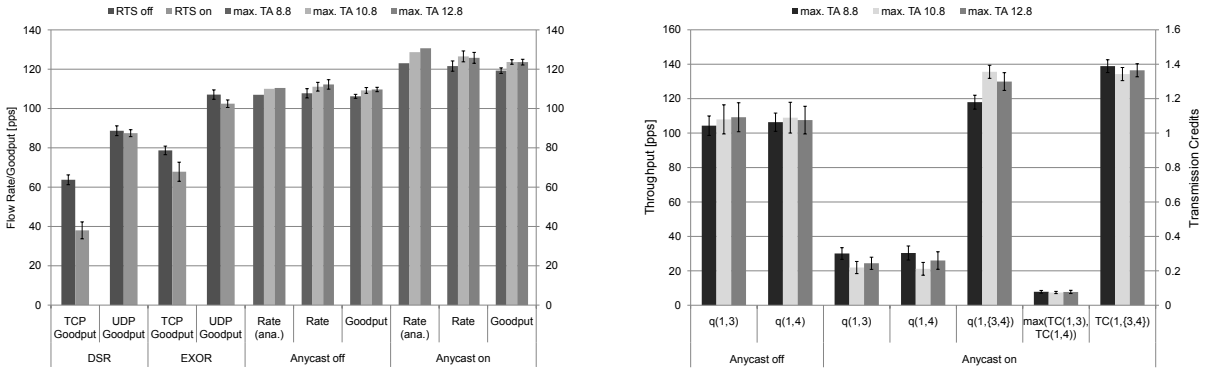

(a) Flow rate and goodput ($\pm std.dev.$).

(b) Throughput and transmission credits on the first hop ($\pm std.dev.$).

Figure 3.35.: Simulation results for the diamond network topology in Figure 3.34.

have plotted the flow rate and the goodput for the considered protocols. DSR achieves the lowest goodput. Nevertheless, remember that it is a single-path routing protocol, which does not benefit from MUD. On the other hand, ExOR performs better. However, it uses anycast on top of a slightly modified IEEE 802.11 MAC. Without anycast, the proposed protocol uses multi-path only, which has no advantages in the considered scenario. In particular, without anycast the goodput of the protocol with single-path (not shown) and multi-path routing is almost identical. With anycast turned on, the proposed protocol increases its rate and goodput due to the available MUD. As expected, larger target TAs result in higher goodput. In either case, the simulation results show a good match with the analytic predictions of the idealized CSMA model. In the analytical model, we have estimated an optimal flow rate of $y = 132.6$ pps in the high efficiency regime.

According to the optimality gap (3.4) of UO-CSMA on page 40, the efficiency of the candidate selection improves when we increase the V parameter and thus the target TA. When using the highest considered target TA of $r_{\text{opt}} = 12.8$, however, Figure 3.35b shows that the system is not able to reallocate further throughput from the unicast to the anycast link. In addition, we have observed that the throughput of the anycast link is generally lower than the model predictions, whereas the throughput on the unicast links is higher. The causes of the observed behavior are manifold. We suppose that virtual transmissions are one of them: The risk of a virtual transmission is higher for anycast links, since a queue overflow at a single receiver will cause a virtual transmission for the whole anycast link. They can be roughly estimated by considering the difference between the flow rate and the end-to-end goodput. Since fading is a random process, there is uncertainty within the channel. The transmitters have to estimate the PSRs via measurements. The resulting TAs are subject to the PSR measurement noise. In addition, the channel may corrupt signaling frames (RTS, CTS, ACK). The risk of signaling errors is higher for anycast links, so that the anycast link may not be able to take all its TXOPs.

The variability of the TCs and the TAs leads to short-term imbalances between paths. According to the analytic model, only the anycast link should have non-zero TCs on

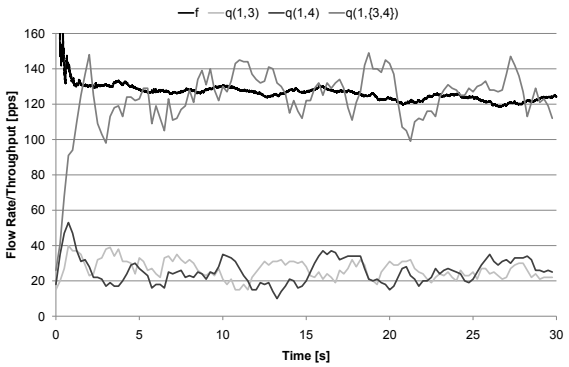

(a) Flow rate and throughput on the first hop (moving average over 1 s.

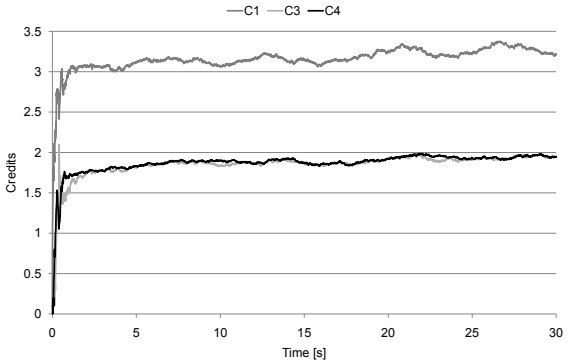

(b) Evolution of the (relative) credits.

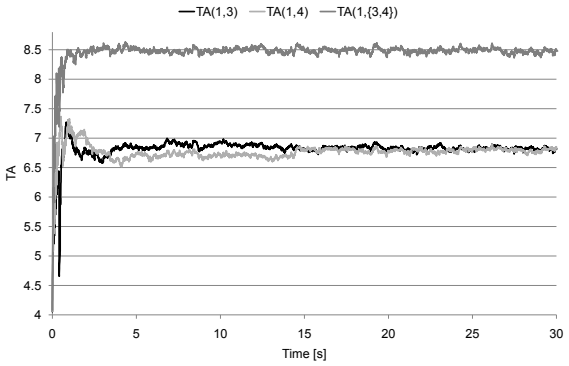

(c) Evolution of the TAs.

Figure 3.36.: Evolution of the system for an individual simulation instance ($r_{\text{opt}} = 8.8$).

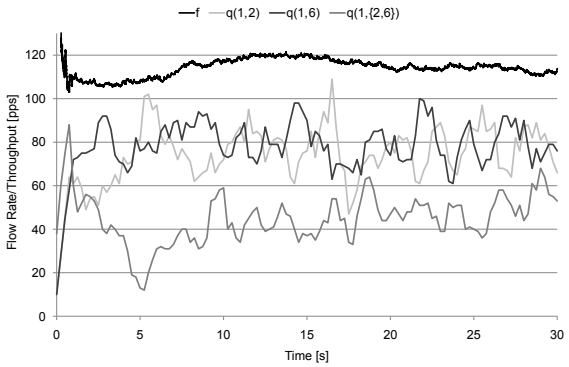

(a) Flow rate and throughput on the first hop (moving average over 1 s).

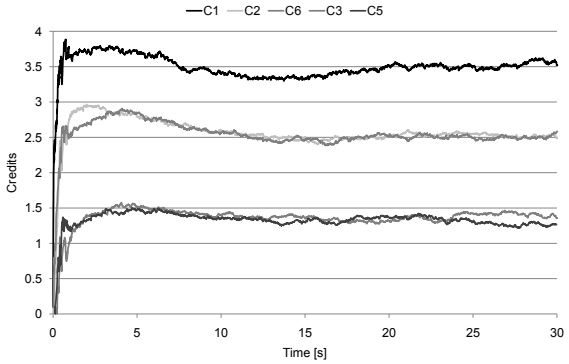

(b) Evolution of the (relative) credits.

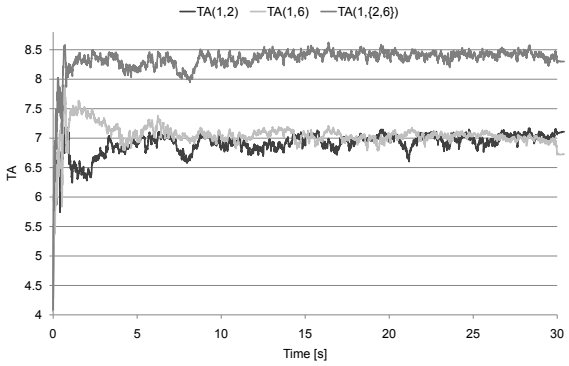

(c) Evolution of the TAs at the first hop.

Figure 3.37.: Evolution of the system for an individual simulation instance ($r_{\text{opt}} = 8.8$, $s_\infty = 0.001$).

the first hop. In Figure 3.35b, we have plotted the TC of the anycast link and the maximum TC of the unicast links. The unicast TCs are not zero in the simulations due to the dynamics of the credit queues. Note that this issue is closely related to both the intra-flow and the step size adaptation. In particular, requesting higher throughput efficiency increases the burstiness of the traffic at the same time. Hence, the imbalance problem between paths will get more serious. On the other hand, a smaller step size will reduce the variability and the imbalances to a certain degree.

3.6.7. Spatial Diversity

Depending on the topology, spatial and multi-user diversity may not be available at the same time. In this section, we illustrate how the system detects the form of diversity that performs best. In the last section, we have considered a topology that provides multi-user but no spatial diversity. On the first hop, the transmitter has considered the PSR of the involved links and decides to prefer the anycast link. In the end, this *local* decision has turned out to be correct for the *global* performance, as well.

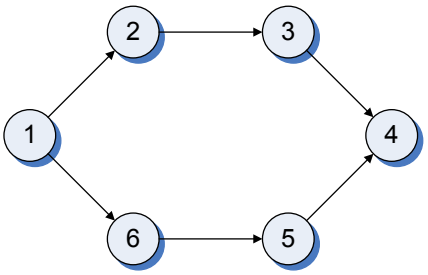

Figure 3.38.: Hexagonal simulation topology with a flow from node 1 to 4. The PSR is 50% (75%) for unicast (anycast) links.

In the following, we consider the hexagonal topology in Figure 3.38 with a traffic flow between nodes 1 and 4. From the perspective of node 1, it is equivalent to the diamond topology from the previous section. Nevertheless, the hexagonal topology provides spatial diversity since there are multiple collision domains. For each unicast link, there is another unicast link that can be activated at the same time. For example, link $(2,3)$ can operate simultaneously with link $(6,5)$. On the other hand, the anycast link $(1,\{2,6\})$ can operate in isolation only. Assuming that a unicast (anycast) link exhibits a PSR of 50% (75%), the local decision of node 1 to prefer the anycast link is *in opposition* to the globally optimal strategy, which activates the unicast links only. The remaining simulation parameters are left unchanged (cf. Table 3.7).

Figure 3.37 shows the results of one particular simulation instance. According to Figure 3.37b and Figure 3.37c, the credits as well as the TAs evolve similarly in both the hexagonal and the diamond network scenario. However, the throughput distribution on the first hop is different. According to Figure 3.37a, the anycast link still achieves a considerable amount of throughput, but the unicast links dominate. On first sight, this seems to be contradictory since the TAs are almost identical to the diamond network from the previous section and thus, node 1 still prefers the anycast link in terms of TA. The difference is within the topology. If link $(3,4)$ is currently active, for example, then only link $(1,6)$ would be allowed to transmit concurrently. Nonetheless, node 1 is not aware of that and may probe link $(1,2)$ or the anycast link. In this case, the probe fails since (one of) the receiver(s) is occupied and the link will be blocked (cf. section 3.2.1).

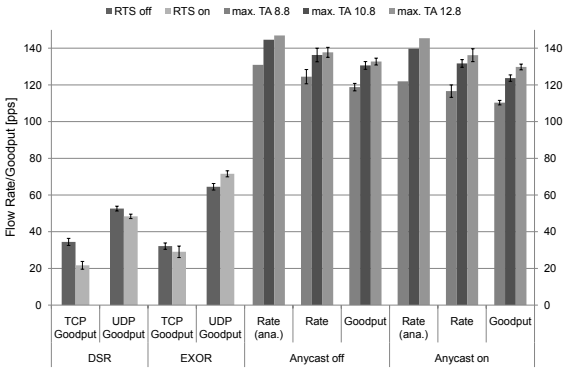

(a) Flow rate and goodput ($s_\infty = 0.001$, $\pm std.dev.$).

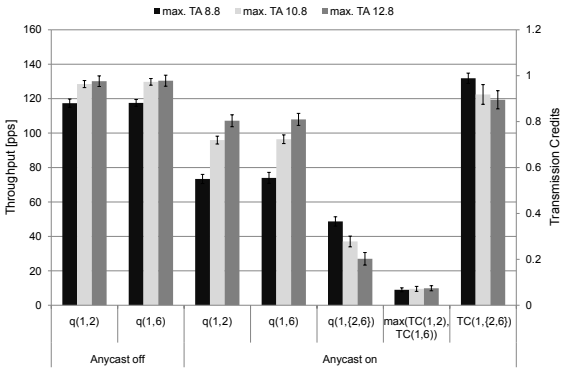

(b) Throughput and transmission credits on the first hop ($s_\infty = 0.001$, $\pm std.dev.$).

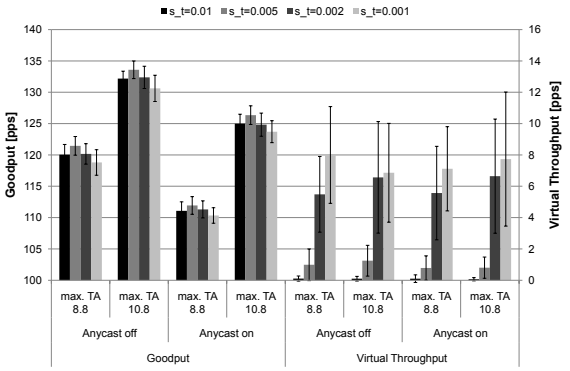

(c) Goodput and virtual throughput in relation to the target step size s_∞ ($\pm std.dev.$).

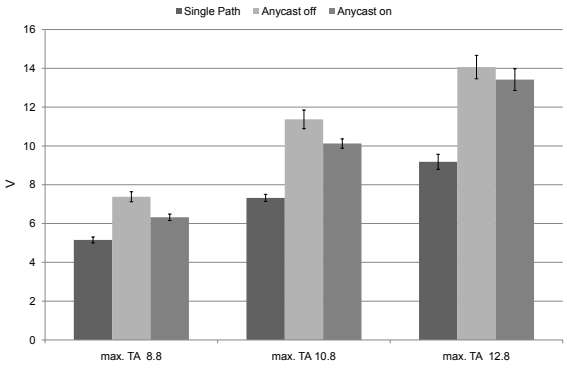

(d) Efficiency Parameter V ($s_\infty = 0.001$, $\pm std.dev.$).

Figure 3.39.: Simulation results for the hexagonal network topology in Figure 3.38.

On the other hand, the backoff of link $(1, 6)$ eventually expires, so that both unicast links will be transmitting concurrently, which takes the transmission opportunity away from the anycast link. The anycast link can only be activated in the less likely case that all other links are idle.

Interestingly, the goodput of ExOR is only slightly better than DSR (cf. Figure 3.39a). Remember that DSR is a single-path routing protocol, whereas ExOR uses multiple paths. However, ExOR is unable to exploit spatial diversity in the hexagonal scenario, since it uses anycast on the first hop only. On the other hand, the proposed protocol performs significantly better in comparison, because it limits its anycast usage as shown in Figure 3.39b.

When increasing the target TA r_{opt} as shown in Figure 3.39a, the system achieves a more efficient working point in terms of flow rate and goodput. We have analytically determined a flow rate of $y = 147.3$ pps in the high efficiency regime, which is achieved without anycast. In Figure 3.39b, we observe that the system gradually decreases the throughput of the anycast link when increasing the target TA. This can be explained as follows. The TAs are proportional to V. The contention becomes more aggressive when

increasing V, so that the average backoff windows get smaller. The anycast link can be activated only if all other unicast links are silent. In particular, the backoff periods of each unicast link pair that can operate concurrently have to overlap. When the backoff periods become smaller, however, the probability of overlapping decreases. In other words, the system persists longer in the states of maximal spatial reuse [65, 167]. Thus, the unicast links benefit from the higher TAs in the first place, since the anycast link is blocked more often after unsuccessful probes.

Starting from *identical initial conditions* and taking the *same actions*, the system implicitly identifies the type of diversity to use based on the differences in the underlying LCG. However, the system needs to actually probe and use *all* available (hyper)-links in order to identify its opportunities. In particular, no link can be excluded in advance, since the system identifies potential spatial or multi-user diversity from the answer of the network to its actions. On the other hand, each additional link introduces costs. It contributes to the aggregated per-hop TA r_{sum}, so that the TA target is reached earlier in the inter-flow adaptation (cf. section 3.5.2). In the hexagonal scenario, for example, the anycast link should not be used at best, although it contributes the most to the sum TA r_{sum} according to Figure 3.37c. By excluding the anycast link, the TAs on the unicast links can be increased without violating the respective target. Disabling anycast results in a larger V (cf. Figure 3.39d) and thus in a higher goodput (cf. Figure 3.39a). The underlying cause is the increase of the optimality gap (3.4) of UO-CSMA on page 40 that increases in the number of involved links. Nonetheless, an interesting question for our future work is whether heuristics can be developed to decide when to use anycast.

Furthermore, we have estimated the influence of the target step size on the performance of the proposed protocol. Interestingly, the highest goodput is achieved with a medium step size of $s_\infty = 0.005$ (cf. Figure 3.39c). We argue that the reasons are within the limitations on the burstiness of the underlying network dynamics. When decreasing the target step size, the variability of the credit queues decreases, so that the short-term imbalances between different routing paths are reduced. However, virtual transmissions emerge when decreasing the target step size further, so that the overall performance suffers (cf. Figure 3.39c). We suppose that the smaller step size renders it more difficult for the system to outweigh the noise of the PSR measurements.

3.7. System Level Evaluation

We have illustrated the operation of the system within small and synthesized topologies in the previous section. In the following, we evaluate the system in larger scenarios. We are particularly interested in the following questions: Does it pay off to design a cross-layer MAC especially for WMNs? And if so, what potential for OR is left to a dedicated mesh MAC? To answer these questions, we have conducted network simulations to compare the performance of the cross-layer protocol and state-of-the-art protocols across a large set of randomized topologies. The use case we are considering is the so-called *community network scenario*: The network nodes have been deployed by members of the community in a spontaneous and unplanned manner resulting in a random topology. Every community member can be both consumer and provider of network services. In the following, we consider the service of long-lasting and elastic

Parameter	Value
Area	square $\{300\text{ m}, 600\text{ m}, 500\text{ m}, 1000\text{ m}\}$[1]
Topology	random with $\{30, 120, 50, 200\}$ nodes[1]
Inter-node distance (min)	$\{30\text{ m}, 30\text{ m}, 50\text{ m}, 50\text{ m}\}$[1]
Path loss	Log-distance with exponent 3
Radio frequency	2.4 GHz
Channel	AWGN
Fading	i.i.d. Rician block fading $K = \{-\infty, 10.8\}$ dB
Reception model	SNR threshold & outage probabilities
Interference	Protocol model (no cumulative interference)
PHY	IEEE 802.11a/g, $\{6, 12, 24, 48\}$ Mbps[2]
SNR thresholds[3]	$\{5.4, 7.0, 11.3, 18.6\}$ dB[2]
TX power	19 dBm
Noise floor	-92.965 dBm
CCA threshold	-88.5 dBm
Routing metric	ETT
(Metric, Hop) stretch	$\{(1.05, 1.5), (1.1, 2.5), (1.3, 3), (1.5, 4), (1.8, 5)\}$
Seeds	100

[1] The same indices belong together, e.g. 300 m is used with 30 nodes and 30 m spacing; 500 m is used with 50 nodes and 50 m, and so on.
[2] The same indices belong together.
[3] 1000 octets, 10% FER.

Table 3.8.: System parameters for the analytic evaluation

file transfer. To start with, we evaluate the potential of WMNs for spatial and multi-user diversity in the community network scenario. We have solved the underlying optimization problem numerically for a large set of topologies in order to get a better understanding of the multi-path and anycast gains that can be expected.

Table 3.8 and Table 3.9 summarize the parameters for the analytic and the simulative evaluation. The fading process is i.i.d. in time, so that the channel is memoryless. We have applied fading to data frames only. Signaling frames are generally more robust against channel impairments because they are shorter and they are often transmitted using a lower bit-rate. Each configuration is repeated 100 times with different random seeds. If not stated otherwise, the average as well as the standard deviation of the resulting distribution is reported. Note that the node placement changes with each random seed. In order to avoid a clustering of nodes within certain areas, we constrain the distance between neighboring nodes to a specified minimal spacing.

3.7.1. Potential of Multi-User and Spatial Diversity

In this section, we evaluate the potential of WMNs for multi-user and spatial diversity in the community network scenario. We assume that UO-CSMA operates at the asymptotical optimum, so that it achieves the performance of MWS. We have solved the opportunistic multi-commodity flow problem [220, 295] for a large set of topologies using a numerical solver. In addition, we put the results in the context of our route

pre-selection heuristics to illustrate its effectiveness (cf. section 3.5.5). The opportunistic multi-commodity flow problem is similar to the opportunistic CSMA problem that we have introduced in section 3.4.1 on page 64. The difference is that the objective does not contain a term for the entropy of the CSMA Markov chain. In the following section, we will consider the extent to which the proposed protocol can realize the prospected potentials at typical operating points in the finite regime.

The considered topologies consist of $30 - 200$ nodes randomly placed in a square area with varying node density (cf. Table 3.8). A single flow traverses the network from left to right. The node closest to the middle of the left (right) edge of the simulation area becomes the source (destination) of the flow. In the following, we use the terms adaptive and fixed bit-rate to refer to the results with all four bit-rates and only 6 Mbps, respectively. The PER is the outage probability P_{out} of the fading channel, which is the a priori probability that the SNR is below a given threshold. Details about the estimation of P_{out} are given in section 2.2.2. The protocol model is used for interference modeling: Two links are in conflict and cannot be activated simultaneously if at least one node of every link (either sender or receiver) is within the CS range of the other, so that the power of the received signal is above the CCA threshold. The protocol model does not consider the impact of the cumulated interference of concurrent transmitters on the CCA and the receiver operation. Thus, the obtained gains of spatial diversity should be understood as upper limits for a physical environment.

Every bar in Figure 3.40 and Figure 3.41 shows the average flow rate of the single-path protocol variant in one particular system configuration with the multi-path and anycast gains on top. Note that the flow rate cannot decrease when going from single-path to multi-path and further to anycast routing, since the optimization gets more opportunities each time and it chooses the best among them. As shown in Figure 3.41a and Figure 3.41b, a Rician channel with $K = 10.8$ dB offers little MUD due to the low channel variability. The gains are below 0.04 in most cases, so that they become almost negligible with bit-rate adaption. On the other hand, Rayleigh fading has more potential for MUD. The gains are about 0.05 for 2 candidates and sufficient stretch parameters (cf. Figure 3.40a). With adaptive bit-rates and 3 or more candidates, they are even higher than 0.08 ((Figure 3.40b).

Interestingly, the relative MUD gains become smaller with bit-rate adaptation. We suppose the additional throughput of a higher bit-rate outweighs the MUD gains, which leaves fewer opportunities for anycast. By construction, the flow rate is non-decreasing in the number of candidates and in the stretch parameters of the route pre-selection. The returns of both parameters are nevertheless diminishing. When increasing the stretch from 1.3 to 1.8, for example, the additional MUD gains are below 0.015 in most cases.

We have observed that two effects determine the achieved multi-path gains. With spatial diversity in a narrow sense, bottlenecks can be mitigated using alternative routes. In some cases, however, the ETT heuristics[9] is not able to find the highest throughput route. With *route selection diversity*, we refer to the effect that additional paths can outweigh a sub-optimal routing decision. The absolute multi-path gains are almost equal across all Rician Ks for fixed bit-rates. With adaptive bit-rates, on

[9]ETT assumes that all nodes share the same collision domain [58].

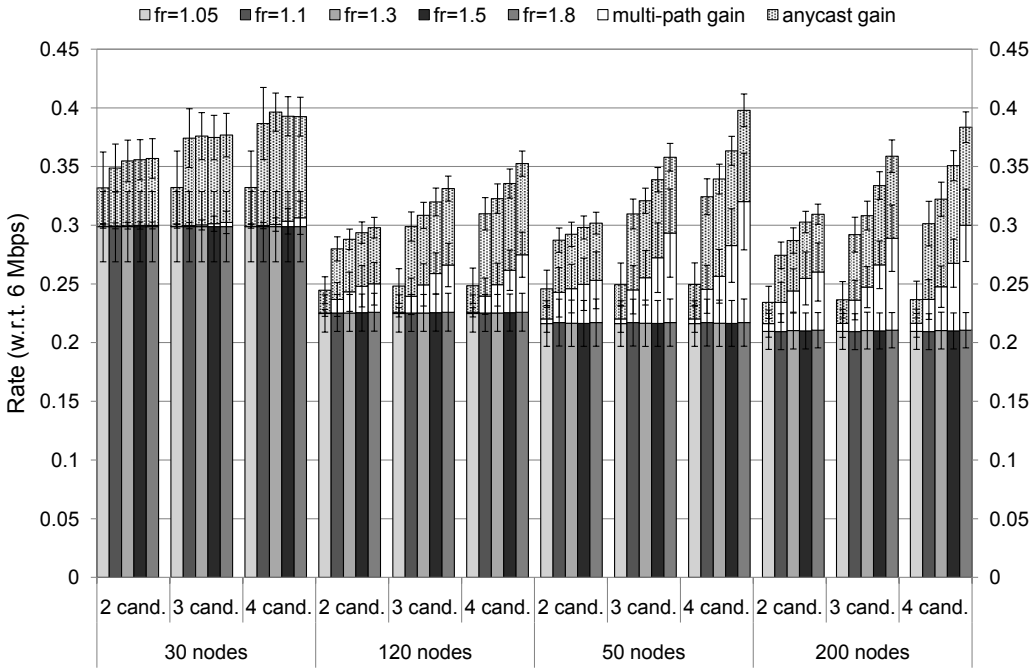

(a) Fixed bit-rate ($\pm std.dev.$).

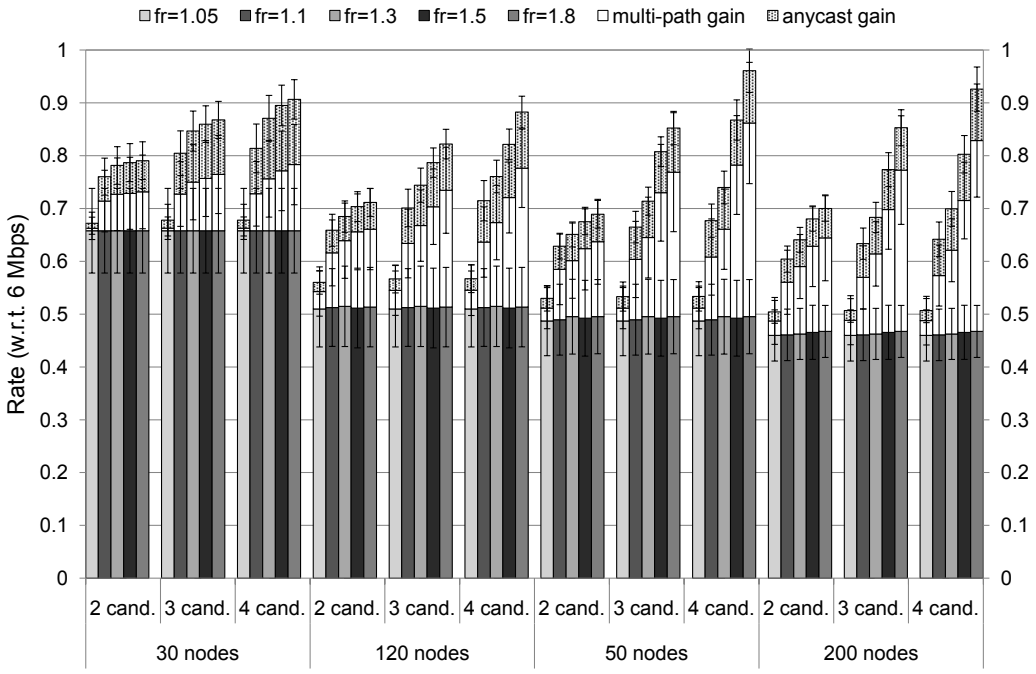

(b) Adaptive bit-rate ($\pm std.dev.$).

Figure 3.40.: Flow rate obtained from numerically solving the opportunistic multi-commodity flow problem ($K = -\infty$ dB, stacked bar charts).

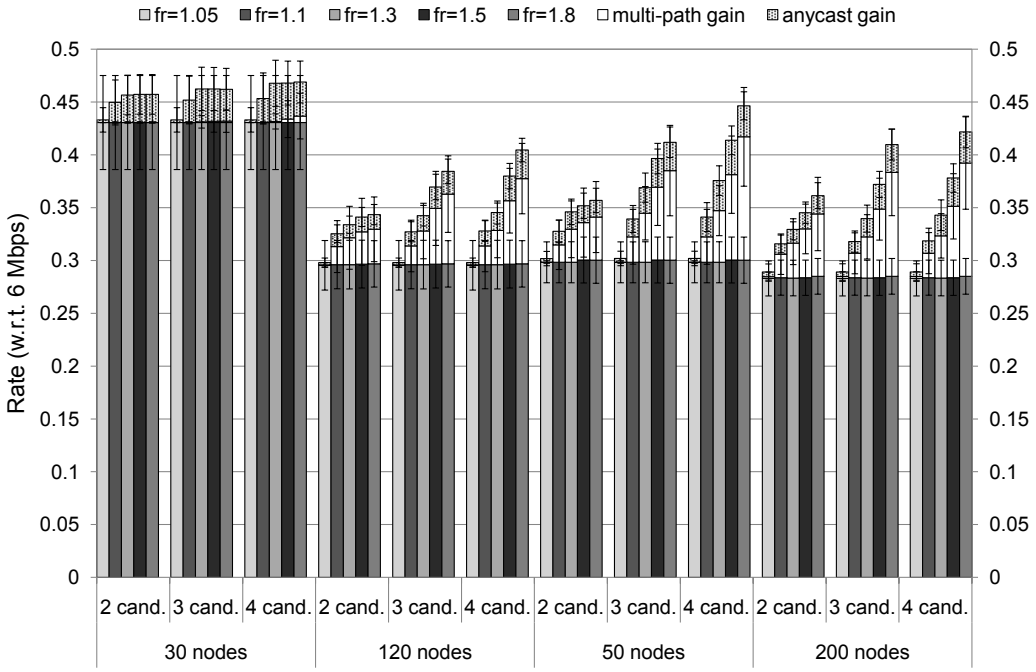

(a) Fixed bit-rate ($\pm std.dev.$).

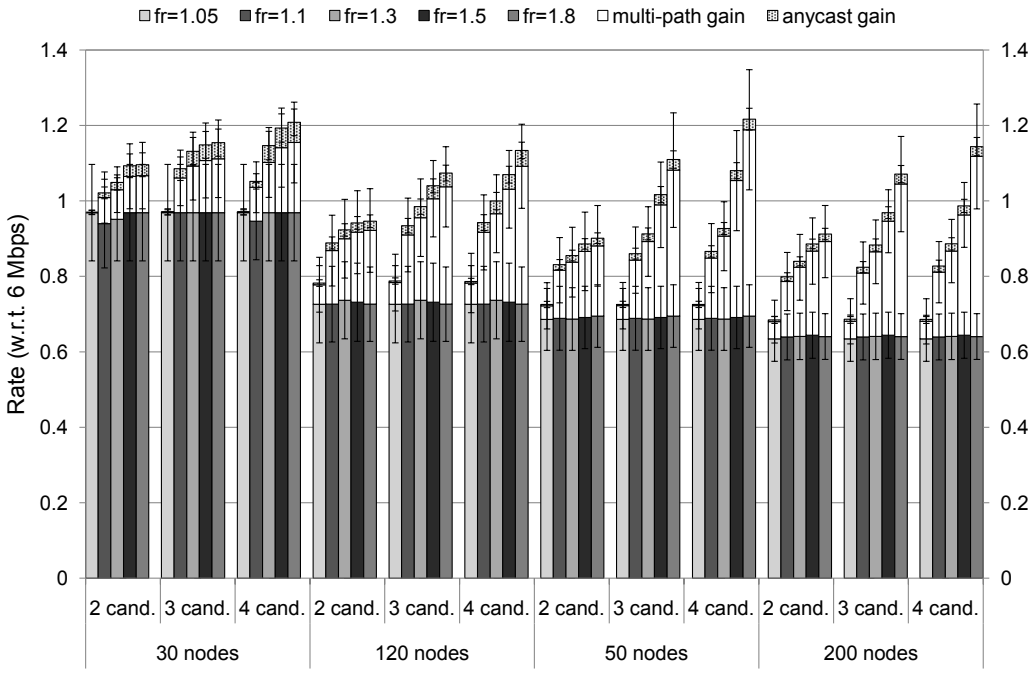

(b) Adaptive bit-rate ($\pm std.dev.$).

Figure 3.41.: Flow rate obtained from numerically solving the opportunistic multi-commodity flow problem ($K = 10.8$ dB, stacked bar charts).

the other hand, the multi-path gains increase with the Rician K when using sufficient large routing stretches and network topologies. In either case, the absolute and relative multi-path gain under adaptive bit-rate selection significantly exceeds the gain when using a fixed bit-rate only. However, remember that our model does not account for cumulative interference and that the LCG is independent from the fading distribution.

The multi-path gain can be increased with larger routing stretches in most cases, although the returns are generally diminishing. With 2 candidates, the returns for stretches larger than 1.1 are small. In contrast, a third or fourth candidate may achieve significant returns beyond a stretch of 1.1 given adaptive bit-rates and a sufficient large network. Thus, we suppose that the multi-path potential of larger networks is not exhausted yet, so that both the number of candidates and the routing stretch are the limiting factors.

In conclusion, the community network scenario has a pronounced potential for multi-path diversity. Nevertheless, the potential for MUD can be significant depending on the fading distribution. With adaptive bit-rates, the MUD potential is generally smaller in relation and it is used up quickly. With 2 candidates, in particular, the anycast gains are about 10% (20%) for adaptive (fixed) bit-rates. Our route pre-selection heuristics succeeds in selecting paths with potential for MUD. The major gains can be realized with small routing stretches, and the topologies offer little additional returns when increasing the stretches further. On the other hand, the proposed route pre-selection is the limiting factor for realizing multi-path gains. Assuming sufficient large networks and routing stretches, multi-path gains in the order of $20\% - 30\%$ ($10\% - 20\%$) can be achieved under adaptive (fixed) bit-rates. However, the multi-path gains are optimistic since we have not accounted for cumulative interference and the LCG is independent from the fading distribution.

At typical working points of UO-CSMA in the finite regime, the system has to pay for every additional (anycast) link in terms of flow rate. The main deficit of the route pre-selection heuristics is that it blindly selects additional nodes and anycast links when increasing the routing stretch or the number of candidates. In our future work, we would like to explore better heuristics that trade the incurring costs of additional relays and anycast links against the expected returns.

3.7.2. Simulative Evaluation: The Single Flow Case

In the following, we evaluate the performance of the proposed cross-layer protocol in the community network scenario using network simulations. Our intention is two-fold. On the one hand, we consider the extent to which the proposed protocol can realize the potentials that we have illustrated in the previous section. On the other hand, we compare the performance of the proposed protocol and state-of-the-art protocols across a large set of randomized topologies to illustrate the benefits of a mesh-enabled MAC and a cross-layer routing protocol that is designed for WMNs.

We present simulation results obtained from a WMN simulator (cf. section 2.5). The system parameters are summarized in Table 3.9. We are using two slightly different fading models: The first one is a synthetic model that halves the PSR of the AWGN channel regardless of the link's SNR (scenario A). The second one is a Nakagami fading [84] with parameter $\mu = 0.75$ (scenario B). The severity of the considered fading

Parameter	Value
Area	300 m × {300 m, 500 m}[1]
Inter-node distance (min)	{30 m, 50 m}[1]
Topology	30 nodes randomly placed
Fading (Scenario A)	i.i.d. synthetic ½PSR
Fading (Scenario B)	i.i.d. Nakagami $\mu = 0.75$
Receiver	SNR-BER & cumulative interference
MAC	CSMA/HBT
CCA	Mode 1, threshold −88.5 dBm
Propagation delay	2 µs
Radio turnaround	9 µs
TXOP duration	2.5 ms
TA limits	$4 - 8.8$
Queue limits	16 - 100
Step size (initial/target)	$0.1 \cdot V^{-1}$ / $0.002 \cdot V^{-1} \cdot C^{-1}$
Step size update interval	200 ms
Target per-hop delay	0.8 s
Flow duration	20 s evaluated (excl. warm-up)
Packet size	1500 Byte

[1] The same indices belong together.

Table 3.9.: Simulation parameters (In addition to Table 3.8)

process is slightly higher compared to Rayleigh fading (cf. section 2.2.2). To get an impression of the dimension of the simulation scenarios, the average hop count across all 100 repetitions for DSR/UDP is shown in Table 3.10.

In Figure 3.42, we have plotted the goodput CDF across all seeds for Nakagami fading with a width of 500 m and adaptive bit-rates. In the figure, DSR and the proposed protocol OPT with a single candidate (in short: 1/1) achieve a shallow CDF. Remember that both approaches rely on single path routing. The CDF gets steeper under multi-path routing. We suppose that this is an indication of diminishing returns, since the diversity gets exhausted in the same way the links are improved. Under multi-path routing without anycast (2/1), the goodput degrades in the high goodput regime (70% and above). Remember that additional links increase the optimality gap (3.4) of UO-

Scenario	Length	Bit-rate	Hop Count
A	300 m	single	2.0
		adaptive	3.2
	500 m	single	3.8
		adaptive	5.3
B	300 m	single	2.4
		adaptive	3.9
	500 m	single	4.2
		adaptive	6.3

Table 3.10.: Average hop count for DSR/UDP in scenario A and B

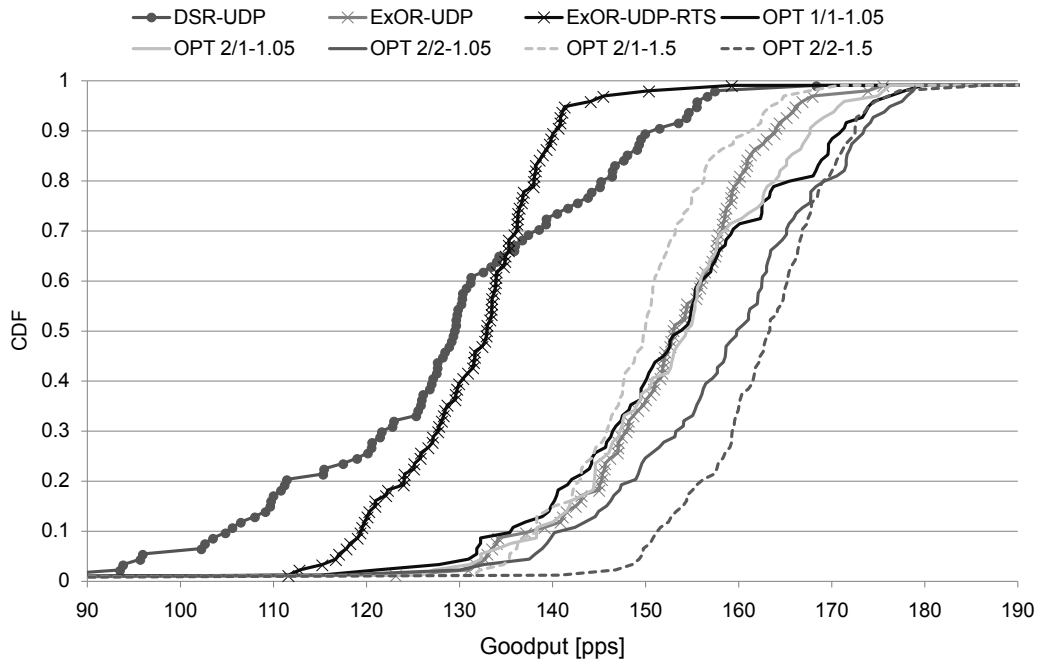

Figure 3.42.: Goodput CDF for the community network scenario B (adaptive bit-rates, 500 m, legend: no. candidates / no. anycast receivers - metric stretch).

CSMA on page 40. The overall goodput suffers if the spatial diversity cannot outweigh this loss. The same holds for anycast (2/2), although the scenarios offer sufficient MUD to increase the overall goodput. The anycast gains are realized in the midrange regime around the median.

With increased routing stretches, the impact of multi-path and anycast routing becomes more pronounced. With a metric stretch of 1.05, for example, the anycast and single path CDFs are close to each other within the low goodput regime ($0\% - 20\%$). A substantial improvement can be observed with a metric stretch of 1.5. If multi-path is used without anycast, on the other hand, a performance loss can be observed with larger routing stretches especially in the high goodput regime.

According to Figure 3.42, the proposed protocol OPT significantly improves the single-path performance. For example, the median goodput increases from 133 pps under DSR/UDP to 154 pps. Thus, we argue that it pays off to consider the characteristics of WMNs in the MAC design. Since many opportunities for the routing layer to outweigh the impairments of the MAC vanish, on the other hand, the OR gains under the cross-layer protocol are generally smaller. For example, anycast increases the median goodput from 154 pps to 163 pps.

The average goodput as well as the estimated flow rate for scenario A and B is shown in Figure 3.43 and Figure 3.44, respectively. As long as our observations are consistent across all diagrams, we refer to an individual figure only if necessary. Using TCP with either DSR or ExOR results in a loss of goodput. The same holds for the usage of RTS in most cases and especially with adaptive bit-rates. Note that both DSR and

ExOR do not use TXOPs, so that the per-packet overhead increases when using RTS at higher bit-rates. Furthermore, ExOR has a higher goodput performance than DSR in the considered scenarios.

The goodput performance of the proposed protocol OPT in its single-path routing variant (1/1) is better than DSR and close to ExOR with a single bit-rate. It even exceeds ExOR with adaptive bit-rates. Nevertheless, remember that both DSR and ExOR are less conservative in terms of MAC exclusion due to the hidden node problem. The proposed protocol, on the other hand, reserves the medium around transmitter and receiver(s), which results in lower spatial reuse. To understand the impact of the larger exclusion region, we have additionally conducted simulations with reduced transmission power P_{bt} of the data busy tone (BTD). In this way, the exclusion region around transmitter and receiver(s) gets smaller. The spatial reuse is increased at the expense of potentially lower SINR margins and thus, an increased risk for receive failures. We have plotted the goodput results for the 500 m topology in Figure 3.45. The diagram illustrates the tradeoff within the selection of P_{bt} especially for the physical fading model in scenario B: The highest goodput is achieved with a slightly reduced power setting. The tradeoff tends towards a more conservative power setting in scenario A, which indicates that the SINR margins are smaller.

Coming back to Figure 3.43 and Figure 3.44, the goodput of the proposed protocol OPT slightly decreases with higher routing stretches in most cases when using multi-path routing without anycast (2/1). According to the previous section, the topology should offer spatial diversity especially with adaptive bit-rate selection. Nevertheless, remember that the simulator relies on the physical interference model. We have used the protocol model in the previous section, which leads to optimistic results in terms of spatial diversity. Furthermore, the multi-path gains are outweighed by the increased optimality gap of UO-CSMA due to the higher number of relays. The end-to-end delay limiting further intensifies the effect: With increasing routing stretches, the estimated flow rate increases in most cases, although the goodput declines at the same time. The difference between flow rate and goodput is roughly the amount of virtual traffic. With higher per-hop delay limits, both flow rate and goodput will converge and the virtual traffic will vanish.

When using anycast (2/2), the goodput of the proposed protocol increases even for small routing stretches. For larger routing stretch, the goodput increases up to a point where the MUD benefits are eventually outweighed by the costs of additional links. The anycast gains are smaller than expect according to section 3.7.1. Especially in scenario B, the performance of the proposed cross-layer protocol with anycast and a single bit-rate is slightly lower compared to ExOR. The reasons are manifold. The SINR margins are larger under Nakagami fading (cf. Figure 3.45). Furthermore, remember that the cross-layer protocol achieves the optimum asymptotically. Sub-optimal decisions cannot be prevented in the considered regime (cf. section 3.6.6). In small topologies, the risk of wrong decisions is lower for ExOR since there are fewer possibilities. With adaptive bit-rates and large topologies, on the other hand, the growth of the possibilities makes a wrong decision more likely for ExOR.

In addition, ExOR splits the traffic among different paths statically. If one path is not able to support the predetermined fraction of traffic, the queues will build up. The genie-aided saturating UDP congestion control assures that the number of in-flight

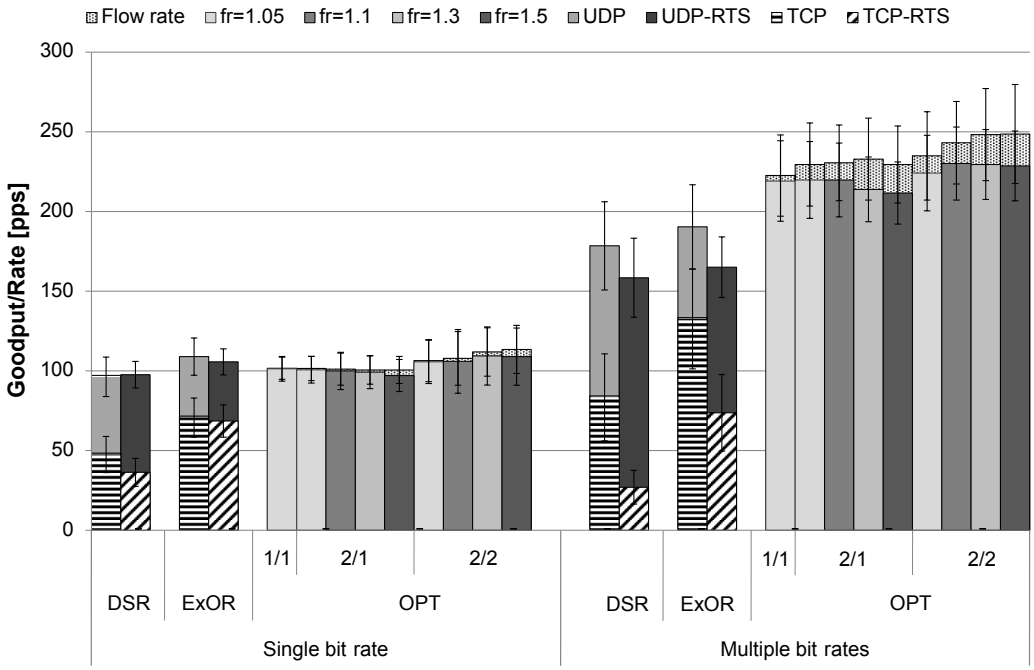

(a) Flow rate and goodput (300 m, $\pm std.dev.$).

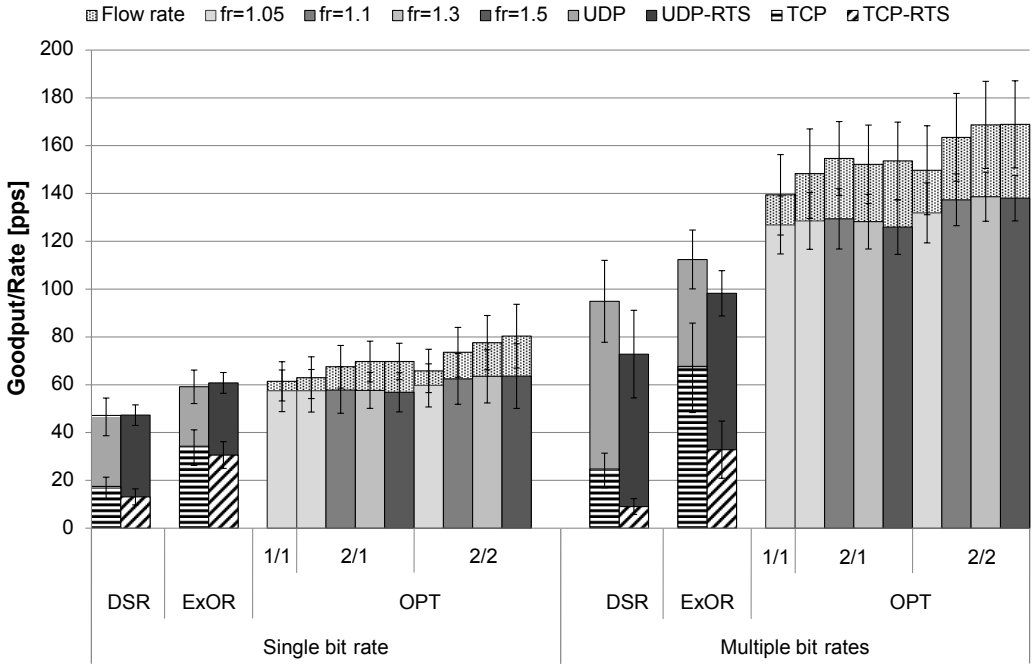

(b) Flow rate and goodput (500 m, $\pm std.dev.$).

Figure 3.43.: Simulation results for the community network scenario A (Synthetic fading ½PSR, overlapped bar charts).

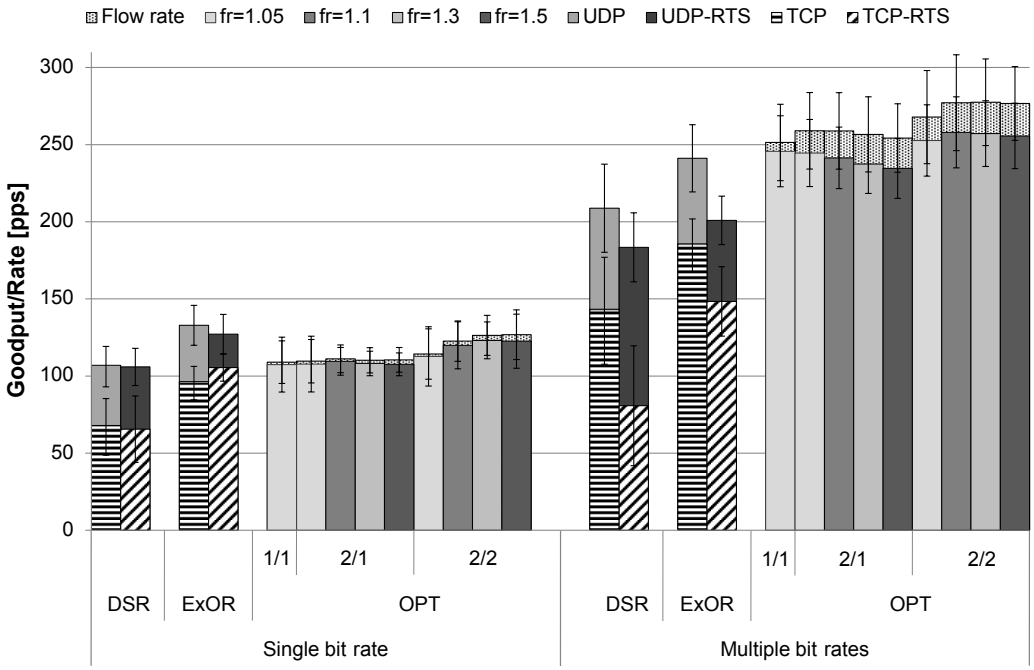

(a) Flow rate and goodput (300 m, $\pm std.dev.$).

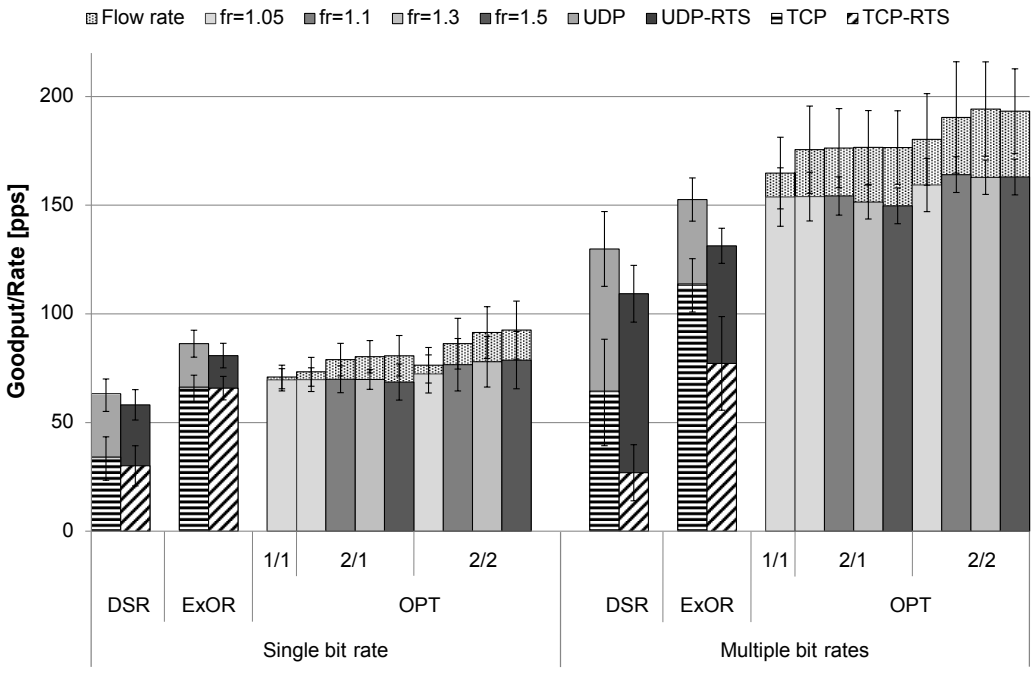

(b) Flow rate and goodput (500 m, $\pm std.dev.$).

Figure 3.44.: Simulation results for the community network scenario B (Nakagami fading $\mu = 0.75$, overlapped bar charts).

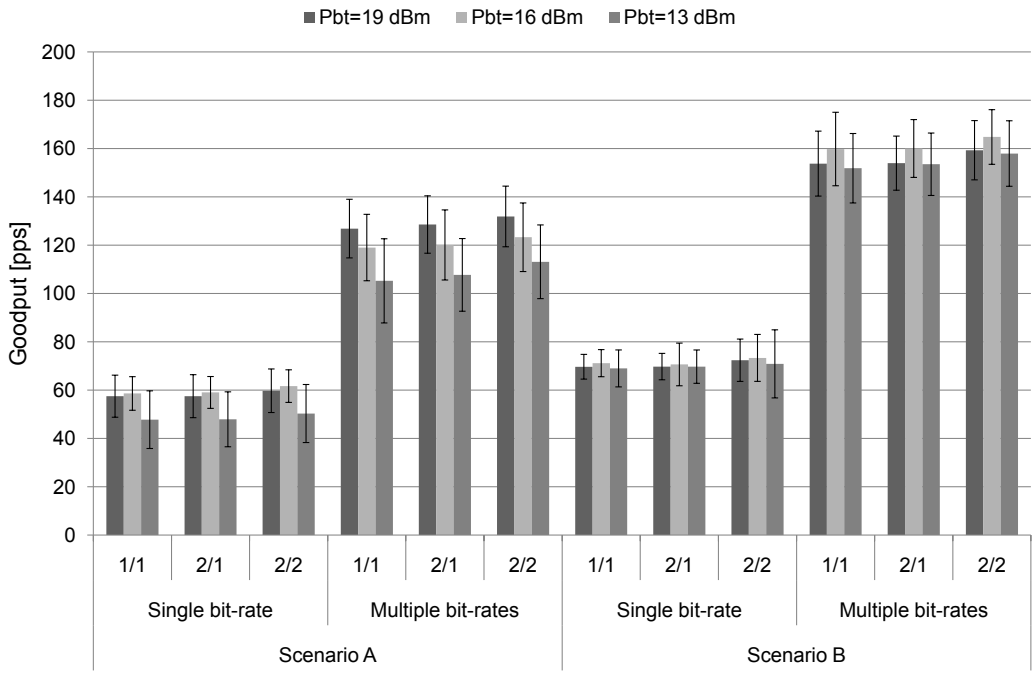

Figure 3.45.: Goodput of the proposed protocol for the community network scenario depending on the power of the data busy tone (500 m, $f_{\mathrm{r}} = 1.05$, $f_{\mathrm{h}} = 1.5$, $\pm std.dev.$).

packets does not exceed a fixed amount of 1000 packets. If the queues along the weaker path have eventually absorbed all available in-flight packets, the congestion controller will throttle its rate. Thus, the goodput on the stronger paths suffers from the static traffic split.

The generation of the link tables for the ETT routing metric [62] has been one particular problem in the simulations. There are conflicting objectives for the estimation of the link quality indicators (LQIs). On the one hand, they should be accurate, and on the other hand, the estimation should consume few medium resources and it should adapt to environmental changes in a timely manner. In the end, the problem boils down to the selection of the interval, packet sizes and bit-rates for link probing. We have used a conservative setting with a very long settling time in order to get acceptable LQIs estimates, so that the results remain comparable. Under typical parameter settings [58], however, the accuracy is very low, which gives rise to *route selection diversity*. In scenarios having neither multi-user nor spatial diversity, multi-path routing offers no advantages. Nevertheless, it might mitigate the uncertainty in the LQIs.

Based on our simulation results, we conclude that it is necessary to consider the mesh nature in the design of MAC protocols. In particular, IEEE 802.11 has been designed for cellular environments. In WMNs, it causes a waste of resources especially on the MAC layer, although opportunistic routing might mitigate the design shortcomings to a certain extent. According to our simulation, however, a mesh-enabled MAC design within a cross-layer protocol achieves the better goodput results in most cases. Conversely, the benefits of MUD become smaller. Opportunistic routing compensates the

Parameter	Value
Area	500 m × 500 m
Inter-node distance (min)	50 m
Topology	50 nodes randomly placed
Fading	i.i.d. Nakagami $\mu = 0.75$
No. flows	$1 - 4$
Flow setup A	horizontal (flow-in-the-middle scenario)
Flow setup B	radial (congested-center scenario)
Inter-flow hysteresis	1.1

Table 3.11.: Simulation parameters (In addition to Table 3.9)

impairments of the lower layers. If less is wasted on the lower layers, then the potential of OR will become smaller.

Furthermore, our results show clearly that every additional link causes high costs in terms of the UO-CSMA optimality gap. Two directions seem promising in order to reduce the gap. New contention technologies might offer a higher dynamic range in terms of contention differentiation, which enables working points for UO-CSMA with higher efficiency. On the other hand, the route pre-selection should be more selective. Instead of blindly including additional links, it should decide on an individual cost-benefit basis. We postpone the further discussion to chapter 5.

3.7.3. Simulative Evaluation: The Multiple Flow Case

When multiple flows share resources of the WMN, the fairness between them becomes a further objective for the network. The concept of utility is generally used to handle the tradeoff between throughput and fairness. In this section, we evaluate the proposed protocol in terms of utility in the community network scenario. Our intention is two-fold. On the one hand, our objective is to characterize the behavior of the system with increasing number of flows in order to identify its limitations. On the other hand, we compare the performance of the system to state-of-the-art approaches within typical multi-flow scenarios.

We consider two well-known scenarios: In the *flow-in-the-middle* scenario, the collision domains of the involved flows overlap to varying degrees. Traditional approaches are reported to handle this scenario unsatisfactory resulting in severe unfairness and starvation [75]. In the *congested-center* scenario, the center area of the network becomes overloaded due to traffic flows, which originate at the edges and cross the network. Generally, a shortest path routing protocol chooses paths through the center of network, so that the center becomes congested with increasing number of flows [181]. Interestingly, Yi *et al.* report that multi-path routing can spatially smooth the traffic in this scenario, so that the congestion at the network center is mitigated [286].

The simulation setup is comparable to the previous section with a few exceptions (cf. Table 3.11). The simulation topology consists of 50 nodes randomly placed in an area of 500 m × 500 m with a minimal neighbor distance of 50 m. We use Nakagami fading only with $\mu = 0.75$ and adaptive bit-rates. There are between 1 and 4 flows that

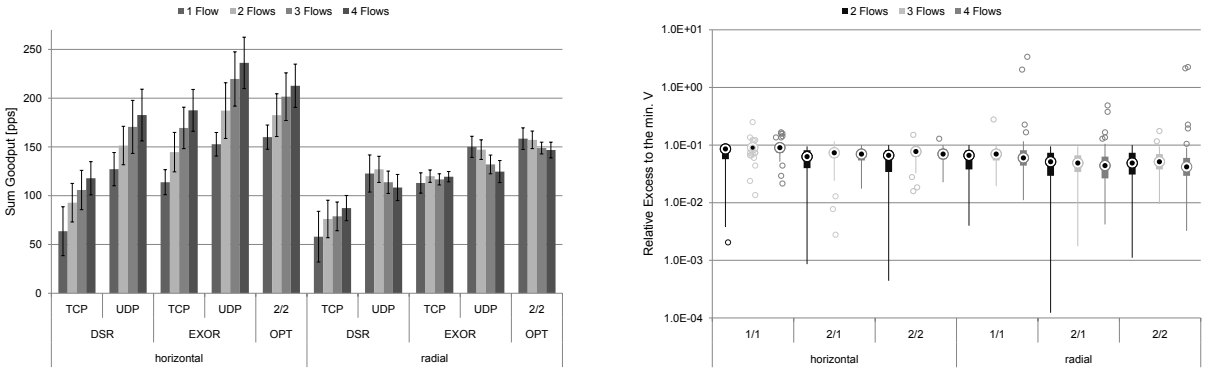

(a) Cumulated goodput (RTS off, $\pm std.dev.$). (b) Excess of the max. V relative to the min. V (Box plot).

Figure 3.46.: Cumulated goodput and excess of V between flows ($f_r = 1.05$).

traverse the network either horizontally or radially. In the latter case, we lay a circle of the same diameter over the network. The ideal positions of the flow sources are placed on the half circle with an equal spacing. The ideal positions of the destinations are placed in opposition. Based on these ideal positions, we select the closest network nodes as respective sources or destinations. For horizontal traffic, we place the ideal positions equally spaced on opposite edges of the network area and determine the actual nodes according to their distance from the determined positions.

We have already reported results for one flow in the previous section. Nonetheless, we have plotted them in Figure 3.47 and Figure 3.48 as a point of reference. Note that the network topology is the same for both horizontal and radial traffic. However, the center of the network will most likely become the bottleneck with radial traffic (*congested-center* scenario). In fact, the cumulated goodput is bounded with radial traffic (cf. Figure 3.46a). With 3 and more flows, the horizontal traffic pattern results in the typical *flow-in-the-middle* scenario.

To start with, let us take a closer look at the effectiveness of the inter-flow fairness adaptation. The inter-flow adaptation ensures that neighboring flows within intersecting collision domains achieve proportional fair flow rates. According to section 3.5.2, the problem boils down to the equalization of the V parameters of all flows. In particular, the involved Vs should not exceed the minimal V by more than a fixed ratio $\delta = 1.1$ (cf. Table 3.9). The box plot in Figure 3.46b shows the distribution of the relative excess in V across all 100 repetitions. The excess of the maximum V relative to the minimum V is defined as $\max_f V^f / \min_f V^f - 1$. We conclude that the inter-flow adaptation is able to meet the given threshold of 10% with only few exceptions.

With increasing number of flows, the advantage of the proposed protocol in terms of aggregated utility increases with respect to DSR and ExOR according to Figure 3.47 and Figure 3.48. The working point is better in terms of proportional fairness as well as the variability of the utilities is lower. With DSR or ExOR, on the other hand, the variability significantly increases especially with horizontal traffic. We suppose that this is an indication of the flow-in-the-middle problem and the starvation. Interestingly, ExOR/TCP exceeds its UDP counterpart in terms of aggregated utility with four flows

in both Figure 3.47b and Figure 3.48b. We conclude that ExOR achieves the higher overall goodput with UDP in Figure 3.46a at the expense of fairness.

With increasing number of flows, larger routing stretches become mostly counterproductive. We suppose that the multi-path and anycast gains do not significantly increase if more flows have to share the same topology. On the other hand, the number of involved links and thus the optimality gap of UO-CSMA increases. The limited multi-path and anycast gains with multiple flows are more often not able to outweigh the incurring costs of additional links. Thus, the proposed protocol achieves the highest utility with multiple flows under generally smaller routing stretches. According to Figure 3.46a, the horizontal traffic pattern offers a higher multi-path and anycast potential. Hence, the system achieves the highest utility with 4 flows and horizontal traffic using a slightly larger routing stretch compared to radial traffic.

With every additional flow, the discrepancy between flow rate and achieved goodput increases due to more virtual throughput. Remember that virtual throughput arises whenever the per-flow queue of a node underflows or overflows. Our delay limiting approach prevents the excessive accumulation of packets at a particular node (cf. section 3.5.3). To a large extent, the throughput capacity of the network has to be shared by all flows (cf. Figure 3.46a). Since the individual arrival rates are generally smaller with multiple flows, the upper queue limits decrease so that the risk of queue overflows is higher. Remember that excessive virtual traffic bears the risk that the physical flow rate deviates from proportional fairness since the congestion controller regulates the joint rate of physical and virtual traffic. The results indicate that this problem is not dominant in our case.

In conclusion, our simulation results indicate that the proposed cross-layer protocol can handle multiple flows more efficiently in the community network scenario. Furthermore, it maintains fairness in the flow-in-the-middle scenario, which traditional approaches do not achieve in general [75]. On the other hand, we have not observed multi-path benefits in the congested-center scenario [286]. We suppose that the considered topology might not possess sufficient potential for spatial smoothing. Furthermore, the spatial spreading of the traffic involves the activation of additional links, so that the optimality gap of UO-CSMA may becomes a limiting factor.

The multi-path and anycast gains are generally smaller with multiple flows. In a given topology, the potential for both does not scale in the number of flows. The potential gets exhausted more quickly, so that the effect of increased routing stretches becomes more often counterproductive. According to our results, the problem of virtual traffic increases with multiple flows, although the consequences are still acceptable. Nevertheless, the problems will intensify in larger scenarios. One promising idea to mitigate the problem might be an architecture, in which the flows share per-neighbor queues as suggested by Bui *et al.* [33].

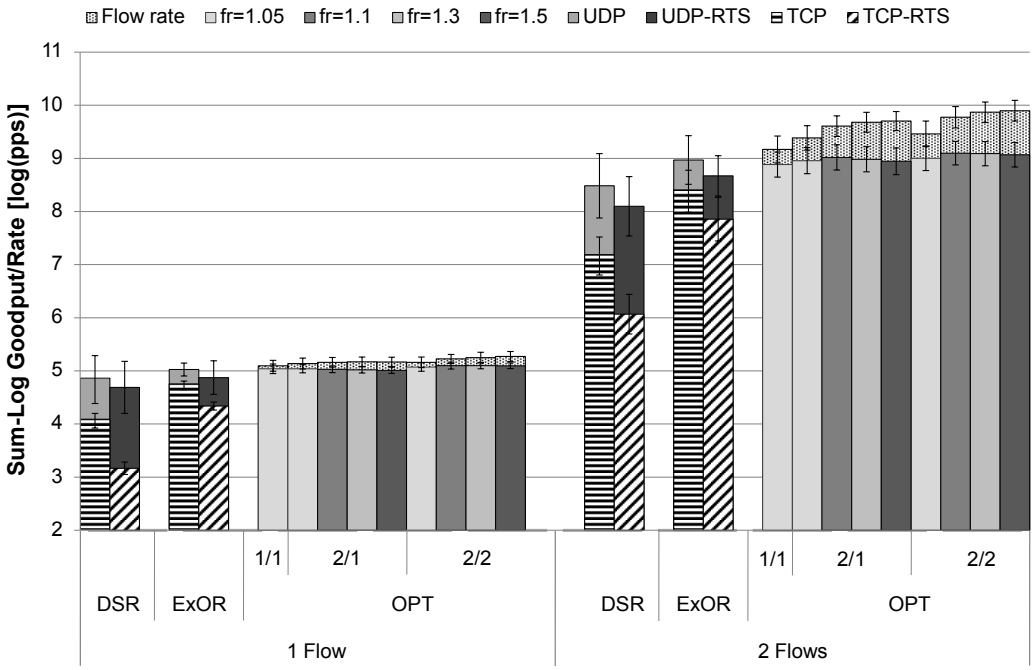

(a) Rate and goodput for 1 and 2 flows ($\pm std.dev.$).

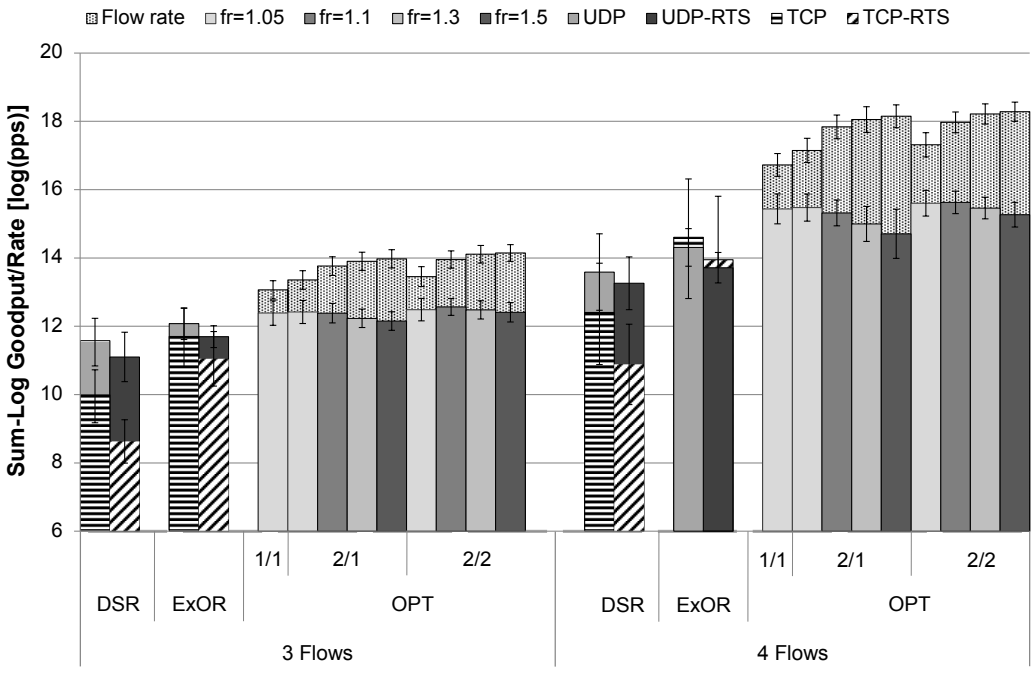

(b) Rate and goodput for 3 and 4 flows ($\pm std.dev.$).

Figure 3.47.: Horizontal flows: Cumulated utility in the community network scenario (Overlapped bar charts).

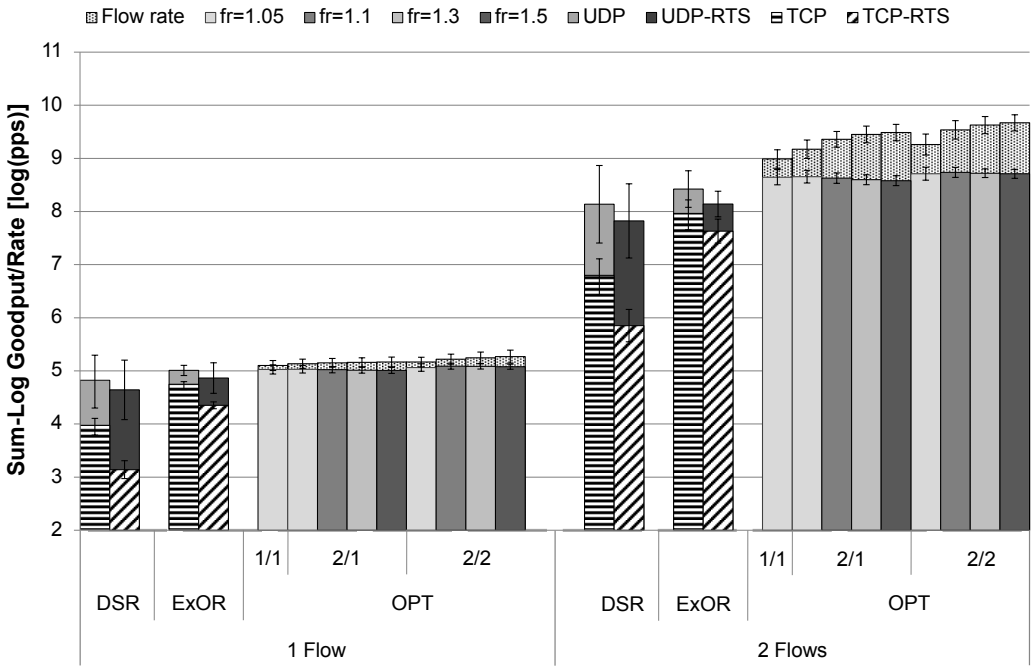

(a) Rate and goodput for 1 and 2 flows ($\pm std.dev.$).

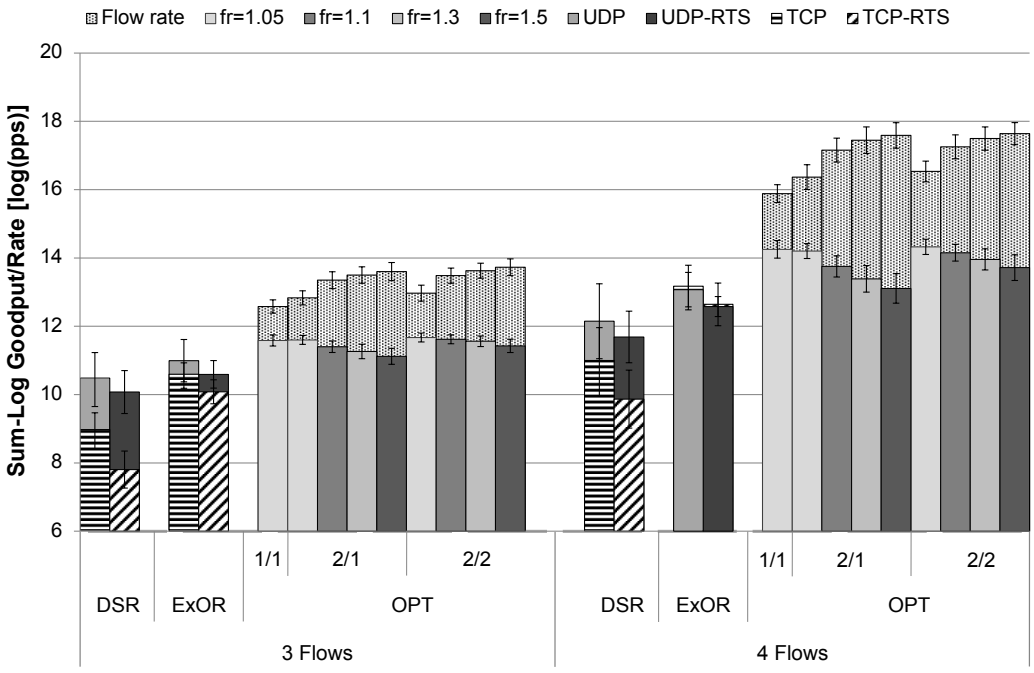

(b) Rate and goodput for 3 and 4 flows ($\pm std.dev.$).

Figure 3.48.: Radial flows: Cumulated utility in the community network scenario (Overlapped bar charts).

3.8. Chapter Summary

In this chapter, we have addressed the question of how opportunistic routing (OR) should be used in WMNs based on CSMA in order to benefit from multi-user and spatial diversity. We have presented a Markov model for CSMA/CA, in which carrier sensing is processed per node. The model captures the characteristic tradeoff of OR between multi-user gain and spatial reuse. Even under node-based carrier sensing, CSMA can be operated in a simple and distributed way if the receiver blocking problem is handled properly. According to the presented model, we have design a CSMA/CA protocol for WMNs called CSMA/HBT based on the idea of dual busy tone multiple access [90]. We have presented a cross-layer algorithm for congestion control, opportunistic routing and CSMA for WMNs with unreliable and memoryless links. The objective of the algorithm is the maximization of the cumulated throughput utility of elastic traffic flows that do not impose (tight) end-to-end delay constraints.

According to the algorithm, we have proposed a cross-layer protocol based on a technology similar to IEEE 802.11. We have defined a working point for CSMA in terms of contention aggressiveness that ensures a high efficiency while avoiding the breakdown of CSMA due to collisions. The working point is approached via an intra- and an inter-flow feedback loop. Furthermore, we have presented an approach to control the throughput-delay tradeoff in UO-CSMA via upper queue limits and virtual transmissions. In this way, the convergence time and the end-to-end delay can be reduced to a level of practical relevance. In addition, we have designed a path pre-selection according to a WMN routing metric in order to exclude non-promising paths in advance.

We have evaluated the proposed protocol through analysis and simulation. According to our analytic results, randomized WMN topologies offer a high potential for both multi-user and spatial diversity. Since neither of them dominates, both forms of diversity should be exploited in a systematic and dynamical way. A simulator prototype has validated the feasibility of the proposed protocol. We have illustrated how the cross-layer protocol handles the tradeoff between spatial reuse and multi-user gain. In particular, it is crucial that a transmitter does not decide for a single anycast link in advance. Instead, all links should properly contend for medium access, and the topology "decides" on the links to activate according to the CS relationship.

Based on our simulation results, we conclude that the prototype is able to increase both throughput and fairness in relation to state-of-the-art single-path and OR protocols. Our more robust MAC significantly increases the single-path throughput. Due to its higher robustness, on the other hand, the MAC leaves fewer opportunities to the higher layers, so that the OR gains of the cross-layer protocol are generally smaller. Furthermore, multi-path and opportunistic routing increases the optimality gap with respect to the analytic potentials. This effect intensifies in the number of competing flows, since the spatial and multi-user gains do not scale in the same way. We close this chapter with the following remarks about current limitations and future directions.

Node-Oriented Carrier Sensing and Hidden Nodes. We have shown that CSMA can be controlled in a simple and distributed way even under node-oriented CS if the receiver blocking problem is handled and the exclusion regions are properly designed.

Both the extended CSMA model and the proposed protocol rely on assumptions. In particular, we have assumed that the synchronization rate is independent from all other TAs in section 3.2. We have assumed that no link becomes inactive as long as there is an ongoing probe within the contention neighborhood. And we have assumed that the PSRs are stationary and i.i.d. in time. The MAC protocol generally allows a small amount of hidden interference, so that the PSRs become dependent on the protocol decisions. Nevertheless, CSMA/HBT should be understood as a straightforward realization of a protocol that complies with the model. We are convinced that better protocol designs exist for the same purpose, which do not rely on high power busy tones and have lower hardware requirements, for example. The design space should be explored in future work.

Carrier Sensing on Real Hardware. The IEEE 802.11 standard defines different types of CCA procedures [76]. In particular, IEEE 802.11g relies on a combination of energy and preamble detection with a mandatory energy threshold of -76 dBm. Thus, the CCA performance for a typical CSMA collision, for example, may be different from cases, in which the preamble can be used [161, 233]. Furthermore, proprietary features like the ambient noise immunity may further change the CS behavior [238]. It remains open whether the implementation decisions are made for technological or physical reasons that impose fundamental limits, or whether they are a compromise with respect to implementation complexity, costs or energy consumption constraints.

We have used the protocol model to derive the MAC protocol. Due to cumulative interference within the physical model, a perfect mutual exclusion requires a large amount of spatial resources. Thus, a relaxed exclusion is often more practical. In addition, the CS detectors are not perfect and their decisions are always subject to uncertainty. Furthermore, the decision to block a link is not always correct. If the CTS is missing due to a blocked receiver, the transmitting link should be blocked. If the CTS is missing due to a CSMA collision, however, the blocking is unnecessary. Nevertheless, the transmitter is unable to distinguish between both events.

Lossy and Time-Varying Channels. The proposed cross-layer protocol is able to handle lossy links that are affected by a memoryless channel error process. The system mitigates the channel impairments using opportunistic routing. The memoryless channel is the best case for OR since the error process cannot be predicted. In the next chapter, we will consider channels with memory, which can be exploited by opportunistic scheduling [264]. We have neglected the impact of channel errors on the signaling traffic and the BTs. It remains open whether and in which way a time-varying LCG affects the control strategy of UO-CSMA.

Throughout this chapter, we have assumed that the channels are stationary. Nevertheless, real links may exhibit non-stationarity at macroscopic time scales from minutes to hours and days due to node mobility, shadowing and environmental mobility. In the long run, the system will adapt to the changed channel statistics. The question is how long it takes to reach the new operating point after abrupt changes, which heavily depends on the current step size used in the parameter updates. It may become necessary to employ a change detection approach that adaptively increases the step sizes in order to reduce the re-convergence delay.

Working Points for the Collision-Efficiency Tradeoff. We have selected a working point for CSMA that maximizes the utility while preventing the collision breakdown of the network as long as the node and flow density remains limited. In the next chapter, we will consider a working point that removes the dependency on the number of flows.

Relays and Their Costs in Multi-Path and Opportunistic Routing. UO-CSMA is utility-optimal in an asymptotic sense. The optimality gap (3.4) on page 40 is determined by the contention aggressiveness V and the number of relay links $|\mathcal{L}|$. The intention of multi-path and opportunistic routing is to achieve spatial and multi-user diversity using additional relay nodes. Thus, a tradeoff arises: Every additional relay achieves further diversity gains, although it causes costs in terms of the optimality gap. In contrast to the costs, the returns of diversity are expected to diminish. Hence, an optimal degree of multi-path and opportunism should exist, so that the diversity gains will be eaten up beyond that point. Our results suggest that the costs are non-negligible especially in the multi-flow case, so that it becomes difficult for the cross-layer OR protocol to outperform its single-path variant.

An in-depth investigation of the interaction between multi-path and opportunism and the optimality gap of UO-CSMA remains an open topic for our future work. In particular, we seek an answer to the questions what the optimal degree of multi-path and opportunism is and how it can be estimated at runtime. We have observed that some cost factors are *preventable*, which otherwise contribute to the optimality gap (3.4). If the underlying unicast links do not experience packet loss, for example, then anycasting has no benefits but incurs costs only. The same applies to dead ends within the topology. In the general case, however, such decisions need global knowledge and it remains an open whether efficient heuristics based on local knowledge exist.

In the context of the route pre-selection, the fairness objective has to be reconsidered and stated more precisely. The larger the degree of multi-path and opportunism, the higher the risk becomes that two previously independent flows come in contact with each other. In this case, one of them generally has to sacrifice some of its efficiency in terms of V due to the inter-flow adaptation.

From our point of view, two directions are promising for our future work. On the one hand, a bias can be introduced into the back-pressure calculation, which encourages the efficient usage of resources but does not affect the optimality. The approach has shown promising results using a routing metric as bias [33, 78, 186, 191, 291]. However, it has caused severe routing oscillations within our preliminary investigation. Alternatively, better designs and heuristics might mitigate the UO-CSMA optimality gap in terms of multi-path and opportunism. For example, sources routes are used with Horizon as proposed by Radunović *et al.* [218]. In this way, the routing decision can be more selective in order to include the most promising paths only. In addition, better heuristics have to be developed that are able to identify the potential of spatial and multi-user diversity. In particular, the route pre-selection should be more selective: Instead of blindly including additional links, it should decide on an individual cost-benefit basis.

Breakdown of the Delay Limiting Approach. Our delay limiting approach is based on queue limits and virtual transmissions. The upper queue limits are adapted according to the packet ingress rate in order to ensure an upper delay limit per hop. Whenever the physical queue limit would be violated in either direction, a virtual transmission takes place. An end-to-end flow of virtual traffic arises from the virtual transmissions. The congestion controller intends to find the fair rate for the joint flow consisting of virtual and physical traffic. Thus, virtual traffic compromises the fairness objective.

The increased usage of multi-path and opportunistic routing generally bears the risk that the delay limiting becomes effective. The more the traffic is spatially spread, the lower the traffic rate becomes on the involved links. The risk of virtual transmission increases due to the smaller queue limits. Since the upper queue bound cannot be decreased beyond a lower limit, the delay control may become ineffective. In the extreme case, the approach might break down in a way that the network does transport virtual packets only instead of physical traffic. The same directions that we have discussed in previous section apply to this problem, as well. We might heuristically prune low-throughput paths if their contribution is marginal according to an individual cost-benefit estimation. Alternatively, the introduction of the delay into optimization problem seems promising [87, 187, 195, 252, 269].

Variability and Flow-Level Dynamics. In the theory on UO-CSMA, it is often assumed that the step sizes properly decrease until they eventually diminish. From a practical point of view, we might not be interested in diminishing step sizes. Due to flow level dynamics or non-stationary changes in the environment, for example, the system has to adapt to the new situation. Arbitrarily diminishing step sizes would slow down the process of convergence to the new operating point. Under non-diminishing step sizes, on the other hand, only a weak convergence can be expected that allows for variations within a small neighborhood of the optimum. In combination with the intra-flow adaptation, the variability causes an additional problem. The intra-flow feedback loop estimates the minimum efficiency parameter along a route. Since all estimates are subject to random variations, however, a bias is introduced into the feedback loop that increases with the length of the route.

4. Distributed Opportunistic Scheduling under Utility-Optimal CSMA

Opportunistic scheduling (OS) is a well known concept to increase the throughput efficiency of wireless multi-user systems [264]. The rationale of OS is to "ride the peaks of the fading process", i.e. use the channel at good instances and refrain from transmission while the channel is in bad conditions. An example is shown in Figure 4.1. Two time-varying links in the same collision domain have to share the wireless resources. Although the average channel quality is identical, the throughput of each link can be increased if the scheduler allocates the channel to the link with the better instantaneous quality in term of achievable bit-rate. OS is already in use in several cellular systems. For example, the IS-856 standard has adopted OS for the downlink transmission [264]. On the other hand, wireless mesh networks (WMNs) have not yet reached that stage of development. In IEEE 802.11 deployments, for example, the contention is not differentiated according to the channel state and if the bit-rate does not remain fixed, then the adaption intervals are often large [21, 153]. A per-frame adaptive modulation and coding (AMC) has been proposed [95, 235], but neither standardization nor hardware manufacturers have adopted the proposal.

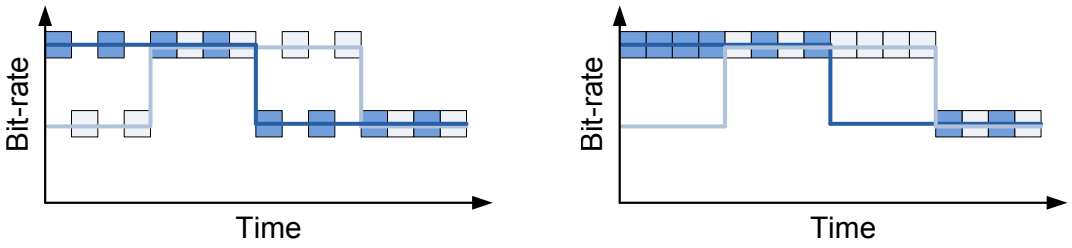

(a) Without channel adaptive scheduling.

(b) With channel adaptive scheduling.

Figure 4.1.: Link quality (lines) and packet transmissions (boxes) over time for two time-varying links (light/dark shaded) within the same collision domain.

Both OS and opportunistic routing (OR) are complementary techniques to achieve multi-user diversity (MUD). The former exploits the knowledge about the instantaneous channel conditions whereas the latter tries to mitigate the missing channel knowledge via multiple candidate receivers. Thus, the question whether OR or OS is better suited for a given system depends on the channel characteristics and the capabilities of the radio hardware. For example, the memoryless fading channel is the best case for OR since the evolution of the channel cannot be predicted. On the other hand, the slow fading channel is better suited for OS given the capabilities for link probing, since it combines predictability and variability in the short and in the long term, respectively.

Throughout this chapter, we will consider a WMN with slow fading links. Nevertheless, real networks are supposed to exhibit a continuum between both extremes and heterogeneity across links.

Altogether, little is known about DOS in WMNs, i.e. achieving OS gains in WMNs in a distributed manner. The architectural difference between cellular and wireless mesh networks is probably one reason for the observed disparity. In cellular networks, a base station directly communicates with its mobile terminals. The number of links is comparatively small. Furthermore, the cells are orthogonalized, so that the costs for acquiring channel quality information (CQI) are low. Due to the centralized architecture, the base station can estimate an efficient schedule autonomously. On the other hand, WMNs have a flat and decentralized architecture. In general, the number of links scales with a squared complexity order, which increases the costs of instantaneous channel quality information (CQI) significantly. Furthermore, no central controller is available. Scheduling decisions have to be made in a cooperative and distributed fashion. The routing decision becomes another degree of freedom that enables multi-hop and multi-path forwarding. From the theoretical point of view, it is known that maximum-weight scheduling (MWS) based on the instantaneous capacity of the fading channels is throughput-optimal [48, 49, 69, 192]. However, this approach does not scale well since MWS is generally NP-hard. Recently, it has been shown that carrier sense multiple access (CSMA) is asymptotically utility-optimal in non-fading environments if the CSMA parameters are properly adapted to the traffic conditions [112].

In this chapter, we address the question whether DOS gains can be obtained in WMNs in a distributed way using a contention technique like CSMA that considers both the traffic and the channel conditions. Our objective is to design and evaluate a cross-layer protocol in order to find an answer to the question. The primary performance metric is utility, which captures both throughput and fairness between flows. We consider applications like FTP that support elastic traffic and do not impose (tight) end-to-end delay or jitter constraints.

Our contributions are as follows. We propose a Markov model of CSMA in WMNs with slow fading channels. We make the following assumptions: Perfect and instantaneous CQI is available at no cost. The channel is block-fading. The fading is mutually independent across different channels. The carrier sensing (CS) is not affected by fading. The hidden node problem is solved and the queues are saturated in a way that they do not run empty. Under these assumptions, the Markov model has a favorable structure that allows for the decomposition into simple and distributed subproblems, which can be solved by each transmitter locally. The foundation of the derived algorithm is the so-called *channel-differentiated contention* that works in the following way: Employ a large backoff if the channel is bad and increase the contention aggressiveness properly with better channel instances. The channel-differentiated contention is the counterpart to AMC for the backoff instead of the transmission phase.

We present a network utility maximization (NUM) problem for congestion control, multi-path and multi-hop routing and CSMA in WMNs with slow fading channels. We derive a technology-agnostic algorithm for the considered problem using the principle of layering as optimization decomposition (LAD). Based on the algorithm, we design a cross-layer protocol for a technology similar to IEEE 802.11 that can readily be implemented in a wireless network simulator. In our design, we consider the following three

issues in particular. Obtaining complete and instantaneous CQI in a WMN is hardly feasible since it involves significant overhead. Instead, the proposed protocol relies on the memory of the slow fading channel. It acquires CQI infrequently via feedback during a frame transmission. Secondly, we propose a windowed congestion control (WCC) that allows for a fine-grained control of the provided buffers. The buffer occupancy affects both the delay performance and the available DOS gain in slow fading channels. In addition, we explore a working point for CSMA in terms of the average backoff duration that maintains a high efficiency independent from the number of contending flows.

We evaluate the proposed protocol through analysis and simulation. Our model relies on strong assumptions, which are hard to fulfill under real world conditions. We study the implications of relaxing the assumptions about infinite buffers and non-hidden channel states. The system's performance becomes dependent on the memory of channel, which is determined by the channel coherence time. Fortunately, the degradation is graceful in the considered cases. In particular, the finite buffers control the characteristic tradeoff between delay and throughput that is inherent to OS. Achieving large OS gains takes a significant and non-negligible amount of end-to-end delay. Furthermore, the channel state is generally hidden from the transmitter. It may change during both the contention and the transmission process. In terms of channel memory, we observe a two-sided tradeoff. If the fading speed increases, the channel uncertainty becomes the limiting factor. The channel loses its memory. The channel estimates are of lower predictive value resulting in more reception errors and lower DOS gains. In the opposite case, the coherence time becomes larger and the window size is the limiting factor since it becomes more difficult to bridge over longer periods of bad channel conditions. Our results indicate that the proposed protocol is able to achieve significant DOS gains when the user population size is large. Furthermore, multi-path forwarding can increase the link capacity in multi-hop WMNs with slow fading channels even if the paths overlap completely.

In order to take the impact of the topology into account, we evaluate both the potential and the actual performance of the channel-differentiated contention in the Internet access network scenario. In particular, the potential of DOS over AMC is significant: With few users, multi-path forwarding offers a way to increase the throughput capacity, whereas the MUD gains dominate under a large user population size. However, the DOS gain over AMC remains moderate in our network simulations, which indicates that the existing potential is not exhausted yet. We suppose that the limiting factor is the limited contention differentiation capability of the IEEE 802.11a/g technology. Nevertheless, the benefits over state-of-the-art protocols are significant in terms of throughput and utility especially with many flows.

4.1. Background and Related Work

In section 3.1, we have already introduced the network utility maximization (NUM) and utility-optimal CSMA (UO-CSMA). In the following, we cover windowed congestion control (WCC), opportunistic scheduling and scheduling with finite buffers.

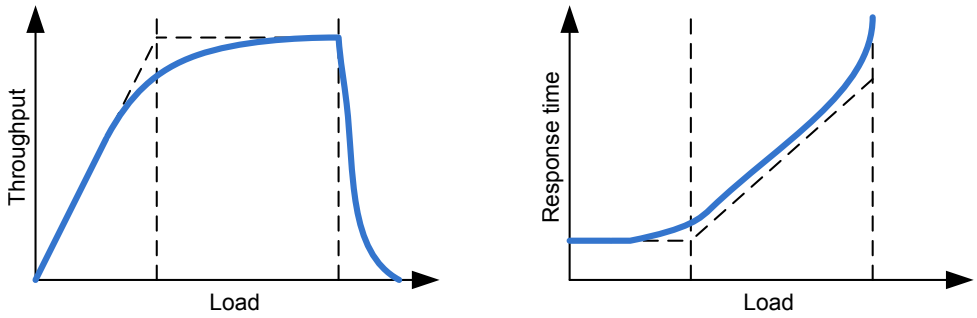

Figure 4.2.: Throughput and response time depending on the offered load (cf. [107, 277]).

4.1.1. Windowed Congestion Control

Windowed congestion control (WCC) has a long history in communication networks. It is a building block of the transmission control protocol (TCP) [39, 206]. TCP provides an end-to-end error control. The TCP sliding window is an efficient ARQ technique that is used to fully utilize the capacity of the communication links. Furthermore, it is important for both the TCP flow and congestion control. The flow control ensures that the receiver queues do not overflow, whereas the congestion control prevents the congestion collapse. In the following, we are interested in the congestion control aspect of TCP only.

In the networks of interest, the route between two communicating nodes generally allows for multiple concurrent transmissions. Sliding window protocols allow for multiple in-flight packets in order to utilize all transmission opportunities. The bandwidth-delay product of a flow represents the maximum amount of in-flight data that can flow in the network without queueing. A simplified model of the relationship between offered load and throughput and delay is shown in Figure 4.2 [107, 277]. If the window and thus the offered load is small, the sliding window protocol is the limiting factor in terms of throughput. As shown in Figure 4.2, the throughput increases linearly in the offered load, whereas the end-to-end delay remains constant. However, if the load passes a threshold, the so-called *knee*, the link capacity becomes the limiting factor. Queues are starting to build up and the delay increases. Depending on the protocol behavior, a *collision collapse* may occur if the offered load exceeds a further threshold, the so-called *cliff*. In that case, the throughput becomes negligible and the delays tend to infinity. The TCP congestion control tries to operate the window size around the congestion knee.

Several TCP congestion control algorithms have been reverse-engineered in order to identify their objectives and the resulting equilibriums [52, 244, 277]. TCP Reno has been designed for wired networks having robust links that exhibit low packet error rates. Its design is based on the assumptions of first-come, first-served (FCFS) queueing, fixed capacity links and single-path routing. In addition, it assumes that packet losses are due to congestion. They are used as input for the congestion control algorithm. During congestion avoidance, the average transmission rate x of TCP Reno is inversely proportional to the round trip time (RTT) T_r and the congestion price q_r of the

route as shown in (4.1). For Reno, the congestion price q_r is the packet loss probability.

$$x \propto \frac{1}{T_r\sqrt{q_r}} \tag{4.1}$$

In addition, TCP Reno has been shown to achieve weighted minimum potential delay fairness according to the utility function (4.2) with constant $\beta \in (0,1)$.

$$U_r(x_r) = -\frac{1}{\beta T_r^2 x_r} \tag{4.2}$$

Vegas is another TCP congestion control algorithm that uses the RTT as the congestion price instead of packet loss. Mo *et al.* have found a generalized utility function that covers both Vegas and Reno [185]. In particular, the objective of Vegas is weighted proportional fairness. Furthermore, they have shown that a window-based congestion controller for proportional fairness can be designed similar to the rate-based controller.

In wireless networks, several assumptions of the initial TCP design do not apply. Plugging together protocols that rely on different premises leads to unintended results, which is illustrated by the following instances. Since wireless links exhibit a distinct error characteristic, the packet loss probability becomes an ineffective congestion price [71]. When considering the hidden node effect without further channel impairments, Fu *et al.* have shown that TCP in WMNs significantly overestimates the optimal window size. The resulting throughput decreases due to lower spatial reuse, increased contention, higher packet loss and more severe hidden node effects. Furthermore, the temporal correlations of the wireless channel significantly affect the performance of TCP [314]. For example, TCP Tahoe outperforms Reno in channels with large memory. The RTT bias of TCP Reno in (4.2) interferes with UO-CSMA, which leads to starvation [50]. Thus, an adaption layer between TCP and back-pressure scheduling like Horizon may translate the cross-layer communication [218].

Tang *et al.* have analyzed the limitations of the fluid model in describing the behavior of TCP [257]. They consider FAST TCP with FCFS queueing in wired networks. FAST is a variant of TCP for networks with large bandwidth-delay products. It adjusts the congestion window according to the queueing delay. The authors analyze the relationship between window size and input rate under delayed and bursty feedback in order to model the effect of perturbations in the window. Burstiness is caused by abrupt changes of the window size and, nevertheless, from the ACK clocking that amplifies the existing burstiness. The authors show that the congestion windows may start to oscillate under certain conditions, so that FAST TCP becomes unstable.

4.1.2. Opportunistic Scheduling

In its most general form, opportunistic scheduling (OS) is the joint optimization of channel adaptation and at least one other resource allocation dimension like time, frequency, user, antenna in order to generate diversity. In the literature, multiple facets of OS have been considered under a diverse set of different constraints. In the following survey, we try to summarize the most important techniques and methods to analyze

OS in wireless networks. For the related work, one differentiation criterion is whether global, correct and/or instantaneous CQI is available, or whether it is incomplete, unreliable and/or delayed. Often, the costs of obtaining CQI are ignored. Another criterion is whether the scheduler is centralized or distributed. The early works on cellular networks have often assumed that a centralized scheduler with global (i.e. cell-wide) CQI is available. Since wireless ad-hoc and mesh networks have a flat architecture, a distributed scheduler that relies on local channel information is favorable. However, a whole continuum of OS designs in-between both extremes can be found in the literature. In the same line, the analytic tools used to tackle the problems differ from NUM, Lyapunov stability, Markov decision processes (MDPs), partially observable Markov decision processes (POMDPs), bandit problems and optimal stopping.

Centralized Opportunistic Scheduling. OS is a well-known concept from the cellular network domain that has already found its way into the IS-856 cellular standard. The rationale of OS is to "ride the peaks of the fading process", i.e. use the channel at good instances and refrain from transmission while the channel is in bad conditions, so that the capacity region is extended [264]. The OS gain depends on the tail of the fading distribution, i.e. the dynamic range of the channel fluctuations. In a cellular system, the implementation requirements remain reasonable since the base station is the central controller within the cell, and adjacent cells are generally orthogonalized. The base station needs to have access to CQI, and it should be able to schedule the transmissions among the users using AMC. Tse *et al.* discuss several system aspects of OS in [264], which include fairness and delay, channel uncertainty and channel fluctuations. In addition, the authors propose a technique called *opportunistic beamforming* to induce and amplify the channel fluctuations in order to maximize the MUD gains [264, 265].

Soret *et al.* have analyzed the tradeoff between delay and throughput in a wireless multiuser system [249]. Remember that the delay performance is related to the queue occupancy via Little's law. A scheduler grants exclusive access to a shared channel on a per-symbol basis. The channels are mutually independent and affected by Rayleigh fading. The authors consider memoryless channels with i.i.d. per-symbol fading as well as channels with memory, which exhibit an autocorrelation with an exponential decay. The channel capacity is continuous in the SNR. The authors derive analytic expressions for the achievable rate region for constant bit-rate (CBR) traffic under different schedulers. In particular, they consider the user rate under a probabilistic delay constraint with target delay D^t and an associated probability ϵ of exceeding D^t. For memoryless channels, the achievable user rates R^u are given in (4.3), where m_u and σ_u^2 are mean and variance of the probabilistic channel capacity, respectively.

$$R^u(D^t, \epsilon) = \frac{m_u}{2} + \frac{1}{2}\sqrt{m_u^2 - 2\sigma_u^2 \frac{-\log \epsilon}{D^t}} \tag{4.3}$$

Thus, the achievable rate region depends on the distribution of the channels, the probabilistic delay constraints, the number of users *and* the scheduler.

Figure 4.3 shows the general relationship between delay and throughput according to (4.3). With increasing delay limit, the user rates asymptotically approach the

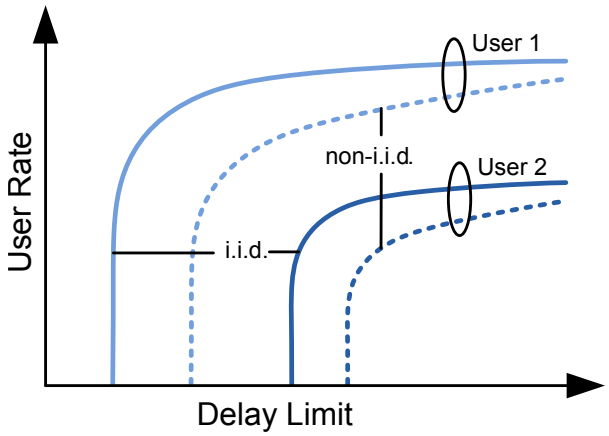

Figure 4.3.: Relationship between user rate and delay limit in a wireless multi-user system with two users (Adapted from [249]).

optimum. However, the achievable user rate decreases under more stringent delay requirements, since the queues gradually lose their ability to bridge over longer periods of bad channel conditions. For a given ϵ, the problem becomes infeasible for delay limits below a certain threshold. The i.i.d. channel is the best case since any memory within the channel reduces the probability of leaving a time period with bad channel conditions. Channel memory shifts the tradeoff curve into the region of larger delays.

Laourine *et al.* consider a single wireless link, on which the fading process evolves according to the Gilbert-Elliot model [154]. They analyze the optimal strategy in the case the transmitter can choose between a weak and a strong code without channel knowledge, or it may decide to use a channel-adaptive, opportunistic strategy that incurs probing costs. The authors cast the problem as a MDP and show that the optimal solution has a threshold structure.

For a wireless downlink with a central controller, Zhou *et al.* derive a PF controller that trades the probing costs against the MUD benefits [310]. They assume that the fading is i.i.d. across all links, whereas the average capacity of each link may vary. In the case that the channel statistics is known so that the expectation can be calculated, the authors solve the problem using optimal stopping theory. If no channel statistics is available, they use the framework of bandit problems to derive a learning algorithm.

Chaporkar *et al.* consider the joint CQI acquisition and scheduling problem with system stability as a performance objective for a wireless downlink [45]. In the same line, they tackle the problem using optimal stopping theory and derive a queue-based scheduling policy. Due to the computational complexity of the optimal stopping problem, they consider an approximate solution that achieves a fraction of the capacity region.

Ouyang *et al.* analyze the impact of uncertainty in the CQI estimates on the throughput performance of single-hop queueing networks with time varying links [197]. The authors show that a MWS type scheduling is throughput-optimal. In addition, they extend their results to the case that the scheduler has only incomplete knowledge of the joint channel and estimator statistics.

According to Ouyang *et al.*, exploiting channel memory outweighs incomplete channel knowledge and leads to significant OS gains [198]. The authors analyze a wireless downlink with Markov-modulated outage channels. The scheduler does not have full

channel knowledge, but it can exploit the channel memory obtained via ARQ feedback. They cast the problem as a POMDP and derive a greedy scheduling policy that has near optimal performance.

A similar setup is analyzed by Li *et al.* [163–165]. They consider a single-hop multi-user wireless downlink with Markov-modulated channels. The instantaneous channel conditions are unknown. The scheduler benefits from the channel memory that is obtained via ARQ feedback. Instead of solving the POMDP directly, the authors establish inner and outer bounds on the capacity region that become tight in the large user regime. Furthermore, they develop a queue-dependent control policy that is stable for input rates within the inner capacity bound.

Distributed Opportunistic Scheduling. Wireless mesh networks and wireless ad-hoc networks (WAHNs) have a flat and decentralized architecture. A scheduler for these networks should be distributed, rely on local channel information only and consider the costs and the uncertainty of CQI. Not surprisingly, a solution complying with all requirements has not been identified yet. The MAC protocol becomes another degree of freedom due to the complexity of optimal TDMA scheduling in WMNs. Since the vanilla MWS is generally not scalable in the number of network nodes, sub-optimal scheduling algorithms and contention-based protocols have attracted interest.

Neely *et al.* present a control policy for flow control, routing and scheduling in general stochastic networks with i.i.d. block-fading channels [192]. The authors show that the control policy achieves queue stability and optimal performance even though it has no knowledge about channel statistics, input rates and the global topology. In essence, it is sufficient for optimality that the back-pressure scheduler solves the MWS for the *instantaneous* capacity region within each time slot. A similar result has been derived by Chen *et al.* [48, 49] and Eryilmaz *et al.* [69]. Nevertheless, the MWS problem remains NP-hard in WMNs, regardless whether it operates on instantaneous or average channel information. In subsequent work, the result has been extended to channels with decaying memory like Markov-modulated channels [193]. It is to note that suboptimal schedulers benefit from considering instantaneous channel conditions, too. The interested reader may refer to Lin *et al.* [170] for a further discussion on that topic.

Ying *et al.* study throughput-optimal scheduling in wireless ad-hoc network with single-hop traffic and time-varying Markov-modulated channels with delayed and incomplete CQI [290]. The authors characterize the capacity region of the network under the geographic disk interference model. They propose a location-based threshold scheduling policy that incorporates location and channel information into back-pressure scheduling and show its throughput optimality. In addition, they present a distributed and low complex scheduler with near-optimal performance, which relies on instantaneous channel state only for local links, whereas delayed CQI for neighboring links is sufficient.

Contention-based medium access has also been considered in literature. Qin *et al.* analyze the asymptotic scaling behavior of channel-adaptive scheduling in an ALOHA uplink network [213, 214]. By observing the local instantaneous channel conditions only, ALOHA can achieve the same asymptotic throughput scaling behavior in terms of user population compared to the optimal scheduling. On the other hand, the ben-

efits of optimal power adaptation via water-filling and optimal ALOHA persistency adaptation are asymptotically negligible under large user populations in relation to channel inversion and an equally distributed persistency, respectively.

In recent literature, the term distributed opportunistic scheduling (DOS) has been established for distributed contention-based scheduling with limited channel information in WAHNs. Zheng *et al.* consider DOS as an optimal stopping problem: Given the instantaneous channel state, should the sender take the transmission opportunity or contend again hoping that the channel quality rises [304, 308]. From the network-centric point of view, the optimal strategy is a pure threshold policy: each transmitter has a fixed threshold as minimal CQI requirement. Thus, the sender depends on local information only in its transmission decision. Nevertheless, computing the threshold is non-trivial and requires global knowledge. The main drawback of the approach is the limitation to fully meshed WAHNs with single-hop traffic and memoryless channels. In combination with a physical SINR-based interference model, the contention probabilities have to be taken into account in addition [77]. The approach of Zhang *et al.* has subsequently been extended to multi-receiver diversity [305], multiple-input multiple-output (MIMO) [209], uncertainty in the channel estimation [306, 307], two level channel probing for mitigating noisy channel estimates [259, 260], delay constraints [255] and wireless relay networks [302].

Inspired by the results above, Zhang *et al.* have derived a heuristic threshold-based MAC for MANETs [299]. In particular, the authors propose a dynamic adaption of the thresholds based on the instantaneous channel conditions and the utilization of the wireless medium around each network node.

Hwang *et al.* present a threshold-based CSMA protocol in order to exploit MUD [100, 101]. They consider an IEEE 802.11 uplink with homogeneous fading distributions. Assuming knowledge about the fading distribution is available, the instantaneous SNR is deterministically mapped to a backoff slot, which gives priority to links experiencing good channel conditions. The objective of the mapping is to maintain a constant access probability within each backoff slot.

Ashraf *et al.* propose a channel-aware MAC protocol that grants access to the channel based on the random fluctuations of the fading channel [8]. In particular, every node maintains a threshold for accessing the channel, which is cooperatively determined in agreement with all network nodes. If the estimated channel quality crosses the threshold in the upward direction and the surrounding wireless medium is idle, the transmitter is granted access the medium. The distributed estimation of the thresholds according to the instantaneous traffic conditions is not considered.

Kanodia *et al.* propose the multi-channel opportunistic auto-rate (MOAR) protocol [129, 234]. MOAR is a MAC protocol for WAHNs based on IEEE 802.11, in which the nodes are equipped with multi-channel and multi-rate capabilities. The authors formulate and solve an optimal stopping problem to handle the tradeoff between the frequency diversity benefits and the costs of obtaining CQI on other RF channels. Thus, MOAR is comparable to the optimal stopping approach of Zheng *et al.* discussed above, although it utilizes frequency diversity via multiple RF channels instead of time diversity. In the same line, Chang *et al.* consider the opportunistic multi-channel probing and transmission problem, in which the channels are not necessary identically distributed and a transmitter may blindly access a channel without prior probing [44].

The *channel-adaptive* bit-rate selection in IEEE 802.11 networks discussed in section 2.3 is an instance of adaptive modulation and coding (AMC). In general, AMC does not comply with our definition of OS, since it is a purely reactive scheme. It does not involve a joint optimization and thus, it does not generate multi-user diversity.

In the context of WMNs, the channel-adaptive bit-rate selection has been extended to the joint bit-rate and relay selection in order to generate MUD [110, 274, 319]. Before initiating the data transmission, the channel towards multiple relays is probed. Depending on the instantaneous bit-rates, the best relay node is chosen. One example for joint bit-rate and relay selection is the medium access diversity (MAD) protocol by Ji *et al.* [110]. Zubow *et al.* propose a similar approach that additionally benefits from the anycast transmission [319].

4.1.3. Scheduling with Small and Finite Buffers

The impact of the buffer size on the system performance is manifold. For window-based protocols like TCP, the window size determines throughput, delay and fairness. In fading environments, the provided buffers additionally affect the OS gains. At the same time, the window size can be seen as the cumulative number of packets that are present within the network and within the associated queues. Thus, it also affects the back-pressure based routing and the underlying MWS problem. In the previous chapter, we have already discussed approaches that consider the delay performance of back-pressure scheduling in general (cf. section 3.5.3). In the following, we review related work that considers small and finite buffers and their impact on MWS.

The fluid model is only an approximation for queue-based back-pressure scheduling since packets are not arbitrarily divisible [183, 257]. According to Neely *et al.* [192], the gap between the optimal utility and the utility of the time-averaged expected flow rates is smaller than BN/V, where N is the number of network nodes, B is a constant and V is a parameter. The cumulative time-averaged expected queue length is bounded above by $^1/_2(BN + VG_{\max})/\mu_{\text{sym}}$, where $G_{\max}$ and μ_{sym} are constants. Thus, by scaling the queues via V, the gap to the optimal solution can be made arbitrarily small at the expense of the delay.

Although MWS is throughput-optimal, its delay properties are generally not optimal. Sadiq *et al.* have derived mean-delay optimal scheduling policies [236, 237] that adapt the scheduling discipline according to the utilization of the queues: With increasing queues, the scheduler switches from the balancing of unequal queues (i.e. MWS with appropriate fairness objective) to (opportunistically) maximizing the instantaneous system throughput. In this way, the asymptotic probability of sum-queue overflows as well as the mean delay is reduced. The extension to multi-hop communication is left open.

Venkataramanan *et al.* consider scheduling policies that maintain a given delay target, i.e. policies that minimize the probability of end-to-end buffer overflows for any flow [269]. Considering upper bounds on the afore-mentioned probability, they derive structural properties that the scheduling should possess: For example, it should give preference to links closer to the destination. The authors derive a class of so-called $\alpha\beta$ algorithms, which modify the link weights according to the derived structural properties.

Maximum-weight scheduling is known to be throughput-optimal under packet level dynamics. However, it becomes unstable under flow level dynamics and the end-to-end delay performance is generally suboptimal [109, 176]. Even worse, packets on low-throughput paths may experience excessive delays, which may easily be interpreted as starvation on the higher layers. Ji *et al.* address these problems using a delay-based back-pressure scheduler instead of considering queue lengths [109]. They assume that multiple flows traverse the WMN using multi-hop and single-path routing. The channel capacity is fixed and deterministic. Under the fluid limit model, the authors establish a linear relationship between the queue length and the differential sojourn time between the head of line packets of neighboring hops along the route. Furthermore, they show that MWS under the delay-based metric is throughput optimal.

In general, MWS assumes infinite buffer space inside the network. The presented approaches so far consider the queue length in terms of averages and overflows, or probabilities and expectations thereof. In the context of buffered crossbar switches, an architecture with finite (and small) buffers has attracted interest. Giaccone *et al.* analyze a flow-controlled MWS, where the queues inside the network are finite [81]. Only at the source of a flow, the ingress queue has infinite buffer space. The optimal scheduling policy under these constraints is difficult to realize. The authors derive a low-complex scheduling policy that is guaranteed to achieve a fraction of the capacity region with a tradeoff in the length of the internal queues. The approach is extended to wireless networks by Le *et al.* [158] using the results of Neely *et al.* [192]. The scheduling is straightforward: Let Q_m^f and Q_n^f be the queue length of flow f at node m and n, respectively. Furthermore, l_f is the internal buffer size per flow and node and $\sigma(f)$ denotes the source node of flow f. The differential backlog ΔQ for link (m,n) and flow f is calculated as follows.

$$\Delta Q_{m,n}^f = \frac{Q_{\sigma(f)}^f}{l_f} \cdot \begin{cases} l_f - Q_n^f & m = \sigma(f) \\ Q_m^f - Q_n^f & m,n \neq \sigma(f) \end{cases}$$

Using these weights in the MWS while providing internal buffers of size $(N-1)/\epsilon$ in the number of network nodes N, the loss in utility is bounded by ϵ.

Xue *et al.* extend the above algorithm by introducing QoS constraints [281]. The finite buffer structure becomes a means to enforce QoS in terms of average delay guarantees and minimum data rate requirements. The resulting algorithm can be operated arbitrarily close to the throughput optimum. Nevertheless, the tradeoff between throughput and delay remains unchanged: Let ϵ be the throughput loss, then the delay scales as $O(\epsilon^{-1})$.

4.2. Modeling CSMA in Slow Fading Channels

In this section, we develop the *fading CSMA model*: A model of CSMA for fading channels with memory, which we use to derive distributed opportunistic scheduling (DOS) policies for CSMA networks in slow fading environments. Each wireless link is modeled as finite-state Markov channel (FSMC) [84]. We extend the MRF model of idealized CSMA according to Jiang *et al.* [112] by another dimension per link, the so-called

channel dimension. The newly introduced dimension captures the instantaneous channel state. Although the theoretical channel capacity is continuous in the SNR, a communication system generally provides a limited set of MCS only. We assume that the available bit-rates are associated with known SNR thresholds. If the channel quality exceeds the threshold, the packet transmission at the associated bit-rate will be successful with high probability. Each transmitter is able to obtain CQI by the means of link probing. The *channel dimension* of each link in the fading CSMA model is driven by the probabilistic channel process according to the channel statistics. We assume that the fading processes on different channels are mutually independent and that the LCG is time-invariant. In the following, we analyze how the remaining *transmission dimension* of each link should be operated in order to maximize the performance in terms of throughput and fairness.

The state of a wireless link is a tuple (w, v) consisting of the transmission state $v \in \{0, 1\}$ in the transmission dimension and the channel state w in the channel dimension. The channel states per link include the bit-rate and a distinct outage state. For illustration purposes, we use the channel states $\{H, N, B\} \ni w$ corresponding to high, normal and bad (outage) quality in the following. When fixing all channel states, the remaining Markov chain is reduced to the idealized CSMA model for non-fading environments. During a single state transition of the fading CSMA model, either the channel state or the transmission state of exactly one link changes. A channel changes its state w independently from all other channels and independent from the transmission state v of all links. In particular, we assume that the Markov property holds, i.e. the transition only depends on the channel's current state w and the associated channel transition rates. Furthermore, we assume that there is a total ordering on the channel states according to their nominal bit-rates, where we use 0 with outages. In the channel dimension, state transitions are possible between neighboring bit-rates only, i.e. we assume that the channel evolves gradually and does not change abruptly. The LCG imposes constraints on the activation of links (cf. chapter 3). In addition, the *outage constraint* states that a link cannot be in the transmission state ($v = 1$) while it is in outage ($w = 0$). In Figure 4.4, our modeling approach is illustrated using a network of two competing links and three channel states as defined above with nominal bit-rates $\{2, 1, 0\}$.

Let K be the number of links and B be the set of channel states per link, which consists of all available bit-rates and the outage state. The K-dimensional vector $\boldsymbol{w} \in B^K$ captures the instantaneous channel state of all links. We assume that the joint channel state space B^K can be indexed, and the index l refers to the l-th vector $\boldsymbol{w}^l \in B^K$. Using a lower index k as in $w_k^l \in B$, we refer to the k-th component of the vector $\boldsymbol{w}^l$. Furthermore, $\gamma_b(w_k^l) = \gamma_{k,b}^l = \mathbb{1}(w_k^l = b) \in \{0, 1\}$ is an indicator function that is evaluated to 1 if link k uses bit-rate b in channel state l. Let $P_{k,b}$ be the unconditional probability that link k is in channel state b. Thus, it holds $\sum_b P_{k,b} = 1 \ \forall k$. In addition, the unconditional probability P_l that the system is in channel state l is defined as product over the state probabilities of all links.

$$P_l := \prod_k P_{k,w_k^l} = \sum_j p(\boldsymbol{w}^l, \boldsymbol{v}^{l,j}; \boldsymbol{r}) \ \ \forall l \tag{4.4}$$

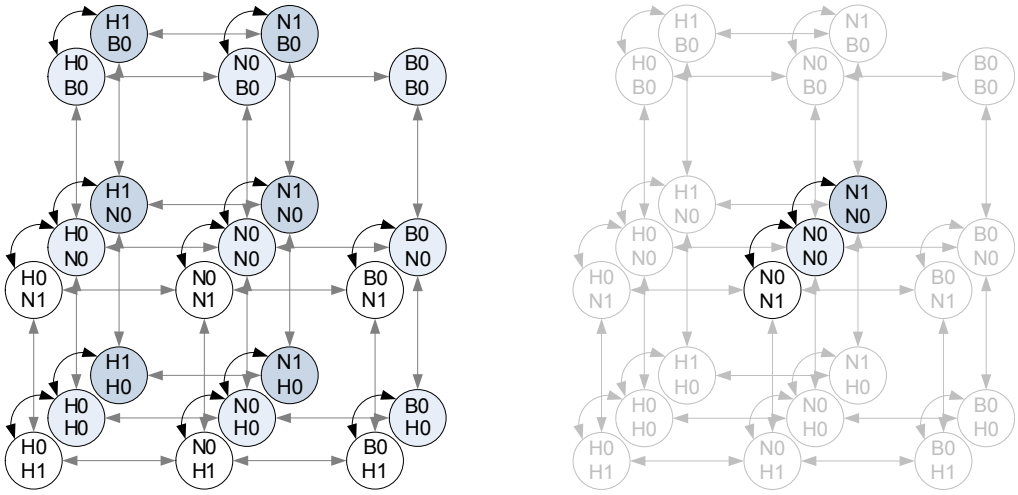

(a) Complete Markov chain.

(b) Channel state fixed at NN. The Markov chain is truncated to the non-gray states.

Figure 4.4.: The fading CSMA model for two competing transmitters in slow fading environments with tree channel states $\{H, N, B\}$ that correspond to the bit-rates $\{2, 1, 0\}$. The rows of the state labels refer to the links. The first and second column in each row denotes the channel and transmission state, respectively. Transitions that alter the transmission (channel) state are marked black (gray). When fixing the joint channel state as shown in (b), the gray states are not reachable anymore and the non-fading idealized CSMA model remains.

Similar to chapter 3, let $\boldsymbol{v} = (v_1, v_2 \dots v_K) \in \{0,1\}^K$ be the transmission state vector that contains the 1 at position k ($v_k = 1$) if link k is transmitting and $v_k = 0$ otherwise. Depending on the channel state $\boldsymbol{w}^l$, the set of available transmission states $V_l \subseteq \{0,1\}^K$ differs. Remember that a link cannot be activated during outages. Thus, the notation $v_k^{l,j}$ refers to the k-th component of the j-th vector of V_l, which is the transmission state space under channel state l. $R_{k,b}$ is the activation rate of link k while the instantaneous bit-rate of the link is b, and $r_{k,b} = \log(R_{k,b})$ denotes the transmission aggressiveness (TA). Note that the TA is dependent on the link *and* the instantaneous bit-rate. Furthermore, we assume saturation at the MAC layer, i.e. each link has always sufficient packets in its queue that can be transmitted as soon as the MAC activates the link.

Let $p(\boldsymbol{w}^l, \boldsymbol{v}^{l,j}; \boldsymbol{r})$ be the stationary distribution of the fading CSMA Markov chain that we intend to construct. When fixing the channel to a particular state l as illustrated in Figure 4.4b, the already known idealized CSMA Markov chain [112] remains. The foundation of our modeling approach relies on the assumption that the channel state distribution P_l depends on link characteristics $P_{k,b}$ only. The medium resources P_l of channel state l have to be shared among the states of the fading CSMA Markov chain as shown in (4.4). In this way, the fading CSMA Markov chain can be thought of as idealized CSMA Markov chains within every channel state l that are weighted according to the probability P_l of the channel state. The resulting stationary distribution is given in (4.5).

$$p(\boldsymbol{w}^l, \boldsymbol{v}^{l,j}; \boldsymbol{r}) = P_l \frac{\exp \sum_{k=1}^{K} v_k^{l,j} r_{k,w_k^l}}{C(\boldsymbol{w}^l; \boldsymbol{r})}, \quad C(\boldsymbol{w}^l; \boldsymbol{r}) = \sum_j \exp \sum_{k=1}^{K} v_k^{l,j} r_{k,w_k^l} \tag{4.5}$$

In contrast to the goodput, the throughput captures the consumed medium time but does not account for the bit-rate that is used in the transmission. Using the abbreviation $p(\boldsymbol{w}^l, \boldsymbol{v}^{l,j}; \boldsymbol{r}) = p_{l,j}(\boldsymbol{r})$, we define the throughput $q_{k,b}$ of link k at bit-rate b as follows.

$$q_{k,b}(\boldsymbol{r}) = \sum_{l,j} \gamma_{k,b}^l v_k^{l,j} p_{l,j}(\boldsymbol{r})$$

Let $\bar{p}$ be the distribution of the fading CSMA Markov chain that the system should achieve under the assumption that the input rates $\lambda_{k,b} = \sum_{l,j} \gamma_{k,b}^l v_k^{l,j} \bar{p}_{l,j}$ are feasible. The TAs $\boldsymbol{r}$ corresponding to the distribution $\bar{p}$ can be found by maximizing the log-likelihood function $F(\boldsymbol{r}) = \sum_{l,j} \bar{p}_{l,j} \log p_{l,j}(\boldsymbol{r})$. When plugging (4.5) into F, we get

$$\begin{aligned} F(\boldsymbol{r}) &= \sum_{l,k} r_{k,w_k^l} \sum_j v_k^{l,j} \bar{p}_{l,j} + \sum_{l,j} \bar{p}_{l,j} \log P_l - \sum_{l,j} \bar{p}_{l,j} \log C(\boldsymbol{w}^l; \boldsymbol{r}) \\ &= \sum_{k,b} r_{k,b} \lambda_{k,b} + \sum_l P_l \log P_l - \sum_l P_l \log C(\boldsymbol{w}^l; \boldsymbol{r}) \end{aligned}$$

and maximizing F with respect to $\boldsymbol{r}$ leads to

$$\begin{aligned} \frac{\partial F(\boldsymbol{r})}{\partial r_{k,b}} &= \lambda_{k,b} - \sum_l \gamma_{k,b}^l P_l \frac{\sum_j v_k^{l,j} \exp \sum_m v_m^{l,j} r_{m,w_m^l}}{C(\boldsymbol{w}^l; \boldsymbol{r})} \\ &= \lambda_{k,b} - \sum_{l,j} \gamma_{k,b}^l v_k^{l,j} p_{l,j}(\boldsymbol{r}) = \lambda_{k,b} - q_{k,b}(\boldsymbol{r}) \end{aligned}$$

Similar to the idealized CSMA Markov chain, we can interpret the result in terms of supply and demand. The throughput supply $q_{k,b}(\boldsymbol{r})$ has to be adapted according to the difference to the demand $\lambda_{k,b}$ via the parameter $r_{k,b}$. However, a problem arises if we want to use the queue backlog for estimating the TA: The demand is generally given in terms of goodput per link λ_k, and the distribution per bit-rate $\lambda_{k,b}$ is left open. The routing layer selects an outgoing link for an incoming packet and places it into the link's queue, but it does not consider the bit-rate to use. On the other hand, we have to estimate the TA $r_{k,b}$ on link k for every bit-rate b.

The Kullback-Leibler (KL) divergence measures the difference between two probability distributions. The KL divergence D_{KL} is defined as follows.

$$D_{\mathrm{KL}} := \sum_{l,j} u_{l,j} \log \frac{u_{l,j}}{p_{l,j}(\boldsymbol{r})} = -\sum_{l,j} u_{l,j} \log p_{l,j}(\boldsymbol{r}) - \left(-\sum_{l,j} u_{l,j} \log u_{l,j} \right)$$

Thus, the KL divergence is the difference of cross-entropy and entropy. It is always non-negative. It reaches its minimum $D_{\mathrm{KL}} = 0$ if and only if $u_{l,j} = p_{l,j}(\boldsymbol{r})$, i.e. if

both distributions are equal. Using $\mu_{k,b} = \sum_{l,j} \gamma_{k,b}^{l} v_k^{l,j} u_{l,j}$ and the observation that the negative cross-entropy corresponds to the log-likelihood function $F(\boldsymbol{r})$, the negative KL divergence becomes

$$-D_{\mathrm{KL}} = -\sum_{l,j} u_{l,j} \log u_{l,j} + \sum_{k,b} r_{k,b} \cdot \mu_{k,b} + \sum_{l} P_l \left(\log P_l - \log C(\boldsymbol{w}^l; \boldsymbol{r}) \right) \tag{4.6}$$

Let us consider the optimization problem (4.7). The objective is to find the distribution $\boldsymbol{u}$ with the maximum entropy subject to constraints (4.8) and (4.9). The channel constraint (4.9) should guarantee that our solution matches the channel distribution $\boldsymbol{P}$. The capacity constraint (4.8) connects the goodput demand λ_k to the supplied throughput $q_{k,b}$ per link k and bit-rate b.

$$\max_{\boldsymbol{u}} -\sum_{l,j} u_{l,j} \log u_{l,j} \tag{4.7}$$

$$\text{s.t.} \sum_{b \in B} b \cdot \sum_{l,j} \gamma_{k,b}^{l} v_k^{l,j} u_{l,j} \geq \lambda_k \ \forall k \tag{4.8}$$

$$\sum_{j} u_{l,j} = P_l \ \ \forall l \tag{4.9}$$

$$u_{l,j} \geq 0, \sum_{l,j} u_{l,j} = 1$$

Relaxing the capacity constraint (4.8) and substituting $\mu_{k,b}$ as defined above leads to the following Lagrangian with dual variables $\boldsymbol{y}$.

$$\mathcal{L}(\boldsymbol{u}; \boldsymbol{y}) = -\sum_{l,j} u_{l,j} \log u_{l,j} + \sum_{k,b} y_k b \cdot \mu_{k,b} - \sum_{k} y_k \lambda_k \tag{4.10}$$

From the discussion above, we know that $-D_{\mathrm{KL}}$ in (4.6) is maximal if $u_{l,j} = p_{l,j}(\boldsymbol{r})$. Comparing (4.6) and (4.10), we conclude that $\mathcal{L}$ becomes maximal in $\boldsymbol{u}$ if $\boldsymbol{u}$ is equal to the steady state $\boldsymbol{p}$ of the fading CSMA Markov chain and we set $r_{k,b} = b y_k$. In this case, the first two sums are equal in both equations, and the last sum does not depend on $\boldsymbol{u}$. Thus, the TAs per channel state should be scaled according to the bit-rates.

$$r_{k,b} = b \cdot r_k \tag{4.11}$$

In other words, the instantaneous TA $r_{k,b}$ should be weighted by the instantaneous bit-rate b as shown in (4.11), which we refer to as *channel-differentiated contention*. The differential queue backlog r_k can be updated via the sub-gradient $r_k \leftarrow [r_k + \alpha(\lambda_k - \sum_b b q_{k,b})]_+$ with positive step size α, i.e. the transmitter has to observe the local goodput supply and demand only.

4.2.1. Example

To illustrate the way the system achieves the OS gain, let us consider the two-link example in Figure 4.4 again. The goodput per bit-rate of both links is shown in Figure 4.5a. The TA on the first link is set to $r_1 = 10$. Let us consider what happens if

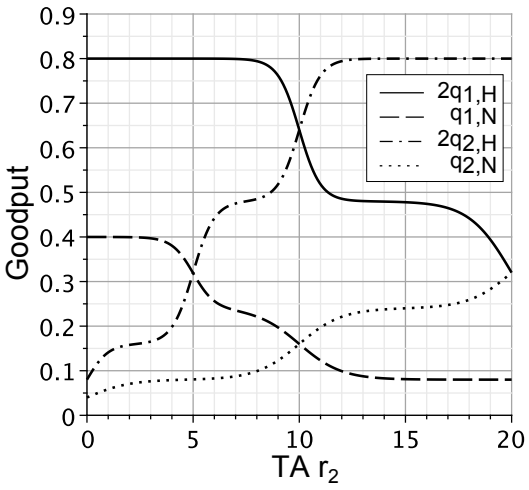

(a) Goodput versus TAs r_2 on the second link. Link 1 is fixed at $r_1 = 10$.

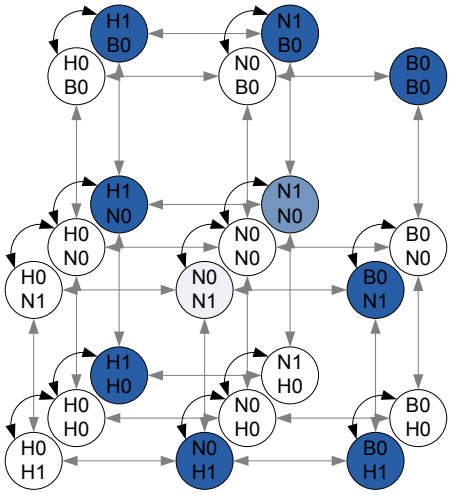

(b) Throughput distribution per channel state for $(r_1, r_2) = (10, 7.5)$. Darker shades represent higher throughput fractions.

Figure 4.5.: Goodput for the two-link example shown in Figure 4.4 with channel states $\{H, N, B\}$ that correspond to the nominal bit-rates $\{2, 1, 0\}$ and occur with probability $\{0.4, 0.4, 0.2\}$. The results are obtained analytically in Maple using (4.5) and channel-differentiated TAs according to (4.11).

the TA on the second link r_2 increases. If r_2 is small, the second link generates significant throughput only while the first link is in outage, i.e. in the channel states $(w_1, w_2) = BH$ and BN shown on the right side of Figure 4.5b. Note that no transmission opportunities are taken away from the first link. However, things change when increasing the TA r_2. Interestingly, the second link generates throughput in the channel state NH first as shown in Figure 4.5b for $r_2 = 7.5$. The channel state NH is more valuable for the second link: it can transmit at a rate of 2 compared to the rate 1 of the first link.

When increasing the TA further, the second link takes over throughput in the channel states HH and NN, which have the same value for both links. At the point $r_1 = r_2 = 10$, both links share the throughput equally in these channel states. In the states of unequal bit-rates HN and NH, only the transmitter that achieves the higher bit-rate generates significant throughput. In this way, the channel-differentiated contention in (4.11) achieves an OS gain that increases the sum goodput. In contrast, when using a single TA only regardless of the channel state, the transmitters would share the throughput equally in the important states of unequal bit-rates. Thus, the sum goodput would be reduced.

Only when increasing the TA further beyond $r_2 = 10$, the second link will take throughput from the first link in the channel state HN, which is more valuable for the latter.

4.2.2. Assumptions and Discussion

In the fading CSMA model presented above, we assume that every node has perfect and instantaneous CQI information available at no costs. Every transmitter is aware of currently occurring channel state changes and reacts immediately on them. If a link is currently transmitting and its channel quality improves, for example, then it switches to a more efficient bit-rate. In addition, the model assumes that no resources are wasted if the channel enters the outage state. Thus, every transmitter acts in perfect synchronization with its channel. This modeling approach has benefits: The steady state distribution is in product form, which allows for the derivations above. As an interesting by-product, the derived policy is agnostic to the temporal correlation of the fading channel. Since every transmitter immediately reacts on channel changes, it is not affected by the speed of fading process.

From the practical point of view, several modeling assumptions may not be fulfilled under the simulation assumptions as well as real world conditions. For example, channel knowledge can only be obtained infrequently from link probing and ARQ feedback, which consumes wireless resources. In contrast to CS, the event of a channel state change is hidden and cannot be observed directly. Thus, the synchronization between channel and transmitter is limited: Adapting the bit-rate during a transmission is generally not possible. Thus, a hidden channel state change leads to a waste of resources due to either underutilization or reception errors. In the same line, a contending node cannot adapt its backoff to the instantaneous channel state since channel changes are hidden. Introducing these issues into the model would result in non-reversible transitions.[1] In this way, the equilibrium distribution would lose the product form and greedy algorithms will not be able to solve the problem anymore.

When applying node-oriented carrier sensing (cf. section 3.2) to the fading CSMA model, an outage event *cannot be distinguished* from a non-responding receiver that is temporarily silenced by the collision avoidance. The problem is that both events generally occur on different time scales, so that different reactions are necessary: In the case of a temporarily silenced receiver, the transmitter should wait until it becomes available again. With outages, on the other hand, a dedicated probing policy should be used in order to identify the end of the outage period.

In the fading CSMA model, we consider fading in terms of receiver performance and ignore its impact on CS. Nevertheless, the link between two transmitters may also be affected by fading. Both links may operate concurrently as long as the inter-transmitter link is in outage. In this case, the LCG is not time-invariant anymore. We intend to consider the effect of fading on CS in our future work.

[1] To see this, consider the fading CSMA Markov chain for a single link. If the link transmits (e.g. in state $N1$) and a hidden outage event occurs, the system would have to enter the newly introduced state $B1$ (outage and transmitting). After some time, it would most likely finish its transmission and proceed to state $B0$. Since the transition $B1 \rightarrow B0$ is crossed in one direction only, however, the modified Markov chain can be distinguished from its time-reversed counterpart or, in other words, it is not reversible. In detail, it is even more involved: Freezing the channel state dimension of the underlying spatial process during an outage corresponds to the truncation of the Markov chain to the states $\{B1, B0\}$. However, the state $B1$ is transient in the truncated Markov chain, while it is generally recurrent in the non-truncated chain. Thus, the modified Markov chain is not a spatial process according to [133, Corollary 9.6].

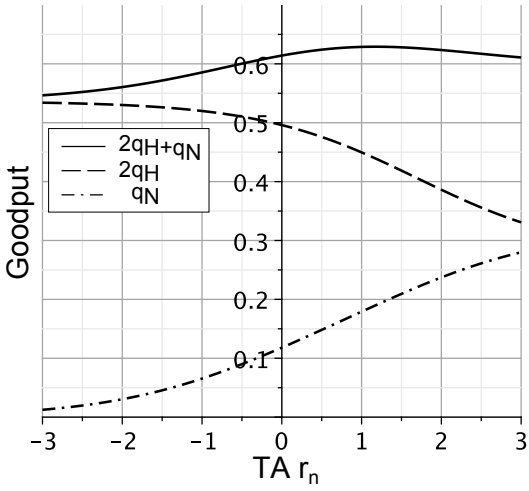

Figure 4.6.: Goodput versus low bit-rate TA $r_n = r_{1,N} = r_{2,N}$ in the two-link scenario (channel states $\{H, N, B\}$, bit-rates $\{2, 1, 0\}$ with marginal probabilities $\{0.4, 0.4, 0.2\}$). The high bit-rate TA is set to $r_{1,H} = r_{2,H} = 1.5$. The goodput is equal on both links.

Due to the additional entropy term in the objective of the optimization problem (4.7), we achieve our actual objective, the utility maximization, only asymptotically (cf. section 3.5.2). In particular, the channel-differentiated contention according to (4.11) may not lead to the highest utility if the associated TAs are small. An example is shown in Figure 4.6 for the already known two-link scenario. The high bit-rate TA is set to $r_{1,H} = r_{2,H} = 1.5$. The diagram shows the resulting goodput when increasing the low bit-rate TA r_n on both links. According to (4.11), r_n should be set to 0.75, whereas it is evident that the highest goodput is achieved around $r_n = 1.17$. The problem is that the benefits of *utilizing idle resources* while the channel is of *moderate quality* are higher compared to the OS gain. In the high TA regime, however, the idle resources vanish, so that there is no benefit when deviating from (4.11).

In summary, the following implications on the system design can be identified. The costs of obtaining CQI should be low, so that the influence of the underlying tradeoff is minimized. In related work, it is repeatedly reported that delayed and imperfect CQI leads to a graceful performance degradation that can be mitigated using channel memory (cf. section 4.1). The channel memory reduces the modeling error since the generally hidden channel state transitions occur less often. Hence, the system should operate in slow fading channels in order to benefit from the channel memory. In section 4.5.3, we will reconsider the assumptions and investigate the impact of their relaxation.

4.3. Optimization Problem

Let N be the set of nodes. The distribution of the fading CSMA Markov chain $\boldsymbol{u}$ subject to a given LCG, the channel state distribution $\boldsymbol{P}$, the bit-rates $b \in B$ and the indicators γ and v are defined as in the previous section. In addition, let F be the set of flows and $\sigma(f)$ ($\delta(f)$) refers to the source (destination) of flow $f \in F$. The throughput, the goodput and the flow rate is denoted by $\boldsymbol{q}$, $\boldsymbol{x}$ and $\boldsymbol{y}$, respectively. The utility function U determines the fairness between flows and V is a tradeoff factor. Using the definitions above, the optimization problem (4.12) captures congestion control, routing and

opportunistic scheduling under the fading CSMA model in WMNs.

$$\max_{\boldsymbol{y},\boldsymbol{x},\boldsymbol{u}} -\sum_{l,m} u_{l,m} \log u_{l,m} + V \sum_{f} U(y^f) \tag{4.12}$$

$$\text{s.t.} \sum_{j} x^f_{j,i} + y^f \, \mathbb{1}(\sigma(f) = i) \leq \sum_{j} x^f_{i,j} \;\; \forall f, \forall i \in N \backslash \delta(f) \tag{4.13}$$

$$\sum_{f} x^f_{i,j} \leq \sum_{b} b \cdot q_{(i,j),b} = \sum_{b} b \sum_{l,m} \gamma^l_{(i,j),b} v^{l,m}_{(i,j)} u_{l,m} \;\; \forall (i,j) \tag{4.14}$$

$$0 \leq x^f_{i,j} \;\; \forall f, i, j \tag{4.15}$$

$$u_{l,m} \geq 0 \;\; \forall l, \forall m, \;\; \sum_{l,m} u_{l,m} = 1, \;\; \sum_{m} u_{l,m} = P_l \;\; \forall l \tag{4.16}$$

The objective (4.12) of the optimization problem contains the maximization of the flow utilities. In particular, we consider $U = \log$ in the following, which corresponds to proportional fairness. As discussed in the previous section, the entropy term in the objective and the constraints (4.16) on the distribution $\boldsymbol{u}$ are the result of our fading CSMA model. The flow conservation constraint (4.13) connects the flow rate $\boldsymbol{y}$ and the goodput $\boldsymbol{x}$, which is furthermore subject to the non-negativity constraint (4.15). The goodput $\boldsymbol{x}$ is connected to the CSMA Markov chain via the capacity constraint (4.14). In the problem above, we assume that the adaptation of the bit-rate to the instantaneous channel conditions is possible in a way that reception errors do not occur.[2]

The solution of the problem (4.12) is straightforward. At first, we relax the flow conservation constraints (4.13), which results in the Lagrangian (4.17) subject to (4.14), (4.15) and (4.16).

$$\begin{aligned} \mathcal{L}(\boldsymbol{y}, \boldsymbol{x}, \boldsymbol{u}; \boldsymbol{\alpha}) = &-\sum_{l,m} u_{l,m} \log u_{l,m} + V \sum_{f} U(y^f) \\ &+ \sum_{f,i} \alpha^f_i \left(\sum_{j} x^f_{i,j} - \sum_{j} x^f_{j,i} - y^f \, \mathbb{1}(\sigma(f) = i) \right) \end{aligned} \tag{4.17}$$

Following the discussion in section 3.4, the dual variables $\boldsymbol{\alpha}$ can be updated using the s_α-weighted difference of the arrived and serviced packets during time interval t as shown in (4.18). Hence, α captures the dynamics of the physical queue. In the following, we use the term node credit (C) for α.

$$\alpha_i(t+1) = \left[\alpha_i(t) - s_\alpha(t) \left(\sum_{j} (x'_{i,j}(t) - x'_{j,i}(t)) - y'(t) \, \mathbb{1}(\sigma(f) = i) \right) \right]_+ \tag{4.18}$$

[2] In slow fading channels, there is a tradeoff between the SNR margin per bit-rate and the conditional reception probability after link probing. The optimization problem can be extended to consider the conditional reception probabilities in a similar way the PSRs have been considered in the previous chapter.

By solving for $\boldsymbol{y} = \arg\max_y \mathcal{L}$, we get the congestion control (4.19).

$$y^f = \frac{V}{\alpha^f_{\sigma(f)}} \tag{4.19}$$

The partial Lagrangian for routing and scheduling subject to (4.14), (4.15) and (4.16) is the following.

$$\mathcal{L}(\boldsymbol{x}, \boldsymbol{u}; \boldsymbol{\alpha}) = -\sum_{l,m} u_{l,m} \log u_{l,m} + \sum_{f,i,j} x^f_{i,j} \left(\alpha^f_i - \alpha^f_j\right)$$

We observe that packets should be routed along links with positive differential back-pressure $(\alpha^f_i - \alpha^f_j)$ only in order to maximize the Lagrangian. Let us fix $\boldsymbol{u}$ and $\boldsymbol{\alpha}$. The problem becomes to distribute the available goodput per link among the flows.

$$\begin{aligned} \max_{\boldsymbol{x}} & \sum_{f,i,j} x^f_{i,j} \left(\alpha^f_i - \alpha^f_j\right) \\ s.t. & \sum_f x^f_{i,j} \leq \sum_b b \cdot q_{(i,j),b} \quad \forall (i,j) \\ & 0 \leq x^f_{i,j} \quad \forall f, (i,j) \end{aligned}$$

The maximum is found by allocating the whole goodput to a flow with maximum positive back-pressure $r_{i,j}$.

$$r_{i,j} = \max_f \left(\alpha^f_i - \alpha^f_j\right) \tag{4.20}$$

Plugging the solutions for $\boldsymbol{x}$ and $\boldsymbol{r}$ into the Lagrangian, it simplifies to (4.21) subject to (4.16).

$$\mathcal{L}(\boldsymbol{u}; \boldsymbol{\alpha}) = -\sum_{l,m} u_{l,m} \log u_{l,m} + \sum_{i,j} r_{i,j} \sum_b b \sum_{l,m} \gamma^l_{(i,j),b} v^{l,m}_{(i,j)} u_{l,m} \tag{4.21}$$

The distribution $\boldsymbol{u}$ that maximizes the Lagrangian above is the stationary distribution of the fading CSMA Markov chain (cf. section 4.2). In other words, the TA per link should be set to the differential queue back-pressure (4.20) weighted according to the instantaneous bit-rate (4.11).

A technology agnostic algorithm can be derived in a straightforward manner similar to section 3.4. We continue with the design of a cross-layer protocol in the following.

4.4. Protocol Design

In this section, we design a cross-layer protocol for congestion control, routing and opportunistic scheduling under CSMA in WMNs based on the solution of the optimization problem (4.12). In addition, we consider the following requirements. The protocol should be completely distributed and it should have a low complexity. The

target environment is a WMN with slow fading channels. The protocol should acquire CQI from link probing and exploit channel memory. The congestion control should be window-based, so that the protocol can control the number of outstanding packets and the associated throughput-delay tradeoff. In addition, the protocol should provide proportional fairness between traffic flows and ensure that the backoff remains within its technological limits in order to prevent excessive collisions on the physical layer (cf. section 3.5.2).

For the sake of clarity, we have subdivided the presentation of the protocol design into three parts. In the next section, we discuss how a WMN node probes the channel and transmits data packets. In section 4.4.2, the window-based congestion control is presented assuming a fixed tradeoff factor V. Algorithm 7 on page 156 summarizes the operation of the protocol that is discussed in both sections. In section 4.4.3, the protocol is extended in order to adapt the tradeoff factor V according to the backoff limits. The resulting protocol is summarized in Algorithm 8 on page 160.

Throughout this section, we use the following notation in addition to section 1.5.

q_i^f	Number of packets of flow f queued at node i
Q_i^f	Shadow queue or back-pressure: cumulative number of packets of flow f along the path from i to the destination of f with the minimum number of packets
W^f	Window size of flow f
$S, S_i^{\mathbf{ack}}$	Packet sequence number; highest acknowledged sequence number as seen by node i
C^f	Credits of flow f
C_i^f	Credit feedback of flow f at node i
V^f	Tradeoff parameter V of flow f
y^f	Flow rate of flow f (averaged)
$r_{i,j}, \bar{r}_{i,j}$	TA and average TA of link (i,j)
$r_{\mathbf{opt}}, r_{\mathbf{min}}$	Target and minimum TA
$b_{i,j}$	Bit-rate of link (i,j)

4.4.1. Channel Probing and Data Transmission

The operation of the MAC is loosely based on EDCA known from IEEE 802.11e and the concept of transmission opportunities (TXOPs) [103]. In order to avoid the problems caused by hidden nodes, we use CSMA/HBT at the MAC layer (cf. section 3.3). The MAC operation consists of the CSMA contention phase, a link probing phase and the actual data transmission. The contention phase starts when the transmitter draws a random backoff for the link from an exponentially distribution. The function SETAVG-BACKOFF adjusts the expectation of the underlying probability distribution (cf. line 15 of Algorithm 7). The backoff is processed according to the deployed CSMA protocol.

The probing phase begins when the backoff has expired. As shown in Figure 4.7, the transmitter and the receiver of the link (i,j) exchange (custom) RTS and CTS frames

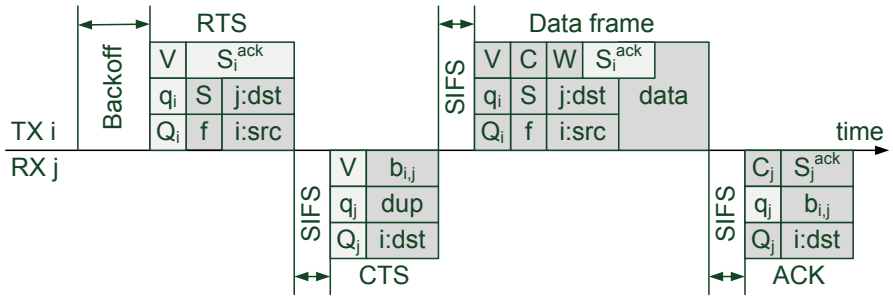

Figure 4.7.: MAC frame format and MAC operation on link (i, j). Lighter shaded fields are intended to be overheard by neighboring nodes and do not have an immediate impact on the MAC operation.

using a robust bit-rate. In addition to the necessary addresses, the RTS frame contains a (globally unique) identification of the flow and the packet to come. In this way, the receiver can detect duplicates even if the affected packets have gone through different routing paths. The transmitter is informed via the duplicates field (dup) in the CTS. In addition, the CTS contains the anticipated bit-rate $b_{i,j}$ to be used with the link, which can be estimated using one of the available methods presented in section 2.3.1 like receiver-based auto-rate (RBAR) and SoftRate. If the channel is reciprocal, then CQI can also be obtained from overheard traffic in order to improve the channel estimation quality. At the end of the probing phase, the function LINKPROBED on line 17 et seq. of Algorithm 7 is called.

If the link probing has not been successful, the function HANDLEOUTAGE on line 25 of Algorithm 7 should implement a policy to handle the outage. As discussed in section 4.2.2, a channel outage cannot be distinguished from a silenced receiver in CSMA/HBT. Hence, we handle outages using the policy for silenced receivers: The link is blocked for the duration of the TXOP. However, the blocking can be released if the link is re-synchronized as described in section 3.3.

If the probing has been successful, the transmitter sends a data frame using the bit-rate $b_{i,j}$ that has been specified in the CTS (cf. Figure 4.7). The data frame contains the control information of the RTS and, in addition, it has fields for the credits C and the window size W of the flow, which are necessary for scheduling at downstream nodes. The receiver acknowledges the reception of the data frame using an ACK frame, which contains the immediate queue feedback Q_j and an end-to-end acknowledgement of the highest received packet sequence number at the destination S_j^{ack} as seen by receiver j. Both values are important during the back-pressure calculation and the maintenance of the packet window at the source node, which we will describe in detail in the next section. Furthermore, the ACK contains a credit feedback C_j, which is explained in section 4.4.3. Optionally, it can contain an estimate of the instantaneous channel conditions in terms of bit-rate $b_{i,j}$ in order to improve the channel adaption. The transmitter continues to send another data frame as long as it has packets to send and the packet transmission is finished within the remaining duration of the TXOP. The function FORWARDPACKETS on line 21 of Algorithm 7 returns the number of successfully transmitted frames during the TXOP.

In the discussion above, we have considered the fields in Figure 4.7 that have an immediate impact on the MAC transaction. The remaining fields are meant to be overheard by neighboring nodes and we introduce them as needed in the following.

4.4.2. Window-Based Congestion Control

In the considered system, both the channel fading and the medium access control interact with the queueing process. Due to the assumption about saturated queues, the queueing process is ignored in the fading CSMA model. The probability that the queue runs empty is small if the number of enqueued packets is large. Reducing the number of enqueued packets leads to smaller end-to-end delays, although the OS gain is reduced at the same time: With a higher probability of empty queues, a transmitter becomes more often unable to benefit from a peak of the fading channel.

The channel memory leads to two opposing implications. On the one hand, the channel memory should be large in order to mitigate the effect of hidden channel state changes. On the other hand, the channel memory should decay sufficiently fast, so that the packet buffers are able to bridge over periods of bad channel conditions.

Due to the importance of the buffer size for the OS gain, we explore an alternative design to the prevalent rate-based approaches in the following. In particular, our objective is to control the number of enqueued packets directly using a windowed congestion control (WCC) at the source of the flow. The sliding window of TCP serves two purposes: In combination with FIFO queueing, it achieves fairness in addition to spatial reuse. However, the window size for optimal spatial reuse is typically small in WMNs. For example, Fu *et al.* have estimated an optimal window size of about ¼ of the number of nodes for a chain topology [71]. Using these window sizes, the OS gains will be limited since there is little freedom left for the opportunistic CSMA scheduler. Hence, we suppose that the window size has to be substantially larger in order to achieve significant OS gains.

We make the following design decisions: Firstly, the window operation is separated from fairness. In this way, we can vary the window size according to the OS gain and delay requirements without worrying about intersecting flows. Secondly, we use a fixed window size in our design and evaluation. In the summary of this chapter, the adaptation of the window size is briefly discussed. However, an in-depth investigation of this topic is not within the scope of this thesis.

The combination of finite buffers according to Le *et al.* [158] and Horizon queueing [218] naturally leads to a WCC that is, nevertheless, different from the TCP sliding window due to the multi-path character of the cross-layer approach. To start with, let us consider the aspect of finite buffers first. Similar to Le *et al.*, we assume that queueing is done per node and flow, and each flow f maintains a fixed buffer size W^f per queue. In contrast to reference [158], we do not distinguish between internal and external queues, so that the buffer constraints apply to all queues. We assume that the source node is able to obtain further packets on demand, e.g. from a storage reservoir at an upper layer as discussed by Neely *et al.* [192]. Later, when using Horizon queueing, we distinguish between the shadow queue (or back-pressure) Q_i^f and the actual packet queue q_i^f. For now, let Q_i^f be the size of the queue of flow f at node i.

Algorithm 7 Cross-Layer CSMA in Slow Fading Channels (Fixed V).

Require: $W^f > W_{\min}$ ▷ Window size

procedure GENERATEPACKETS(Flow f) ▷ Runs continuously at source of flow f
  $\Delta q \leftarrow \left[W^f - Q^f_{\sigma(f)}\right]_+$
  $q^f_{\sigma(f)} \leftarrow q^f_{\sigma(f)} + \Delta q$ ▷ Fill window
  $y^f \leftarrow \text{MOVINGAVERAGE}(y^f, \Delta q)$ ▷ Estimate avg. flow rate
  UPDATEQ$(\sigma(f), f)$
end procedure

procedure UPDATEQ(Node i, Flow f) ▷ Routing
  $Q^f_i \leftarrow q^f_i + \min_{j \in N_i} Q^f_j$
  for $j \in N_i$ **do**
    UPDATETA(i, j)
  end for
end procedure

procedure UPDATETA(Link (i, j)) ▷ Adapt CSMA
  $f_{i,j} \leftarrow \arg\max_f C^f \left[\frac{Q^f_i - Q^f_j}{W^f}\right]_+$, $r_{i,j} \leftarrow b_{i,j} C^{f_{i,j}} \left[\frac{Q^{f_{i,j}}_i - Q^{f_{i,j}}_j}{W^{f_{i,j}}}\right]_+$
  SETAVGBACKOFF$(\exp(-r_{i,j}))$ ▷ Deactivate link if $r_{i,j} = 0$
end procedure

Require: $\gamma \in (0, 1)$ ▷ EWMA smoothing factor
procedure LINKPROBED(Link (i, j), Bit-rate b) ▷ After RTS/CTS
  if $b \neq 0$ **then**
    $b_{i,j} \leftarrow b$ ▷ Instantaneous channel condition
    $\bar{r}_{i,j} \leftarrow -\log\left(\exp(-\bar{r}_{i,j})(1-\gamma) + \gamma \exp(-r_{i,j})\right)$ ▷ Estimate avg. TA
    $t \leftarrow \text{FORWARDPACKETS}(i, j, b)$ ▷ Transmit t packets during TXOP
    $q^{f_{i,j}}_i \leftarrow q^{f_{i,j}}_i - t$; $q^{f_{i,j}}_j \leftarrow q^{f_{i,j}}_j + t$
    UPDATEQ(i, f) ; UPDATEQ(j, f)
  else
    HANDLEOUTAGE(i, j) ▷ Outage policy
  end if
end procedure

Require: $t_{\text{up}} > 0$ ▷ Update interval
Require: $V > 0$ ▷ Fixed tradeoff factor
procedure UPDATEV(Flow f) ▷ At source of f
  $C^f \leftarrow V / y^f$
  SLEEP(t_{up}) ; UPDATEV(f)
end procedure

In Algorithm 7, the WCC in function GENERATEPACKETS ensures that the queue of the source node is constantly filled, so that it holds $Q^f_{\sigma(f)} = W^f$. In particular, the generated packets should have a fixed and reasonable size. In function UPDATETA, the differential back-log is used in relation to W^f (the queue size of the source) and weighted by the credits of the flow C^f. The resulting TA $r_{i,j}$ on line 14 is the product of the differential back-log and the most recent bit-rate estimate $b_{i,j}$ (cf. section 4.3). Thus, three factors determine the value of $r_{i,j}$:

1. The instantaneous channel state and its estimate $b_{i,j}$,
2. The distribution of the packets q^f belonging to flow f along the routing path(s) and the derived differential back-pressure ΔQ^f and
3. The credits C^f.

According to Le *et al.* [158], we can think of the credits C^f as the size of a hypothetical rate-controlled transport layer queue, which holds packets that have not been admitted to the finite network layer queues. Nevertheless, the credits C^f are simple counters in our design. Since each flow f uses its own credit value C^f with all links, they affect the inter-flow contention in the first place. In other words, the credits determine the fairness between flows. To achieve PF, the estimation of the credits on line 29 of Algorithm 7 is based on the above derived flow control law (4.19). The average flow rate y^f is calculated on line 4 and, for now, we assume that the parameter V is fixed. The averaging horizon of y^f should be sufficiently large to average out the short-term fading dynamics of the channel, although excessively large values should be avoided in order to maintain the reactivity. The function UPDATEV updates the credits of the flow C^f in regular intervals t_{up} based on the most recent estimate of the flow rate y^f.

In the vanilla approach of back-pressure routing, the queues length increases towards the source (cf. section 3.4.1). Via Horizon queueing [218], the buffering efforts can be considerably reduced. The rationale is as follows. The physical queue q^f_i stores the differential back-log $Q^f_i - Q^f_j$ with respect to the least cost neighbor j only. Hence, the shadow queue Q^f_i is actually a counter that can be estimated via function UPDATEQ of Algorithm 7 in a distributed way. As shown in function LINKPROBED, the dynamics of the physical queue is straightforward (cf. line 22 of Algorithm 7).

Figure 4.8 shows an example of the queueing structure for a hexagonal network with two disjoint paths between source and destination nodes 1 and 6, respectively. Each node has a queue of fixed size W, which we refer to as *window* in the following. A window can contain data packets, downstream back-pressure and empty spaces. For example, the window of node 2 consists of the number of enqueued packets q_2, the minimum back-pressure of its downstream nodes, which is Q_4 in this case, and empty spaces in the remaining region between Q_2 and W. At node 1, the downstream back-pressure of node 2 is considered in the window since it is smaller than Q_3. The flow controller ensures that there are no empty spaces in the window of the source node. In contrast to TCP, the window size W is generally smaller than the number of outstanding packets under multi-path routing.

The instantaneous values of C, W and Q are exchanged during the MAC operation using the frame formats in Figure 4.7. Additionally, we have introduced an end-to-end

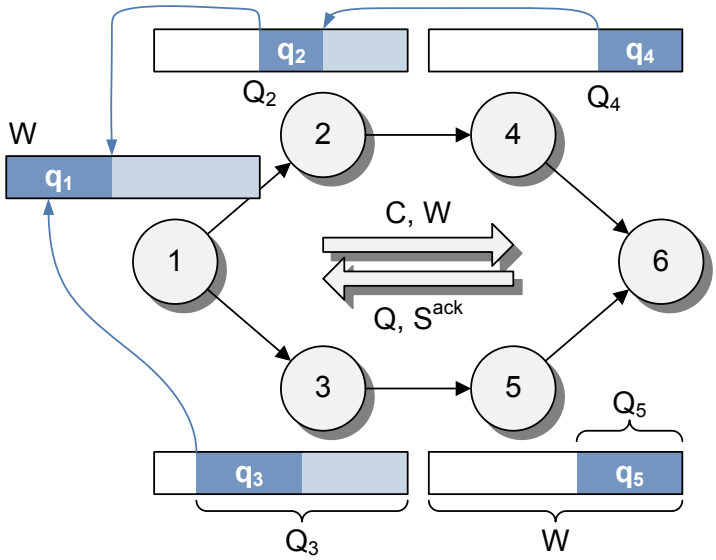

Figure 4.8.: Window structure and control information exchange. A single flow traverses the network from node 1 to 6 using multi-hop and multi-path routing. The window of size W can contain data packets q (dark shading), downstream back-pressure Q (light shading) and empty spaces (white). The acknowledgements S^{ack} and the back-pressure Q are propagated upstream. The source distributes the flow credits C and the window size W downstream.

acknowledgement scheme similar to TCP, so that the window maintenance becomes more robust. The source node of the flow assigns an increasing sequence number S to each data packet. The destination determines the largest sequence number S^{ack} among the arrived packets. Every node exchanges the sequence number to acknowledge with its upstream neighbors. Eventually, the source node will receive S^{ack} and can use it to improve the window maintenance in the function GENERATEPACKETS.

The feedback in the upstream direction is physically transported in CTS and ACK frames. In addition, the network nodes benefit from the broadcast nature of the wireless medium and try to overhear information from downstream nodes. In particular, the back-pressure Q is contained in all frame types shown in Figure 4.7. Additionally, both RTS and data frames contain the acknowledgement number S^{ack}. Nevertheless, the physical packet flow is in downstream direction only. If the upstream feedback arrives at a node that has upstream neighbors with empty queues only, it may get stuck and the feedback loop is interrupted. For this case, we introduce an active mechanism for upstream feedback consisting of an empty data and an ACK frame, which transport the control information to the upstream node. As shown in Figure 4.7, the actual queue length q_i is additionally contained in all MAC frames. Knowing the queue size of all upstream neighbors, the decision for passive or active upstream feedback is straightforward.

In section 3.5.5, we have discussed a routing heuristics that tries to exclude non-promising routing paths in advance via routing metrics. The heuristics can be used with the presented protocol as well, and we apply it during our evaluations.

4.4.3. Adaption of the Tradeoff Factor *V*

The algorithm presented above adapts the TAs without considering the technological constraints. As discussed in section 3.5.2, it is hardly possible to find a single value for the V parameter that fits in all cases. The resulting working point has either a low throughput efficiency or causes severe CSMA collisions. In this section, we extend Algorithm 7 in a way that the system dynamically adapts the V parameter in order to find a suitable working point. Our objective is slightly different from the previous chapter. In particular, the system should maximize the sum utility subject to an upper limit on the *average sum TA per node*. Optionally, an additional constraint on the instantaneous TA per link can be imposed to prevent excessive high TAs during channel peaks. The bounds on peak and average TA should be sufficiently spaced to allow for a backoff differentiation under a wide range of channel conditions.

Our starting point is the flow control law (4.19) on page 152. In Algorithm 7, we have estimated the credits C^f using a fixed V parameter and the averaged flow rate y^f. Now, the parameter $V \leftarrow f(y^f, C^f)$ is updated using the flow rate y^f and the flow credits C^f, which are determined in the network and fed back to the source. We refer to this operation as *intra-flow adaptation*. The source node propagates the estimate of V^f in the downstream direction using dedicated fields of the MAC header shown in Figure 4.7. If multiple flows contend for resources within the same collision domain, then the system can achieve proportional fairness by equalizing the Vs between them. In the following, we use the term *inter-flow adaptation* for this operation.

Let us start with the intra-flow adaptation. Each forwarder i locally estimates the largest credit value C_i^f for the flow f that complies with the average TA constraints in the following way. It maintains the average TA per link $\bar{r}_{i,j}$ on line 20 of Algorithm 7. In Algorithm 8, the average sum TA per node r_{sum} is determined in function UPDATEC. Similar to section 3.5.2, we assume that the relationship between V and C is linear in the following step. Given linearity, the anticipated credit value of node i is $C_i^f = \alpha C^f$ since the average sum TA r_{sum} becomes equal to the target TA r_{opt} in this case. The processing step on line 8 of Algorithm 8 is necessary for the inter-flow adaptation, which we will consider in the next paragraph. In a distributed fashion, the minimum of C_i^f across all forwarders is fed back upstream to the source node of flow f (cf. line 10). As illustrated in function UPDATEV of Algorithm 8, the source updates the credits C^f according to the received feedback. Furthermore, it updates the instantaneous V^f using the averaged flow rate y^f and the most recent credit estimate C^f. The source propagates the updated values of V^f and C^f. We have observed that the convergence is considerably accelerated if flow credit changes are anticipated in the TA averages $\bar{r}$, i.e. if $\bar{r}$ is scaled by the ratio of the new to the current credit value whenever a new credit estimate C^f is received from upstream nodes.

The vanilla approach of UO-CSMA acts on the assumption that each node can increase its TA and take a larger share of the throughput whenever it is treated unfairly by its neighbors. Due to the technological constraints, the assumption does not hold in systems that we are considering. Instead, the inter-flow adaptation has to ensure that flows, which take throughput away from others in an unfair manner, decrease their contention aggressiveness. An indicator for unfairness is the difference between the

Algorithm 8 Adaption of the Tradeoff Parameter V.

1: **procedure** LINKPROBED(Link (i,j), Bit-rate b)
2: ... ▷ As in Algorithm 7
3: UPDATEC(i)
4: **end procedure**

Require: $\delta > 1$ ▷ Hysteresis factor
Require: $r_{\text{opt}}, r_{\min}$ ▷ Target and minimum TA
5: **procedure** UPDATEC(Node i)
6: $r_{\text{sum}} \leftarrow \log \sum_j \exp \bar{r}_{i,j}$ ▷ Sum of avg. TAs $\bar{r}$
7: $\alpha \leftarrow \dfrac{r_{\text{opt}} - r_{\min}}{r_{\text{sum}} - r_{\min}}$
8: $V \leftarrow \min\left(\alpha \min_{f \in F(i)} V^f, \delta \min_{f \in F(N_i) \setminus F(i)} V^f\right)$
9: **for** $f \in F(i)$ **do**
10: $C_i^f \leftarrow \min\left(\dfrac{V}{V^f} C^f, \min_{j \in N_{\text{DS}}^f(i)} C_j^f\right)$
11: **end for**
12: **end procedure**

Require: $t_{\text{up}} > 0$ ▷ Update interval
13: **procedure** UPDATEV(Flow f) ▷ At source of f
14: $C^f \leftarrow C_{\sigma(f)}^f$
15: $V^f \leftarrow y^f C^f$
16: SLEEP(t_{up}) ; UPDATEV(f)
17: **end procedure**

parameters V^f. Each node i considers these differences during the estimation of its credit feedback C_i^f in function UPDATEC of Algorithm 8.

To start with, we consider the case of multiple flows per node first and extend the discussion to additional flows in the neighborhood afterwards. The flows $f \in F(i)$ traversing node i may have different parameters V^f. Let $g = \arg\min_{f \in F(i)} V^f$ be the flow that experiences the highest unfairness among them. Note that V^g is estimated in the first expression on line 8 of Algorithm 8. Using the assumption about linearity between V and C, we scale the credit feedback C_i^f of each flow f by the ratio V^g/V^f, in addition (cf. line 10). Due to the feedback loop, all flows that behave in an unfair manner will experience a reduction in C^f and thus a lower V^f in the next adaption period.

Now, let us consider contending flows in the neighborhood of node i, in addition. The RTS and CTS frames contain the flow identification and the instantaneous value of V^f in dedicated header fields (cf. Figure 4.7). Both types of control frames are transmitted using a robust bit-rate to maximize the reception range. In this way, each node i is able to maintain a list of contending but not-intersecting flows $f \in F(N_i) \setminus F(i)$ in its

neighborhood along with their V^f values. As shown on line 8 of Algorithm 8, neighboring flows are considered slightly different in the update of the credit feedback C_i^f . The α scaling does not apply since these flows do not contribute to the local TA limits r_{opt}. Instead, we apply a hysteresis factor δ to prevent the livelock-like situation mentioned in section 3.6.2: Due to the mutual reduction, it becomes impossible to increase the value of the V parameter of any involved flow f. By setting the hysteresis factor δ to a value slightly larger than one, the involved flows are able to mutually increase their V^f values at the expense of a deviation from proportional fairness at the working point.

4.5. Evaluation in Illustrative Scenarios

In the following, we evaluate the proposed protocol within small and synthesized scenarios. We present analytic and simulation results in order to illustrate the system's operation. On the one hand, we will validate the effectiveness of the designed protocol. On the other hand, we will evaluate the efficiency of the system when relaxing the buffer and channel assumptions and characterize the impact of the number of users and routing paths.

The analytic results are obtained in Maple and the simulations have been conducted in JiST/SWANS, which is a packet level simulator for wireless mesh and ad-hoc networks (cf. section 2.5). In our simulations, we use CSMA/HBT at the MAC layer in order to mitigate the hidden node problem (cf. section 3.3). The simulator generates Rician fading coefficients according to the approach of Punnoose *et al.* [210]. Estimating the fading coefficients on the fly is a resource intensive task (cf. [142]). Thus, the authors propose to pre-calculate normalized coefficients, which possess the typical distribution and temporal correlation properties of Rician fading. During runtime, the coefficients are scaled in time and amplitude according to the Doppler shift f_{D} and the Rician K. A single fading coefficient is drawn per frame and link at the beginning of the transmission, which results in a block fading per frame. The fading process is frequency flat and independent across different channels. Note that this model does not account for any possible evolving of the fading process during the frame transmission. The path loss in the data and the BT channels is identical. Furthermore, the fading process is positively correlated across the data and the BT channels, so that both the reception of frames and the CCA operation is affected by the fading process in the same way. Thus, the CS relationship between nodes becomes time-variant. Unless stated otherwise, we use the parameters in Table 4.2 in the following.

4.5.1. Channel-Adaptive Contention and Bit-Rate Selection

To start with, let us reconsider the example from section 4.2 in order to illustrate the gains of the proposed channel-differentiated contention approach. The scenario consists of two links with one flow each, which are within one contention domain and share the same wireless spectrum resources. The bit-rates 6 Mbps and 12 Mbps are available. The channel is in the associated states for about 45% of the medium time for each bit-rate. In the remaining 10% of the time, the channel is in outage. The win-

Parameter	Value
Radio frequency	2.4 GHz
Signal bandwidth B	20 MHz
Path loss	Log-distance, exponent 6, ref. dist. 1 m
Channel	AWGN
Fading	Rician $K = 0$ dB, $f_D = 8$ Hz
Noise floor N	-92.965 dBm
TX power	19 dBm
Receiver	SINR-BER & cumulative interference
PHY	IEEE 802.11a/g
PHY bit-rates	$\{6, 12\}$ Mbps[2]
SNR thresholds[1]	$\{5.4, 14.6\}$ dB[2]
CCA	Mode 1, threshold -88.5 dBm
Propagation delay	0 µs
Radio turnaround	0 µs
TXOP duration	2.5 ms
min, avg. & peak TA	$4, 8.8, 9.6$
Inter-flow hysteresis δ	1.05
Window size W	100 packets
TA EWMA	0.025
Flow rate EWMA γ_y, τ_y	$0.025, 100$ ms
Flow duration	20 s (excl. warm-up)
Packet size	1500 Byte
Seeds	100

[1] 1000 octets, 10% FER.
[2] The same indices belong together.

Table 4.2.: Evaluation parameters

dow size is not relevant for single-hop flows: The packet queues will not run empty since the source nodes ensure that their windows are always filled. Both links experience slow Rician fading under the parameter setting $K = 0$ dB. The coherence time is about 22 ms for the chosen Doppler shift of $f_D = 8$ Hz [228]. A link is blocked for the duration of a TXOP (2.5 ms) if an outage leads to an unsuccessful RTS exchange (cf. section 4.4.1). The propagation delays and the radio turnarounds are set to zero, which allows us to compare the simulation and analytic results in the high TA regime without a bias due to collisions. Table 4.2 shows the remaining parameters.

Using simulation and analytic results, we compare the achieved goodput of the proposed protocol (referred to as OPT) to a channel-adaptive and a non-adaptive protocol variant referred to as RBAR and fixed bit-rate, respectively. In contrast to the latter, both OPT and RBAR determine the bit-rate for data transmission from the RTS/CTS exchange. However, only OPT differentiates its backoff according to the instantaneous channel state. Figure 4.9a shows the simulation results under varying TA targets r_{opt}. For comparison, a single transmitter achieves a transmission rate of 412 pps (801 pps) on an error-free link when using a bit-rate of 6 Mbps (12 Mbps) and an average back-

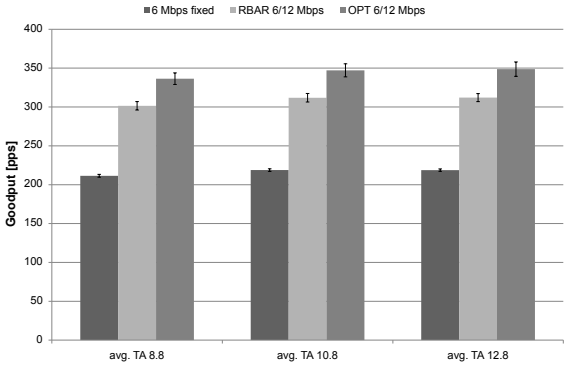

(a) Simulation results ($\pm std.dev.$)

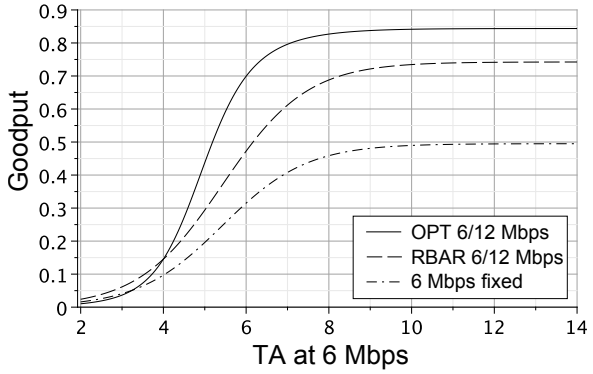

(b) Analytic results. For OPT, the abscissa shows the TA at 6 Mbps, i.e. the avg. TA is correspondingly higher.

Figure 4.9.: Per-flow goodput of two contending one-hop flows under slow fading. The channel has three states $\{0, 6, 12\}$ Mbps with the marginal distribution $\{0.1, 0.45, 0.45\}$. The proposed protocol (OPT) is compared to RBAR and no bit-rate adaptation.

off of 150 µs $\approx \exp(-8.8)$ µs. Even with fixed bit-rates, an OS gain is achieved due to channel outages: In sum, both flows almost achieve the goodput of an error-free channel. If the channel of one flow is in outage, the other channel remains operational with a high probability. When using the fixed bit-rate goodput as baseline, the gains of channel adaptation according to RBAR are about 42%. However, the OS gains are increased to 59% when applying backoff differentiation in addition to channel adaptation. According to the analytic results in Figure 4.9b, the gains of RBAR and OPT are about 50% and 70%, respectively, in the high TA regime. Note that we have assumed equal transmission durations for all bit-rates in the analytic evaluation, which is not feasible in the simulations due to the static overhead that cannot benefit from higher bit-rates.

The proposed protocol OPT outperforms RBAR by about 20% due to the channel-differentiated contention. Let us consider the fading CSMA Markov chain in Figure 4.4 again. Without channel-differentiated backoffs, both links equally share the wireless medium within all channel states and, in particular, in the channel states $(6, 12)$ and $(12, 6)$. From the point of view of throughput efficiency, the transmitter with the instantaneous weaker channel should refrain from contention and compensate the short-term throughput loss in the future when its channel becomes the stronger one.

In summary, we have illustrated the effectiveness of the proposed channel-differentiated contention in a particular scenario. Significant OS gains over non-adaptive approaches are observable even with two users and two bit-rates only. In slow fading channels, outages limit the performance of individual links similar to channel errors that we have considered in the previous chapter. However, outages are different from reception errors since they can be detected in advance. As illustrated in this section, the reallocation of precious resources to operational links achieves OS gains.

4.5.2. Credit Adaptation and Fairness

In this section, we illustrate the effectiveness of the proposed adaptation according to the technological limits presented in section 4.4.3. To start with, we evaluate the intra-flow adaptation under a single flow. Afterwards, we consider multiple flows in several constellations in order to illustrate how the inter-flow adaptation achieves fairness.

Intra-Flow Adaption

The objective of the intra-flow adaptation is the distributed estimation of a credit value C^f for the flow, so that the average TA $\bar{r}$ at the bottleneck meets a given average TA target r_{opt}. According to Algorithm 7 on page 156, the TA determines the absolute size of the CSMA backoffs. Due to the imperfectness of the receivers and physical impairments, severe collisions will arise when arbitrarily decreasing the average backoffs. We have evaluated the impact of collisions due to radio turnaround delays for CSMA/HBT in section 3.3.1 (cf. p. 52ff.). Remember that the instantaneous TAs are scaled by the credits C^f and the instantaneous bit-rate estimate b. In essence, the intra-flow adaptation is an end-to-end feedback loop. According to Algorithm 8 on 160, each forwarder calculates a flow credit estimate C_i^f from the discrepancy between the current and the targeted average TA value, which is communicated in the upstream direction. On arrival, the source of the flow updates the flow credits C^f and the fairness parameter V^f and propagates them in the downstream direction.

Similar to the previous chapter, we consider a single flow on a chain topology consisting of 3 and 7 links, respectively. Each link experiences the same channel characteristics: For 45% of the medium time, the channel supports each of the bit-rates 6 and 12 Mbps and it is in outage for the remaining 10% of the medium time. Since the window size is not the focus in this section, it is set to a conservative value of $W = 100$ packets per hop, i.e. the window consists of 300 (700) packets in the 3 (7) link topology.

We compare the proposed protocol (OPT) against two variants (RBAR, 6 Mbps) and two conventional approaches (UDP, TCP). The RBAR protocol variant employs AMC, whereas the backoffs are not differentiated according to the instantaneous channel conditions. In the second variant, the bit-rates are additionally restricted to 6 Mbps only. For the latter competitors, the transport layer protocols UDP and TCP are used in combination with DSR, IEEE 802.11 and AARF bit-rate selection [153]. In particular, a genie-aided congestion control is used with UDP, so that the number of in-network packets per flow is limited to 1400. All simulations are probabilistically repeated 20 times. The remaining parameters are set according to Table 4.2.

Figure 4.10a shows the goodput results obtained from simulation. The TCP goodput remains negligible due to its inability to differentiate congestion losses from channel impairments [71]. The goodput of UDP is in the order of the 6 Mbps variant. In other words, the AARF bit-rate selection is not able to benefit from the slow fading channel. On the other hand, the RBAR and OPT variants achieve a considerable OS gain of about 40% and 60%, respectively, compared to the fixed bit-rate transmissions. However, the analytic goodput in Figure 4.10a slightly differs from the simulation results especially in the 7 link topology. We suppose that the strong modeling assumptions are the main cause for the observed disparity. In particular, the model ignores the impact of fading

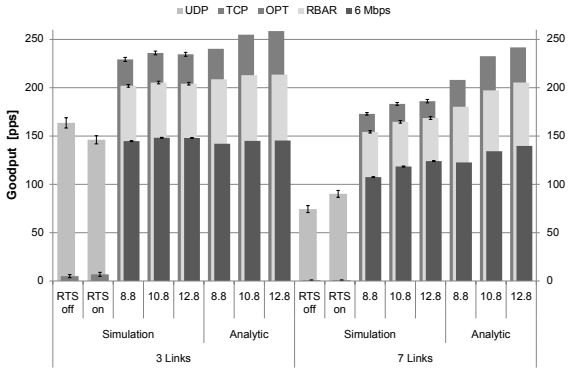

(a) Goodput results ($\pm std.dev.$). The results for TCP and saturating UDP under DSR are also shown.

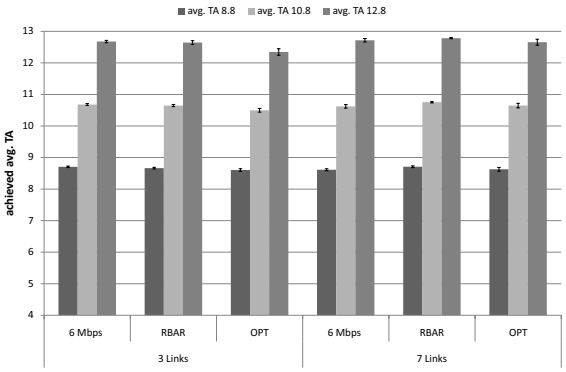

(b) Achieved average TA at the bottleneck link ($\pm std.dev.$).

Figure 4.10.: Results for a single flow on a chain topology of 3 and 7 links, respectively. The slow fading channel has three states $\{0, 6, 12\}$ Mbps with the marginal distribution $\{0.1, 0.45, 0.45\}$. The proposed protocol (OPT) is compared to RBAR and fixed bit-rate transmissions.

on carrier sensing and the underlying link conflict graph. Furthermore, the buffers are finite and the channel state changes are hidden in the simulation, which we will investigate in detail in section 4.5.3. Nevertheless, the proposed algorithm is able to operate the average TAs near the anticipated operating point as shown in Figure 4.10b.

Inter-Flow Adaption

In this section, we illustrate the effectiveness of the inter-flow adaption according to Algorithm 8 on page 160 using several example topologies. The inter-flow adaption should equalize the V values between competing flows in order to provide proportional fairness. We reconsider the scenarios already introduced in Figure 3.19 on page 78, in which a long and short flow share either a common link or wireless resources within a collision domain. In addition, we consider two and three single-path flows that are placed parallel to each other on a regular grid as shown in Figure 4.11. The latter corresponds to the well-known *flow in the middle* scenario, for which severe fairness problems have been reported with state-of-the-art protocols [74, 75]. For both grid topologies, we vary the number of hops between one and four. All simulations are probabilistically repeated 20 times.

Similar to the previous section, each link supports the bit-rates $\{0, 6, 12\}$ Mbps with the marginal distribution $\{0.1, 0.45, 0.45\}$. The same holds for the interfering links shown in Figure 4.11. The hysteresis factor for the inter-flow adaption is set to $\delta = 1.05$. We compare the results for the proposed protocol (OPT) with two of its variants (RBAR, 6 Mbps) and two conventional approaches (UDP, TCP), which have been described in the previous section. For presentation purposes, we report the values of V relative to $(r_{\text{opt}} - r_{\min})$. The relative difference ΔV is the range of the V values across all flows

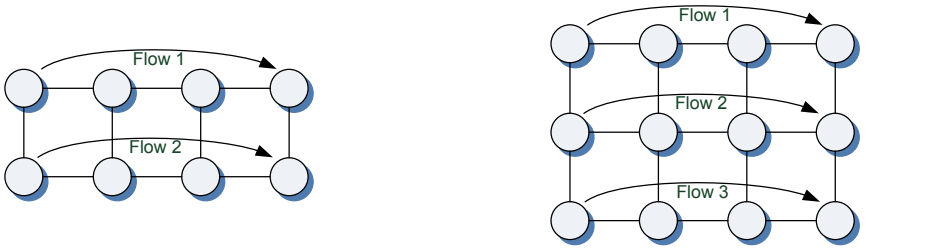

(a) Two-flow scenario.

(b) Three-flow scenario (flow in the middle).

Figure 4.11.: Simulation topologies: Multiple flows on a regular grid.

within one simulation in relation to the largest V:

$$\Delta V = \frac{\max_f V_f - \min_f V_f}{\max_f V_f}$$

Figure 4.12a shows the per-flow goodput and the sum utility for the three scenarios in Figure 3.19 on page 78. TCP achieves low utilities since the longer flow is starved in almost all cases. In comparison, the utility under UDP is significantly larger. However, the shorter flow is generally favored over the longer one. Thus, the achieved utility of OPT and its variants is comparatively larger, i.e. it offers a higher degree of proportional fairness. The proposed protocol (OPT) dominates its variant RBAR in terms of per-flow goodput and utility, whereas RBAR dominates the variant 6 Mbps in the same way. With OPT and its variants, the standard deviation of both goodput and utility across all randomized repetitions is significantly lower. Hence, they are able to maintain their working points with a higher stability.

Figure 4.12b presents the achieved V values and their relative difference ΔV for the proposed protocol (OPT). In scenario A and B, the flows are coupled via a shared link. Hence, they interact with each other via the first expression of the minimum on line 8 of Algorithm 8 (cf. p. 160). The results suggest that the proposed algorithm is able to equalize the Vs in both scenarios. The relative difference between them is below 1% on average. In scenario C, on the other hand, the flows share wireless resources within a collision domain. They interact via the second expression of the above considered minimum in the algorithm. In this case, we have to accept a slight deviation from proportional fairness (equal Vs) that is expressed by the hysteresis factor δ in order to prevent the downward spiral, in which the Vs cannot be increased anymore. However, the relative differences ΔV are in good match with the predetermined hysteresis factor $\delta = 1.05$.

For the grid scenarios with two and three parallel flows, the above observations apply to the goodput and utility results in Figure 4.13a and Figure 4.14a in the same way. Although there is no shared link in the scenarios in Figure 4.11 and thus, the flows interact via the hysteresis expression, the achieved Vs in Figure 4.13b show a small imbalance only. In particular, the relative difference ΔV is below 1%. The reason is the symmetry of the scenario: The working point in terms of V is the same for both flows. In the three flow scenario, the flow in the middle contends with both outer

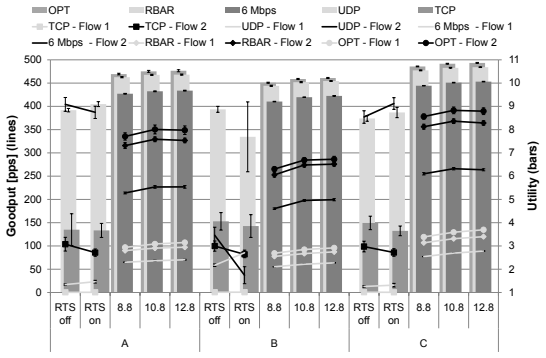

(a) Per-flow goodput and sum utility are shown as lines and bars, respectively ($\pm std.dev.$).

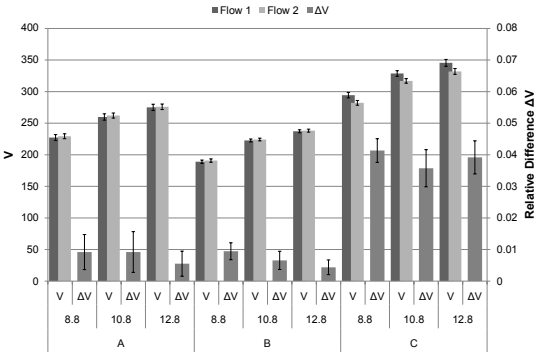

(b) Average V and relative V difference between both flows (OPT, $\pm std.dev.$).

Figure 4.12.: Simulation results for the 3 topologies in Figure 3.19 on page 78 with 2 flows each depending on the scenario, the TA target and the RTS usage ($W = 25$).

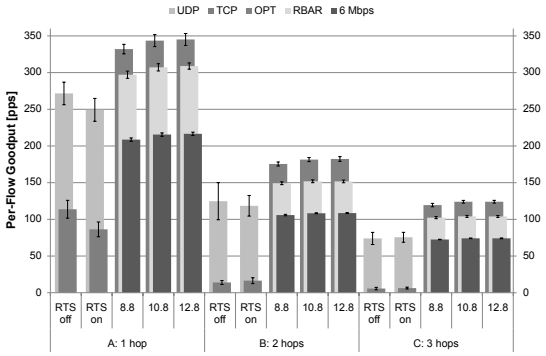

(a) Per-flow goodput ($\pm std.dev.$). Due to symmetry, the per-flow goodput is not distinguished.

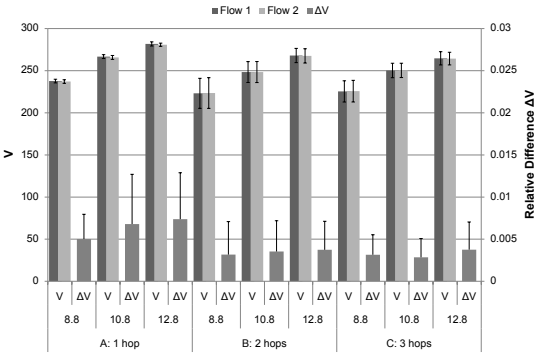

(b) Average V and relative V difference between both flows (OPT, $\pm std.dev.$).

Figure 4.13.: Simulation results for the grid topology in Figure 4.11 with 2 flows depending on the number of hops, the TA target and the RTS usage ($W = 100$).

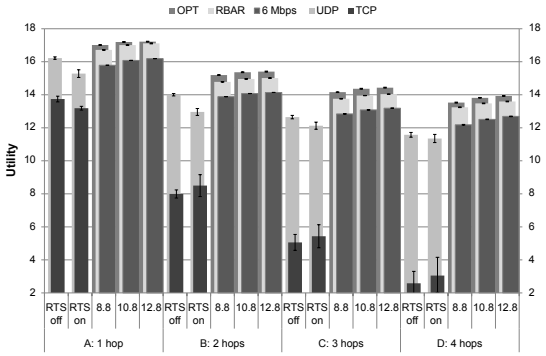

(a) Sum utility ($\pm std.dev.$).

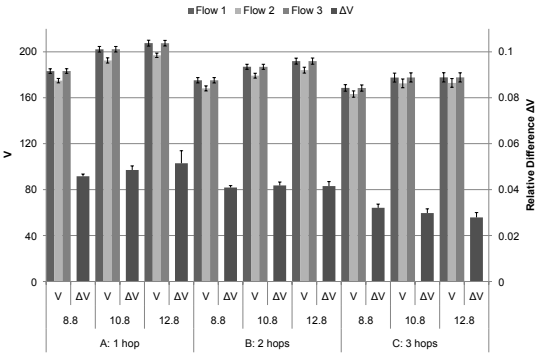

(b) Average V and relative V difference (OPT, $\pm std.dev.$).

Figure 4.14.: Simulation results for the grid topology in Figure 4.11 with 3 flows (flow in the middle) depending on the number of hops, the TA target and the RTS usage ($W = 100$).

flows, whereas they share the wireless medium with the flow in the middle only. Due to the hysteresis factor, the flow in the middle achieves slightly lower Vs. Nevertheless, the relative difference ΔV in Figure 4.14b remains within the bounds of the hysteresis factor.

In summary, we have evaluated the adaption algorithm presented in section 4.4.3 in terms of approaching and maintaining a working point for the TAs (intra-flow adaptation) and, furthermore, in terms of providing proportional fairness among contending flows (intra-flow adaption). We conclude that the algorithm is effective in the considered cases. It dynamically approaches a small neighborhood of the proportional fair working point subject to the TA targets. The hysteresis may lead to a small deviation from proportional fairness. Nevertheless, it effectively prevents the situation, in which competing flows mutually limit their V values in a way that an increase becomes impossible.

4.5.3. Finite Buffers and the Slow Fading Channel

In the system we are considering, the queues, the medium access and the channels are driven by random processes that interact with each other. Each channel evolves independently according to the underlying fading process, which is assumed to be independent from the users' actions. This assumption is not straightforward since techniques like random beamforming [264] actively influence the fading process. On the other hand, both the medium access and the queueing process are driven by the actions of the users and the fading process. The interacting random processes render it hard to evaluate the impact of finite buffers and hidden channel state changes separately.

The WCC influences the end-to-end delay and the OS gain and thus the achievable throughput capacity. In contrast to TCP, the window size determines not only the efficiency of the resource utilization, but also the amount of available capacity resources. Order results and bounds are known for the arising tradeoff under MWS and several channel models [158]. We are interested in the numerical characterization of the tradeoff for the considered system using the proposed protocol. The model of CSMA in slow fading channel relies on several assumptions about the fading process, which we have already introduced in section 4.2.2. Among them, the most important assumptions are:

1. *Perfect and instantaneous CQI* is available at *no cost*. In this way, the transceivers synchronize their actions with the channel and react immediately on channel changes.

2. The channel is *block-fading*. The fading process does not advance while a transmission occupies the channel.

3. *Mutually independent* fading on different channels.

4. Fading does not affect the *carrier sensing* on both communication and interference links.

The third assumption is reasonable for a sufficient antenna separation [84]. Zubow *et al.* have experimentally validated that the third assumption applies to their in-door mesh network based on IEEE 802.11 hardware [318]. We are particularly interested in the

impact of the first two assumptions. Since channel state changes are generally hidden, they remain unrevealed until the channel is probed once again, which consumes resources and incurs measurement errors and feedback delay. Clearly, there is a tradeoff between the timeliness and accuracy of the probes and the necessary resources. In order to cope with the incomplete knowledge, our proposed protocol employs a strategy that reduces the resource costs for the exchange of CSI: Such information is exchanged only during MAC transactions in a piggy-back fashion at negligible extra costs (cf. section 4.4.1). The accuracy of the channel information over time relies on the memory of the fading process. In addition, the speed of the fading process determines the extent to which the block-fading assumption holds.

Finite Buffers with Perfect Channel Knowledge

In the following, we investigate the interaction between the queueing and the channel process under slow fading and WCC. Our intention is to analyze the relationship independent from CSMA in order to derive upper bounds for any online algorithm. Hence, we abstract from contention-based medium access and assume that a central controller is available, which has perfect knowledge about channel conditions and queue sizes. We assume that the system operates in slotted time. The central controller schedules the transmissions via MWS. A single flow traverses the network using single-path routing, and we associate a queue with every link of the route. Since the WCC guarantees saturated queues for single-hop flows, we will consider multi-hop routing only. For the sake of clarity, we constrain our analysis to a single collision domain without any concurrent transmissions.

Closed queueing networks and Gordon-Newell networks, in particular, can be used to model systems with WCC [26, 31]. In the following, we derive a discrete time Markov model for a closed queueing network, in which each link and thus each queue is associated with a channel-dependent service rate. The state of each link i consists of the current queue size $w_i \in \{0 \dots W\}$ and the current channel state $b_i \in B$. In addition, $\mathrm{P}(b_i)$ denotes the a priori probability of the channel state $b_i \in B$. We assume that a total order of the channel states B exists according to the nominal bit-rates. The increment operation $b_i + 1$ (decrement operation $b_i - 1$) selects the predecessor (successor) of b_i according to the total order, or it is the identity b_i if no such element exists. The system state $(\boldsymbol{w}, \boldsymbol{b})$ consists of the joint link state. Furthermore, we assume that both state spaces can be indexed, and the notation $\boldsymbol{w}^l$ ($\boldsymbol{b}^l$) refers to the l-th element of the queue (channel) state space.

The frame structure is as follows. The time is divided into slots. The system changes its state only at slot boundaries. With a fixed probability S, the channel state $\boldsymbol{b}$ changes at the slot boundary and the queue state $\boldsymbol{w}$ remains unchanged, and with probability $1 - S$ a queue related transition occurs without altering the channel. Both types of transitions are denoted by C and $TXOP$ in Figure 4.15.

Figure 4.16 shows a sketch of the resulting discrete-time Markov chain for two links, a window size of $W = 2$ packets and three channel states $\{B, N, H\}$, which correspond to the nominal data rates of $\{0, 1, 2\}$ packets per TXOP. For the sake of readability, we have neglected some channel transitions and the transition probabilities. In the figure, every transition that stays within the same depth of the shown three-dimensional

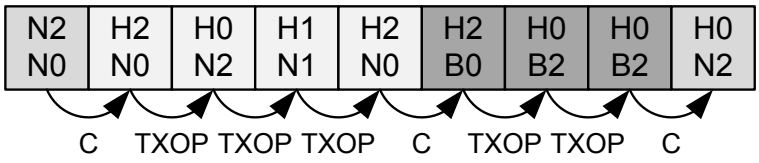

Figure 4.15.: Frame structure of the finite buffer model. A transition is either a channel state change (C) or a transmission (TXOP) that changes the queue state. If no packets are available for transmission like in state $H0B2$, the TXOP remains unused.

Markov chain is a channel transition. They are shown in gray. Let us neglect the queue component $\boldsymbol{w}$ of the system state for the moment, since it is unaffected by channel transitions. Every state $\boldsymbol{b}^l$ has an outgoing transition to any other state $\boldsymbol{b}^k$ that differs in each link channel state b_i^k by up to one adjacent bit-rate, i.e. $b_i^k \in \{b_i^l - 1, \ldots, b_i^l + 1\} \forall i$. The transition probabilities $\mathrm{P}(\boldsymbol{b}^l \to \boldsymbol{b}^k)$ are defined as follows.

$$\mathrm{P}(\boldsymbol{b}^l \to \boldsymbol{b}^k) = \begin{cases} S \cdot \prod_i \mathrm{P}(b_i^k) & l \neq k \textbf{ and } b_i^k \in \{b_i^l - 1, \ldots, b_i^l + 1\} \forall i \\ S - \sum_{m \neq l} \mathrm{P}(\boldsymbol{b}^l \to \boldsymbol{b}^m) & l = k \end{cases}$$

Furthermore, the self-transition with probability $\mathrm{P}(\boldsymbol{b}^l \to \boldsymbol{b}^l)$ ensures that the probabilities of all outgoing channel transitions sum up to S. In Figure 4.16, we have neglected the channel transitions that alter both channel states at the same time, which includes the transition $H2H0 \to N2N0$, for example. On the other hand, the transition $H2H0 \to B2B0$ is *not* part of the model since the channel states H and B are *not* adjacent, so that a direct transition is not supported.

Queue-related transitions may alter the queue state $\boldsymbol{w}^l \to \boldsymbol{w}^k$ but not the channel state $\boldsymbol{b}$. In Figure 4.16, these transitions are shown as black arrows. They occur along the depth axis of the depicted Markov chain. A queue-related transition consumes a TXOP in the physical network, which is either used for packet transmission, or it is left unused depending on the channel and queue state. For a given system state $(\boldsymbol{b}, \boldsymbol{w}^l)$, the set O covers all links and thus all queues that are allowed to transmit. It is defined as follows.

$$O(\boldsymbol{w}^l | \boldsymbol{b}) = \Big\{ i : w_i^l > \min(W, b_i) \textbf{ and } b_i > 0 \textbf{ and } \Big[b_i > b_j \textbf{ or } b_i = b_j \textbf{ and } w_i^l >= w_j^l \Big] \forall j : w_j^l > \min(W, b_j) \Big\}$$

The definition of O consists of three constraints. At first, the considered queue w_i^l has to provide sufficient packets to utilize the whole TXOP. The minimum term in the first constraint ensures that the system remains operational under small window sizes that are not able fill the whole TXOP. Secondly, the associated link has to be in non-outage. The MWS is encoded in the third constraint: Among all links that satisfy both the first and the second constraint, only the links with the highest bit-rate and the largest queue size are selected for transmission. In particular, the bit-rate is the dominant criterion, and the queue size is considered in the case of ties only.

Although the state $N1N1$ has two queue-related transitions, state $H1N1$ in Fig-

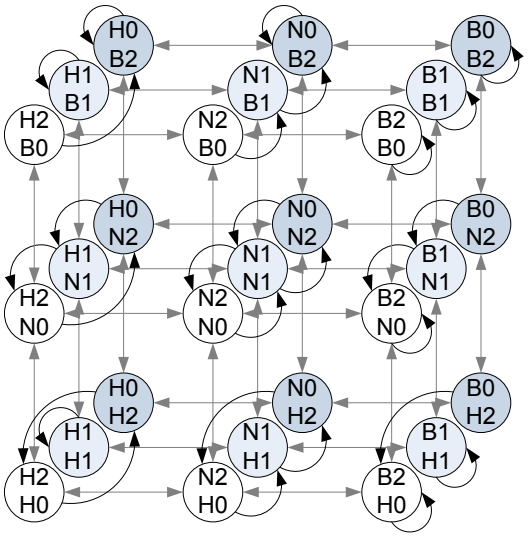

Figure 4.16.: Sketch of the discrete time Markov chain of the closed queueing network under slow fading channels.

ure 4.16 has only one since the first queue does not provide sufficient packets to cover the whole TXOP. Note that the first constraint leads to the curious case that state $H1H1$, for example, has no outgoing transition into other states. However, these curiosities vanish with larger window sizes. Let $R(i)$ be the next hop link along the route from source to destination. If i is the last hop, $R(i)$ becomes the first hop of the route. The probability P of the queue-related transition $\boldsymbol{w}^l \rightarrow \boldsymbol{w}^k$ in channel state $\boldsymbol{b}$ is defined as follows.

$$\mathrm{P}(\boldsymbol{w}^l \rightarrow \boldsymbol{w}^k|\boldsymbol{b}) = \begin{cases} \dfrac{1-S}{|O(\boldsymbol{w}^l|\boldsymbol{b})|} & \begin{array}{l} \forall i \in O(\boldsymbol{w}^l|\boldsymbol{b}) : w_i^k = w_i^l - \min(W, b_i) \\ \textbf{and } w_{R(i)}^k = w_{R(i)}^l + \min(W, b_i) \\ \textbf{and } w_j^l = w_j^k \; \forall j \notin \{i, R(i)\} \end{array} \\ 1-S & l = k \textbf{ and } O(\boldsymbol{w}^l|\boldsymbol{b}) = \emptyset \end{cases}$$

The definition of $\mathrm{P}(\boldsymbol{w}^l \rightarrow \boldsymbol{w}^k|\boldsymbol{b})$ is straightforward: The queue-related transition probability $1 - S$ is shared equally between all outgoing transitions. If no outgoing transitions are available, we add a self-transition back into the state.

Every queue-related transition in the model consumes a TXOP in the network and thus, it determines the link and system throughput. Let i be the transmitting link in the transition $\boldsymbol{w}^l \rightarrow \boldsymbol{w}^k$ under channel state $\boldsymbol{b}$. Then, link i generates throughput by transmitting $(w_i^l - w_i^k) = \min(W, b_i)$ packets. On the other hand, the self-transition $\boldsymbol{w}^l \rightarrow \boldsymbol{w}^l$ does not generate any throughput. The throughput of a link is the number of transmitted packets in relation to the overall sum of processed TXOPs in the considered time period t. Since the probability of a queue-related transition is $(1 - S)$ in every time slot, the expected number of processed TXOPs is $(1 - S) \cdot t$. Let p be the stationary distribution of the considered Markov chain. During time period t, the expected number of transmitted packets in channel state $\boldsymbol{b}$ due to the transition $\boldsymbol{w}^l \rightarrow \boldsymbol{w}^k$

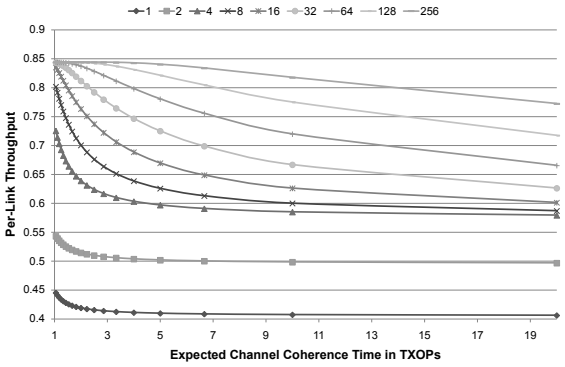

(a) Per-link throughput depending on coherence time (in TXOPs) and window size (in packets).

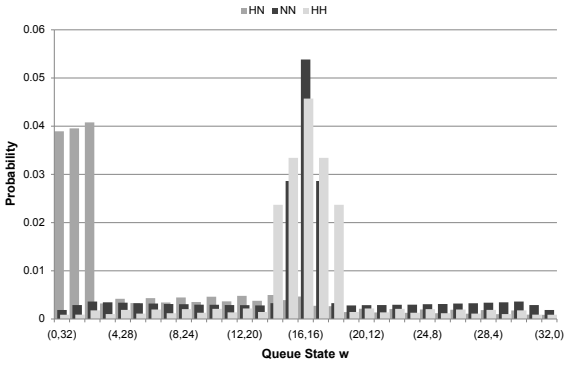

(b) Stationary distribution of the packets for several channel states ($T_c = 10$ TXOPs, $W = 32$ packets).

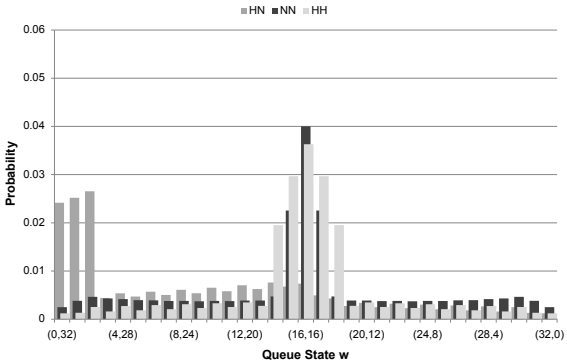

(c) Stationary distribution of the packets for several channel states ($T_c = 5$ TXOPs, $W = 32$ packets).

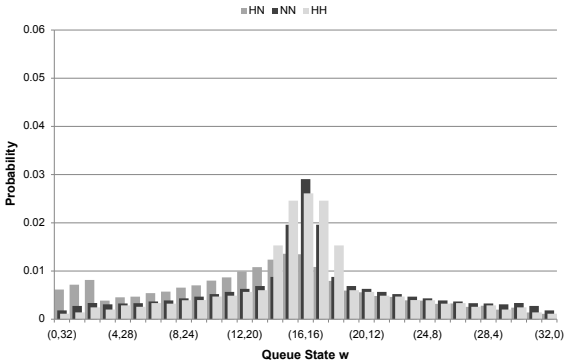

(d) Stationary distribution of the packets for several channel states ($T_c = 2$ TXOPs, $W = 32$ packets).

Figure 4.17.: Numeric evaluation of the stationary distribution of the joint fading and closed queueing model. The scenario consists of two fading links and a single flow. Each link is in one of the channel states $\{B, N, H\}$ with probability $\{0.1, 0.45, 0.45\}$.

with transmitter i is $t \cdot p(\boldsymbol{b}, \boldsymbol{w}^l)(1-S)|O(\boldsymbol{w}^l|\boldsymbol{b})|^{-1} \min(W, b_i)$. Thus, the *throughput* T of link i can be calculated as follows.

$$T(i) = \sum_k \min(W, b_i^k) \sum_{l:O(\boldsymbol{w}^l|\boldsymbol{b}^k)\ni i} \frac{p(\boldsymbol{b}^k, \boldsymbol{w}^l)}{|O(\boldsymbol{w}^l|\boldsymbol{b}^k)|}$$

We refer to the average number of slots, in which the channel remains in the same channel state, as *expected channel coherence time* T_c that is measured in TXOPs. Due to the fixed per-slot probability of a channel state change S, the channel coherence time has a geometric distribution with mean $T_c = S^{-1}$. For example, let the channel transition probability be $S = 0.1$, then the expected coherence time is $T_c = 10$. However, the channel state change can also be a self-transition: If the considered link is in state N and $\mathrm{P}(N) = 0.45$, then its channel state does not change with a probability of 45%.

The stationary distribution p does not have the product form. We have numerically

estimated the stationary distribution p and the throughput T for a two-hop flow using a Maple solver. The results are plotted in Figure 4.17a. In several configurations, the system operates near the optimal throughput of 0.84 as shown in Figure 4.17a. However, the throughput significantly decreases with larger channel memory and smaller window sizes. Using a window of 32 packets and a coherence time of 10 TXOPs, for example, the resulting throughput reduces to 0.67.

Let us consider Figure 4.17b to understand the reasons. The figure shows the stationary distribution across the queue states within three channel states of interest. In the states NN and HH, both links operate with equal bit-rates and the MWS considers their queues only. Thus, the system tries to balance both queues, i.e. it tries to push the queues into the neighborhood of queue state $(16, 16)$. However, the channel evolves too slowly, so that the queues are not able to bridge over channel states with unequal channel conditions. For example, let us consider the channel transition $HH \rightarrow HN$ within queue state $(16, 16)$. The system is able to transmit 16 packets on the first link using 8 TXOPs. Afterwards, both links have to take turns as shown by the peaks of the distribution within the states $(0, 32) - (2, 30)$. Remember that taking turns in channel state HN is less efficient in terms of throughput. As shown in Figure 4.17c and Figure 4.17d, the weight of the distributions can be shifted to more efficient states by reducing the channel coherence time. Note that we assume block fading and the channel does not change within a TXOP even if the coherence time is small. We will investigate the effect of the block fading assumption in the next section.

In contrast to the TCP assumptions, the results in Figure 4.17 clearly show a significant dependency of the channel capacity on the channel distribution and the window size. According to Fu *et al.* [71], the optimal TCP window size should be one for our two-hop scenario. However, such a small window size would result in severe throughput losses as shown above. Thus, the congestion controller is not only responsible for the efficient utilization of the capacity resources, but it determines the amount of available capacity, in addition.

The implications on the system design are manifold. The ability to influence the coherence time is limited since it is a physical property of the channel. Nevertheless, the fading process can be accelerated via random beamforming using dumb antennas as proposed by Tse *et al.* [264]. Furthermore, the length of a TXOP is a design parameter that can be appropriately adapted within certain technological limits. On the other hand, the window size is the parameter that the system can easily adapt. Unfortunately, the above results suggest that the OS capacity scales rather shallow with the window size in the large window regime. In other words, it takes a significant and non-negligible amount of end-to-end delay to achieve high capacities. The throughput and delay requirements of applications are generally diverse. We argue that the *applications* and eventually the *users* should be able to specify their preferences according to their requirements.

Data Transmission under Hidden Channel State Changes

Both our model and our design rely on several strong assumptions. In the following, we are going to take a deeper look at the block fading assumption using an enhanced model of CSMA in fading environments. The block fading assumption guarantees that

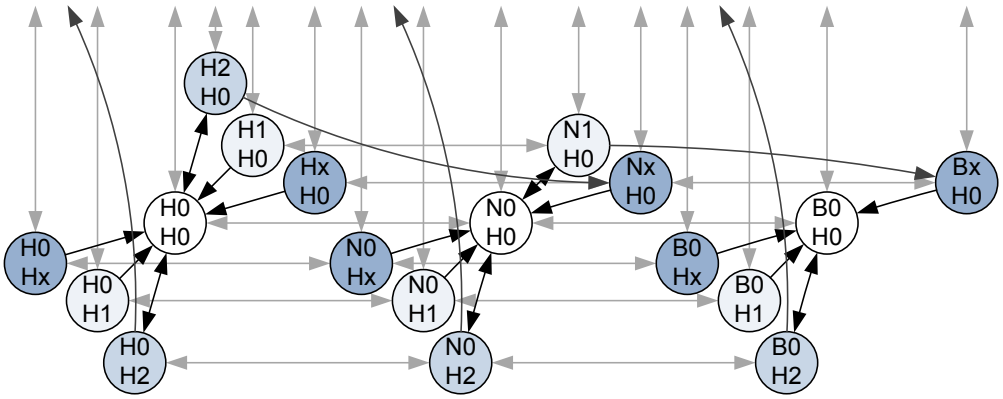

Figure 4.18.: An excerpt of the enhanced fading CSMA Markov chain for two competing transmitters in slow fading environments and tree channel states $\{H, N, B\}$. Transmission and channel transitions are shown in shown in black and grey, respectively. The transmission state additionally stores the selected bit-rate and whether the channel has been in outage during the transmission. The excerpt corresponds to the bottom layer of the chain in Figure 4.4 on page 145.

the channel does not change during a transmission. In other words, the CSI acquired at the beginning of a transmission is sufficient to describe the channel at the transmission's end.

When relaxing the block fading assumption, a transmission fails if the channel quality decreases. In the opposite case, the transmission cannot benefit from potential channel improvements. Hence, we differentiate the transmission states of the idealized fading CSMA model (cf. section 4.2) according to the bit-rate at the beginning of the TXOP and whether the channel has been in outage since the transmission started, which is captured in the failure state. An example is given in Figure 4.18. In contrast to the corresponding fading CSMA model in Figure 4.4 (cf. p. 145), the transmission states indicate both bit-rate and failure status, in addition. In particular, if the transmission state of a link is larger than zero, then the transmission has been started with the given bit-rate *and* it has not failed yet. The transmission state x refers to an ongoing failed transmission. The state transitions of the Markov chain can be classified into *transmission* and *channel* transitions. The former refer to the activation and the inactivation of links. If a link starts transmitting, it selects the highest bit-rate available. Thus, exactly two transmission transitions leave the Markov chain state $H0H0$ in Figure 4.18, which are $H0H0 \rightarrow H2H0$ and $H0H0 \rightarrow H0H2$. The transmission length is independent from the bit-rate and the failure status, so that the figure contains the transition $H0Hx \rightarrow H0H0$, for example. For most of the states, a channel transition changes the channel state of the link only. As shown for $N1H0 \rightarrow H1H0$, the selected bit-rate of a transmitting link remains unchanged. However, a channel transition for a currently transmitting link may cause an outage. In this case, the transmission state is changed to x, in addition, as shown for $H2H0 \rightarrow NxH0$.

Let us define the Markov chain using the notation from section 4.2: The transmission and channel state vectors are denoted by $\boldsymbol{v} \in V^K$ and $\boldsymbol{w} \in W^K$, respectively. The set W contains all available bit-rates and an additional element for outages that is de-

noted by 0. We assume that W does not contain duplicates and the notation W_i refers to the i-th element of W according to the natural ordering of the nominal bit-rates. The states of the Markov chain can be generated as follows. At first, generate the set of channel states $W^K \ni \boldsymbol{w}$, where K is the number of links. Similar to the previous chapters, we assume that the set W^K can be indexed and the notation $\boldsymbol{w}^l$ refers to the l-th element of the set. The j-th component of the vector $\boldsymbol{w}^l$ can be accessed via $\boldsymbol{w}^l_j$. The set of transmission states contains the elements $V = \{x, 0, 1, \ldots\}$, where 0 indicates a listening link. Otherwise, the link is transmitting and a value larger than zero indicates the initial bit-rate at the beginning of the transmission. A transmission failure due to the channel conditions is denoted by the value x, which we assign the nominal value -1. For each joint channel state $\boldsymbol{w}^l$, generate the transmission states $\{\boldsymbol{v}^{l,k}\} \subseteq V^K$ according to the LCG and the following additional rule: If the idealized CSMA Markov chain according to Jiang *et al.* [112] that corresponds to the considered topology contains a state, in which link i is transmitting, then there should be several states k having $v_i^{l,k} \in \{x, 0, \ldots, w_i^l\}$ within the joint channel state $\boldsymbol{w}^l$. In particular, we have to generate all combinations across the links i that comply with the LCG constraints. In the following, we neglect the channel index l at transmission state expressions $\boldsymbol{v}^{l,k}$ if the channel state $\boldsymbol{w}^l$ the index refers to is given in the context.

Let us consider the transmission transitions next. They occur within a fixed joint channel state $\boldsymbol{w}$. The transition rates Q are defined as follows.

$$Q(\boldsymbol{v}^l \to \boldsymbol{v}^k | \boldsymbol{w}) = \begin{cases} \exp(w_i r_i) & v_j^l = v_j^k \ \ \forall j \neq i \textbf{ and } v_i^l = 0 \textbf{ and } v_i^k > 0 \\ & \quad \textbf{and } v_i^k \geq \max_m v_i^m \\ 1 & v_j^l = v_j^k \ \ \forall j \neq i \textbf{ and } v_i^l \neq 0 \textbf{ and } v_i^k = 0 \end{cases}$$

The first alternative expresses that a link always selects the highest instantaneous bit-rate if it decides to start a transmission. Thereby, the TA r_i of the link is scaled by the instantaneous bit-rate w_i. The second alternative determines the frame length, which is normalized in our case.

The channel transitions Q determine how fast the channel changes. They are defined as follows.

$$\begin{aligned} & Q\left((\boldsymbol{w}^l, \boldsymbol{v}^{l,m}) \to (\boldsymbol{w}^k, \boldsymbol{v}^{k,n})\right) \\ & = \begin{cases} R_c(w_i^l \to w_i^k) & w_j^l = w_j^k \ \ \forall j \neq i \textbf{ and } w_i^k \in \{W_{-1}(w_i^l), W_{+1}(w_i^l)\} \\ & \quad \textbf{and } \boldsymbol{v}^{l,m} = \boldsymbol{v}^{k,n} \textbf{ and } v_i^{l,m} \leq w_i^k \\ R_c(w_i^l \to w_i^k) & w_j^l = w_j^k \ \ \forall j \neq i \textbf{ and } w_i^k \in \{W_{-1}(w_i^l), W_{+1}(w_i^l)\} \\ & \quad \textbf{and } v_j^{l,m} = v_j^{k,n} \ \ \forall j \neq i \textbf{ and } v_i^{l,m} > 0 \textbf{ and } v_i^{k,n} = x \\ & \quad \textbf{and } v_i^{l,m} > w_i^k \end{cases} \end{aligned}$$

In the expressions above, $W_{-1}(w) \in W$ and $W_{+1}(w) \in W$ refer to the adjacent bit-rates of w in W in the down- und upward direction, respectively. In addition, R_c denotes the average fade rate that we will explain in the next paragraph. The first alternative is a simple channel state change without changes to the transmission state. The second alternative captures the case that the channel quality decreases in a way that the selected

bit-rate cannot be supported anymore. In this case, the transition ends in an x state and the further consumed medium time is wasted.

The average fade rate R_c is related to the AFD and the ANFD. In particular, they are reciprocal when considering two channel states only. We differentiate the average fade rate R_c into upward and downward channel state changes: $R_c(W_i \rightarrow W_{i+1})$ is the rate, at which the channel improves from state W_i to the adjacent state W_{i+1}. With multiple non-outage states, we use the finite-state Markov channel (FSMC) model [84] in continuous time in the following way.

$$R_c(W_i \rightarrow W_{i+1}) = \frac{L(W_{i+1})}{\mathrm{P}(W_i)} = \frac{L(\rho_{i+1})}{\mathrm{P}_{\mathrm{out}}(\rho_{i+1}|1) - \mathrm{P}_{\mathrm{out}}(\rho_i|1)} \tag{4.22}$$

$$R_c(W_i \rightarrow W_{i-1}) = \frac{L(W_i)}{\mathrm{P}(W_i)} = \frac{L(\rho_i)}{\mathrm{P}_{\mathrm{out}}(\rho_{i+1}|1) - \mathrm{P}_{\mathrm{out}}(\rho_i|1)} \tag{4.23}$$

Let us assume that every channel state W_i has an associated signal amplitude threshold ρ_i, which must be satisfied by the received signal in order to support the bit-rate. In the expressions above, $L(W_i)$ refers to the level crossing rate (LCR) of the transition $W_i \rightarrow W_{i-1}$, i.e. it holds $L(W_i) = L(\rho_i)$. Furthermore, $\mathrm{P}(W_i) = \mathrm{P}_{\mathrm{out}}(\rho_{i+1}|1) - \mathrm{P}_{\mathrm{out}}(\rho_i|1)$ is the a priori probability of the channel state W_i. For Rician fading, the outage probability $\mathrm{P}_{\mathrm{out}}$ and the LCR L can be estimated according to (2.5) and (2.6), respectively (cf. p. 17).

Let p be the stationary distribution of the Markov chain. The *throughput* $q_{i,b}$ of link i while the channel is in state b is defined as follows.

$$q_{i,b} = b \sum_{l,k} \mathbb{1}(v_i^{l,k} = b) p(\boldsymbol{w}^l, \boldsymbol{v}^{l,k})$$

In the equation above, $\mathbb{1}$ is an indicator function that is evaluated to one if the argument is true, whereas it is zero otherwise. The *throughput* q_i of link i defined as $q_i = \sum_{b>0} q_{i,b}$. Note that our enhanced fading CSMA model has the following limitation: Only the medium time *after* the transition into the x state is wasted, whereas the medium time *before* is assumed to generate throughput. There are several systems like IEEE 802.11, which behave differently. Thus, our results are optimistic for these systems. On the other hand, there are techniques like partial packet recovery [94, 108, 150, 169] that try to extract the usable information from corrupted packets.

The stationary distribution p does not have the product form. We have evaluated the enhanced fading CSMA model numerically using Maple. We consider a single flow traversing two links, which can be in three channel states. Due to the symmetry of the scenario, we can use the same TA to generate the same throughput on both links. The results are shown in Figure 4.19. In one of the next sections, we will present simulation results where we have set the TXOP duration to 2.5 ms. A Doppler frequency of $f_{\mathrm{D}} = 1$ Hz in the simulations corresponds to $1\ \mathrm{Hz} \cdot 2.5\ \mathrm{ms}/(1\ \mathrm{s})$ in the model, since it uses a normalized frame length. Nevertheless, we report the Doppler frequencies in relation to a TXOP, e.g. 1 Hz in the above example, in order to provide comparability with the simulation results. In scenario A, we have used the signal thresholds from the simulations, which results in the channel distribution $\mathrm{P}(\{0,1,2\}) = \{0.11, 0.52, 0.37\}$

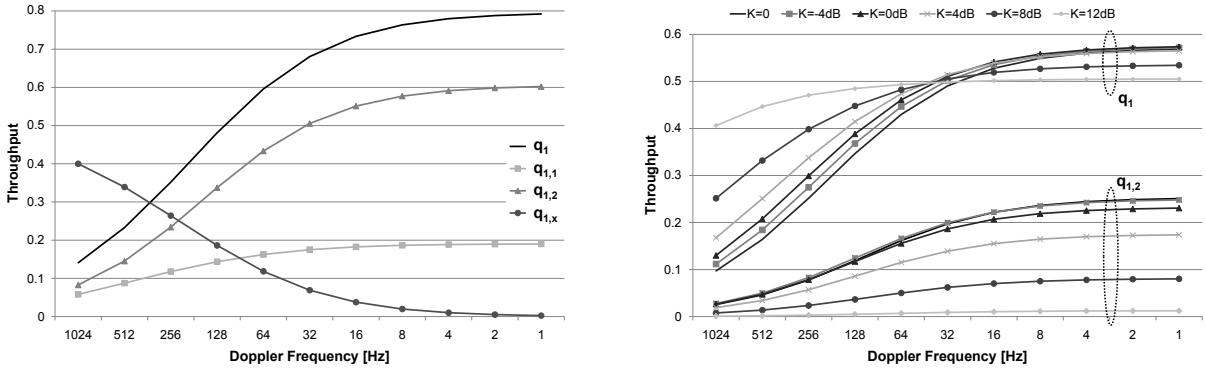

(a) Scenario A: $(\rho_1^2, \rho_2^2) = (-9.26, -0.06)$ dB, $K = -\infty$ dB.

(b) Scenario B: $(\rho_1^2, \rho_2^2) = (-4, 3)$ dB.

Figure 4.19.: Per-link throughput for a single flow traversing two hops with three states per channel depending on the Doppler frequency, (a) the bit-rate and (b) the Rician K parameter. The results are obtained by solving the stationary distribution of the enhanced Markov chain numerically using the TA $r_1 = r_2 = 6$.

for $K = -\infty$ dB. Table 4.3 shows the associated average fade rates R_c in terms of TXOPs for $f_D = 32$ Hz. The entry $R_c(0 \to 1) = 0.549$, for example, means that the channel spends $1/0.549 = 1.82$ TXOPs on average in outage before proceeding to state 1. Remember that R_c is directly proportional to f_D. The throughput for scenario A is shown in Figure 4.19a. As supposed, an increased Doppler frequency results in throughput losses. When the fading process is accelerated, the wasted throughput $q_{1,x}$ grows since a channel state change occurs more often during a transmission. The throughput losses are moderate when starting with a large Doppler frequency. However, there is a *critical Doppler frequency* at which the losses start to accelerate, so that the system has to cope with severe losses. In the figure, the critical point is located around $f_D = 32$ Hz. At this point, the average duration the channel spends within a state is in the order of a few TXOPs only.

In scenario B, we have selected different bit-rate thresholds in order to illustrate the impact of the Rician K parameter. For the sake of clarity, Figure 4.19b shows q_1 and $q_{1,2}$ only. The above observations about throughput and Doppler frequency apply to sce-

Scenario	K	$R_c(0 \to 1)$	$R_c(1 \to 0)$	$R_c(1 \to 2)$	$R_c(2 \to 1)$
A	$-\infty$ dB	0.549	0.119	0.144	0.199
B	$-\infty$ dB	0.218	0.215	0.129	0.252
B	-4 dB	0.190	0.177	0.111	0.222
B	0 dB	0.179	0.138	0.095	0.210
B	4 dB	0.187	0.091	0.070	0.212
B	8 dB	0.224	0.049	0.042	0.235
B	12 dB	0.294	0.017	0.018	0.289

Table 4.3.: Average fade rate R_c (normalized to a TXOP) for both scenarios and several Rician Ks ($f_D = 32$ Hz).

nario B in the same way. By increasing the Rician K, the strength of the LOS component of the signal is increased with respect to the NLOS signal components and thus, the fading severity is reduced. In particular, the channel distribution with $K = -\infty$ dB is $\mathrm{P}(\{0,1,2\}) = \{0.33, 0.53, 0.14\}$ and becomes $\{0.02, 0.97, 0.01\}$ with $K = 12$ dB. Hence, it happens less often that the channel is within one of the "extreme" states, which is reflected in the average fade rates in Table 4.3, too. The implications are diverse. On the one hand, the throughput in the slow channel regime is reduced with large Ks, since there are fewer opportunities to benefit from. On the other hand, the critical Doppler frequency is pushed into the direction of larger Doppler frequencies since both the good and the bad extremes of the channel are reduced in the same way.

Differentiated Contention under Hidden Channel State Changes

So far, we have investigated two assumptions of our design: The assumption about finite buffers and block fading in time-varying channels. When relaxing the latter assumption, data transmissions are affected by hidden channel state changes. In the following, we relax the assumption about *perfect and instantaneous CQI* and investigate whether and how the CSMA contention can cope with hidden channel state changes. Our proposed cross-layer protocol tries to minimize the costs of acquiring channel knowledge via passive link probing and thus, it relies on the inherent memory of the slow fading channel.

The focus of this section lies on the fact that the hidden fading process causes inconsistencies between the instantaneous and the empirically observed channel state of a link. The CQI that has been obtained via link probing characterizes a point in the past, whereas the fading process may evolve in the meantime. Hence, we have to differentiate between the *instantaneous* and the *observed* channel state. In a nutshell, we are going to extend the fading CSMA Markov chain (cf. section 4.2) through the introduction of a further dimension per link that captures the observed channel state. An example of our modeling approach is given in Figure 4.20. It shows an excerpt of the resulting Markov chain for the instantaneous channel state NN. As shown in Figure 4.4b on page 145, the corresponding excerpt of the fading CSMA chain contains the tree states $N0N0$, $N1N0$ and $N0N1$ only. Due to the three possible observed channel states $\{B, N, H\}$ per link, the state space is increased by a factor of 9. The rationale of this modeling approach is as follows. Let us assume both the instantaneous and observed channel state is HN and the channel state changes to NN while both transmitters process their backoff. Thus, the system state evolves according to the transition $HH0NN0 \rightarrow NH0NN0$ and the first transmitter contends with outdated channel knowledge. If it wins the contention, then the system proceeds via $NH0NN0 \rightarrow NH1NN0 \rightarrow NN0NN0$, i.e. a transmission takes place on the first link and the observed channel state of the first transmitter is synchronized to the instantaneous channel state. Afterwards, both transmitters have correct channel knowledge and do not leave the three states in the middle of Figure 4.20 until the next hidden channel state change occurs.

Let us define the above described Markov chain using the terminology and notations from section 4.2. In addition to the instantaneous channel state vector $\boldsymbol{w} \in W^K$ and the binary vector of transmission states $\boldsymbol{v} \in V^K$, we introduce an additional vector of observed channel states $\boldsymbol{o} \in W^K$. As above, we assume that the sets W^K and V^K are

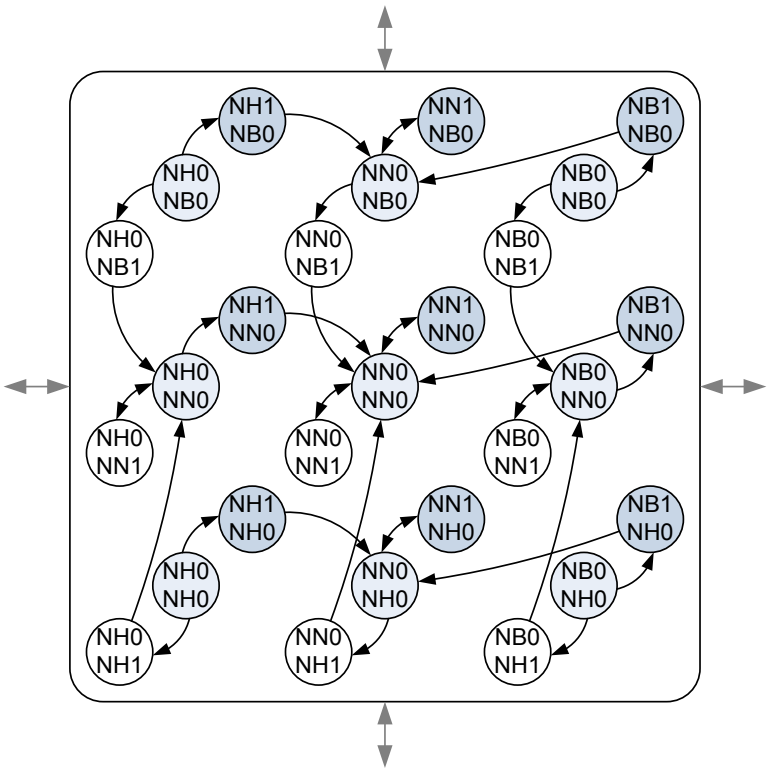

Figure 4.20.: An excerpt of the enhanced fading CSMA Markov chain that captures hidden channel state changes during the contention. The excerpt corresponds to the highlighted states of the vanilla model shown in Figure 4.4b (cf. p. 145) and uses the same notation. The modeling idea is as follows. A further state per link is introduced, which is denoted as second column in the state labels and accounts for the observed channel state. The instantaneous and the observed channel states are synchronized via link probing.

indexable and $\boldsymbol{w}^l$ ($\boldsymbol{v}^l$, $\boldsymbol{o}^l$) refers to the l-th element of the corresponding set. A component of each state vector can be selected via a lower index. The set of joint channel and transmission states can be generated as follows. Take the transmission states of the corresponding idealized CSMA Markov chain according to [111] and combine them with every possible joint instantaneous and observed channel state from $W^K \times W^K$.

The transitions that connect the above generated states fall within two categories. They are either channel transitions that alter the instantaneous channel state, or they are transmission transitions, which change the transmission and possibly the observed channel state. The definition of the former is straightforward.

$$Q\left(\boldsymbol{w}^l \to \boldsymbol{w}^k | \boldsymbol{o}^m, \boldsymbol{v}^n\right) = \begin{cases} R_c(w_i^l \to w_i^k) & w_i^k \in \{W_{-1}(w_i^l), W_{+1}(w_i^l)\} \\ & \quad \textbf{and } w_j^l = w_j^k \ \ \forall j \neq i \\ 0 & \text{otherwise} \end{cases}$$

In the above expression, R_c is the average fade rate, which can be estimated according

to (4.22) and (4.23). $W_{-1}(w) \in W$ and $W_{+1}(w) \in W$ refer to the adjacent bit-rates of w in W in the down- und upward direction, respectively. According to the definition, every state has up to two channel transitions per link, one for channel improvements and one in the opposite direction. The observed channel state and the transmission state remain unchanged. In contrast to the vanilla fading CSMA Markov chain, the above definition allows a transmitting link to proceed into outage and vice versa. The transmission transitions are defined as follows.

$$
\begin{aligned}
&Q\left((\boldsymbol{o}^l, \boldsymbol{v}^m) \to (\boldsymbol{o}^k, \boldsymbol{v}^n) | \boldsymbol{w}^f\right) \\
&= \begin{cases}
\exp(o_i^l r_i) & v_j^m = v_j^n \ \ \forall j \neq i \textbf{ and } v_i^m = 0 \textbf{ and } v_i^n = 1 \\
& \quad \textbf{and } \boldsymbol{o}^l = \boldsymbol{o}^k \\
1 & v_j^m = v_j^n \ \ \forall j \neq i \textbf{ and } v_i^m = 1 \textbf{ and } v_i^n = 0 \\
& \quad \textbf{and } o_j^l = o_j^k \ \ \forall j \neq i \textbf{ and } o_i^k = w_i^f \textbf{ and } w_i^f > 0 \\
d_{\text{out}} & v_j^m = v_j^n \ \ \forall j \neq i \textbf{ and } v_i^m = 1 \textbf{ and } v_i^n = 0 \\
& \quad \textbf{and } o_j^l = o_j^k \ \ \forall j \neq i \textbf{ and } o_i^k = w_i^f \textbf{ and } w_i^f = 0
\end{cases}
\end{aligned}
$$

The first alternative applies to the activation of links. In this case, only the transmission state of the considered link v_i is changed. Note that the average backoff is determined by the link's TA r_i and the *observed* channel state o_i^l instead of the instantaneous channel state w_i^f. Hence, a hidden channel state change does *not* alter the backoff decision of a transmitter. As shown in the remaining two alternatives, the observed channel state of link i is updated at the end of each transmission. In particular, the success of the transmission attempt is determined by the instantaneous channel state w_i^f only. If it has been successful, the transmitter proceeds. We assume a normalized frame length as shown in the second alternative. If the channel is in outage, however, the transmitter may decide to give up the remaining TXOP after an unsuccessful channel probe via a deactivation rate $d_{\text{out}} > 1$ in the third alternative. In contrast to the vanilla fading CSMA model, the transmitter has to probe the channel even during observed outages in order to locate the next usable channel instance. There is a tradeoff between the reactivity of the probing technique and the associated overhead: When the channel is probed more often, less medium time is wasted after the channel becomes usable again. According to the first alternative in the definition above, a backoff in the order of a TXOP is used to probe the channel during outages.

Let p be the stationary distribution of the Markov chain. The *throughput* $q_{i,b}$ of link i while the instantaneous channel is in state b is defined as follows.

$$q_{i,b} = b \sum_{j,k,l} \mathbb{1}(w_i^j = b) v_i^l p(\boldsymbol{w}^j, \boldsymbol{o}^k, \boldsymbol{v}^l)$$

In the equation above, $\mathbb{1}$ is an indicator function that is evaluated to one if the argument is true, whereas it is zero otherwise. The *throughput* q_i of link i defined as $q_i = \sum_{b>0} q_{i,b}$. In difference to the previous section, the definition accounts for the entire throughput of link i regardless whether the channel has been in outage before.

Figure 4.21 shows results for the per-link throughput, which we have obtained by

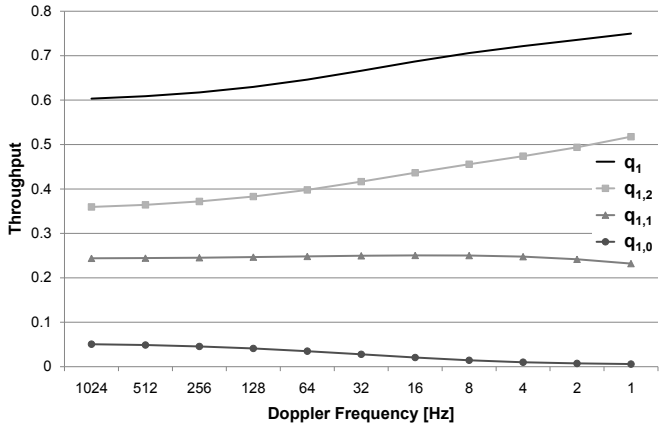

(a) Scenario A: $(\rho_1^2, \rho_2^2) = (-9.26, -0.06)$ dB.

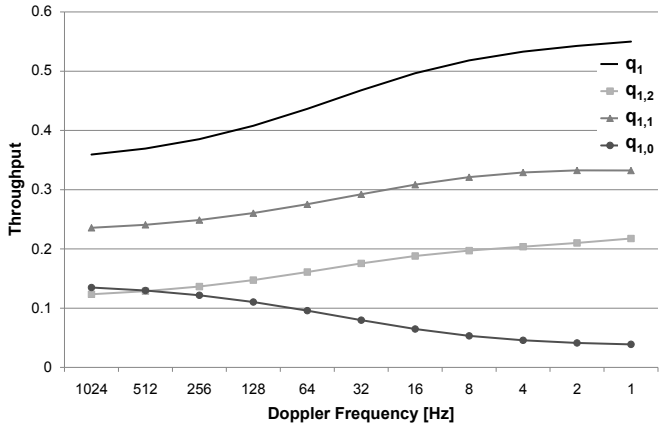

(b) Scenario B: $(\rho_1^2, \rho_2^2) = (-4, 3)$ dB.

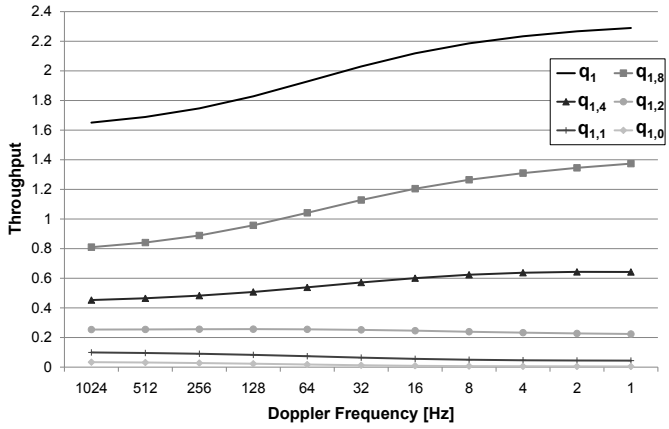

(c) Scenario C: $(\rho_1^2, \rho_2^2, \rho_3^2, \rho_4^2) = (-9.66, -3.66, -0.36, 2.04)$ dB.

Figure 4.21.: Per-link throughput for a single flow traversing 2 hops depending on the Doppler frequency and the bit-rate. The results are obtained by solving the stationary distribution of the enhanced CSMA Markov chain numerically using $d_{\text{out}} = 1$ and a-b) 2 bit-rates, $r_1 = r_2 = 6$, $K = -\infty$ dB or c) 4 bit-rates, $r_1 = r_2 = 2$, $K = 0$ dB.

W_i	0	1	2	4	8
$R_c(W_i \to W_{i+1})$	0.577	0.346	0.304	0.261	
$R_c(W_i \to W_{i-1})$		0.239	0.340	0.390	0.254

Table 4.4.: Average fade rate R_c (normalized to a TXOP) for scenario C ($f_D = 32$ Hz, $K = 0$ dB).

numerically solving the stationary distribution of the Markov chain. Similar to the previous section, the scenarios A and B consist of a single flow, two links and three channel states with varying thresholds. In addition, four bit-rates and five channel states are considered in the scenario C. Due to the symmetry of each scenario, we can use the same TA on both links in order to equalize their throughput. We will consider the throughput of link 1 only in the following. The TXOP duration is set to 2.5 ms and we report the Doppler frequencies in relation to a TXOP as explained above to simplify the comparison with the simulation results in the next section.

In scenario A, the channel distribution is $P(\{0,1,2\}) = \{0.11, 0.52, 0.37\}$. The channel transition rates can be found in Table 4.3 on page 177. As shown in Figure 4.21a, the throughput distribution for scenario A is close to its optimum (cf. Figure 4.19a) if the Doppler frequency is small. When increasing the speed of the fading process, the overall throughput q_1 and the throughput within the best channel state $q_{1,2}$ start to decline. At the same time, the throughput in the remaining channel states $q_{1,1}$ and $q_{1,0}$ increases. The throughput distribution levels off at the point that corresponds to the memoryless channel. Due to the higher fading speed, *the channel loses its memory* and looks more and more like an i.i.d. channel to the transmitter, in which OS gains cannot be achieved.

For the scenarios B and C, the observations are qualitatively identical as shown in Figure 4.21b and Figure 4.21c, respectively. In scenario B, the channel distribution is $P(\{0,1,2\}) = \{0.33, 0.53, 0.14\}$. We have used 4 bit-rates in scenario C. Under a Rician $K = 0$ dB, the associated distribution is $P(\{0,1,2,4,8\}) = \{0.08, 0.22, 0.27, 0.23, 0.20\}$ and the fade rates are shown in Table 4.4. In both scenarios, the DOS gain is even more pronounced. For example, the throughput in scenario C is increased from 1.65 to 2.29 when the channel offers sufficient memory. Note that the DOS gains can be obtained without any further hardware or significant protocol efforts by simply changing the scheduling discipline.

Finite Buffers under Hidden Channel State Changes: Simulation Results

We have conducted packet level simulations to evaluate the impact of both the window size and the Doppler frequency on the performance of the proposed protocol. We are particularly interested in comparing the performance of the proposed protocol to the above derived results. Similar to the analytic evaluation, we consider a single flow on an equal-spaced chain topology of nodes. We vary the window size W and the speed of the fading process, i.e. the Doppler frequency f_D of the Punnoose fading model. For ease of exposition, we will consider Rayleigh fading only in the following ($K = -\infty$ dB). The presented results are averages over 20 randomized repetitions. The

remaining simulation parameters can be found in Table 4.2 on page 162.

Without fading, the SNR on the considered links is $\gamma_r = 14.66$ dB. Given the SNR thresholds in Table 4.2, we get $\rho_1^2 = -9.26$ dB and $\rho_2^2 = -0.06$ dB. The average fade rates R_c according to the FSMC model of Wang *et al.* [84, 272] are shown in Table 4.5. Results for other Doppler frequencies f_D can be easily obtained since R_c is directly proportional to f_D. Note that the derivation above is an approximation only since the impact of the AWGN channel is not considered.

Table 4.5.: Average fade rate R_c (normalized to a TXOP, $f_D = 32$ Hz).

W_i [Mbps]	0	6	12
$R_c(W_i \rightarrow W_{i+1})$	0.549	0.144	
$R_c(W_i \rightarrow W_{i-1})$		0.119	0.199

Simulation results for throughput and delay are shown in Figure 4.22. In particular, we observe *a two-sided tradeoff* in Figure 4.22a: The maximal throughput is achieved with a window size $W = 512$ around a Doppler frequency of 8 Hz. The throughput is reduced by either decreasing or increasing the Doppler frequency. In the former case, the coherence time becomes larger and the window size is the limiting factor. In the latter case, the channel exhibits less memory leading to a lower predictive value of the channel estimates. Hence, the differentiated contention will identify opportunities less often and reception errors become increasingly important. When using smaller window sizes, the maximal throughput is achieved at larger Doppler frequencies, since the limitations due to the finite buffers are further amplified.

Figure 4.22b shows the throughput difference between the proposed protocol and the variant RBAR, which does not use the channel-differentiated contention. Similar to the throughput results above, the maximal DOS gain over RBAR is achieved with the largest window size of $W = 512$ at about $f_D = 8$ Hz. For smaller window sizes, the maximal DOS gain becomes smaller, and it is achieved at higher Doppler frequencies. It can be observed that the proposed protocol performs worse than RBAR for $W \leq 4$ and small Doppler frequencies. We suppose that this observation is an artifact of the intra-flow TA adaption (cf. section 4.4.3). The end-to-end delay is presented in Figure 4.22c. The delay results are in good match with Little's law. Nevertheless, the figure illustrates the costs in terms of delay for achieving the DOS gain: The end-to-end delay is in the order of $1.6 - 2.0$ s for the 10% gain over RBAR under $W = 512$. On the other hand, the DOS gain declines only slowly with reduced window sizes: It remains at 9.2% (8.4%) for one half (one quarter) of the previous window size, whereas the scaling of the end-to-end delays is linear.

It remains to note that the analytical models derived above apply only partially to simulations under very small window sizes and especially $W = 1$. In the Markov model with finite buffers at the beginning of section 4.5.3, we have assumed that every transmission consumes a TXOP. Nevertheless, the transmitter in the simulations will release the wireless medium after one packet in the case $W = 1$ even if the channel condition would allow for 12 Mbps. In this way, medium resources are preserved in the simulations. Furthermore, the ACK processing at the end of each MAC transaction is considered in the simulations whereas it has been neglected in our analysis.

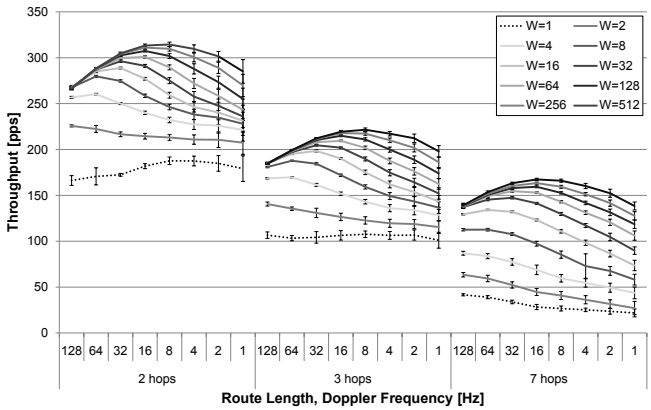

(a) Throughput of the proposed protocol depending on the route length, the Doppler frequency and the window size ($\pm std.dev.$).

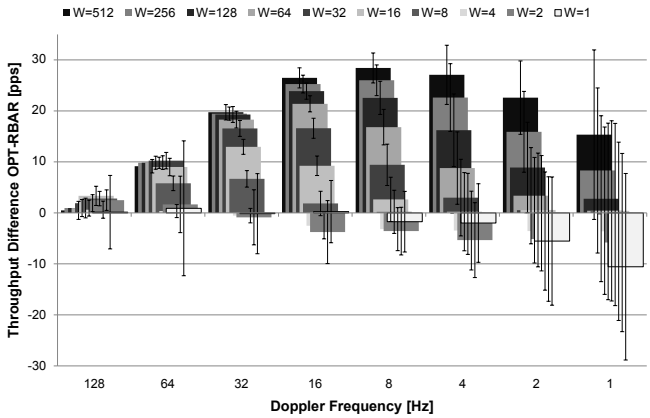

(b) The DOS gain: Throughput difference between the proposed protocol OPT and the variant RBAR without channel-differentiated contention (2 hops, $\pm std.dev.$).

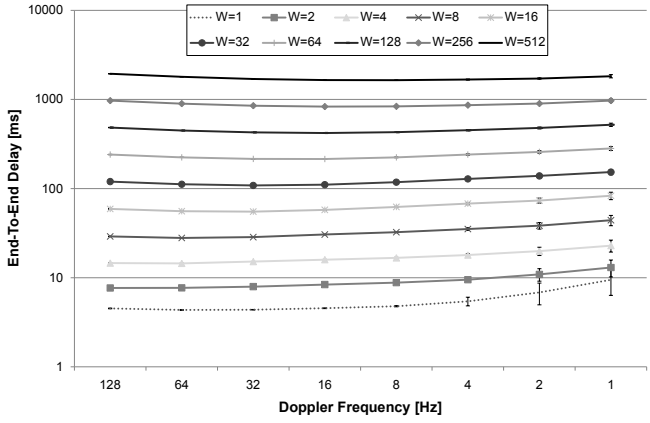

(c) Average end-to-end delay (2 hops, $\pm std.dev.$).

Figure 4.22.: Simulation results for a single flow on a chain topology, depending on the window size W and the Doppler frequency ($r_{\text{opt}} = 8.8$, Rayleigh fading). The slow fading channel has 3 states $\{0, 6, 12\}$ Mbps with the distribution $\{0.11, 0.52, 0.37\}$.

K	0 Mbps	6 Mbps	12 Mbps	24 Mbps	48 Mbps
$-\infty$ dB	0.103	0.247	0.252	0.196	0.202
0 dB	0.079	0.223	0.269	0.229	0.200
4 dB	0.039	0.182	0.313	0.289	0.177
8 dB	0.006	0.107	0.378	0.387	0.122
12 dB	0.000	0.027	0.413	0.509	0.051
16 dB	0.000	0.001	0.376	0.616	0.007

Table 4.6.: Channel state distributions for both links of the two-hop chain scenario under Rician fading.

Impact of the Fading Distribution on the Simulation Results

In order to illustrate the combined effect of finite buffers and the fading distribution, we have jointly varied the window size and the parameters of the Rician fading process: the Doppler frequency f_{D} that controls the fading speed and the Rician K parameter, which determines the variability of the fading process. The simulation setup is similar to the previous section. The topology is a chain of two links traversed by one flow. The SNR on both links is $\gamma_{\mathrm{r}} = 14.66$ dB when considering the path loss effect only without any fading. In order to support a broader range of bit-rates, the SNR thresholds for the bit-rates $(6, 12, 24, 48)$ Mbps are set to $\gamma_{\mathrm{t}} = (5, 11, 14.3, 16.7)$ dB. The remaining simulation parameters can be found in Table 4.2 on page 162.

Table 4.6 lists the probabilities that the channel supports a given bit-rate depending on the selection of the Rician K parameter, which have been derived from the outage probabilities (cf. chapter 2). By increasing the K parameter of the Rician fading process, the variability of the received power is reduced. In addition, the mean received power and thus the expected bit-rate changes, too. The average fading rates R_c according to the finite-state Markov channel (FSMC) model of Wang *et al.* [84, 272] for a Doppler frequency of $f_{\mathrm{D}} = 32$ Hz are shown in Table 4.7. Remember that the average fading rate R_c is directly proportional to the Doppler frequency f_{D}.

Figure 4.23 shows the simulation results. The average throughput of the proposed protocol for different values of the Rician K parameter is presented in Figure 4.23a and Figure 4.23b. Similar to the previous section, the two-sided tradeoff is present in the

K	$-\infty$ dB	0 dB	4 dB	8 dB	12 dB	16 dB
$R_c(0 \text{ Mbps} \rightarrow 6 \text{ Mbps})$	0.577	0.428	0.388	0.440	0.601	0.891
$R_c(6 \text{ Mbps} \rightarrow 0 \text{ Mbps})$	0.239	0.152	0.083	0.023	0.001	0.000
$R_c(6 \text{ Mbps} \rightarrow 12 \text{ Mbps})$	0.346	0.268	0.251	0.262	0.333	0.477
$R_c(12 \text{ Mbps} \rightarrow 6 \text{ Mbps})$	0.340	0.222	0.146	0.074	0.022	0.001
$R_c(12 \text{ Mbps} \rightarrow 24 \text{ Mbps})$	0.304	0.229	0.189	0.153	0.136	0.144
$R_c(24 \text{ Mbps} \rightarrow 12 \text{ Mbps})$	0.390	0.269	0.204	0.149	0.111	0.088
$R_c(24 \text{ Mbps} \rightarrow 48 \text{ Mbps})$	0.261	0.185	0.132	0.075	0.029	0.005
$R_c(48 \text{ Mbps} \rightarrow 24 \text{ Mbps})$	0.254	0.212	0.214	0.238	0.293	0.395

Table 4.7.: Average fade rate R_c (normalized to a TXOP, $f_{\mathrm{D}} = 32$ Hz).

K	$-\infty$ dB	0 dB	4 dB	8 dB	12 dB	16 dB
$q^\star$ [pps]	323	343	373	407	448	498
$b^\star$ [Mbps]	48	24	24	24	24	24

Table 4.8.: Estimated throughput for fixed bit-rate transmissions in the two-hop chain scenario according to (4.24) and Table 4.6.

results when varying the Doppler frequency. When increasing the Doppler frequency beyond the optimum, the reduced channel memory becomes the limiting factor instead of the finite buffers. The maximum throughput is achieved around $f_\mathrm{D} = 16$ Hz under the window size $W = 512$. The optimal Doppler frequency becomes larger when reducing the window size since the smaller buffers are less often able to bridge over periods of bad channel conditions.

There is a significant loss in throughput if the window size limits the parallelism or the efficient utilization of a TXOP. This effect is observable for a Rician $K = 16$ dB in Figure 4.23b, for example, when using a window size smaller than $W = 4$. Remember that a TXOP can carry almost eight frames at 48 Mbps if a single frame fits within a TXOP at 6 Mbps. Under large Rician Ks, increasing the window size beyond the above threshold does not bring significant benefits. In the simulations with a Rician $K = 16$ dB, the difference between highest and lowest throughput for a window size $W > 4$ is only 73 pps. The large Rician K removes variability from the fading channel, so that the potential for DOS becomes low. These types of channels comply with the TCP assumptions, where the objective of the window size adaptation is the maximization of the concurrency within the communication system and increasing the window size further will only contribute to the experienced end-to-end delays [71]. At lower Rician Ks like 0 dB, however, the throughput difference for window sizes $W > 4$ is increased to 334 pps and thus, the potential for DOS is higher. In these types of channels, the window size determines the available multi-user MAC capacity due to the DOS gain. Hence, increasing the internal buffers *beyond* the optimal TCP windows size improves the throughput efficiency of the system.

Let us compare the results in Figure 4.23 with an estimate of the throughput, which a non-adaptive protocol would achieve under the channel state distribution in Table 4.6. In particular, we assume that a non-adaptive protocol selects a fixed bit-rate $w \in W$ and transmits data packets without any channel measurements. Let $\mathrm{P}(w)$ be the probability of the channel state w. The maximum throughput $q^\star$ and the optimum bit-rate $b^\star$ for both links in the two-hop chain scenario can be estimated as follows.

$$\begin{aligned} b^\star &= \arg\max_{w \in W} w \sum_{v \geq w} \mathrm{P}(v) \\ q^\star &= \frac{b^\star}{2} \sum_{v \geq b^\star} \mathrm{P}(v) \end{aligned} \tag{4.24}$$

The factor ½ stems from the fact that both links have identical channel distributions and they have to share the available wireless resources. To make the estimates comparable with the throughput results in Figure 4.23, the throughput $q^\star$ in Table 4.8 has

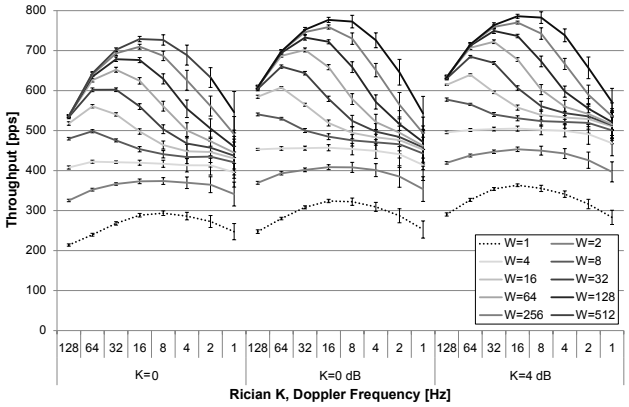

(a) Throughput of the proposed protocol depending on Rician K, Doppler frequency f_{D} and the window size W ($\pm std.dev.$).

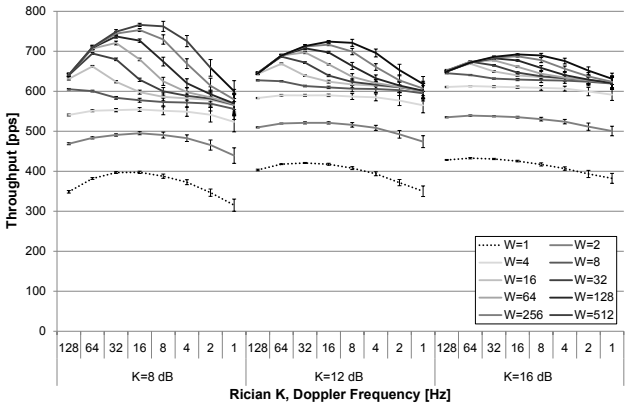

(b) Throughput of the proposed protocol depending on Rician K, Doppler frequency f_{D} and the window size W ($\pm std.dev.$).

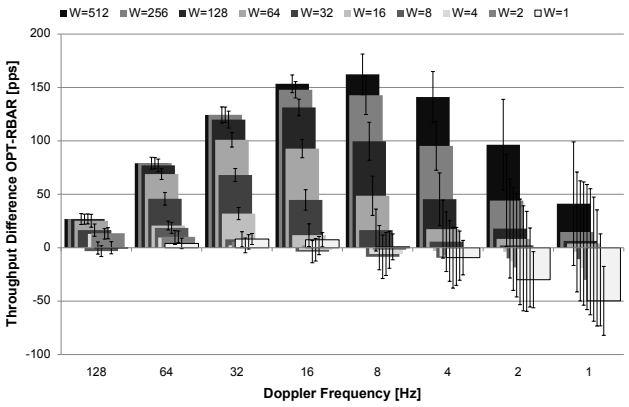

(c) The DOS gain: Throughput difference between the proposed protocol OPT and the variant RBAR without channel-differentiated contention ($K = 0$ dB, $\pm std.dev.$).

Figure 4.23.: Simulation results for a single flow on a chain topology, depending on the window size W and the Doppler frequency f_{D} and the severity K of the Rician fading process ($r_{\mathrm{opt}} = 8.8$). The channel distribution is given in Table 4.6.

been converted to packet per second using the factor 400 pps/6 Mbps. It can be observed that the proposed protocol, which relies on channel-adaptive contention and transmission, achieves substantial DOS gains over the non-adaptive variant that uses a fixed bit-rate only.

Let us evaluate the effect of the channel-differentiated contention in isolation. Figure 4.23c shows the throughput difference between the proposed protocol and the RBAR variant for the Rician $K = 0$ dB. Remember that both RBAR and OPT perform AMC, i.e. the bit-rate is adapted according to the instantaneous channel conditions. In contrast to RBAR, OPT uses the channel-differentiated contention. The figure illustrates that that the channel-differentiated contention is able to release additional DOS gains of up to 162 pps or 26% over RBAR under a large window size and a Doppler frequency $f_{\mathrm{D}} = 8$ Hz. The DOS gains also show the two-sided tradeoff that can be explained in the following way. At higher Doppler frequencies, the channel memory is reduced so that the channel prediction and thus the channel-differentiated contention become less effective. In the opposite case, the window size as limiting factor applies to the proposed protocol and the RBAR variant in the same way, which reduces the relative benefits of the channel-differentiated contention. For smaller window sizes, the maximum DOS gain over RBAR is achieved at higher Doppler frequencies. The channel-differentiated contention of the proposed protocol becomes counterproductive at low Doppler frequencies and small window sizes. We suppose that this observation is an artifact of the intra-flow TA adaption (cf. section 4.4.3).

Conclusion

Both our system model and our protocol design rely on several simplifying assumptions about the fading process: Perfect and instantaneous CQI should be available at no cost, the channel fading should be a block-fading, the fading processes on different channels should be mutually independent and the CS relationships should not be affected by fading. Due to the relaxation of the first two assumptions, the performance of the protocol becomes dependent on the temporal correlation within the fading process.

In this section, we have illustrated that both the finite buffers and the fading process have a crucial impact on the achievable throughput. In particular, we have evaluated the effect of finite buffers with perfect channel knowledge using a Markov model. The results indicate that the window size becomes the limiting factor in terms of throughput efficiency if the channel memory increases. Due to the larger coherence time, it becomes more difficult to bridge over longer periods of bad channel conditions. TCP relies on a WCC in order to maximize the efficiency of the resource utilization. The WCC of the proposed protocol additionally determines the OS gain and thus the amount of available throughput capacity.

Furthermore, we have presented Markov models to evaluate the system's performance under channel uncertainty during both the transmission and the contention period. The results reveal that the channel uncertainty becomes the limiting factor if the channel memory decreases. Our simulation results have validated the two-sided structure of the tradeoff in terms of channel memory. In addition, we have illustrated that the channel-differentiated contention is able to achieve substantial DOS gains. In particular, we have observed that a gain of 26% can be obtained over RBAR via a sim-

ple change in the CSMA contention procedure. The gains of the channel-differentiated contention also show the two-sided tradeoff structure in terms of channel memory.

Although the above described tradeoffs are fundamental in nature, there are several ways to alter the working point that should be explored in future work. Techniques like opportunistic beamforming may speed up and amplify the channel fluctuations in order to maximize the MUD gains [264, 265]. Acquiring CQI more often may mitigate the channel uncertainty at the expense of additional probing overhead. Furthermore, both the MAC frame size and the TXOP duration can be adapted to the available memory within the channel. Longer frames may mitigate the limitations due to finite buffers under high channel memory, whereas the channel uncertainty can be reduced via shorter frames and smaller TXOPs.

4.5.4. Multi-User and Cooperative Diversity

The concept of multi-user diversity (MUD) was first explored by Knopp *et al.* in a cellular multi-user system [141]. The classical approach to MUD is the introduction of additional users, which provides the system with further scheduling opportunities in order to select the best channel instance for transmission. In multi-hop WMNs, however, the introduction of relay nodes offers another way to achieve diversity gains. Due to the cooperation of additional relays, the number of available forwarding paths can be increased. In contrast to the diversity concepts for point-to-point links (cf. [84, chap. 7]), the channel statistics varies vastly across multi-user channels. In the following, we are going to examine the potential of the proposed protocol for multi-user and cooperative diversity.

Impact of the User Population Size

To start with, we will investigate in which way the proposed protocol is able to benefit from classical MUD in terms of the user population size. We are considering the so-called *AP scenario*: Within a single wireless collision domain, all stations directly communicate with the AP node. Depending on the communication direction, we distinguish between uplink and downlink traffic, i.e. traffic from the stations towards the AP and vice versa. In our simulations, each station carries a single traffic flow. We vary the number of flows F between 1 and 16. Furthermore, all single-hop flows experience i.i.d. Rician fading channels with $K = -\infty$ dB and varying Doppler frequencies. The SNR of each link without the fading component is $\gamma = 14.66$ dB. The SNR thresholds for the bit-rates $(6, 12, 24, 48)$ Mbps are set to $\gamma_t = (5, 11, 14.3, 16.7)$ dB. Since all flows are single-hop only, the window size $W = 8$ has no impact on the performance. We compare the proposed protocol with the variants RBAR and fixed bit-rate. The former uses AMC to adapt to the instantaneous channel conditions, whereas the latter uses a predetermined bit-rate of 24 Mbps only. The hysteresis factor for the inter-flow fairness adaption is set to $\delta = 1.1$ (cf. section 4.4.3). The error bars on the goodput results indicate the standard deviation across all 20 random repetitions. All remaining simulation parameters are listed in Table 4.2 on page 162.

The goodput results for the uplink scenarios are presented in Figure 4.24. In particular, the sum goodput of the proposed protocol is shown in Figure 4.24a. The diagram

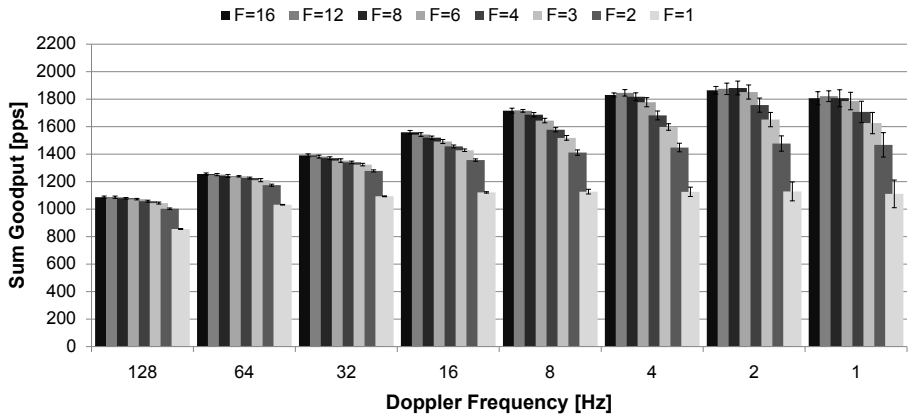

(a) Goodput of the proposed protocol ($\pm std.dev.$).

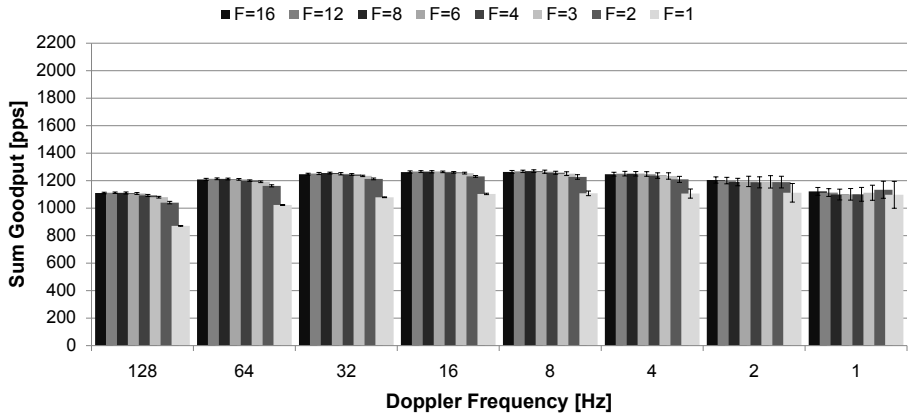

(b) Goodput of the RBAR variant without differentiated contention ($\pm std.dev.$).

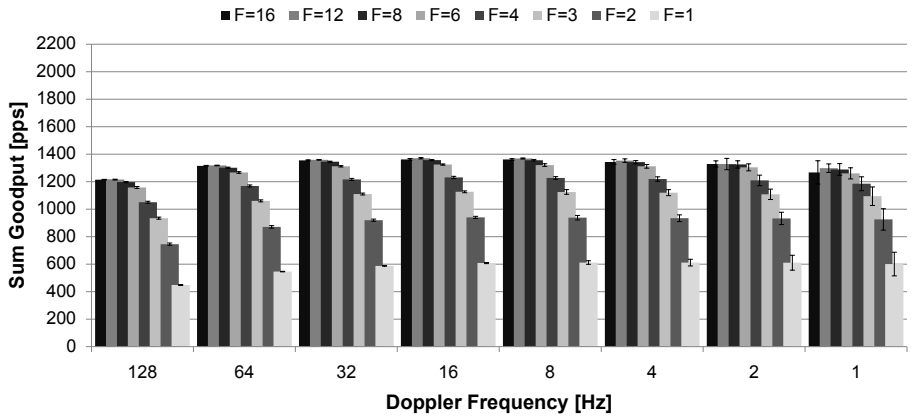

(c) Goodput of the 24 Mbps fixed bit-rate variant ($\pm std.dev.$).

Figure 4.24.: Simulation results for multiple single-hop flows in the *uplink* AP scenario ($r_{\text{opt}} = 8.8$, $\tau_y = 20$ ms, $\gamma_y = 0.025$). All F flows experience i.i.d. Rayleigh fading channels at varying fading speeds ($K = -\infty$ dB). The SNR threshold γ_{t} for the bit-rate 6,12,24 and 48 Mbps is set to 5, 11, 14.3 and 16.7 dB, respectively.

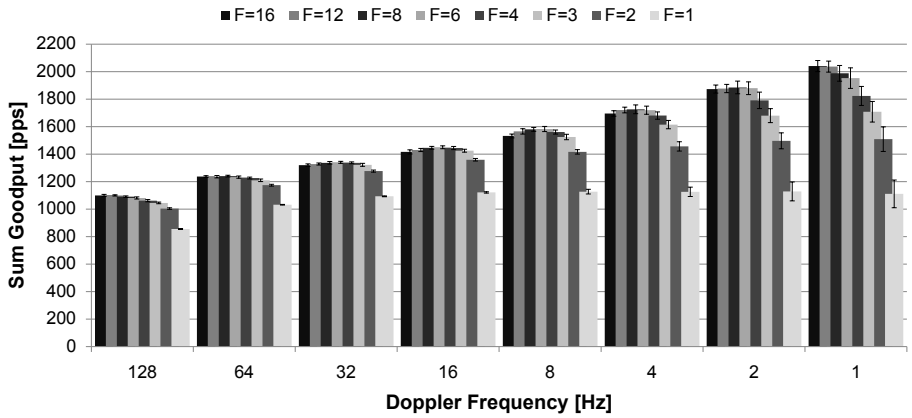

(a) Uplink, $\tau_y = 100$ ms ($\pm std.dev.$).

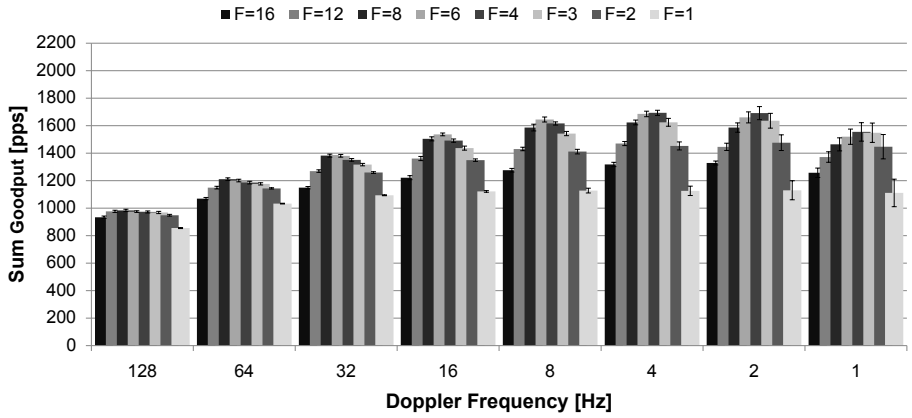

(b) Downlink, $\tau_y = 20$ ms ($\pm std.dev.$).

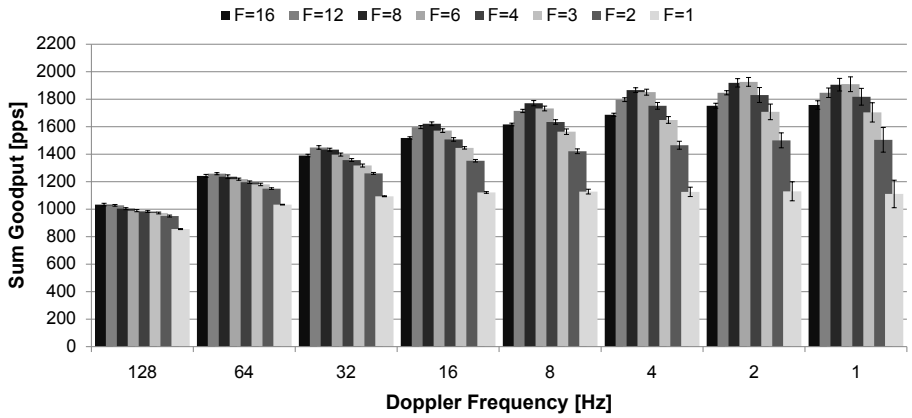

(c) Downlink, $\tau_y = 100$ ms ($\pm std.dev.$).

Figure 4.25.: Goodput of the proposed protocol for multiple single-hop flows in the AP scenario ($r_{\text{opt}} = 8.8$, $\gamma_y = 0.025$). All F flows experience i.i.d. Rayleigh fading channels at varying fading speeds ($K = -\infty$ dB). The SNR threshold γ_{t} for the bit-rate 6,12,24 and 48 Mbps is set to 5, 11, 14.3 and 16.7 dB, respectively.

indicates that higher sum goodputs are achieved with increasing number of flows or under a decelerated fading process. However, this trend is reversed beyond a certain point in both parameters, which is around a Doppler frequency $f_D = 2$ Hz and $F = 8$ concurrent flows in our case. When increasing the speed of the fading process, the channel-differentiated contention becomes less effective as previously explained in section 4.5.3. Nevertheless, the limited window size does not cause the reduction of the sum goodput at low Doppler frequencies because no multi-hop forwarding is involved. On the other hand, the returns of additional flows are generally diminishing and become even negative beyond the mentioned point. In part, this observation can be traced back to the coarse and fixed SNR thresholds for the bit-rates: For example, a link cannot benefit from channel conditions above 16.7 dB SNR (48 Mbps), whereas the probability of having no link above 14.3 dB SNR (24 Mbps) gradually decreases with each additional flow.

We have identified the averaging horizon of the flow rate y^f as another factor that leads to the reduction of the sum goodput under large user populations and low Doppler frequencies. As shown in Algorithm 7 on page 156, the flow rate y^f is averaged before it is processed further in UPDATEV and within the inter-flow adaption in section 4.4.3. The following averaging method is applied. The source considers discrete time epochs of duration τ_y. The empirical flow rate for each epoch is calculated as the number of emitted frames during the epoch divided by its length τ_y. The per-epoch estimates are averaged via an EWMA. Thus, the averaging process has two parameters: the length of the epoch τ_y and the EWMA smoothing factor γ_y. In Algorithm 8 on page 160, we have illustrated how the tradeoff parameter V can be adapted to increase the efficiency subject to fairness and the technological CS constraints. The V adaption depends on the estimation of the flow rate y^f. The averaging horizon determines the reactivity of the inter-flow V adaptation. In particular, the shorter the averaging horizon becomes, the more sensitive the adaption reacts on short-term unfairness, which in turn reduces the burst length or lowers the node's patience to wait for better channel conditions. By comparing Figure 4.24a and Figure 4.25a, we observe that the larger averaging epoch in the latter diagram results in a larger sum goodput at low fading speeds and under a large number of flows. In the downlink, the observations are similar (cf. Figure 4.25b and Figure 4.25c). The question is to which extend the flow rate estimate should average out the channel variability at the expense of short-term unfairness. We come back to this issue in the chapter summary.

For comparison, we have plotted the sum goodput results of the variants RBAR and 24 Mbps fixed bit-rate in Figure 4.24b and Figure 4.24c, respectively. Both the fading speed and the number of flows do not have a significant impact on the performance of RBAR: Only a small increase of the goodput can be observed when using two instead of only one flow. RBAR does not perform OS: It always uses all opportunities for transmission regardless of the channel conditions, although outages are an exception. Due to the high SNR of the links, however, outages occur less often especially with a larger number of flows. On the other hand, the sum goodput of the fixed bit-rate variant strongly depends on the number of flows. It is around 600 pps for a single flow. Nevertheless, it rises up to 1400 pps with 16 flows. Since the fixed bit-rate variant treats every transmission opportunity not supporting 24 Mbps as an outage, it is able to benefit from OS in a higher degree than RBAR. Thus, it may become counter-

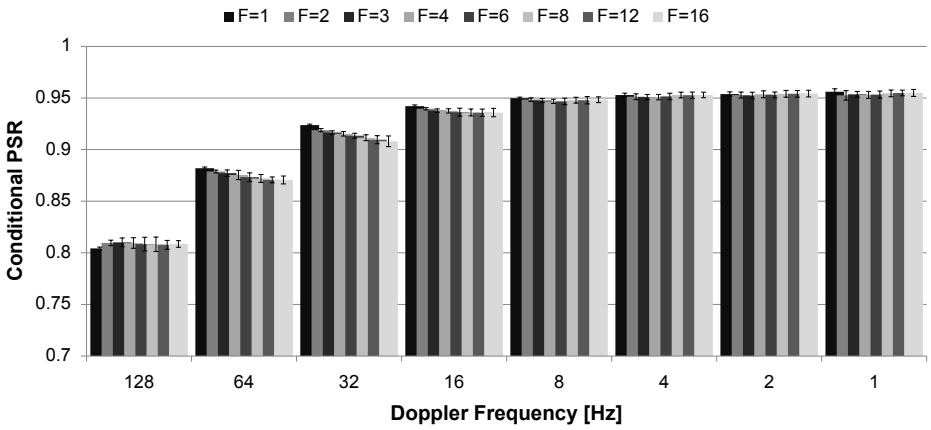

Figure 4.26.: Conditional PSR after a successful channel probe in the AP scenario (Uplink and downlink, $r_{\text{opt}} = 8.8$, $\gamma_y = 0.025$, $\tau_y = 20$ ms, $\pm std.dev.$).

productive to use every opportunity in the way RBAR does. In comparison with both variants, the proposed protocol performs significantly better especially if the channel offers sufficient memory.

All above-mentioned observations also apply to the downlink scenario shown in Figure 4.25b and Figure 4.25c. In the downlink, however, the sum goodput is smaller in most cases compared to the uplink scenarios. Especially under a large number of flows, a goodput degradation is observable. The reason lies within the adaption of the tradeoff parameter V (cf. section 4.4.3). Our objective is the limitation of the average TA per node, so that the average backoffs per node remain within the feasible technological boundaries. In the uplink scenario, there is only one flow per transmitter. In the downlink, however, all flows originate from the AP node. With each additional flow, the TA of the other flows is reduced, so that the sum TA remains within the technological limits. Due to the lower per-flow TAs, the goodput efficiency decreases in the downlink scenario especially under a large user population.

In summary, the simulation results indicate that the proposed protocol is able to achieve significant MUD gains when the user population size is large. In particular, the sum goodput can be increased from about 1300 pps to 1900 pps by using channel-adaptive contention and transmissions. In addition, we have identified several factors that limit the system's performance.

- A high *Doppler frequency* reduces the memory of the channel, so that the channel-differentiated contention becomes less effective regardless of the user population size. In addition, it increases the uncertainty whether the channel quality remains constant during the transmission. The latter effect can be observed in Figure 4.26, which shows the PSRs under the condition that the channel probe has been successful. If the memory of the channel is reduced, the channel-blind diversity techniques discussed in chapter 3 become more efficient in relation to OS.

- The PHY should provide a sufficient *number of bit-rates* at *SNR thresholds* matching the operational regime of the considered link.

- The *averaging horizon* within the estimation of the *flow rate* can be used to control the tradeoff between long-term goodput and short-term unfairness. The same observation applies to the averaging of the TAs at each node.

- The CQI may become *outdated* while processing the backoff. Especially if the instantaneous channel quality is very low, the backoffs can become substantially larger than the channel coherence time. However, the large backoffs may cause short-term unfairness and thus, they can interfere with the flow rate averaging.

- The V *adaption* is sensitive to *variations between flows*. As shown in Algorithm 8 on page 160, a single flow may cause a reduction of the V value of all other flows. On the other hand, the V value can only be increased simultaneously by all involved flows in a step by step fashion. Maintaining the working point becomes harder with every additional flow involved. Furthermore, we have encountered that outdated information about the neighboring flows may slow down the convergence.

Impact of Multi-Path Routing

Adding relay nodes to a communication system that is based on multi-hop and multi-path routing generates throughput capacity in slow fading channels similar to each additional user in the AP scenario. In order to validate the conjecture, we evaluate the proposed protocol on the so-called *double chain topology* shown in Figure 4.27 in the following. In particular, we consider a single flow that traverses a varying number of hops with two nodes per relaying stage. The distance between the relays at the same stage is kept small, so that all forwarding links experience i.i.d. Rician fading channels with $K = -\infty$ dB and varying Doppler frequencies. With the exception of the last relaying stage, two equally suited next hop candidates are available for every forwarding node. In order to evaluate the impact of the multi-path forwarding, we vary the number of outgoing paths R per node and flow between one and two using the route pre-selection technique described in section 3.5.5. In addition to the parameters in Table 4.2 on page 162, the PHY supports the bit-rates $(6, 12, 24, 48)$ Mbps with the SNR thresholds $\gamma_t = (5, 11, 14.3, 16.7)$ dB. The results are averaged over 40 s of simulation time, which are taken after an initial warm-up period of 10 s. The error bars indicate the standard deviation across 20 repetitions.

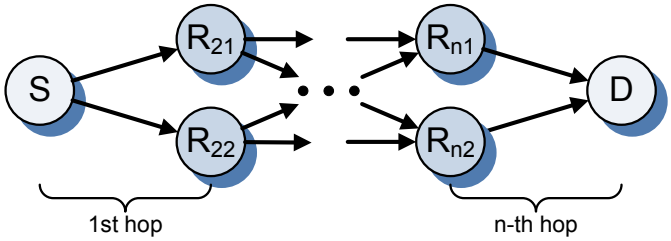

Figure 4.27.: Double chain topology: A single flow traverses the network from source S to destination D. Both nodes are connected via two chains of relay nodes.

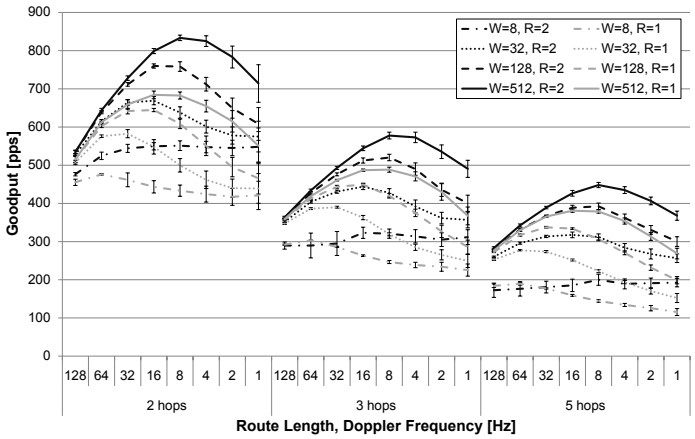

(a) Goodput of the proposed protocol ($\pm std.dev.$).

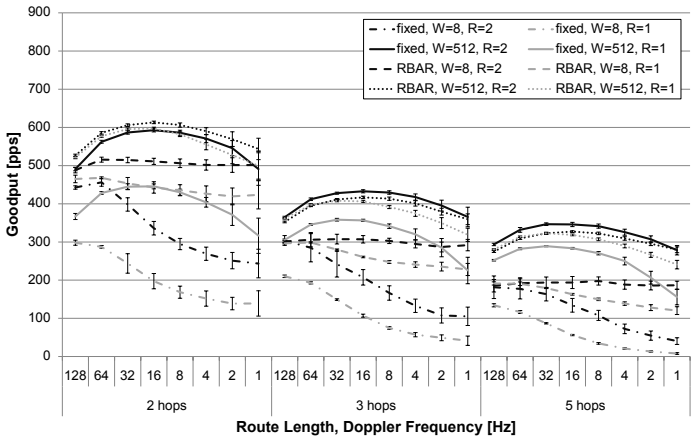

(b) Goodput of the variants RBAR and 24 Mbps fixed bit-rate ($\pm std.dev.$).

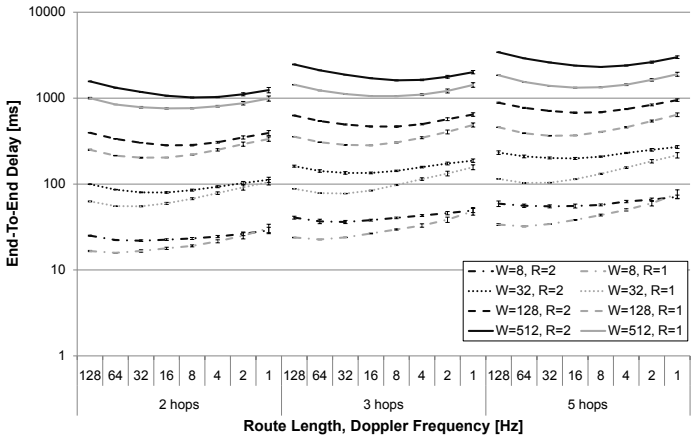

(c) End-to-end delay of the proposed protocol ($\pm std.dev.$).

Figure 4.28.: Simulation results for a single multi-path flow on the topology shown in Figure 4.27 depending on the window size W, the number of outgoing links per node R and the Doppler frequency of the i.i.d. Rician fading links ($K = -\infty$ dB).

Figure 4.28a shows the goodput of the proposed protocol. Regarding the window size W and the Doppler frequency f_D, the already known tradeoff structure is observable in the results. When reducing the channel memory, the channel-differentiated contention gradually becomes ineffective. On the other hand, the window size is the limiting factor in the case of a large channel memory since the smaller buffers are less often able to bridge over periods of bad channel conditions.

Nevertheless, an interesting insight can be drawn from a comparison of the number of forwarders R. In the high Doppler regime, the setting of the parameter R has only marginal influence. However, the cooperative diversity gains significantly increase in the way the channel-differentiated contention becomes effective. The gains can even be preserved within the low Doppler regime. For example, cooperative diversity gains of up to 170 pps or 29% can be achieved in the two hop case. In other words, the results show that *multi-path routing increases the throughput capacity* in the presence of slow fading channels even if the paths overlap completely.

The goodput results of both protocol variants are shown in Figure 4.28b for the case of an either large or small window size. As expected, the RBAR variant cannot benefit from the additional forwarding path if the window size is large. In this case, the goodput difference between one and two forwarding candidates is marginal. On the other hand, the fixed bit-rate variant achieves significant cooperative diversity gains even under a large window size due to the additional forwarding path. However, the more stringent channel quality requirements cause outages and, eventually, lead to a goodput reduction when only a single candidate is used. The diversity gains compensate for these goodput losses in the first place, whereas they are not able to catch up with the proposed protocol. When reducing the window size W, the performance of the proposed protocol gradually converges to the RBAR results (cf. Figure 4.28a and Figure 4.28b). If the window size is small so that, in an extreme case, only a single transmitter contends for medium access at a time, the channel-differentiated contention does not offer any benefits. Remember that the average bit-rate on all links is above 24 Mbps, i.e. up to four packets fit within a single TXOP.

Figure 4.28c shows the average end-to-end delay when using the proposed protocol. Similar to our previous observations in section 4.5.3, the costs in terms of delay for achieving the diversity gain are considerable. The system is affected by the number of forward candidates per node R in the following way. In the high Doppler regime, the additional forwarding paths increase the average end-to-end delay. Since the goodput is almost identical in this regime regardless of the number of forwarding paths, the number of outstanding packets has to be higher according to Little's law. Remember that the windowed congestion control (WCC) introduced in section 4.4.2 does not limit the total number of enqueued packets per flow, but their aggregated number along each routing path instead. Hence, the number of outstanding packets is limited between W and $2W$ for the simulation topology in Figure 4.27, because two node-disjoint paths exist at most. Interestingly, the delay differences between $R = 1$ and $R = 2$ gradually become smaller and even vanish in some cases in the low Doppler regime. Thus, the goodput gains due to cooperative diversity are able to compensate the delay costs in this regime.

In conclusion, we have illustrated that multi-path forwarding offers significant potential for cooperative diversity in slow fading environments, which the proposed pro-

tocol is able to exploit in order to increase the throughput performance at the expense of the end-to-end delay. Cooperative diversity can be seen as the counterpart to MUD for multi-path forwarding. In particular, the results show that multi-path forwarding is able to increase the link's capacity in slow fading environments. In contrast to memoryless channels like the AWGN channel, this observation gives additional incentives to use multi-path forwarding in WMNs that have to cope with slow fading. Furthermore, our results identify the cross-layer interactions. The Doppler frequency f_D is a characteristic parameter of the fading process at the PHY. The number of candidates R is a routing parameter of the network layer. In the TCP/IP stack, the transport layer is responsible for the window size parameter W. Considering the cross-layer interaction, the system architect is able to tune the underlying tradeoffs according to given requirements. The speed of the fading process can be changed via the TXOP length or via opportunistic beamforming. The system designer may decide for a working point in terms of throughput and delay via the window size and the number of paths in multi-path forwarding.

4.6. System Level Evaluation

Our cross-layer design enhances CSMA in WMNs with opportunistic scheduling (OS) capabilities. In the previous section, the operation as well as the performance of the proposed protocol has been illustrated using small and synthesized examples. In the following, we are going to investigate the system's performance in large and randomized scenarios. Our intentions are two-fold. We start with an investigation of the benefits of OS within the targeted application domain. Since we have controlled the synthesized topologies in the previous section, it remains unclear whether and to which extend larger and randomized networks offer any potential in terms of OS gains under more representative use cases. On the other hand, we consider both the benefits and costs of our cross-layer design under conditions similar to IEEE 802.11. We are interested whether the proposed channel-differentiated contention is able to exploit the potential of these networks under more relevant conditions.

A typical use case for a WMN is an *Internet access network* (cf. section 2.1). The Internet connectivity is established via the meshed network. A gateway node is a distinguished node of the access network that shares its Internet connection with all other network nodes wirelessly. Depending on the covered area, an Internet access network contains several gateway nodes. On accessing the Internet, a client node selects a suitable gateway (cf. [20, 248]) and sends its Internet traffic to the selected gateway using multi-hop routing. In the following, the system is evaluated within the access network scenario. All nodes are randomly placed in a rectangular area. The node closest to the middle of the network area becomes the gateway. Multiple traffic flows are established between the gateway and randomly selected client nodes. Note that we neglect the Internet in our evaluation and terminate all flows at the gateway. We assume that the traffic is long-lasting and elastic like an FTP transfer of a large file. All traffic flows are either uplink or downlink. In the downlink case, the direction of the information flow is from the gateway to the client nodes. Downlink traffic is possibly the more common use case for an Internet access network like a campus or an office network. We as-

Parameter	Value
Area	Square $\{300 \times 300, 500 \times 500\}$ m[1]
Topology	Random with $\{30, 50\}$ nodes[1]
Inter-node distance (min)	$\{30, 50\}$ m[1]
Radio frequency	2.4 GHz
Path loss	Log-distance, exponent 3, ref. dist. 1 m
Channel	AWGN
Fading	Block-fading Rician, $K = -\infty$ dB
Noise floor N	-92.965 dBm
TX power	19 dBm
Receiver	SNR thresholds (no cumulative interference)
PHY bit-rates	$\{1, 1.5, 2, 3, 4, 6, 8, 9\}$ packets/slot[2]
Bit-rate SNR thresholds	$\{5.4, 5.8, 7.0, 9.5, 11.3, 14.9, 18.6, 20.6\}$ dB[2]
CCA	Mode 1, threshold -88.5 dBm
V	1000
No. candidates	$\{1, 2, 3\}$
Routing metric	ETT
(Metric, Hop) stretch	$\{(1.05, 1.5), (1.1, 2.5), (1.5, 4)\}$
Simulated time slots	$1 \cdot 10^5$
No. flows	$\{1, 2, 4, 8, 12\}$
Seeds	99

[1] The same indices belong together.
[2] The same indices belong together.

Table 4.9.: Evaluation parameters

sume that the capacity of the gateway's Internet connection is sufficient and the WMN is the bottleneck, which may not be the case with today's consumer Internet connections. Nevertheless, uplink traffic is also an important use case. With the advent of Web 2.0 and user-generated content, being able to upload YouTube videos, photos or files in general is increasingly important. In addition, the consumer market is moving towards all-wireless designs. Thus, we will see more wireless devices that offer more resources within home and community networks, so that the typical usage patterns we know from IEEE 802.11 infrastructure networks will most likely change.

4.6.1. Potential of Opportunistic Scheduling

In the following, we evaluate the potential of WMNs for OS in the access network scenario using high level MATLAB simulations. We are favoring simulations over analytically solving the optimization problem (4.12) on page 151 because the number of constraints increases exponentially in the number of links due to the temporal correlation of the fading process. Thus, the problem quickly becomes too large to be solved numerically. Table 4.9 lists the simulation parameters. At the PHY, a physical model is deployed that uses SNR thresholds to decide upon transmission success but does not account for cumulative interference. All links are subject to an i.i.d. Rician block-fading with $K = -\infty$ dB, and the centralized scheduler has perfect CQI knowledge.

The results are averaged over 99 repetitions using different seeds for the random number generator. For each seed, a different topology is created. The nodes are placed at random within given boundaries. While randomly placing nodes, we enforce a minimum distance between each node pair in order to avoid spatial clustering of nodes. The node closest to the center of the simulation area becomes the gateway. Based on the time-averaged link capacities, the routing path(s) are constructed as discussed in section 3.5.5 using the ETT routing metric, several routing stretches and a varying number of candidates.

The time is divided into slots. A simulation consists of $1 \cdot 10^5$ slots. A central scheduler generates the LCG based on the CS relationship. For each time slot, the scheduler determines the schedule having the largest weight and activates the respective links if they have pending packets. We use three different weight functions: W_{opt} considers instantaneous CQI and AMC, W_{rbar} uses AMC considering average CQI and instantaneous outages and W_{fixed} does not employ AMC and schedules based on average CQI and instantaneous outage knowledge. In particular, let L be the number of links and N be the number of nodes. In addition, let $\Delta\boldsymbol{Q} \in \mathbb{R}_+^L$, $\boldsymbol{C} \in \mathbb{R}_+^L$ and $\bar{\boldsymbol{C}} \in \mathbb{R}_+^L$ be instantaneous back-pressure and the instantaneous and the average channel capacity vectors, respectively. The back-pressure is calculated as the difference between the shadow queue lengths $\boldsymbol{Q} \in \mathbb{R}_+^N$ of the nodes belonging to the considered link as proposed by Radunović *et al.* [218]. In addition, let $\boldsymbol{m}_j \in \{0,1\}^L$ be a vector denoting the j-th schedule. The l-th component of the schedule $\boldsymbol{m}_j$ is either 1 if link l is contained in the schedule or 0 otherwise. The scheduler selects the schedule $j^\star$ for activation in the following way, where $\langle .,. \rangle$ denotes the dot product.

$$j^\star = \arg\max_j \langle W(\boldsymbol{C}, \Delta\boldsymbol{Q}), \boldsymbol{m}_j \rangle$$

The scheduling policies are defined as follows.

$$\begin{aligned} W_{\text{opt}}(C_l, \Delta Q_l) &= C_l \cdot \Delta Q_l \\ W_{\text{rbar}}(C_l, \Delta Q_l) &= \mathbb{1}\left(C_l > 0\right) \bar{C}_l \cdot \Delta Q_l \\ W_{\text{fixed}}(C_l, \Delta Q_l) &= \mathbb{1}\left(C_l \geq \lfloor \bar{C}_l \rfloor\right) \lfloor \bar{C}_l \rfloor \cdot \Delta Q_l \end{aligned}$$

In the expressions above, $\lfloor \bar{C}_l \rfloor$ denotes largest available bit-rate that is smaller or equal to the average channel capacity $\bar{C}_l$ of link l. If the selected schedule $j^\star$ contains link l, the number of transmitted packets per slot corresponds to the instantaneous channel capacity C_l under the policies W_{opt} and W_{rbar}, whereas it is determined by the average channel capacity $\lfloor \bar{C}_l \rfloor$ under W_{fixed}. In either case, the queue at the transmitter of link l is an upper bound on the number of packets that can be transported in the considered time slot. If link l is not contained in the selected schedule, it remains silent. In order to achieve proportional fairness, the utility function is logarithmic. The number of generated packets per time slot at the source of a flow f is Poisson distributed with rate $Y_f = V / Q_{\sigma(f)}$.

We have conducted simulations with 30 and 50 nodes and between $1 - 12$ flows. In Figure 4.29, the sum throughput is shown instead of the aggregated utility since both show similar trends whereas the presentation of the former is clearer. Our observa-

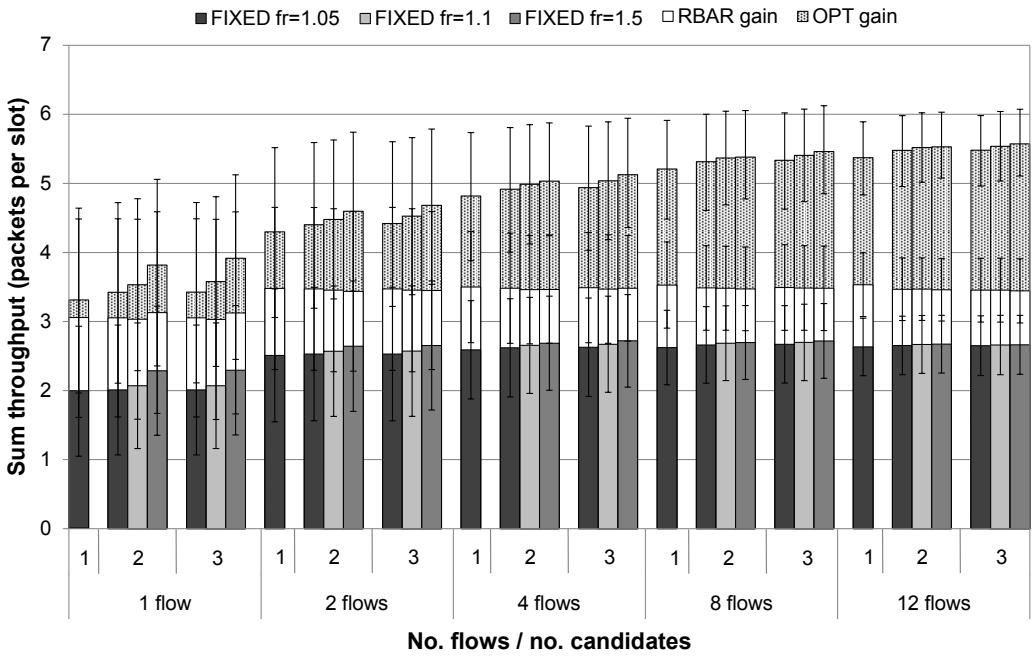

(a) 30 nodes ($\pm std.dev.$).

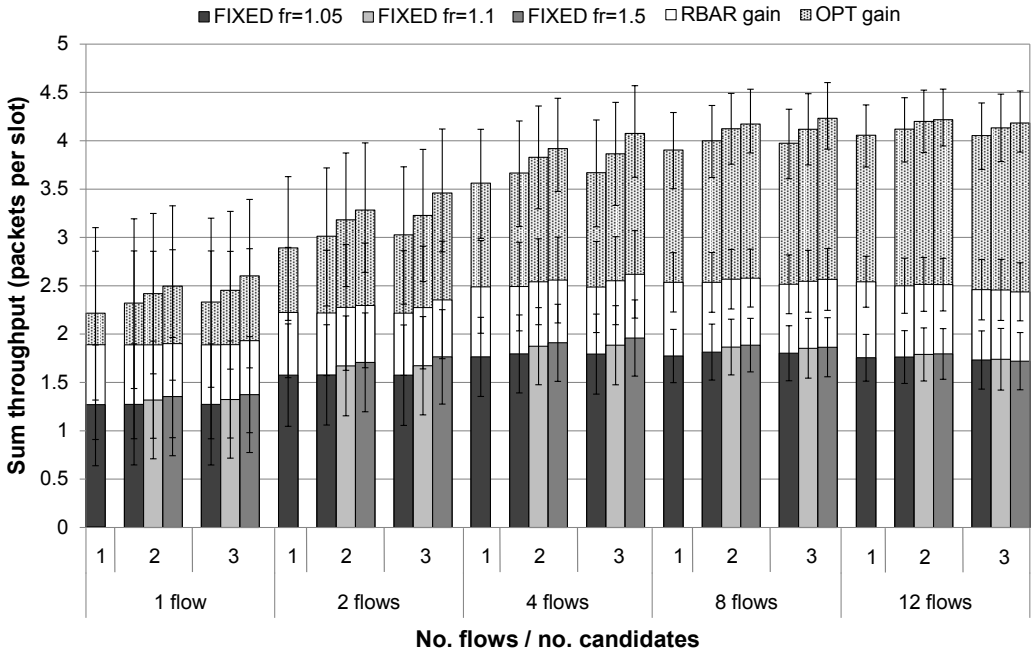

(b) 50 nodes ($\pm std.dev.$).

Figure 4.29.: Average sum throughput across all flow in the Internet access network scenario obtained from high level simulations (stacked bar charts).

tions are consistent across both topology sizes in Figure 4.29a and Figure 4.29b. The results show that there is a strict dominance in terms of sum throughput between OPT and RBAR as well as RBAR and the baseline FIXED. With 12 flows and single-path routing, for example, the sum throughput can be increased from 1.76 to 2.54 and 4.05 when using RBAR and OPT, respectively, instead of FIXED. Using the policies FIXED and RBAR, the sum throughput increases only marginally in the number of flows, the number of candidates and the routing stretch. Both policies react on channel outages, which is a basic form of OS. The gains of multi-path routing are almost negligible. The throughput gain of RBAR over FIXED remains almost constant across all parameters.

Under the policy OPT, on the other hand, the sum throughput significantly increases in the number of flows. In particular, the sum throughput in Figure 4.29b increases from 2.2 to 4.2 packets per slot when increasing the number of flows from 1 to 12. Furthermore, the throughput performance of the system can be increased via multi-path routing under the policy OPT. For a small number of flows, the gains of larger routing stretches or more candidates are moderate. If the number of flows becomes large, however, the returns for multi-path routing are diminishing, which is probably an indication that the diversity gets exhausted.

The results above highlight the potential benefits of channel-adaptive scheduling and bit-rate selection. However, they do not account for imperfect and delayed CQI, variations of the CQI during a transmission, the randomness of the channel noise, receiver impairments, cumulative interference, the memory of the fading process, the window size of the flow, the collisions inherent to CSMA and the efficiency loss of CSMA due to the non-asymptotic working point of the contention process that is expressed in the entropy term in (4.12) on page 151. Nevertheless, we draw the conclusion that the Internet access network scenario offers a significant potential for joint channel-adaptive contention and transmission. Even though the gateway and the associated collision domains will probably saturate quickly and become the dominant bottleneck, the inclusion of a further flow generates throughput capacity due to the additional scheduling opportunities (cf. [264, chap. 6.6]).

4.6.2. Simulative Evaluation

Now that we are aware of the OS potentials of an Internet access network, we will investigate whether and to which extend the proposed system is able to materialize them in terms of throughput gains. In order to answer the question, we have conducted network simulations (cf. section 2.5). Similar to the previous section, a different topology is created for each seed. The nodes are placed at random within the simulation area. A minimum distance between each node pair is enforced in order to avoid spatial clustering of nodes. The node closest to the center of the simulation area becomes the gateway.

Table 4.10 lists the simulation parameters. We are using a Rician fading process with parameter $K = -\infty$ dB and temporal correlations according to Punnoose *et al.* [210]. The path loss exponent is reduced to 3, which corresponds to indoor and obstructed NLOS environments (cf. [228]). The receiver parameters are adjusted to the IEEE 802.11a/g standard. The chosen target and peak TAs correspond to an average backoff of about 150 µs and 55 µs, respectively. Thus, the average backoff is comparable to

Parameter	Value
Area	Square 500×500 m
Topology	Random with 50 nodes
Inter-node distance (min)	50 m
Radio frequency	2.4 GHz
Path loss	Log-distance, exponent 3, ref. dist. 1 m
Channel	AWGN, noise floor $N = -92.965$ dBm
Fading	Rician $K = -\infty$ dB, $f_D = \{4, 16\}$ Hz
TX power	19 dBm
Receiver	SINR-BER & cumulative interference
PHY	IEEE 802.11a/g, $\{6, 9, 12, 18, 24, 36, 48, 54\}$ Mbps[2]
SNR thresholds[1]	$\{5.4, 5.8, 7.0, 9.5, 11.3, 14.9, 18.6, 20.6\}$ dB[2]
MAC	CSMA/HBT
CCA	Mode 1, threshold -88.5 dBm
Propagation delay	2 µs
Radio turnaround	9 µs
TXOP duration	2.5 ms
min, avg. & peak TA	$4, 8.8, 9.8$
Inter-flow hysteresis δ	1.1
Per-hop window size W	$\{8, 32, 128\}$ packets per hop
TA EWMA	0.025
Flow rate EWMA γ_y, τ_y	0.025, 100 ms
Routing metric	ETT
(Metric, hop) stretch	$\{(1.05, 1.5), (1.1, 2.5)\}$
Flow duration	15 s warm-up, 25 s evaluated
Packet size	1500 Byte
No. flows	$\{1, 2, 4, 8, 12\}$
Seeds	50

[1] 1000 octets, 10% FER.
[2] The same indices belong together.

Table 4.10.: Evaluation parameters

IEEE 802.11g with 20 µs slot time and 31 contention window slots. The CSMA/HBT protocol is deployed at the MAC layer in order to mitigate the hidden node problem (cf. section 3.3). In our evaluation, we are considering the CSMA inherent collisions. The radio turnaround delays are set according to IEEE 802.11a. The routing path(s) are constructed as described in section 3.5.5 (cf. p. 91ff.) based on the ETT routing metric. Furthermore, we vary the number of candidates, the routing stretch, the window size and the number of flows. In contrast to the previous section, we now use a *per-hop window size*. Thus, the window size is not fixed anymore, but depends on the length of the best routing path according to the ETT routing metric. If the best route consists of 4 hops and the per-hop window size is set to $W = 8$ packets per hop, for example, the total window size per flow is 32 packets. In this way, we try to keep the impact of the window size (cf. section 4.5.3) independent from the length of the flow.

The results are compared with the RBAR variant of the protocol, which only performs AMC but does not apply the channel-differentiated contention. In addition, we compare the results with both DSR and ExOR forwarding, which operate on top of an IEEE 802.11a/g PHY and MAC. In the latter case, the MAC is sufficiently modified to support the anycast transmission (cf. [22, 316]). Remember that OR does not offer any benefits if the channel can be estimated reliably in advance. However, if the a priori channel estimation is not possible as it is the case with the IEEE 802.11 DCF under the basic access mode, then multiple receiver candidates may achieve additional diversity and throughput gains even in channel with large memory. The bit-rate for packet transmission is selected by the routing layer according to the long-term average channel conditions [62]. At the transport layer, either TCP or a genie-aided saturating UDP is deployed. The former is a Reno-like TCP implementation according to the RFCs 793 and 2581 [7, 206]. The latter, on the other hand, is a vanilla UDP [204] that is enhanced with an error-free and zero-latency out-of-band feedback channel in order to control the number of outstanding packets, which is chosen sufficiently large in order to saturate the flow.

Uplink Traffic Flows

Figure 4.30 and Figure 4.31 show the sum goodput, the sum utility and the end-to-end delay for the uplink of the Internet access network scenario. The accumulated goodput shown in Figure 4.30a possess a dominance relationship similar to the potentials in the previous section. The proposed protocol (OPT) performs strictly better than its RBAR counterpart and all DSR and ExOR variants in terms of sum goodput with only one exception: DSR-UDP is slightly better without RTS in the case of only one flow and the smallest per-hop window size of $W = 8$.

Our observations about the potentials of multi-path routing apply to the simulation results to a large extend. Especially if the number of flows is small, there is a considerable gain when using two candidates ($C = 2$) and larger routing metric stretches f_{r}. If the number of flows is large, however, multi-path routing becomes counter-productive and a large per-hop window size seems to intensify this behavior. We suppose that the CSMA inherent collisions contribute to this observation. Remember that we are using non-negligible turnaround delays whenever the radio switches from receive to transmit mode and vice versa (cf. Table 4.10), which will cause collisions that CSMA cannot prevent. A higher degree of multi-path routing increases the number of contending nodes within the collision domains and thus, CSMA collisions become more likely (cf. section 3.3.1). On the other hand, the returns for an additional multi-path usage are generally small for a high number of nodes (cf. Figure 4.29).

In the previous section, we have observed that the gain of the channel-differentiated contention over RBAR increases in the number of flows. In our network simulations, however, we observe only a moderate gain of about 69 pps or 11% that is achieved with 4 flows. We suppose that the CSMA collisions are one cause for the observation. Furthermore, the CSMA contention under IEEE 802.11a/g cannot be sufficiently aggressive in order to operate the system in the regime of high OS efficiency (cf. section 4.5.1). Thus, a limited fraction of the potentials can be achieved only. We will come back to this issue in our conclusions.

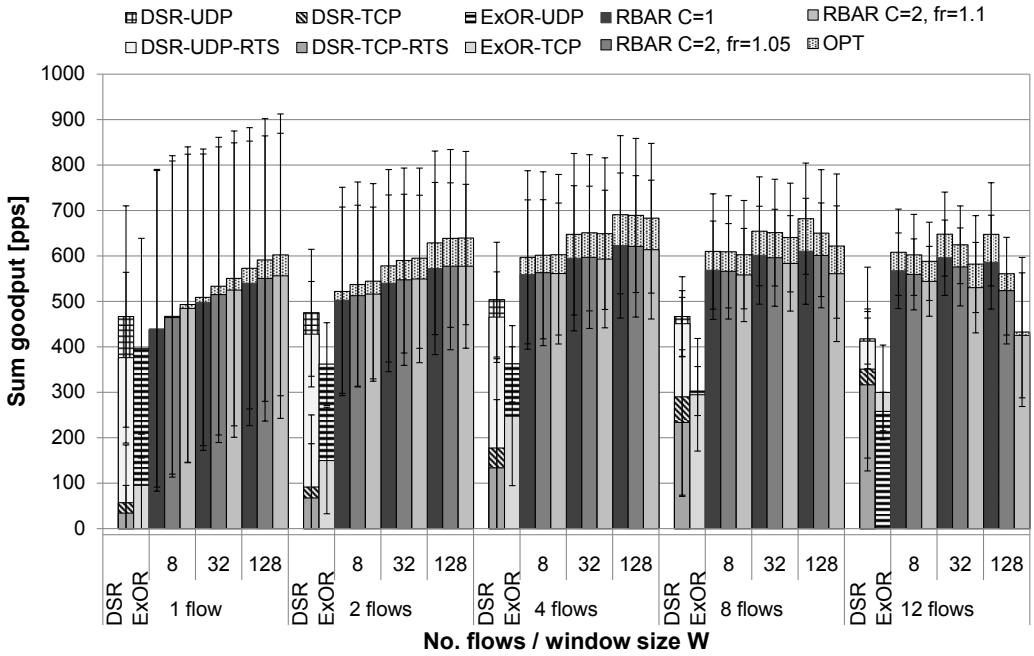

(a) Sum goodput ($\pm std.dev.$).

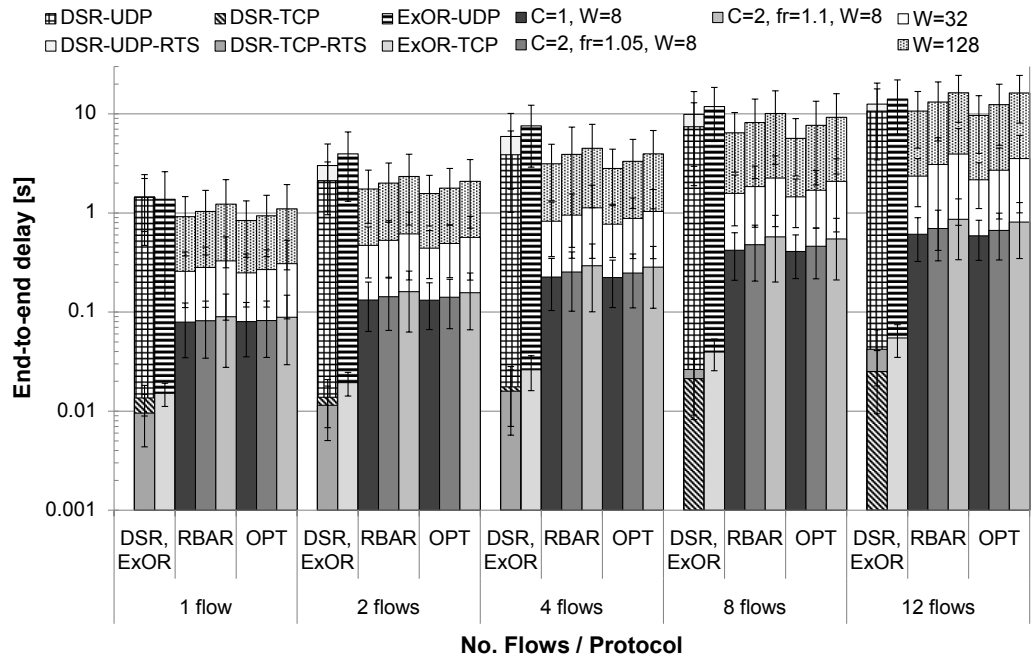

(b) Per-flow end-to-end delay ($f_{\mathrm{D}} = 4$ Hz, $\pm std.dev.$).

Figure 4.30.: Goodput and end-to-end delay results for the uplink of the Internet access network scenario ($f_{\mathrm{D}} = 4$ Hz, overlapped bar charts).

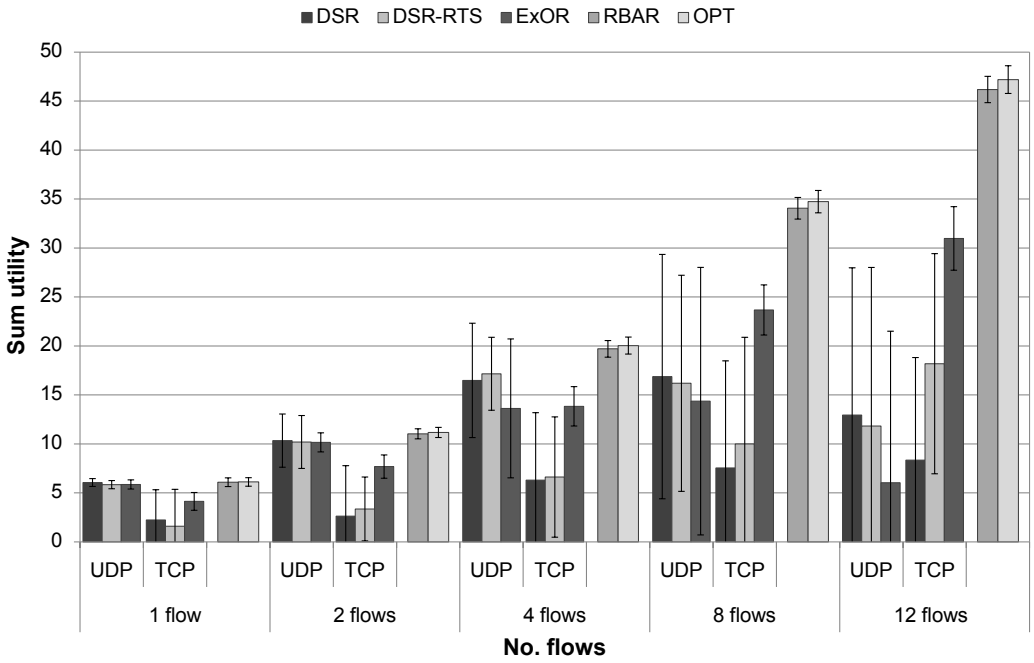

(a) Sum utility, based on the packet arrival rates ($f_{\mathrm{D}} = 4$ Hz, $\pm std.dev.$).

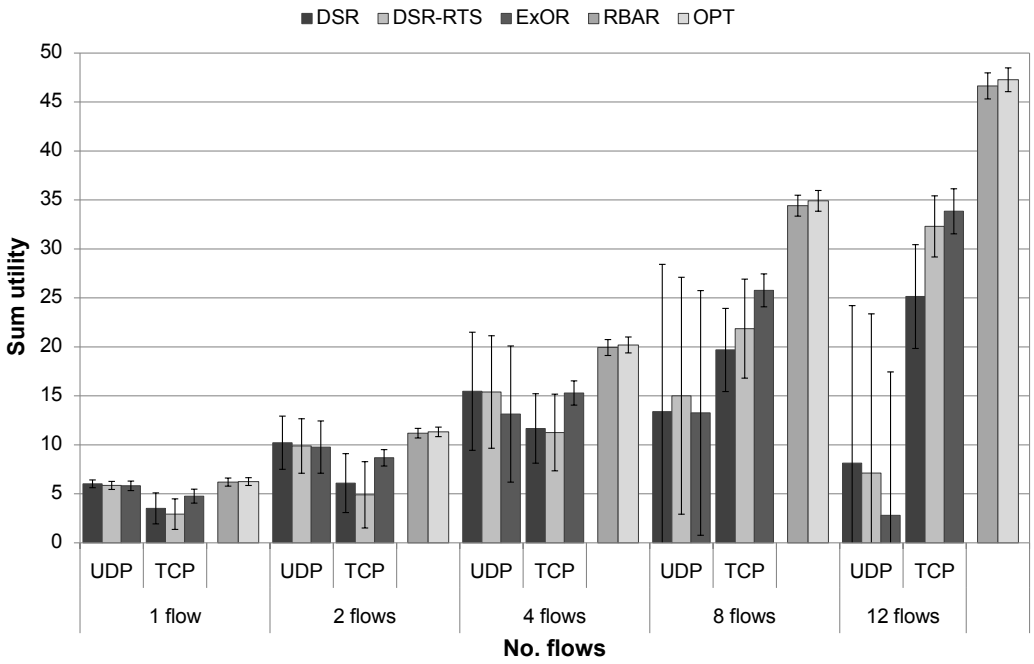

(b) Sum utility, based on the packet arrival rates ($f_{\mathrm{D}} = 16$ Hz, $\pm std.dev.$).

Figure 4.31.: Utility results under different Doppler frequencies for the uplink of the Internet access network scenario ($W = 32$, $C = 1$).

In section 4.5.3, we have already discussed the impact of the finite buffers and the hidden channel state on the throughput performance. In Figure 4.30a, the sum goodput of the system increases with larger buffers as expected. However, large buffers become counter-productive in combination with multi-path routing and a large number of flows. We suppose that this observation is related to the CSMA inherent collisions due to the increased number of contenders in the collision domains. The small buffers become a further limiting factor for the number of activatable transmitters having non-empty queues, which mitigates the problem of the CSMA collisions. Remember that almost 9 packets fit within a TXOP of 2.5 ms. We have plotted the accumulated utility in Figure 4.31 for single-path routing and under both Doppler frequencies. The relative benefit of the proposed protocol OPT over RBAR is slightly smaller at higher Doppler frequency

The sum goodput of DSR and ExOR is smaller compared to OPT if the buffers are sufficiently large (cf. Figure 4.30a). As shown in Figure 4.31, the performance gap in terms of utility between the conventional and the proposed protocols significantly increases under a large number of flows. This observation indicates that the conventional protocols maintain the sum goodput under many flows at the expense of higher unfairness. However, TCP has been designed for a fairness function different from proportional fairness [52]. The saturating UDP traffic does not employ any fairness objective at all and solely relies on the MAC layer fairness. In addition, we observe that DSR performs better without RTS.

The goodput results under saturating UDP are generally higher compared to TCP, although the difference between UDP and TCP seems to vanish under many flows. In the case of ExOR, TCP even exceeds UDP in terms of sum goodput under 12 flows. The UDP goodput degrades under a large number of flows. We suppose that this observation is related to the higher probability of CSMA collisions. At the same time, the TCP goodput increases, most probably due to a lower packet loss probability at the MAC layer. With an increasing number of flows, the higher contention increases the average inter-transmission delay experienced at the MAC layer. Thus, from the perspective of an individual transmitter, the fading process accelerates with each additional flow. The *virtually reduced* channel memory increases the success probability of the link's ARQ process. The average TCP congestion window can become larger since TCP generally misinterprets channel-related packet loss as an indication of congestion. The impact of the channel memory on the TCP performance is directly observable in the sum utility shown in Figure 4.31 under different Doppler frequencies. Interestingly, it depends upon the transport layer protocol which of the conventional routing protocols performs better in terms of cumulated utility. Especially if the number of flows is large, DSR outperforms ExOR under saturating UDP, whereas the reverse holds true for TCP.

The per-flow end-to-end delay is shown in Figure 4.30b. As predicted by Little's law, the delay performance of the proposed protocol and its RBAR variant greatly differs depending on the selected per-hop window size W: It increases from 90 ms to 300 ms and 1000 ms when increasing the window size W from 8 to 32 and 128, respectively. The proposed protocol has a slight advantage over RBAR since it achieves higher goodput. We observe that the end-to-end delay increases under multi-path routing. When the number of flows is small, multi-path routing generates additional through-

put. However, the generated throughput is not able to outweigh the additional delays since further packets have to be injected into the additional routing paths as discussed in section 4.4.2. Furthermore, the end-to-end delays increase in the number of flows. The sum goodput capacity of the considered scenario does scale with the flow population. With each addition flow, the per-flow goodput decreases. Since the occupied buffer size per flow remains constant, the delays increase according to Little's law. The delay results of saturating UDP are comparable to OPT under the per-hop window size $W = 128$. The average delay of TCP is between 10 ms $-$ 60 ms. Compared to OPT, the TCP delays are smaller by an order of magnitude. On the other hand, the TCP sum goodput differs from OPT and RBAR by a factor of about two only under many flows. Thus, the TCP congestion window remains small according to Little's law.

Downlink Traffic Flows

For the downlink traffic, the gateway is the origin of all flows. From the point of view of the protocol proposed in section 4.4, the difference to the uplink is that all flows share at least one transmitter. At the gateway, the flows interact with each other within their V adaption via the first term in the minimum expression on line 8 of Algorithm 8 on page 160. In contrast to the uplink, all flows have to share the sum TA r_{sum} of the gateway. If the number of flows increases, the gateway will probably become the bottleneck that determines the working point for all flows in terms of V and TA. Furthermore, the working point is most likely not as efficient as in the uplink case due to the shared transmitter, so that both throughput and utility should decrease to some extent.

The goodput and utility results for the downlink Internet access network scenario are shown in Figure 4.32. The observations that we have made for the uplink apply to the downlink in most cases, as well. In particular, the accumulated goodput shown in Figure 4.32a is similar to the uplink case for the proposed protocol OPT and its RBAR variant when the number of flows is smaller than 8, although the gain of OPT over RBAR is slightly larger with up to 16%. However, both the goodput and the utility under many flows and large window sizes significantly lag behind the uplink results. We will consider this issue in the next paragraph. Considering both DSR and ExOR, we observe that the sum goodput slightly decreases for all of them except ExOR-UDP. Comparing the utility results in Figure 4.32b with the uplink, we observe that both routing protocols perform significantly better in the case of UDP traffic. However, the observation is probably influenced by our genie-aided saturating UDP flow controller. Remember that vanilla UDP does not apply any flow control and the scheduling discipline at the IP layer is FCFS.

In order to understand the above-mentioned performance loss under large window sizes and many flows, let us consider Figure 4.33. The figure shows the evolution of the individual Vs of 12 flows and, in addition, the accumulated queue size at the gateway in one particular simulation instance of the downlink scenario. All flows start at the same time and emit a large amount of packets in order to fill their window of outstanding packets. The V parameter is set to an empirically determined initial value. Due to the large number of flows, however, the system cannot support the initial value of V and reduces it drastically. During the startup of the flow, the gateway enqueues the whole window of packets for all flows, which further increases the TA and thus

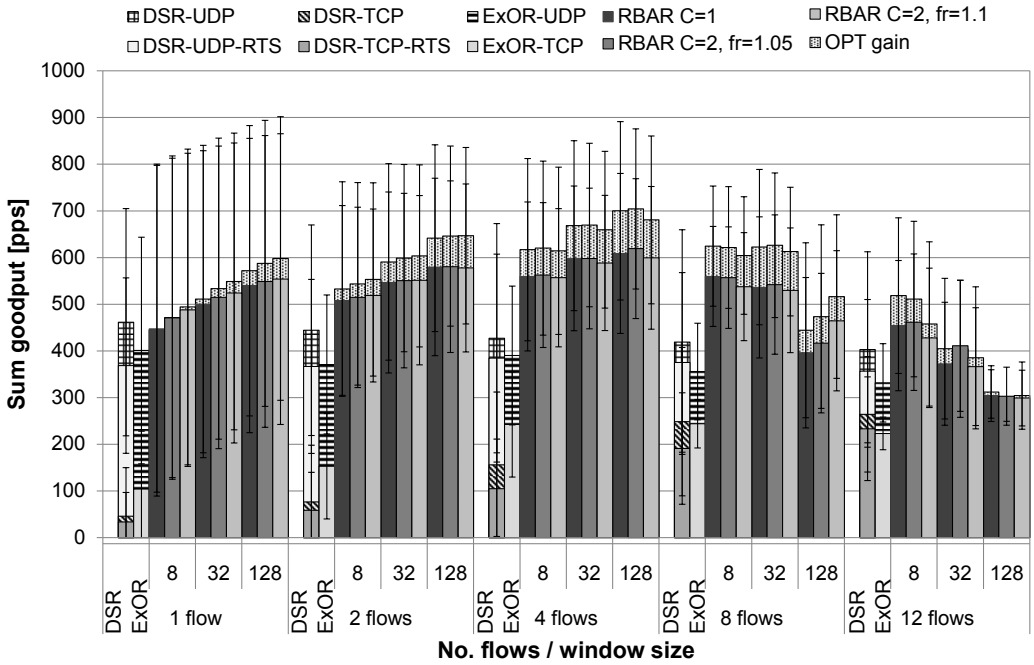

(a) Sum goodput ($\pm std.dev.$, overlapped bar chart).

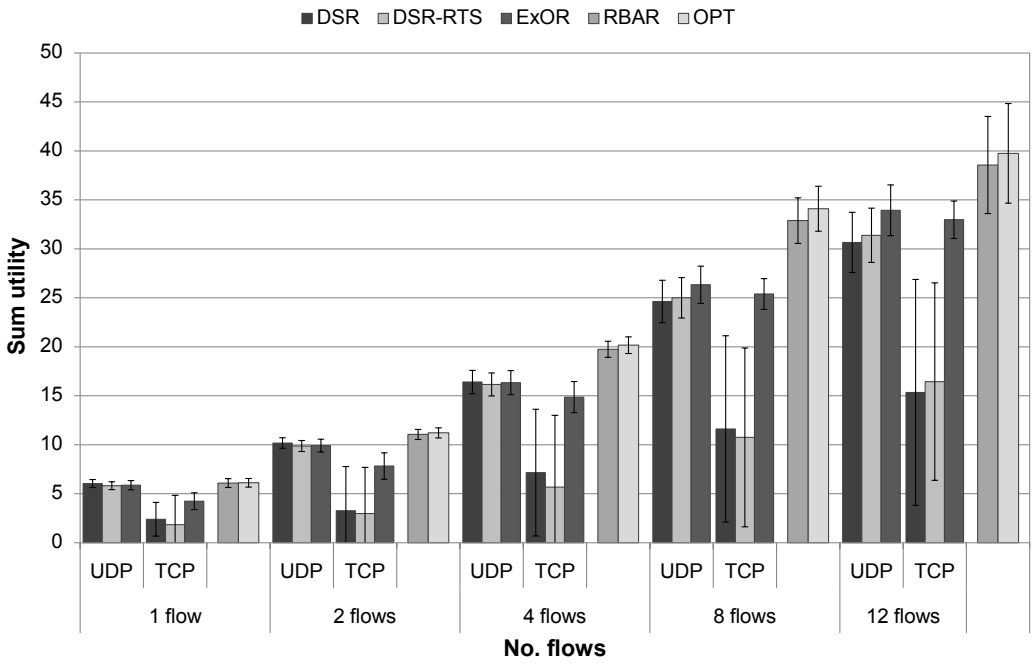

(b) Sum utility, based on the packet arrival rates ($W = 32$, $C = 1$, $\pm std.dev.$).

Figure 4.32.: Goodput and utility results for the downlink of the Internet access network scenario ($f_{\mathrm{D}} = 4$ Hz).

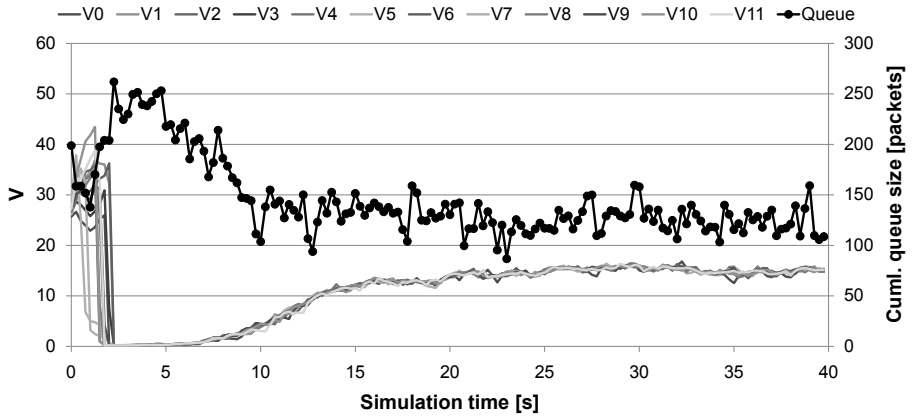

(a) Per-hop window size $W = 8$.

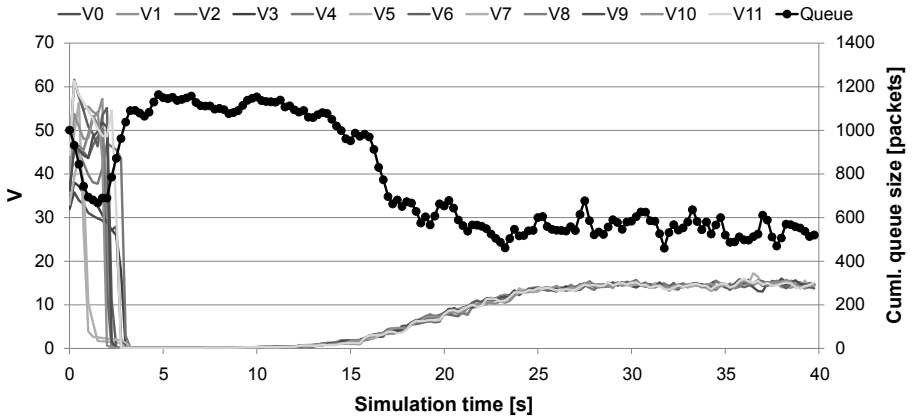

(b) Per-hop window size $W = 32$.

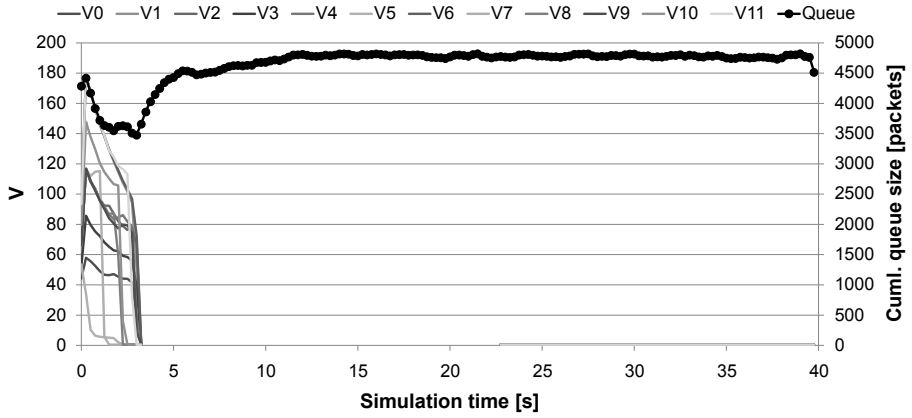

(c) Per-hop window size $W = 128$.

Figure 4.33.: Evolution of the V parameter and the cumulated queue size at the gateway under the proposed protocol for one particular instance of the downlink Internet access network scenario depending on the window size W (12 flows, $f_D = 4$ Hz, $C = 1$, averaged over 250 ms).

triggers an additional reduction of V. Under the small per-hop windows size $W = 8$, Figure 4.33a illustrates that it takes about 8 s until the buffered packets are sufficiently drained from the gateway's queue and distributed along the routing path, so that the value of V can be raised and eventually approach its working point. This process takes longer when the windows are larger as shown in Figure 4.33b and Figure 4.33c for $W = 32$ and $W = 128$, respectively. Under the per-hop windows of $W = 128$ packets, in particular, the adaption does not finish within the 40 s simulation time. Thus, the system operates with very small TA values, which eventually reduce the observable throughput efficiency.

In summary, the uplink as well as the downlink of an Internet access network can benefit from channel-differentiated contention in combination with AMC. Especially with many flows, the benefits over state-of-the-art protocols are significant in terms of sum goodput and utility. In contrast to the expected potentials, we have observed a moderate sum goodput gain of about 16% over the RBAR variant. Our results indicate that the potentials are not exhausted yet. We suppose that the limited backoff differentiation abilities of the IEEE 802.11a/g technology contribute to this observation. It remains open whether a more aggressive contention technology is able to operate the system close to the potential OS gains.

On the other hand, the costs for achieving the observed DOS gains are considerable. However, the tradeoff between the DOS gain and the end-to-end delay can be controlled via the provided buffer space. Multi-path routing has shown to increase the throughput capacity especially when the number of flows is small. If the number of flows increases, the multi-user gains become more pronounced even with small buffers and single-path routing. In the system level evaluation, the propagation and turnaround delays cause CSMA collisions. Especially with many flows and multi-path routing, the CSMA collisions become a limiting factor. The objective of our adaption approach of the CSMA parameter V is the limitation of the average backoff *per node* according to the technological constraints (cf. section 4.4.3).

A topic for future research is the V adaption between contending flows. All flows that contend with each other depend on the smallest V parameter among them. We have observed that the estimated minimum V value tends to decrease with increasing number of flows, presumably due to the variability of the underlying channel and queueing processes as well as the averaging and the feedback delay. Hence, it becomes harder for the system to maintain an efficient working point in terms of TA. In addition, the V adaptation introduces a form of coupling between contending flows, which may easily involve all flows of the WMN and thus become a global coupling. It remains open whether large WMNs can be efficiently operated under these circumstances, or if a decoupling becomes necessary.

4.7. Chapter Summary

In this chapter, we have addressed the question whether DOS gains can be obtained in WMNs in a distributed way by adapting the CSMA parameters according to both the traffic and the channel conditions and, in a nutshell, the answer is positive. We have presented a Markov model of CSMA in WMNs with slow fading channels. It

possesses a favorable structure that allows for a decomposition into simple and distributed subproblems under some assumptions. We have presented a NUM algorithm for congestion control, multi-path and multi-hop routing and CSMA in WMNs with slow fading channels. The foundation of the algorithm is the so-called *channel-differentiated contention*. The rationale is to employ a large backoff if the channel is bad and increase the contention aggressiveness properly with better channel instances. The channel-differentiated contention is the counterpart to AMC since it adapts the backoff to the instantaneous channel conditions. According to the algorithm, we have designed a cross-layer protocol that addresses how CQI is obtained in a WMN, how the sender maintains the window of in-flight packets and how efficient backoff durations can be preserved in the contention process.

We have evaluated the proposed protocol through analysis and simulation. Our results indicate that DOS is feasibly in WMNs using the concept of contention that is inherent to CSMA. When relaxing the modeling assumptions about infinite buffers and non-hidden channel states, the system's performance becomes dependent on the memory of the channel and fortunately, it degrades gracefully. In particular, we have observed a two-sided tradeoff. When reducing the memory, the channel uncertainty becomes the limiting factor. The channel estimates are of lower predictive value resulting in more reception errors and lower DOS gains. In the opposite case, the coherence time becomes larger and the window size is the limiting factor since it becomes more difficult to bridge over longer periods of bad channel conditions. The characteristic tradeoff between delay and throughput that is inherent to OS [264] can be controlled via the window size. However, the costs of high OS gains in terms of end-to-end delay are significant and non-negligible. Similar to classical MUD [141], the DOS gains of the proposed protocol depend on the size of the user population. In addition, multi-path forwarding is an alternative approach to increase the throughput efficiency in WMNs.

In order to take the impact of the topology into account, we have evaluated both the potential and the actual performance of the channel-differentiated contention in the Internet access network scenario. In particular, the potential of DOS over AMC is significant: With few users, multi-path forwarding offers a way to increase the throughput capacity, whereas the MUD gains dominate under a large user population size. However, the DOS gain over AMC remains moderate in our network simulations, which indicates that the existing potential is not exhausted yet, which leaves room for more aggressive contention approaches in our future work. Nevertheless, the benefits over state-of-the-art protocols are significant in terms of sum goodput and utility especially with many flows. We close this chapter with the following remarks about current limitations and future directions.

Architectural Implications. The architectural differences between cellular and wireless mesh networks have been discussed in the introduction of this chapter. A lesson learned is that the rich topological structure of WMNs is an important advantage. According to our evaluation results, the *contention aggressiveness* of the IEEE 802.11a/g technology is probably not sufficient to exhaust the DOS potential of WMNs especially under a large number of links and flows. Thus, increasing the differentiation capabilities within the contention process is one option that we will discuss in the next chapter.

Between the cellular and the wireless mesh topology, however, an architectural continuum exists that needs to be explored. Given the contention aggressiveness of IEEE 802.11a/g, for example, it would be an option to prune the topology of the WMN in order to focus on the more important links. The CQI could be monitored more frequently [227] or (randomized) beamforming techniques could be used to shape the channel statistics as desired. On the other hand, we are already seeing relaying techniques finding their way into cellular networks. Both candidate proposals for the upcoming ITU IMT-Advanced standard, which are LTE-Advanced and IEEE 802.16m WiMAX, contain multi-hop relaying elements [1, 247]. As the scheduling domains grow in these networks, contention procedures carried out on the wired backbone can enhance their scalability.

Controlling the Memory of the Channel. Since the channel state is hidden from each transmitter, the system's performance depends on the memory of the fading channel. Throughout this chapter, we have assumed that the channel coherence time and the length of the TXOPs are both fixed parameters. Nevertheless, the memory of the channel can be adjusted in several ways. If the channel does not offer sufficient memory, for example, the TXOP can be shortened in order to slow down the fading process and vice versa. In non-fading environments, the adaption of the backoff duration is equivalent to the TXOP adaptation in terms of CSMA optimality. Furthermore, the optimality in discrete time has been established using a fixed-sized backoff window and TXOP adaptation [111]. However, the interaction between the TXOP adaptation and the slow fading channel is not yet understood.

Beamforming techniques can be used to generate fading channels that have the desired dynamic range and memory properties [264]. In this case, the channel state probabilities P of the fading CSMA model presented in section 4.2 become optimization variables and conditional independence cannot be guaranteed anymore. It remains open how the joint optimization over both the channel state and the CSMA backoffs can be solved efficiently and, in addition, how both nodes belonging to a wireless link can be coordinated accordingly.

Slow Fading and Carrier Sensing. In the derivation of the fading CSMA model in section 4.2, we have assumed that the LCG is time-invariant. In other words, carrier sensing is assumed to be independent from the fading process. In our network simulations, on the other hand, the CS relationship has been time-dependent since the instantaneous fading affects both the data and the busy tone channels. Nevertheless, we have observed that the model has had a reasonable predictive value for the simulation results in the illustrative scenarios. It remains open to analyze the impact of fading on the CS process for both the model and the protocol.

Contention-Based Probing of Multiple Links. Throughout this chapter, we have considered a straightforward approach to link probing, in which one link is probed at a time during the actual data transmission. An interesting question for our future work is whether contention methods are able to enhance the link probing process in terms of

timeliness, probing intensity and overhead. In the context of cooperative communication, for example, Bletsas *et al.* have proposed a probabilistic relay selection scheme, in which the relays contend for cooperation according to their instantaneous channels to both source and destination [25].

One way to apply the idea to link probing is to group individual candidate receivers into receiver sets similar to the concept of hyperlinks that was used with OR in the previous chapter. A transmitter does not probe a single receiver but a receiver set instead. On receiving the probe request, each receiver contends for the transmission of the reply considering both the instantaneous queue and channel state. Eventually, the contention process will select the instantaneous best receiver to send the probe reply. The transmitter cannot observe the individual channels towards each receiver anymore, since it only sees the instantaneous best of them. In this way, both the probing overhead and the CQI uncertainty can be reduced at the expense of collisions and an efficiency loss due to the probabilistic nature of contention.

Short Time Fairness and the Averaging Horizon. The adaption of the V parameter shown in Algorithm 8 on page 160 relies on averages of both flow rate y and link TA $\bar{r}$. As already discussed in section 4.5.4, the performance of the system depends on both the method and the horizon for averaging. A small averaging window increases the sensitivity of the system to short-term unfairness. With longer averaging windows, on the other hand, the reactivity of the averages to short-term unfairness is reduced and the system exhibits more patience in waiting for better channel conditions. Thus, the averaging horizon can be used to control the tradeoff between DOS gains and short-term unfairness.

The averaging horizon of both flow rate y and TA r should ideally be identical. The flow rate is maintained at the source of the flow, whereas the TA averages are estimated by each forwarder along the multi-hop route. The feedback of the latter to the source incurs delay that is hard to predict since the feedback is passive by design and additionally subject to outages. Furthermore, different averaging methods are used. The averaging of the flow rate y proceeds in fixed intervals, whereas the TA average is updated irregularly after a successful probe. The TAs are averaged arithmetically in the time domain (cf. line 20 of Algorithm 7), so that the estimate $\bar{r}$ characterizes the average backoff. However, the time domain averaging renders the relationship between credits C^f and average TA $\bar{r}$ sub-linear since the weight of higher bit-rate samples is smaller in comparison due to the involved exp expression. Remember that the linearity was one of our assumptions for the V adaption algorithm in section 4.4.3. The linearity can be preserved by an arithmetic average in the TA domain. In this case, however, the high bit-rate samples have a higher weight, so that the efficiency of the resulting working point is generally lower.

Adaption of the Window Size. The tradeoff between DOS gain and end-to-end delay is determined by the window size. The costs of high DOS gains are considerable. In the first place, the application should be able to specify the available delay budget that can be spend on DOS. Furthermore, several problems can be addressed if the system is able to adapt the window size within the specified bounds. In section 4.6.2, for

example, we have already mentioned the problems with large windows during the startup of a flow. Incrementally increasing the window after startup might speed up the convergence process. In addition, we have observed that large windows might not be necessary if the number of flows is large, since the returns are smaller in this regime. Thus, it remains open whether and to which extend the user satisfaction can be increased via the adaption of the window size based on the number of flows and possibly further indicators of the instantaneous network state.

Working Points and Advanced Methods for the *V* Adaption. We have selected a working point in terms of TA and V that prevents the breakdown of the network due to CSMA collision as long as the node density remains limited (cf. section 4.4.3). In comparison with the previous chapter, we have removed the dependency on the number of flows. It remains open to explore further working points and their properties. Interesting work points are, for example, the ones that consider the transmission aggressiveness per collision domain, so that they are independent from both the node and flow density. Furthermore, it remains open whether it is possible to optimize over the CSMA collision probability within the NUM framework.

We have validated the effectiveness of the V adaptation by simulations. However, analytic results about the convergence properties of the algorithm would be valuable. In addition, it remains open to explore the implications of a joint adaption of the backoff window and the TXOP duration similar to Jiang *et al.* [111] on the adaption of the tradeoff parameter V.

According to our design, the inter-flow adaptation introduces a form of coupling between contending flows, which may easily involve all flows of the WMN and thus become a global coupling. It remains open whether the scalability is maintained in this case, or if a decoupling becomes necessary. In particular, all flows that contend with each other depend on the smallest V parameter among them. We have observed that the estimated minimum V value tends to decrease with increasing number of flows (cf. section 4.5.4), presumably due to the variability of the underlying channel and queueing processes as well as the averaging and the feedback delay. Hence, it becomes harder for the system to maintain an efficient working point in terms of TA. It remains open whether an inter-flow adaptation exists that addresses both scalability and efficiency in the same way.

Relays and Their Costs in Multi-Hop and Multi-Path Routing. We have already discussed the costs of relays in the previous chapter. From the theoretical point of view, every additional relay node introduces further opportunities for DOS, but the returns are generally diminishing. On the other hand, the optimality gap (3.4) on page 40 is determined by the contention aggressiveness V and the number of relay links $|\mathcal{L}|$. Thus, there is generally a point at which the costs of an additional relay will outweigh the prospective benefits. It remains open whether the system can identify and adapt to the optimal degree of multi-path and opportunism.

5. Conclusion and Outlook

When comparing cellular to wireless mesh networks, a disparity can be observed in terms of innovation at the lower layers. Advanced concepts and technologies that have been developed in recent years already found their way into cellular standards and system. However, the multi-user nature that is inherent to most technologies breaks with the network stack abstraction and introduces both vertical and horizontal dependencies. Resources have to be allocated cooperatively, which is difficult due to the flat and decentralized architecture of wireless mesh networks. Recently, it has been reported that CSMA is utility-optimal in WMNs if its parameters are updated in a traffic-adaptive manner. The result is promising since CSMA is a simple contention-based algorithm that is furthermore completely distributed.

The question arises whether CSMA and the underlying concept of contention allows for the assimilation of advanced PHY technologies into WMNs. The objective of this thesis is to answer the question for the advanced PHY concept of opportunistic communication. We have developed models of CSMA that consider the important aspects of opportunistic communication. Using network utility maximization and layering as optimization decomposition, cross-layer algorithms have been derived for both opportunistic routing and opportunistic scheduling. In the design of protocols, we have addressed several practical problems like buffer provisioning, acquiring of channel knowledge, end-to-end delay limitation and the preservation of efficient backoff durations.

Based on our evaluation results from analysis and simulation, we argue that opportunistic communication via contention techniques is feasible in WMNs using a technology similar to IEEE 802.11. Nevertheless, the costs are generally high in terms of delay. The optimality gap with respect to utility is considerable for the underlying technology. Further promising results have recently been reported for CSMA in combination with other innovative technologies like MIMO spatial multiplexing [211], multiple RF channels [28, 168, 208] and superposition coding [245]. Thus, we are optimistic that the principle of contention will be a building block for future wireless mesh networks that allows them to keep up with the speed of innovation at the lower layers. We dedicate the remaining pages of this thesis to a short discussion of future directions.

A Bottom-Up Design for CSMA. A lesson that we have learned is that the cross-layer design leaves room for interpretation. An optimization problem possesses a declarative nature only. The "how" is left to the system designer. The alert reader might have noticed that we have already given an example how the same facet of a NUM problem can be designed in two different ways. In particular, the congestion control algorithm in chapter 3 assumes a given parameter V and derives the flow rate y accordingly, whereas it is the other way around in chapter 4.

Considering the freedom in the design process, an interesting direction for further investigations is the so-called *bottom-up design* for CSMA. To start with, let us reconsider the state-of-the-art approach first. According to the top-down design, the traffic intensity on a link determines its contention aggressiveness. In particular, the size of the backoff window is set according to the queue size. If the traffic intensity on the considered link is high, then the backoffs are small, but the queueing delay is large. With low traffic intensities, on the other hand, the queues as well as the queueing delays are small, whereas the backoff durations will be large.

On the other hand, what would be the implication of using a small and fixed backoff window? On the one hand, the queues do not have to grow in order to satisfy the high traffic intensity in the above-mentioned scenario. Under a low traffic intensity, on the other hand, the fixed backoff window keeps the medium access delay small, although the queue will run empty more often. In other words, the approach effectively postpones the greater part of the formerly large backoffs until after the actual medium access. More general, the rationale behind the bottom-up design is to reverse the relationship between queue size and backoff. Instead of setting the backoff according to the queue size, the backoff determines the expected queue size. However, the expected queue size should not be mistaken for the actual size of the physical queue. Instead, it can be understood as a credit counter. In particular, the effective backoff is estimated from the time the medium has been idle regardless whether the transmitter actually processes a backoff or its queue is empty. The expected queue lengths are calculated based on the effective backoffs. Both the routing and the congestion control problem can be addressed using the expected queue lengths.

The advantage of the bottom-up design is that it does not rely on the adaption of backoff windows or TXOP lengths, which makes it well suited for IEEE 802.11 based systems. According to the discussion within the last paragraph, we suppose that the bottom-up approach has furthermore the better delay performance. Nevertheless, it is still an open problem how the approach can distinguish between outages and empty queues during multi-hop forwarding in fading environments.

Adaption to IEEE 802.11 and TCP/IP. In this thesis, we have presented a clean slate design for CSMA and opportunistic communication in WMNs. Since the design space was limited by neither technological nor architectural constraints, we have been able to focus on the functional dependencies. Nevertheless, compromises have to be made on the way from a research prototype to a production level protocol. In the short term, both IEEE 802.11 on the lower and TCP/IP on the higher layers cannot be replaced. What remains is a solution on *layer 2.5*, which operates in-between the MAC and the network layer. The bottom-up design idea presented in the previous section is one step in this direction. How TCP can be controlled from a lower layer has been illustrated by Radunović *et al.* [218]. The question is which assumptions should be relaxed and what the incurring costs are. For example, IEEE 802.11 does not employ hierarchical busy tones and it remains open to which degree they can be substituted by RTS/CTS and virtual carrier sensing.

Contention Procedures. We suppose that the key to success for UO-CSMA lies within a generalization of the view on contention, which particularly involves two key factors. On the one hand, we have to become aware, reconsider and come up with new *means of contention*. The contention procedures are the building blocks for future WMN protocols. The advances on the physical layer offer opportunities to develop new and innovative contention concepts. We will illustrate this point in the following. On the other hand, we have to reconsider the *granularity of contention*. In particular, we have to become aware of the resources and their respective quantities that we contend for. We will address this issue in the next section.

The vanilla UO-CSMA offers two means of contention [111]. The transmitter may adapt the backoff windows, or it can decide for frame length adaptation. Both approaches are interchangeable in terms of effectiveness, but they differ from each other with respect to the resulting properties of the system. In this thesis, we have considered the adaption of the backoff durations only. The consideration of the TXOP adaptation and mixed strategies [175] is left for future work.

Nowadays, the term carrier sensing refers to several different concepts and technologies. For example, the IEEE 802.11 standard defines several CCA methods. Energy detection is employed in mode 1, whereas mode 2 relies on preamble detection [76]. The standard additionally permits virtual carrier sensing similar to MACA and derivates [17, 73, 131]. Furthermore, out-of-band solutions for carrier sensing in wireless networks have been proposed like BTMA and derivates [90, 263]. Due to its higher reliability and lower complexity, we have used busy tones in the derivation of the CSMA/HBT protocol.

New contention procedures can be developed by reconsidering existing techniques, or they may emerge as a byproduct of revolutionary technological innovations. An example for the former is given by Jose *et al.* They do not think of carrier sensing as a binary decision anymore. Instead, they propose a technique called *measuring* [126]. In contrast to CSMA, it allows for concurrent transmissions in a way that it tries to estimate the available SINR and the remaining power margins. Knowing the instantaneously available SINR budgets, links can contend for these resources in order to pack concurrent transmissions in a spatial more efficient way. On the other hand, the advent of MIMO represents a technological revolution. In general, the state of a MIMO link is no longer binary due to the spatial multiplexing capabilities. Coviello *et al.* propose a CS technique for MIMO networks that tries to estimate the number of simultaneously active data streams [57]. In addition, Qian *et al.* have extended the CSMA model to MIMO links that contend for spatial streams [211].

Due to its asynchronous operation, CSMA is well suited for WMNs. Nevertheless, synchronous contention is also an option. For example, Coupechoux *et al.* have presented a distributed, slotted MAC protocol that uses the Global Positioning System (GPS) for synchronization [56]. Ni *et al.* have shown that the principle of UO-CSMA applies to frame-slotted contention, as well [195, 196].

CSMA tries to arbitrate the access to a shared resource within one round of contention. It fails if either multiple or no contenders survive the contention phase. The failure probability crucially depends on the number of contenders. On the other hand, the well-known binary countdown concept achieves a better scaling behavior with increasing number of participants [256]. The rationale is to use multiple contention

rounds. A fraction of contenders is eliminated in each round. For example, carrier sense multiple access/bitwise arbitration (CSMA/BA) is a binary countdown protocol that is used in the controller area network (CAN) domain. The binary countdown technique has also been discussed in the context of medium access for wireless LANs [2] and in the context of relay self-selection for opportunistic routing [12].

The concept of binary countdown can also be extended to both the time and frequency domain. Recently, Roman *et al.* have proposed a protocol called multi-carrier burst contention (MCBC) [229–231]. It is an efficient contention technique for dense ad-hoc and wireless mesh networks that is based on OFDMA. In particular, the countdown bit vector is mapped onto dedicated contention subcarriers and modulated using on-off keying. If a bit is set, the contender emits a blind energy burst on the corresponding OFDMA subcarrier. Within each round, the protocol eliminates a fraction of the active contenders, resulting in a logarithmic time complexity. A hardware prototype is used to validate the feasibility of MCBC. In addition, Dutta *et al.* present a further hardware prototype for a similar contention method [66].

MCBC operates in a half-duplex manner. One round of contention consists of two time slots. The contention takes place in the first time slot. In the second time slot, idle nodes repeat the received signal that consists of a superposition of contention vectors. In some application domains, however, a full-duplex operation may be possible via additional antennas. For example, Sen *et al.* consider a contention approach similar to MCBC, but they equip each node with two antennas and receive chains [239]. One antenna is used to transmit the contention signals and the second antenna receives the superimposed countdown vectors. The self-interference between both antennas is reduced due to the physical separation between them. As discussed by Radunović *et al.*, interference cancelation techniques in the analogue and digital domain can reduce the self-interference further [219, 221]. Choi *et al.* point out that the concept of destructive signal alignment can be used, in addition, via a dedicated antenna placement [53]. Spreading codes may further improve the detection performance in the presence of strong self-interference [240]. However, the dynamic range of the analog-to-digital converters (ADCs) may still not be large enough to support the full-duplex operation across all necessary transmit power ranges. Thus, these technologies will possibly emerge in the low-power segment first [92]. Nevertheless, it is impressive that hardware prototypes have been presented for all approaches discussed above.

The binary countdown in the frequency domain is appealing for several reasons. First of all, the technique supports an arbitrary contention aggressiveness since the number of rounds is variable. We suppose that increasing the contention aggressiveness will reduce the optimality gap that we have observed in the previous chapters. Furthermore, the contention overhead of the IEEE 802.11 DCF is non-negligible, although the frequency domain is not used at all. Hence, the contention efforts can be balanced between time and frequency domain. In addition, the scaling capabilities of the DCF are limited. In contrast, the binary countdown approach should be able to cope with a large number of contenders due to its logarithmic complexity.

The exchange of contention information can be either implicit or explicit. Carrier sensing is an instance of implicit information exchange, whereas MCBC exchanges the contention information in an explicit way. Furthermore, the contention process can take place either in-band or out-of-band in dedicated channels. Several examples for

the former are given above. In addition, an in-band control channel can also be realized using overlay techniques as proposed by [278]. In this thesis, we have considered a busy-tone based approach, which is an instance of out-of-band channels. Dedicated contention channels are attractive since they generally involve fewer technological constraints reducing the design complexity. Nowadays, the hardware costs of an additional radio are generally low. Nevertheless, the wired backbone may also be a feasible channel for contention depending on the application domain. For example, Hung *et al.* consider the downlink AP scenario, which seems to be perfect for contention on the wired backbone [97, 98].

Contention Granularity. In addition to the contention procedures discussed above, we suppose that the contention granularity is the second key factor in future wireless mesh networks. Using the term granularity, we refer to the resources and their respective quantities that are allocated within the contention process. In an infrastructure IEEE 802.11 network, for example, the contention granularity is a frame duration across the frequency spectrum within the cell. With IEEE 802.11e, the granularity in time has changed to a TXOP. In ad-hoc and wireless mesh networks based on the DCF, on the other hand, the sharp spatial distinction vanishes due to the overlapping collision domains. Exposed nodes are a direct consequence of this design.

We have already given examples for alternative resources to contend for. They can be SINR budgets [126], MIMO spatial streams [211], RF channels [28, 168, 208] and superposition coding opportunities [245]. In the chapters 3 and 4, we have considered hyperlinks and channel states as resources in the contention process.

The frequency resources are particularly appealing within wireless mesh networks for several reasons. First of all, both the PHY and the MAC overhead can be reduced if the channel is additionally shared in the frequency dimension [42, 254]. The capacity of the wireless channel as well as the number of users increases steadily. However, allocating the whole channel to a single user at a time becomes inefficient. The consumed medium time per packet becomes smaller due to the higher capacities, although the fixed overhead like the preamble and backoff duration remains. For example, the efficiency of IEEE 802.11a/g at 54 Mbps with a typical Ethernet maximum transmission unit (MTU) is about 60%. Under the same conditions, the efficiency of IEEE 802.11n drops below 10% at 600 Mbps, i.e. only about 60 out of 600 Mbps remain for the higher layers [254]. Sharing the wireless channel in both time and frequency will help to amortize the fixed overhead of the lower layers in a multi-user system. In addition, it may significantly reduce the medium access delay especially if the user population size is large [168]. Under multi-user communication, a frequency diversity gain can be achieved if the channel variations across both frequency and user dimension are exploited similar to opportunistic scheduling [171]. In particular, Rahul *et al.* have presented a software radio prototype that performs OFDM subcarrier AMC and point-to-multipoint communication in order to benefit from both frequency and multi-user diversity [222].

In a broader sense, the discussion also applies to white spaces in the wireless spectrum. They are licensed frequency resources that are unused or underutilized. For example, the standardization efforts behind IEEE 802.11af target at the TV white spaces.

Similar to the allocation of RF channels mentioned above, contention techniques can help to utilize the white spaces more efficiently.

In addition to the resources itself, their respective quantities within the contention process becomes another degree of freedom. We have already mentioned the introduction of the TXOP concept into IEEE 802.11. In the same way, the contention granularity can be varied across different resource dimensions. The hyperlink approach presented in chapter 3, for example, aggregates multiple wireless links that have the same transmitter. Due to the aggregation, a new communication primitive is introduced at the MAC layer. On the other hand, innovations at the lower layers demand for further levels of granularity. Let us consider the Transmit Diversity based Cooperative Opportunistic Routing (TDiCOR), for example, which is a combined opportunistic and cooperative protocol for WMNs that we have proposed recently [149]. The rationale is that the concurrent transmission of multiple forwarder nodes can be constructive if they share the same data to transmit and apply an appropriate coding and synchronization. A new link layer communication primitive is introduced that coordinates and synchronizes the involved transmitters. Recently, the feasibility has been validated using a hardware prototype [223]. In general, multi-user communication demands for coarser contention granularities in the form of more comprehensive communication primitives. For example, technologies like MIMO, OFDMA and superposition coding benefit from additional nodes on both the transmitter and the receiver side. Thus, a single transaction involves an increased number of nodes and the efficient coordination and synchronization of the participating nodes becomes the main challenge within the MAC design.

In the long term, a question of interest is whether a hierarchical system can be designed that combines both contention and scheduling-based medium access control. The evolution towards the envisioned system is driven by coarser contention granularities: Instead of the contention between individual links, they are aggregated into so-called TDMA clusters. Within each cluster, a highly efficient scheduling algorithm is used. Between clusters, a contention protocol decouples the scheduling domains. Such a hierarchical approach is appealing since it covers both the application domains of cellular as well as ad-hoc and wireless mesh networks. In the discussion above, we have given an overview of how the principle of contention can be generalized. We suppose that both the contention procedures and the contention granularity are the success factors for WMNs to catch up with the speed of innovations that we see on the lower layers.

A. Appendix

A.1. BER Estimation for IEEE 802.11a: Parameters

PHY Bit-Rate	MCS	d_f	$a(d_f)$	$a(d_f+1)$
6 Mbps	BPSK 1/2	10	11	
9 Mbps	BPSK 3/4	5	8	
12 Mbps	QPSK 1/2	10	11	0
18 Mbps	QPSK 3/4	5	8	31
24 Mbps	16-QAM 1/2	10	11	0
36 Mbps	16-QAM 3/4	5	8	31
48 Mbps	64-QAM 2/3	6	1	16
54 Mbps	64-QAM 3/4	5	8	31

A.2. Partial Balance in the Extended CSMA Markov Chain

According to [133, Corollary 9.7], a spatial process is a Markov random field (MRF) if it satisfies the partial balance equations

$$\pi(\boldsymbol{v}) \sum_w q(\boldsymbol{v}, \Theta_l^w \boldsymbol{v}) = \sum_w \pi(\Theta_l^w \boldsymbol{v}) q(\Theta_l^w \boldsymbol{v}, \boldsymbol{v})$$

with state vector $\boldsymbol{v}$, stationary distribution π and transition rates q for each link $l \in G$. The operator Θ_l^w changes the state of link l to w, i.e. the l-th component of the resulting state vector $\boldsymbol{v}' = \Theta_l^w \boldsymbol{v}$ becomes $v_l' = w$. Plugging (3.6) on page 48 into the definition above, we get the following.

$$\begin{aligned}
\frac{\prod_k P(v_k)}{C(\boldsymbol{r})} \sum_w R(v_l, w) &= \sum_w \frac{\prod_k P((\Theta_l^w \boldsymbol{v})_k)}{C(\boldsymbol{r})} R(w, v_l) \\
\prod_k P(v_k) \sum_w R(v_l, w) &= \sum_w \prod_k P((\Theta_l^w \boldsymbol{v})_k) R(w, v_l) \\
P(v_l) \prod_{k \neq l} P(v_k) \sum_w R(v_l, w) &= \sum_w P(w) \prod_{k \neq l} P(v_k) R(w, v_l) \\
P(v_l) \sum_w R(v_l, w) &= \sum_w P(w) R(w, v_l)
\end{aligned}$$

According to the derivation above, the partial balance equation for the truncated Markov chain remains, in which all links except l are frozen. Thus, the CSMA Markov chain (3.6) is a MRF if the truncated Markov process satisfies the partial balance equations.

The conflict relation of link l is determined by one of the conflict types in Figure 3.4. Since only link l remains unfrozen, we can think of the truncation process in the de-

pictured Markov chains as the removal of all other columns except for the column that corresponds to the frozen state of the remaining links. What remains is a Markov chain with either three, two or only one state, and it can be shown that the partial balance holds in all cases. Note that it is important that the truncated Markov chain does not contain a transition from state 2 to 0 if there is no probing state (1). Otherwise the truncated Markov chain would be non-reversible, which means that the unfrozen chain is not an MRF anymore.

A.3. Statistical Entropy of the Extended CSMA Markov Chain

Jiang *et al.* pointed out that directly using the maximum likelihood (ML) estimate leads to non-convexity [112]. Instead, they propose to use the statistical entropy. In the following, we show that this approach is also feasible for our formulation of the extended CSMA model (cf. section 3.2). The statistical entropy is defined as

$$H(\tau, \boldsymbol{r}) = -\sum_l u_l(\tau) \log \frac{u_l(\tau)}{p_l(\boldsymbol{r})}.$$

By using the definition of p_l in (3.6) and $\mu_k^a(\tau) = \sum_l u_l(\tau)\delta_{l,k}^a \ \forall a$, we get

$$\begin{aligned}
H(\tau, \boldsymbol{r}) &= -\sum_l u_l(\tau)[\log(u_l(\tau)) - \log(p_l(\boldsymbol{r}))] \\
&= -\sum_l u_l(\tau)\log(u_l(\tau)) - \log(C(\boldsymbol{r})) \\
&+ \sum_l u_l(\tau) \sum_k \left[\delta_{l,k}^1(r_k - r^s) + \delta_{l,k}^2(r_k - r^l) + \delta_{l,k}^3(r^x - r^s)\right] \\
&= -\sum_l u_l(\tau)\log(u_l(\tau)) - \log(C(\boldsymbol{r})) \\
&+ \sum_k \left[\mu_k^1(\tau)(r_k - r^s) + \mu_k^2(\tau)(r_k - r^l) + \mu_k^3(\tau)(r^x - r^s)\right]
\end{aligned}$$

The UO-CSMA algorithm solves the following optimization problem:

$$\begin{aligned}
&\max_u -\sum_l u_l \log(u_l) \\
&\text{s.t.} \sum_l \delta_{l,k}^a u_l \geq \lambda_k^a, \ \forall k, a \in \{1,2,3\} \\
&u_l \geq 0, \sum_l u_l = 1
\end{aligned}$$

If λ_k^2 is zero, there is no traffic on the link. Hence, it is not necessary to consider the link in the optimization. The partial Lagrangian is

$$\begin{aligned}
\mathcal{L}(\boldsymbol{u}; \boldsymbol{y}) &= -\sum_l u_l \log(u_l) + \sum_{k,a} y_k^a (\sum_l \delta_{l,k}^a u_l - \lambda_k^a) \\
&= -\sum_l u_l \log(u_l) + \sum_{k,a} y_k^a \mu_k^a - \sum_{k,a} y_k^a \lambda_k^a
\end{aligned}$$

The $\boldsymbol{y}$s are dual variables subject to the first constraint. Given $\boldsymbol{r}$, we know that the equilibrium distribution $u_l = p_l(\boldsymbol{r})$ maximizes $H(\tau, \boldsymbol{r})$. However, the equilibrium distribution also maximizes the above Lagrangian with $y_k^1 = r_k - r^s$, $y_k^2 = r_k - r^l$ and $y_k^3 = r^x - r^s$ because the coefficients $\sum_{k,a} y_k^a \lambda_k^a$ and $\log(C(\boldsymbol{r}))$ do not depend on $\boldsymbol{u}$. In particular, both y_k^1 and y_k^2 only depend on r_k and y_k^3 is fixed, which shows that the a priori knowledge of λ_k^3 is not necessary in order to update r_k. The partial derivate of the Lagrangian with respect to r_k is $\partial\mathcal{L}/\partial r_k = \mu_k^1 - \lambda_k^1 + \mu_k^2 - \lambda_k^2$. From the KKT conditions, we know that $\mu_k^2 = \lambda_k^2$ if $y_k^2 > 0$ or, in other words, $r_k > r^l$. In addition, it holds $\mu_k^1 > \lambda_k^1$ iff $\mu_k^2 > \lambda_k^2$ and vice versa for $r_k > r^l$ by construction. Hence, we do not need a priori knowledge of λ_k^1 because $r_k \leftarrow r_k + \alpha[\lambda_k^2 - \mu_k^2]$ is a sub-gradient algorithm to update the dual variables. We conclude that the UO-CSMA algorithm updates the TAs via sub-gradients.

A.4. Anycast Goodput Region with Polynomial Number of Constraints

If we restrict the maximum number of (simultaneous usable) candidates J, we can reduce the number of necessary constraints to describe the anycast goodput region (3.13) to a polynomial number. From the practical point of view, it is often favorable to restrict the number of candidates, because an additional candidate generally causes constant costs for diminishing returns. Let N be the number of neighbors. If we upper bound the number of candidates to a fixed constant C, the number of possible candidate sets is

$$\sum_{c=1}^{C} \binom{N}{c} \leq \sum_{c=1}^{C} N^c \leq CN^C.$$

Hence, the number of candidate sets is polynomial bounded in the number of neighbors up to a degree of C. In this way, the number of necessary equations also reduces to a polynomial number, because all constraints in (3.13) having $|J| > C$ are linearly depending on the set of equations with $|J| \leq C$. To see this, consider the constraint for a fixed candidate set with $|J^\star| > C$. Because the throughput $q_{i,J}$ is zero for all J with $|J| > C$, (3.13) simplifies to

$$\sum_{j \in J^\star} x_{i,j} \leq \sum_{k=1}^{C} \sum_{K \in \mathcal{P}_k(J^\star)} p_{i,K} \cdot R_{i,K} \cdot q_{i,K}, \tag{A.1}$$

where the k-subsets are given by $\mathcal{P}_k$. For reasons of clarity, we denote the PSRs p without superscripts since they coincide with the subscripts. By summing the constraints having exactly C times an "x" on the left-hand side (LHS) over all combinations which contain the nodes $J^\star$, we get

$$\sum_{J \in \mathcal{P}_C(J^\star)} \sum_{j \in J} x_{i,j} \leq \sum_{J \in \mathcal{P}_C(J^\star)} \sum_{K \in \mathcal{P}(J)} p_{i,K} \cdot R_{i,K} \cdot q_{i,K}$$

$$\sum_{j\in J^\star}\binom{|J^\star|-1}{C-1}x_{i,j} \leq \sum_{k=1}^{C}\sum_{K\in\mathcal{P}_k(J^\star)}\binom{|J^\star|-k}{C-k}p_{i,K}\cdot R_{i,K}\cdot q_{i,K}$$

The introduced factor on the LHS corresponds to the number of times the term $x_{i,j}$ appears in the sum. We generate all C-subsets of a set of $|J^\star|$ elements and we are interested in how often a particular term appears. Hence, this corresponds to choosing $C-1$ from $|J^\star|-1$ elements, since we demand that the considered element is already contained. The introduced factor on the RHS can be derived in the same way.

$$\begin{aligned}
\sum_{j\in J^\star} x_{i,j} &\leq \sum_{k=1}^{C}\sum_{K\in\mathcal{P}_k(J^\star)}\binom{|J^\star|-k}{C-k}\binom{|J^\star|-1}{C-1}^{-1}\cdot p_{i,K}\cdot R_{i,K}\cdot q_{i,K}\\
\sum_{j\in J^\star} x_{i,j} &\leq \sum_{k=1}^{C}\sum_{K\in\mathcal{P}_k(J^\star)}\frac{(|J^\star|-k)!(C-1)!}{(|J^\star|-1)!(C-k)!}\cdot p_{i,K}\cdot R_{i,K}\cdot q_{i,K}\\
\sum_{j\in J^\star} x_{i,j} &\leq \sum_{k=1}^{C}\sum_{K\in\mathcal{P}_k(J^\star)}\prod_{l=1}^{k-1}\frac{C-l}{|J^\star|-l}\cdot p_{i,K}\cdot R_{i,K}\cdot q_{i,K} \qquad \text{(A.2)}
\end{aligned}$$

Using the relations $|J^\star| > C$ and $k-1 < C$, the product term on the RHS can be bounded in the following way.

$$0 < \prod_{l=1}^{k-1}\frac{C-l}{|J^\star|-l} \leq 1$$

The upper bound can be plugged into (A.2) in the following way.

$$\sum_{j\in J^\star} x_{i,j} \leq \sum_{k=1}^{C}\sum_{K\in\mathcal{P}_k(J^\star)} 1\cdot p_{i,K}\cdot R_{i,K}\cdot q_{i,K}$$

We conclude that (A.1) is a superset of the given linear combination of C-"x" constraints. Hence, it is sufficient to consider the constraints for candidates set sizes less or equal to C, which is polynomial in the number of neighbors.

A.5. Simultaneously Active Constraints of the Anycast Goodput Region

The anycast capacity region (3.13) is given as

$$\sum_{j\in J} x_{i,j} \leq \sum_{L\in\mathcal{P}(J)}\sum_{K\in\mathcal{P}(N\setminus J)} p_{i,L}^{i,L\cup K}\cdot R_{i,L\cup K}\cdot q_{i,L\cup K},\quad \forall i\in N, \forall J\in\mathcal{P}(N)$$

For the ease of notation, we consider a single bit-rate only, i.e. we substitute $p_{i,L}^{i,L\cup K}\cdot R_{i,L\cup K}$ with $p_{i,L}$. It is straightforward to show that the results apply to multiple bit-rates if the assumptions about diminishing returns are updated accordingly. Further-

more, we drop the index i in the following. Let us associate a Lagrangian multiplier β_J with each constraint. Furthermore, let us assume without loss of generality (WLOG) $x_j > 0$ for all $j \leq j'$ ($j' \geq 1$) and $x_j = 0$ otherwise. The set J' covers all receivers $1, \ldots, j'$. In addition, we assume $p_L > 0$, which means that we consider the neighbors of node i only. The correlation of the PSR across different receivers can be arbitrary. However, the return for another candidate has to be diminishing, but it must remain non-negative. In particular, given p_A and p_B for the non-empty receiver sets A and B, the joint packet success probability must satisfy $\max(p_A, p_B) \leq p_{A\cup B} < p_A + p_B$. Furthermore, given a shared receiver set C, the return of using the additional candidates B together with $A \cup C$ should not exceed the returns of adding B to the smaller set A: $p_{A\cup B\cup C} - p_{A\cup C} \leq p_{B\cup C} - p_C$.

In our CSMA model, the routing layer suggests a set of neighbors as potential forwarding candidates C. The throughput of each used hyperlink $J \in \mathcal{P}(C)$ is positive $q_J > 0$, but possibly arbitrarily small. For all unused hyperlinks having at least one receiver out of $N\backslash C$, the throughput q is zero and the associated constraints β are not considered. This decision is justified in the next paragraph.

We observe that for all $M \not\subseteq J'$, or equally $M : \exists j \in M \wedge x_j = 0$, the TCs β_M are zero. To see this, let us consider the case $M = J \cup \{m\}$ with $J \subseteq J'$ and $m \notin J'$. We assume that constraint β_M is tight and equality holds. By substituting the LHS of β_J in β_M, we get the following.

$$
\begin{aligned}
x_m &\geq \sum_{L\in\mathcal{P}(M)} \sum_{K\in\mathcal{P}(N\backslash M)} p_L q_{L\cup K} - \sum_{L\in\mathcal{P}(J)} \sum_{K\in\mathcal{P}(N\backslash J)} p_L q_{L\cup K} \\
x_m &\geq \sum_{L\in\mathcal{P}(J)} \sum_{K\in\mathcal{P}(N\backslash M)} \left(p_{\{m\}\cup L} - p_L\right) q_{\{m\}\cup L\cup K} \\
x_m &\geq p_m q_m + \sum_{L\in\mathcal{P}(J)\backslash\emptyset} \sum_{K\in\mathcal{P}(N\backslash M)\backslash\emptyset} \left(p_{\{m\}\cup L} - p_L\right) q_{\{m\}\cup L\cup K}
\end{aligned}
$$

The RHS of the above expression is positive since we approach $q_m = 0$ only asymptotically within our CSMA model. Thus, a contradiction is shown and we conclude that the constraint β_M cannot be active.

On the other hand, at least one constraint must be active. Otherwise, we have strict inequality in all constraints. Thus, we can pick one arbitrary hyperlink having $q_J > 0$, and decrease its throughput until the first constraint becomes tight.

We observe that at each *level* $k = |J|$, at most one constraint $\beta_J > 0$ can be active. The observation holds for level j': Only the constraint $\beta_{J'}$ can be active, since all other candidate sets J at level j' contain at least one receiver m with $x_m = 0$, so that β_M cannot be positive. We proceed as follows: We consider level $m < j'$ and assume that there are at least two active constraints β_{M1} and β_{M2} at that level, what should lead to a contradiction. We partition $J' = A \cup B \cup C \cup D$ in a way that $A = M1\backslash M2, B = M2\backslash M1, C = M1 \cap M2, D = J'\backslash M1\backslash M2$. Since both $M1$ and $M2$ are at the same level and it holds $M1 \neq M2$, we know that $A \neq \emptyset$ *and* $B \neq \emptyset$. The summation of both

constraints β_{M1} and β_{M2} that are assumed to be active leads to

$$\sum_{j \in A \cup B \cup C} x_j + \sum_{j \in C} x_j = \sum_{a \in \mathcal{P}(A)} \sum_{b \in \mathcal{P}(B)} \sum_{c \in \mathcal{P}(C)} \sum_{d \in \mathcal{P}(D)} q_{a \cup b \cup c \cup d} (p_{a \cup c} + p_{b \cup c})$$

Now, we consider the sum of the constraints $\beta_{A \cup B \cup C} + \beta_C$. Note that we have to use inequalities because nothing is known about the activity of the involved constraints.

$$\sum_{j \in A \cup B \cup C} x_j + \sum_{j \in C} x_j \leq \sum_{a \in \mathcal{P}(A)} \sum_{b \in \mathcal{P}(B)} \sum_{c \in \mathcal{P}(C)} \sum_{d \in \mathcal{P}(D)} q_{a \cup b \cup c \cup d} (p_{a \cup b \cup c} + p_c)$$

Substituting the LHS with the above derived expression results in

$$0 \leq \sum_{a \in \mathcal{P}(A)} \sum_{b \in \mathcal{P}(B)} \sum_{c \in \mathcal{P}(C)} \sum_{d \in \mathcal{P}(D)} q_{a \cup b \cup c \cup d} \Big[(p_{a \cup b \cup c} - p_{a \cup c}) - (p_{b \cup c} - p_c) \Big] \tag{A.3}$$

The term in squared brackets does not depend on D. It is negative for all $c = \emptyset, a \neq \emptyset, b \neq \emptyset$ and non-positive otherwise due to the assumption about diminishing returns. Since it exists at least one negative term by construction, the RHS of the expression is negative. Thus, the contradiction is shown and we conclude that there can be at most one active constraint per level. On the other hand, this means that *the number of active constraints is bounded above by the number of candidates*.

In addition, we observe that the constraint $\beta_K > 0$ at level k cannot be active if there exists an active constraint $\beta_L > 0$ at level $l < k$ with $L \not\subset K$. To see this, we assume both constraints are active and show the contradiction in the same way as above. The set J' is partitioned according to K and L as above. Note that neither A nor B are empty due to the construction. By summing the constraints $A \cup B \cup C$ and C and subtracting K and L, we get (A.3), as well. Due to our assumption about diminishing returns, the expression in squared brackets is non-positive in general, and negative in the cases $c = \emptyset, a \neq \emptyset, b \neq \emptyset$. Thus, the RHS becomes negative and we conclude that, *if an active constraint $\beta_L > 0$ exists at level l, then at higher levels each active constraint $\beta_K > 0$ contains $K \supset L$.*

A.6. Opportunistic Back-Pressure Routing with Linear Queueing Complexity

In the following, we assume WLOG that the neighbors are sorted according to ascending costs, i.e. it holds $C_j^f \leq C_{j+1}^f$. Using Algorithm 1, the resulting flow rate $\boldsymbol{y}$ and the goodput $\boldsymbol{x}$ maximize the problem (3.14) if the system is in steady state with $\alpha_i^f = C_i^f$ and $\beta_{i,J}^f = TC_{i,j}, J = \{1, \ldots, j\}, C_j^f < C_i^f$ or $\beta_{i,J}^f = 0$ otherwise. Furthermore, $\boldsymbol{\gamma}$ denotes the dual variable for the non-negativity constraint (3.17). We show this point in a way similar to Radunović *et al.* [218]. In particular, the KKT conditions for (3.14) are noted below, and we show that they are satisfied by the proposed approach. As pointed out in the given reference, however, this does not guarantee the existence of the steady state nor the convergence.

$$\sum_j x_{j,i}^f + y^f \, \mathbb{1}(\sigma(f) = i) \leq \sum_j x_{i,j}^f \tag{A.4}$$

$$\sum_{j \in J} x_{i,j}^f \leq \sum_{L \in \mathcal{P}(J)} \sum_{K \in \mathcal{P}(N \setminus J)} p_{i,L}^{i,L \cup K} \cdot R_{i,L \cup K} \cdot q_{i,L \cup K}^f \tag{A.5}$$

$$0 \leq x_{i,j}^f, 0 \leq y^f, 0 \leq q_{i,J}^f, 0 \leq u_l, 0 \leq \alpha_i^f \tag{A.6}$$

$$0 \leq \beta_{i,J}^f \tag{A.7}$$

$$0 \leq \gamma_{i,j}^f \tag{A.8}$$

$$0 = \alpha_i^f \left(\sum_j x_{i,j}^f - \sum_j x_{j,i}^f + y^f \, \mathbb{1}(\sigma(f) = i) \right) \tag{A.9}$$

$$0 = \beta_{i,J}^f \left(\sum_{L \in \mathcal{P}(J)} \sum_{K \in \mathcal{P}(N \setminus J)} p_{i,L}^{i,L \cup K} \cdot R_{i,L \cup K} \cdot q_{i,L \cup K}^f - \sum_{j \in J} x_{i,j}^f \right) \tag{A.10}$$

$$0 = \gamma_{i,j}^f \cdot x_{i,j}^f \tag{A.11}$$

$$\alpha^f = V U'(y^f) \tag{A.12}$$

$$\alpha_i^f + \gamma_{i,j}^f = \alpha_j^f + \sum_{J \ni j} \beta_{i,J}^f \tag{A.13}$$

If the system is in steady state, the conditions (A.4) are satisfied with equality. This means, in turn, conditions (A.9) is satisfied, as well. Furthermore, the throughput, the goodput, and the flow rates are non-negative by construction. Using the proposed approach, the costs $\boldsymbol{C}$ are non-negative. Thus, the conditions (A.6) are satisfied. (A.12) follows from (3.24).

Traffic will be routed along link (i, j) ($x_{j,i}^f > 0$) iff node j is included in the routing decision ($C_j^f < C_i^f$). In this case, we set $\gamma_{i,j}^f = 0$ and conditions (A.8), (A.11) and (A.13) are satisfied. Furthermore, condition (A.7) holds since $\beta_{i,J}^f$ is either zero or equal to $TC_{i,j}$, which is non-negative by construction.

In the case $x_{i,j}^f = 0$, we do not assign credits to the link ($TC_{i,j} = 0$). Thus, it holds $\beta_{i,J}^f = 0 \;\; \forall J \ni j$. We set $\gamma_{i,j}^f = \alpha_j^f + \sum_{J \ni j} \beta_{i,J}^f - \alpha_i^f$. Hence, conditions (A.7), (A.13) (A.11) and (A.8) are satisfied, since it holds $\gamma_{i,j}^f = C_j^f + 0 - C_i^f \geq 0$.

In addition, the condition (A.5) is satisfied due to our steady state assumption. If equality applies, the condition (A.10) is satisfied. If (A.5) is a strict inequality, then we consider the associated dual variable $\beta_{i,J}^f$. If J contains a node m carrying no traffic ($x_{i,m}^f = 0$), then node m does not have lower costs than node i ($C_i^f \leq C_m^f$). According to our construction above, we know that the TCs $\beta_{i,J}^f = 0 \;\; \forall J \ni m$ and (A.10) applies. Otherwise, all nodes $j \in J$ have lower costs than i ($C_j^f < C_i^f$) and carry traffic ($x_{i,j}^f > 0$). If J cannot be written as $J = \{1, 2, \ldots, j\}$ in the notation from above ($C_1^f \leq \ldots \leq C_j^f <$

C_i^f), then $\beta_{i,J}^f = 0$ and condition (A.10) applies. In the remaining case, J can be written as $J = \{1, 2, \ldots, j\}$. Due to the strict inequality in condition (A.5), the goodput supply for these receivers is higher than the demand. Thus, the costs C_j^f will increase. Let $K = J \cup \{j+1, \ldots, k\}$ be the smallest set of receivers containing J, for which $\beta_{i,K}^f > 0$. If no such $\beta_{i,K}^f$ exists, the costs C_j^f will eventually reach C_i^f and no traffic will be allocated to node j ($x_{i,j}^f = 0$). If $\beta_{i,K}^f$ exists, then equality applies to the associated constraint. Hence, C_j^f cannot increase above C_k^f and will settle there, which results in $\beta_{i,J}^f = TC_{i,j} = C_k^f - C_j^f = 0$. We conclude that (A.10) applies in all cases.

Bibliography

[1] E. 3rd Generation Partnership Project (3GPP). Feasibility study for Further Advancements for E-UTRA (LTE-Advanced), 2010.

[2] Z. Abichar and J. M. Chang. A Medium Access Control Scheme for Wireless LANs with Constant-Time Contention. *IEEE Transactions on Mobile Computing*, 10(2), 2011. ISSN 1536-1233. doi: 10.1109/TMC.2010.157.

[3] M. Afanasyev, T. Chen, G. M. Voelker, and A. C. Snoeren. Usage Patterns in an Urban WiFi Network. *IEEE/ACM Transactions on Networking*, 18(5), 2010. ISSN 1063-6692. doi: 10.1109/TNET.2010.2040087.

[4] D. Aguayo, J. Bicket, S. Biswas, G. Judd, and R. Morris. Link-level measurements from an 802.11b mesh network. *ACM SIGCOMM Computer Communication Review*, 34(4), 2004. ISSN 01464833. doi: 10.1145/1030194.1015482.

[5] I. F. Akyildiz and X. Wang. *Wireless mesh networks*. John Wiley and Sons, 2009. ISBN 0470032561.

[6] U. Akyol, M. Andrews, P. Gupta, J. Hobby, I. Saniee, and A. Stolyar. Joint Scheduling and Congestion Control in Mobile Ad-Hoc Networks. In *2008 IEEE INFOCOM - The 27th Conference on Computer Communications*. IEEE, 2008. ISBN 978-1-4244-2026-1. doi: 10.1109/INFOCOM.2008.111.

[7] M. Allman, V. Paxson, and W. Stevens. TCP Congestion Control. RFC 2581 (Proposed Standard), 1999. Obsoleted by RFC 5681, updated by RFC 3390.

[8] M. Ashraf, A. Jayasuriya, and S. Perreau. Channel MAC Protocol for Opportunistic Communication in Ad Hoc Wireless Networks. *EURASIP Journal on Advances in Signal Processing*, 2009, 2009. ISSN 1687-6172. doi: 10.1155/2009/368209.

[9] E. Athanasopoulou, L. Bui, T. Ji, R. Srikant, A. Stoylar, and N. I. May. Backpressure-based Packet-by-Packet Adaptive Routing in Communication Networks, 2010. arXiv:1005.4984.

[10] A. Aziz, D. Starobinski, and P. Thiran. Elucidating the Instability of Random Access Wireless Mesh Networks. In *2009 6th Annual IEEE Communications Society Conference on Sensor, Mesh and Ad Hoc Communications and Networks*. IEEE, 2009. ISBN 978-1-4244-2907-3. doi: 10.1109/SAHCN.2009.5168930.

[11] A. Aziz, D. Starobinski, P. Thiran, and A. El Fawal. EZ-Flow. In *Proceedings of the 5th international conference on Emerging networking experiments and technologies - CoNEXT'09*. ACM Press, 2009. ISBN 9781605586366. doi: 10.1145/1658939.1658948.

[12] F. Baccelli, B. Blaszczyszyn, E. Ermel, and P. Muhlethaler. An optimized relay self selection technique for opportunistic routing in mobile ad hoc networks. In *2008 14th European Wireless Conference*. IEEE, 2008. ISBN 978-3-8007-3102-2. doi: 10.1109/EW.2008.4623843.

[13] F. Baccelli, B. Blaszczyszyn, and P. Muhlethaler. Time-Space Opportunistic Routing in Wireless Ad hoc Networks: Algorithms and Performance Optimization by Stochastic Geometry. *The Computer Journal*, 53(5), 2009. ISSN 0010-4620. doi: 10.1093/comjnl/bxp049.

[14] F. Bai, D. D. Stancil, and H. Krishnan. Toward understanding characteristics of dedicated short range communications (DSRC) from a perspective of vehicular network engineers. In *Proceedings of the sixteenth annual international conference on Mobile computing and networking - MobiCom '10*. ACM Press, 2010. ISBN 9781450301817. doi: 10.1145/1859995.1860033.

[15] R. Barr. *SWANS - Scalable Wireless Ad hoc Network Simulator User Guide*. Cornell University, Ithaca, NY, 2004.

[16] R. Barr, Z. J. Haas, and R. van Renesse. JiST: an efficient approach to simulation using virtual machines. *Software: Practice and Experience*, 35(6), 2005. ISSN 0038-0644. doi: 10.1002/spe.647.

[17] V. Bharghavan, A. Demers, S. Shenker, and L. Zhang. MACAW. In *Proceedings of the conference on Communications architectures, protocols and applications - SIGCOMM '94*. ACM Press, 1994. ISBN 0897916824. doi: 10.1145/190314.190334.

[18] U. N. Bhat. *An Introduction to Queueing Theory: Modeling and Analysis in Applications (Statistics for Industry and Technology)*. Birkhäuser Boston, 1 edition, 2008. ISBN 0817647244.

[19] G. Bianchi, F. Formisano, and D. Giustiniano. 802.11b/g Link Level Measurements for an Outdoor Wireless Campus Network. In *2006 International Symposium on a World of Wireless, Mobile and Multimedia Networks(WoWMoM'06)*. IEEE, 2006. ISBN 0-7695-2593-8. doi: 10.1109/WOWMOM.2006.6.

[20] J. Bicket, D. Aguayo, S. Biswas, and R. Morris. Architecture and evaluation of an unplanned 802.11b mesh network. In *Proceedings of the 11th annual international conference on Mobile computing and networking - MobiCom '05*. ACM Press, 2005. ISBN 1595930205. doi: 10.1145/1080829.1080833.

[21] J. C. Bicket. Bit-rate selection in wireless networks. Master's thesis, Massachusetts Institute of Technology, 2005.

[22] S. Biswas and R. Morris. Opportunistic routing in multi-hop wireless networks. *ACM SIGCOMM Computer Communication Review*, 34(1), 2004. ISSN 01464833. doi: 10.1145/972374.972387.

[23] S. Biswas and R. Morris. ExOR. In *Proceedings of the 2005 conference on Applications, technologies, architectures, and protocols for computer communications -*

SIGCOMM '05, number 4 in 35. ACM Press, 2005. ISBN 1595930094. doi: 10.1145/1080091.1080108.

[24] A. Bletsas, A. Khisti, D. Reed, and A. Lippman. A simple Cooperative diversity method based on network path selection. *IEEE Journal on Selected Areas in Communications*, 24(3), 2006. ISSN 0733-8716. doi: 10.1109/JSAC.2005.862417.

[25] A. Bletsas, H. Shin, and M. Win. Cooperative Communications with Outage-Optimal Opportunistic Relaying. *IEEE Transactions on Wireless Communications*, 6(9), 2007. ISSN 1536-1276. doi: 10.1109/TWC.2007.06020050.

[26] G. Bolch. *Queueing networks and Markov chains: modeling and performance evaluation with computer science applications*. John Wiley and Sons Ltd, 2006. ISBN 9780471565253.

[27] T. Bonald and M. Feuillet. On the stability of flow-aware CSMA. *Performance Evaluation*, 67(11), 2010. ISSN 01665316. doi: 10.1016/j.peva.2010.08.001.

[28] T. Bonald and M. Feuillet. On User-Level CSMA for Multi-Channel Wireless Networks, 2010. arXiv:1011.5317.

[29] V. C. Borges, M. Curado, and E. Monteiro. Cross-layer routing metrics for mesh networks: Current status and research directions. *Computer Communications*, 2010. ISSN 01403664. doi: 10.1016/j.comcom.2010.12.001.

[30] S. Boyd and L. Vandenberghe. *Convex Optimization*. Cambridge University Press, 2004. ISBN 0521833787.

[31] L. Breuer and D. Baum. *An introduction to queueing theory and matrix-analytic methods*. Springer, 2005. ISBN 9781402036309.

[32] R. Bruno, M. Conti, and M. Nurchis. Opportunistic packet scheduling and routing in wireless mesh networks. In *2010 IFIP Wireless Days*, Venice, Italy, 2010. IEEE. ISBN 978-1-4244-9230-5. doi: 10.1109/WD.2010.5657736.

[33] L. Bui, R. Srikant, and A. Stolyar. Novel Architectures and Algorithms for Delay Reduction in Back-Pressure Scheduling and Routing. In *IEEE INFOCOM 2009 - The 28th Conference on Computer Communications*. IEEE, 2009. ISBN 978-1-4244-3512-8. doi: 10.1109/INFCOM.2009.5062262.

[34] F. Buschmann, R. Meunier, H. Rohnert, and P. Sommerlad. *A System of Patterns: Pattern-Oriented Software Architecture*. John Wiley & Sons, 2001. ISBN 978-0471958697.

[35] A. S. Cacciapuoti, M. Caleffi, and L. Paura. Optimal Constrained Candidate Selection for Opportunistic Routing. In *2010 IEEE Global Telecommunications Conference GLOBECOM 2010*, Miami, FL, 2010. IEEE. ISBN 978-1-4244-5636-9. doi: 10.1109/GLOCOM.2010.5683490.

[36] J. Camp and E. Knightly. Modulation rate adaptation in urban and vehicular environments. In *Proceedings of the 14th ACM international conference on Mobile computing and networking - MobiCom '08*. ACM Press, 2008. ISBN 9781605580968. doi: 10.1145/1409944.1409981.

[37] M. Carroll and T. Wysocki. Fading characteristics for indoor wireless channels at 5 GHz unlicensed bands. In *SympoTIC'03. Joint 1st Workshop on Mobile Future and Symposium on Trends in Communications*. IEEE, 2003. ISBN 0-7803-7993-4. doi: 10.1109/TIC.2003.1249099.

[38] a. Caruso, S. Chessa, S. De, and A. Urpi. GPS free coordinate assignment and routing in wireless sensor networks. In *Proceedings IEEE 24th Annual Joint Conference of the IEEE Computer and Communications Societies.* IEEE, 2005. ISBN 0-7803-8968-9. doi: 10.1109/INFCOM.2005.1497887.

[39] V. Cerf and R. Kahn. A Protocol for Packet Network Intercommunication. *IEEE Transactions on Communications*, 22(5), 1974. ISSN 0096-2244. doi: 10.1109/TCOM.1974.1092259.

[40] V. G. Cerf and E. Cain. The DoD internet architecture model. *Computer Networks (1976)*, 7(5), 1983. ISSN 03765075. doi: 10.1016/0376-5075(83)90042-9.

[41] S. Chachulski, M. Jennings, S. Katti, and D. Katabi. Trading structure for randomness in wireless opportunistic routing. *ACM SIGCOMM Computer Communication Review*, 37(4), 2007. ISSN 01464833. doi: 10.1145/1282427.1282400.

[42] R. Chandra, R. Mahajan, T. Moscibroda, R. Raghavendra, and P. Bahl. A case for adapting channel width in wireless networks. *ACM SIGCOMM Computer Communication Review*, 38(4), 2008. ISSN 01464833. doi: 10.1145/1402946.1402975.

[43] H. Chang, V. Misra, and D. Rubenstein. Fairness and Physical Layer Capture in Random Access Networks. In *2007 4th Annual IEEE Communications Society Conference on Sensor, Mesh and Ad Hoc Communications and Networks*. IEEE, 2007. ISBN 1-4244-1268-4. doi: 10.1109/SAHCN.2007.4292850.

[44] N. B. Chang and M. Liu. Optimal channel probing and transmission scheduling for opportunistic spectrum access. In *Proceedings of the 13th annual ACM international conference on Mobile computing and networking - MobiCom '07*. ACM Press, 2007. ISBN 9781595936813. doi: 10.1145/1287853.1287858.

[45] P. Chaporkar, A. Proutière, H. Asnani, and A. Karandikar. Scheduling with limited information in wireless systems. In *Proceedings of the tenth ACM international symposium on Mobile ad hoc networking and computing - MobiHoc '09*. ACM Press, 2009. ISBN 9781605585314. doi: 10.1145/1530748.1530759.

[46] C.-K. Chau, M. Chen, and S. C. Liew. Capacity of large-scale CSMA wireless networks. In *Proceedings of the 15th annual international conference on Mobile computing and networking - MobiCom '09*. ACM Press, 2009. ISBN 9781605587028. doi: 10.1145/1614320.1614332.

[47] K. Chebrolu, B. Raman, and S. Sen. Long-distance 802.11b links. In *Proceedings of the 12th annual international conference on Mobile computing and networking - MobiCom '06*. ACM Press, 2006. ISBN 1595932860. doi: 10.1145/1161089.1161099.

[48] L. Chen, S. H. Low, M. Chiang, and J. C. Doyle. Cross-Layer Congestion Control, Routing and Scheduling Design in Ad Hoc Wireless Networks. In *Proceedings IEEE INFOCOM 2006. 25TH IEEE International Conference on Computer Communications*. IEEE, 2006. ISBN 1-4244-0221-2. doi: 10.1109/INFOCOM.2006.142.

[49] L. Chen, S. H. Low, and J. C. Doyle. Cross-layer design in multihop wireless networks. *Computer Networks*, 55(2), 2011. ISSN 13891286. doi: 10.1016/j.comnet.2010.09.005.

[50] W. Chen, Y. Wang, M. Chen, and S. C. Liew. TCP over Adaptive CSMA, 2010. arXiv:1007.5239.

[51] L. Cheng, B. Henty, R. Cooper, D. Stancil, and F. Bai. A Measurement Study of Time-Scaled 802.11a Waveforms Over The Mobile-to-Mobile Vehicular Channel at 5.9 GHz. *IEEE Communications Magazine*, 46(5), 2008. ISSN 0163-6804. doi: 10.1109/MCOM.2008.4511654.

[52] M. Chiang, S. H. Low, A. R. Calderbank, and J. C. Doyle. Layering as Optimization Decomposition: A Mathematical Theory of Network Architectures. *Proceedings of the IEEE*, 95(1), 2007. ISSN 0018-9219. doi: 10.1109/JPROC.2006.887322.

[53] J. I. Choi, M. Jain, K. Srinivasan, P. Levis, and S. Katti. Achieving single channel, full duplex wireless communication. In *Proceedings of the sixteenth annual international conference on Mobile computing and networking - MobiCom '10*. ACM Press, 2010. ISBN 9781450301817. doi: 10.1145/1859995.1859997.

[54] T. Clausen and P. Jacquet. Optimized Link State Routing Protocol (OLSR). RFC 3626 (Experimental), 2003.

[55] T. Clausen, C. Dearlove, and J. Dean. Mobile Ad Hoc Network (MANET) Neighborhood Discovery Protocol (NHDP), 2010.

[56] M. Coupechoux, B. Baynat, C. Bonnet, and V. Kumar. CROMA - An Enhanced Slotted MAC Protocol for MANETs. *Mobile Networks and Applications*, 10(1/2), 2005. ISSN 1383-469X. doi: 10.1023/B:MONE.0000048554.50262.c1.

[57] E. Coviello, A. Bhorkar, F. Rossetto, B. D. Rao, and M. Zorzi. A Robust Approach to Carrier Sense for MIMO Ad Hoc Networks. In *2009 IEEE International Conference on Communications*. IEEE, 2009. doi: 10.1109/ICC.2009.5198664.

[58] D. S. J. De Couto, D. Aguayo, J. Bicket, and R. Morris. A high-throughput path metric for multi-hop wireless routing. In *Proceedings of the 9th annual international conference on Mobile computing and networking - MobiCom '03*. ACM Press, 2003. ISBN 1581137532. doi: 10.1145/938985.939000.

[59] R. de Francisco. Indoor Channel Measurements and Models at 2.4 GHz in a Hospital. In *2010 IEEE Global Telecommunications Conference GLOBECOM 2010*, Miami, FL, 2010. IEEE. ISBN 978-1-4244-5636-9. doi: 10.1109/GLOCOM.2010.5683218.

[60] D. S. J. DeCouto. *High-Throughput Routing for Multi-Hop Wireless Networks*. PhD thesis, Massachusetts Institute of Technology, 2004.

[61] M. Dohler, R. W. Heath Jr, A. Lozano, C. Papadias, and R. A. Valenzuela. Is the PHY Layer Dead? *Communications Magazine, IEEE*, 49(4), 2011. ISSN 0163-6804. doi: 10.1109/MCOM.2011.5741160.

[62] R. Draves, J. Padhye, and B. Zill. Routing in multi-radio, multi-hop wireless mesh networks. In *Proceedings of the 10th annual international conference on Mobile computing and networking - MobiCom '04*. ACM Press, 2004. ISBN 1581138687. doi: 10.1145/1023720.1023732.

[63] H. Dubois-Ferriere, M. Grossglauser, and M. Vetterli. Least-Cost Opportunistic Routing. In *Allerton Conference on Communication, Control, and Computing*, Monticello, IL, 2007.

[64] H. Dubois-Ferriere, M. Grossglauser, and M. Vetterli. Valuable Detours: Least-Cost Anypath Routing. *IEEE/ACM Transactions on Networking*, 2010. ISSN 1063-6692. doi: 10.1109/TNET.2010.2070844.

[65] M. Durvy. *Modelling the IEEE 802.11 protocol in wireless multi-hop networks*. PhD thesis, École polytechnique fédérale de Lausanne, 2007.

[66] A. Dutta, D. Saha, D. Grunwald, and D. Sicker. SMACK. *ACM SIGCOMM Computer Communication Review*, 39(4), 2009. ISSN 01464833. doi: 10.1145/1594977.1592572.

[67] J. Eriksson, M. Faloutsos, and S. V. Krishnamurthy. DART: Dynamic Address RouTing for Scalable Ad Hoc and Mesh Networks. *IEEE/ACM Transactions on Networking*, 15(1), 2007. ISSN 1063-6692. doi: 10.1109/TNET.2006.890092.

[68] A. Eryilmaz and R. Srikant. Joint congestion control, routing, and MAC for stability and fairness in wireless networks. *IEEE Journal on Selected Areas in Communications*, 24(8), 2006. ISSN 0733-8716. doi: 10.1109/JSAC.2006.879361.

[69] A. Eryilmaz and R. Srikant. Fair Resource Allocation in Wireless Networks Using Queue-Length-Based Scheduling and Congestion Control. *IEEE/ACM Transactions on Networking*, 15(6), 2007. ISSN 1063-6692. doi: 10.1109/TNET.2007.897944.

[70] A. Eryilmaz, P. Marbach, and A. Ozdaglar. A Fluid-Flow Model for Backlog-Based CSMA Policies. In *International Conference on Wireless Internet*, 2008. doi: 10.1145/1554126.1554222.

[71] Z. Fu, P. Zerfos, H. Luo, S. Lu, L. Zhang, and M. Gerla. The impact of multihop wireless channel on TCP throughput and loss. In *IEEE INFOCOM 2003. Twenty-second Annual Joint Conference of the IEEE Computer and Communications Societies (IEEE Cat. No.03CH37428)*, volume 3. IEEE, 2003. ISBN 0-7803-7752-4. doi: 10.1109/INFCOM.2003.1209197.

[72] T. Fuhrmann. A Self-organizing Routing Scheme for Random Networks. *IFIP International Federation For Information Processing*, 2005. doi: 10.1007/11422778_116.

[73] C. L. Fullmer and J. J. Garcia-Luna-Aceves. Floor acquisition multiple access (FAMA) for packet-radio networks. *ACM SIGCOMM Computer Communication Review*, 25(4), 1995. ISSN 01464833. doi: 10.1145/217391.217458.

[74] V. Gambiroza and E. W. Knightly. Congestion control in CSMA-based networks with inconsistent channel state. In *Proceedings of the 2nd annual international workshop on Wireless internet - WICON '06*. ACM Press, 2006. ISBN 159593510X. doi: 10.1145/1234161.1234169.

[75] M. Garetto, T. Salonidis, and E. W. Knightly. Modeling Per-Flow Throughput and Capturing Starvation in CSMA Multi-Hop Wireless Networks. In *Proceedings IEEE INFOCOM 2006. 25TH IEEE International Conference on Computer Communications*. IEEE, 2006. ISBN 1-4244-0221-2. doi: 10.1109/INFOCOM.2006.194.

[76] M. Gast. *802.11 Wireless Networks: The Definitive Guide, Second Edition (Definitive Guide)*. O'Reilly Media, Inc., 2005. ISBN 0596100523.

[77] W. Ge, J. Zhang, J. Wieselthier, and X. Shen. PHY-aware distributed scheduling for ad hoc communications with physical interference model. *IEEE Transactions on Wireless Communications*, 8(5), 2009. ISSN 1536-1276. doi: 10.1109/TWC.2008.080798.

[78] L. Georgiadis, M. J. Neely, and L. Tassiulas. Resource Allocation and Cross-Layer Control in Wireless Networks. *Foundations and Trends in Networking*, 1(1), 2005. ISSN 1554-057X. doi: 10.1561/1300000001.

[79] J. Ghaderi and R. Srikant. On the design of efficient CSMA algorithms for wireless networks. In *49th IEEE Conference on Decision and Control (CDC)*. IEEE, 2010. ISBN 978-1-4244-7745-6. doi: 10.1109/CDC.2010.5717965.

[80] B. Ghimire, G. Auer, and H. Haas. Busy Bursts for Trading off Throughput and Fairness in Cellular OFDMA-TDD. *EURASIP Journal on Wireless Communications and Networking*, 2009, 2009. ISSN 1687-1472. doi: 10.1155/2009/462396.

[81] P. Giaccone, E. Leonardi, and D. Shah. Throughput Region of Finite-Buffered Networks. *IEEE Transactions on Parallel and Distributed Systems*, 18(2), 2007. ISSN 1045-9219. doi: 10.1109/TPDS.2007.30.

[82] C. Gkantsidis, W. Hu, P. Key, B. Radunović, P. Rodriguez, and S. Gheorghiu. Multipath code casting for wireless mesh networks. In *Proceedings of the 2007 ACM*

CoNEXT conference on - CoNEXT '07. ACM Press, 2007. ISBN 9781595937704. doi: 10.1145/1364654.1364667.

[83] D. Gokhale, S. Sen, K. Chebrolu, and B. Raman. On the Feasibility of the Link Abstraction in (Rural) Mesh Networks. In *2008 IEEE INFOCOM - The 27th Conference on Computer Communications*. IEEE, 2008. ISBN 978-1-4244-2026-1. doi: 10.1109/INFOCOM.2008.21.

[84] A. Goldsmith. *Wireless Communications*. Cambridge University Press, 2005. ISBN 0521837162.

[85] G. R. Gupta and N. Shroff. Delay Analysis for Multi-Hop Wireless Networks. In *IEEE INFOCOM 2009 - The 28th Conference on Computer Communications*. IEEE, 2009. ISBN 978-1-4244-3512-8. doi: 10.1109/INFCOM.2009.5062162.

[86] G. R. Gupta and N. B. Shroff. Delay Analysis for Wireless Networks with Single Hop Traffic and General Interference Constraints. *IEEE/ACM Transactions on Networking*, 18(2), 2010. ISSN 1063-6692. doi: 10.1109/TNET.2009.2032181.

[87] P. Gupta and T. Javidi. Towards Throughput and Delay Optimal Routing for Wireless Ad-Hoc Networks. In *2007 Conference Record of the Forty-First Asilomar Conference on Signals, Systems and Computers*. IEEE, 2007. ISBN 978-1-4244-2109-1. doi: 10.1109/ACSSC.2007.4487207.

[88] P. Gupta and A. Stolyar. Optimal Throughput Allocation in General Random-Access Networks. In *2006 40th Annual Conference on Information Sciences and Systems*. IEEE, 2006. ISBN 1-4244-0350-2. doi: 10.1109/CISS.2006.286657.

[89] Z. Haas. A new routing protocol for the reconfigurable wireless networks. In *Proceedings of ICUPC 97 - 6th International Conference on Universal Personal Communications*. IEEE, 1997. ISBN 0-7803-3777-8. doi: 10.1109/ICUPC.1997.627227.

[90] Z. Haas and J. Deng. Dual busy tone multiple access (DBTMA)-a multiple access control scheme for ad hoc networks. *IEEE Transactions on Communications*, 50(6), 2002. ISSN 0090-6778. doi: 10.1109/TCOMM.2002.1010617.

[91] A. Hac. *Mobile Telecommunications Protocols for Data Networks*. Wiley, 2003. ISBN 0470850566.

[92] D. Halperin, T. Anderson, and D. Wetherall. Taking the sting out of carrier sense. In *Proceedings of the 14th ACM international conference on Mobile computing and networking - MobiCom '08*. ACM Press, 2008. ISBN 9781605580968. doi: 10.1145/1409944.1409983.

[93] D. Halperin, W. Hu, A. Sheth, and D. Wetherall. Predictable 802.11 packet delivery from wireless channel measurements. In *Proceedings of the ACM SIGCOMM 2010 conference on SIGCOMM - SIGCOMM '10*. ACM Press, 2010. ISBN 9781450302012. doi: 10.1145/1851182.1851203.

[94] B. Han, A. Schulman, F. Gringoli, N. Spring, B. Bhattacharjee, L. Nava, L. Ji, S. Lee, and R. Miller. Maranello: Practical Partial Packet Recovery for 802.11. In *USENIX Symposium on Networked Systems Design and Implementation (NSDI)*, 2010.

[95] G. Holland, N. Vaidya, and P. Bahl. A rate-adaptive MAC protocol for multi-Hop wireless networks. In *Proceedings of the 7th annual international conference on Mobile computing and networking - MobiCom '01*. ACM Press, 2001. ISBN 1581134223. doi: 10.1145/381677.381700.

[96] F.-Y. Hung and I. Marsic. Performance analysis of the IEEE 802.11 DCF in the presence of the hidden stations. *Computer Networks*, 54(15), 2010. ISSN 13891286. doi: 10.1016/j.comnet.2010.04.015.

[97] K.-L. Hung and B. Bensaou. Throughput analysis and rate control for IEEE 802.11 Wireless LAN with hidden terminals. In *Proceedings of the 11th international symposium on Modeling, analysis and simulation of wireless and mobile systems - MSWiM '08*. ACM Press, 2008. ISBN 9781605582351. doi: 10.1145/1454503.1454530.

[98] K.-l. Hung and B. Bensaou. Distributed rate control and contention resolution in multi-cell IEEE 802.11 WLANs with hidden terminals. In *Proceedings of the eleventh ACM international symposium on Mobile ad hoc networking and computing - MobiHoc '10*. ACM Press, 2010. ISBN 9781450301831. doi: 10.1145/1860093.1860101.

[99] P. J. Husted and W. J. McFarland. Method and system for noise floor calibration and receive signal strength detection, 2002. United States Patent 7245893.

[100] C.-s. Hwang and J. M. Cioffi. Using Opportunistic CSMA/CA to Achieve Multi-User Diversity in Wireless LAN. In *IEEE GLOBECOM 2007-2007 IEEE Global Telecommunications Conference*. IEEE, 2007. ISBN 978-1-4244-1042-2. doi: 10.1109/GLOCOM.2007.939.

[101] C.-s. Hwang, K. Seong, and J. Cioffi. Opportunistic p-persistent CSMA in wireless networks. In *2006 IEEE International Conference on Communications*. IEEE, 2006. ISBN 1-4244-0354-5. doi: 10.1109/ICC.2006.254725.

[102] IEEE 802 LAN/MAN Standards Committee. Wireless LAN Medium Access Control (MAC) and Physical Layer (PHY) Specifications. IEEE Standard 802.11, 1999.

[103] IEEE 802 LAN/MAN Standards Committee. Wireless LAN Medium Access Control (MAC) and Physical Layer (PHY) Specifications Amendment 8: Medium Access Control (MAC) Quality of Service Enhancements, 2005.

[104] IEEE 802 LAN/MAN Standards Committee. Wireless LAN Medium Access Control (MAC) and Physical Layer (PHY) Specifications Amendment: ESS Mesh Networking (Draft), 2006.

[105] IEEE 802 LAN/MAN Standards Committee. Wireless LAN Medium Access Control (MAC) and Physical Layer (PHY) Specifications Amendment 5: Enhancements for Higher Throughput, 2009.

[106] P. Jacquet, P. Muhlethaler, T. Clausen, A. Laouiti, A. Qayyum, and L. Viennot. Optimized link state routing protocol for ad hoc networks. In *Proceedings. IEEE International Multi Topic Conference, 2001. IEEE INMIC 2001. Technology for the 21st Century.* IEEE, 2001. ISBN 0-7803-7406-1. doi: 10.1109/INMIC.2001.995315.

[107] R. Jain, K. K. Ramakrishnan, and D.-M. Chiu. *Congestion avoidance in computer networks with a connectionless network layer*, chapter 12. Artech House, 1988. ISBN 0890063370.

[108] K. Jamieson and H. Balakrishnan. PPR. In *ACM SIGCOMM Computer Communication Review*, number 4 in 37. Massachusetts Institute of Technology Computer Science and Artificial Intelligence Laboratory, 2007. doi: 10.1145/1282427.1282426.

[109] B. Ji, C. Joo, and N. B. Shroff. Delay-Based Back-Pressure Scheduling in Multi-Hop Wireless Networks. INFOCOM 2011 (to appear), 2010. arXiv:1011.5674.

[110] Z. Ji, Y. Yang, J. Zhou, M. Takai, and R. Bagrodia. Exploiting medium access diversity in rate adaptive wireless LANs. In *Proceedings of the 10th annual international conference on Mobile computing and networking - MobiCom '04*. ACM Press, 2004. ISBN 1581138687. doi: 10.1145/1023720.1023754.

[111] L. Jiang. *Optimization and Incentives in Communication Networks*. PhD thesis, University of California, Berkeley, 2009.

[112] L. Jiang and J. Walrand. A Distributed Algorithm for Optimal Throughput and Fairness in Wireless Networks with a General Interference Model. In *Allerton Conference on Communication, Control, and Computing*, 2008.

[113] L. Jiang and J. Walrand. Approaching Throughput-optimality in a Distributed CSMA Algorithm with Contention Resolution. Technical Report EECS-2009-37, Electrical Engineering and Computer Sciences, University of California at Berkeley, CA, 2009.

[114] L. Jiang and J. Walrand. Approaching throughput-optimality in a distributed CSMA algorithm. In *Proceedings of the 2009 MobiHoc S3 workshop on MobiHoc S3 - MobiHoc S3 '09*. ACM Press, 2009. ISBN 9781605585215. doi: 10.1145/1540358.1540361.

[115] L. Jiang and J. Walrand. Convergence and Stability of a Distributed CSMA Algorithm for Maximal Network Throughput. Technical Report EECS-2009-43, Electrical Engineering and Computer Sciences, University of California at Berkeley, CA, 2009.

[116] L. Jiang and J. Walrand. A Novel Approach to Model Control Throughput CSMA/CA Wireless Networks. Technical Report EECS-2009-8, Electrical Engineering and Computer Sciences, University of California at Berkeley, CA, 2009.

[117] L. Jiang and J. Walrand. Approaching Throughput-Optimality in Distributed CSMA Scheduling Algorithms with Collisions. *IEEE/ACM Transactions on Networking*, 2010. ISSN 1063-6692. doi: 10.1109/TNET.2010.2089804.

[118] L. Jiang and J. Walrand. A Distributed CSMA Algorithm for Throughput and Utility Maximization in Wireless Networks. *IEEE/ACM Transactions on Networking*, 18(3), 2010. ISSN 1063-6692. doi: 10.1109/TNET.2009.2035046.

[119] L. Jiang, M. Leconte, J. Ni, R. Srikant, and J. Walrand. Fast Mixing of Parallel Glauber Dynamics and Low-Delay CSMA Scheduling, 2010. arXiv:1008.0227.

[120] L. Jiang, J. Ni, R. Srikant, and J. Walrand. Performance bounds of distributed CSMA scheduling. In *2010 Information Theory and Applications Workshop (ITA)*. IEEE, 2010. ISBN 978-1-4244-7012-9. doi: 10.1109/ITA.2010.5454123.

[121] L. Jiang, D. Shah, J. Shin, and J. Walrand. Distributed Random Access Algorithm: Scheduling and Congestion Control. *IEEE Transactions on Information Theory*, 56 (12), 2010. ISSN 0018-9448. doi: 10.1109/TIT.2010.2081490.

[122] L. B. Jiang and S. C. Liew. Improving Throughput and Fairness by Reducing Exposed and Hidden Nodes in 802.11 Networks. *IEEE Transactions on Mobile Computing*, 7(1), 2008. ISSN 1536-1233. doi: 10.1109/TMC.2007.1070.

[123] D. Johnson, Y. Hu, and D. Maltz. The Dynamic Source Routing Protocol (DSR) for Mobile Ad Hoc Networks for IPv4. RFC 4728 (Experimental), 2007.

[124] D. B. Johnson and D. A. Maltz. Dynamic Source Routing in Ad Hoc Wireless Networks. *Mobile Computing*, 353, 1996. doi: 10.1007/978-0-585-29603-6_5.

[125] C. Joo, G. Sharma, N. B. Shroff, and R. R. Mazumdar. On the Complexity of Scheduling in Wireless Networks. *EURASIP Journal on Wireless Communications and Networking*, 2010, 2010. ISSN 1687-1472. doi: 10.1155/2010/418934.

[126] J. Jose and S. Vishwanath. Distributed Rate Allocation for Wireless Networks, 2010. arXiv:1002.2813.

[127] C. H. Kai and S. C. Liew. Temporal Starvation in CSMA Wireless Networks, 2010. arXiv:1009.3415.

[128] A. Kamerman and L. Monteban. WaveLAN-II: a high-performance wireless LAN for the unlicensed band. *Bell Labs Technical Journal*, 2(3), 2002. ISSN 10897089. doi: 10.1002/bltj.2069.

[129] V. Kanodia, A. Sabharwal, and E. Knightly. MOAR: a multi-channel opportunistic auto-rate media access protocol for ad hoc networks. In *First International Conference on Broadband Networks*. IEEE Comput. Soc, 2004. ISBN 0-7695-2221-1. doi: 10.1109/BROADNETS.2004.46.

[130] H. Karl and A. Willig. *Protocols and Architectures for Wireless Sensor Networks*. John Wiley & Sons, 2005. ISBN 0470095105.

[131] P. Karn. MACA - a new channel access method for packet radio. In *ARRL/CRRL Amateur Radio 9th Computer Networking Conference*, 1990.

[132] B. Karp and H. T. Kung. GPSR. In *Proceedings of the 6th annual international conference on Mobile computing and networking - MobiCom '00*. ACM Press, 2000. ISBN 1581131976. doi: 10.1145/345910.345953.

[133] F. P. Kelly. *Reversibility and Stochastic Networks (Probability & Mathematical Statistics)*. John Wiley and Sons Ltd, 1979. ISBN 0471276014.

[134] F. P. Kelly, A. K. Maulloo, and D. K. H. Tan. Rate Control for Communication Networks: Shadow Prices, Proportional Fairness and Stability. *The Journal of the Operational Research Society*, 49(3), 1998. ISSN 01605682. doi: 10.2307/3010473.

[135] K.-H. Kim and K. G. Shin. On accurate measurement of link quality in multi-hop wireless mesh networks. In *Proceedings of the 12th annual international conference on Mobile computing and networking - MobiCom '06*. ACM Press, 2006. ISBN 1595932860. doi: 10.1145/1161089.1161095.

[136] T. H. Kim, J. Ni, R. Srikant, and N. H. Vaidya. On the Achievable Throughput of CSMA under Imperfect Carrier Sensing. Technical report, Coordinated Science Laboratory, University of Illinois at Urbana-Champaign, IL, 2010.

[137] T. H. Kim, J. Ni, and N. H. Vaidya. A Distributed Throughput-Optimal CSMA/CA. Technical report, Coordinated Science Laboratory, University of Illinois at Urbana-Champaign, IL, 2010.

[138] T. H. Kim, J. Ni, and N. H. Vaidya. A Distributed Throughput-Optimal CSMA with Data Packet Collisions. In *2010 Fifth IEEE Workshop on Wireless Mesh Networks*. IEEE, 2010. ISBN 978-1-4244-7975-7. doi: 10.1109/WIMESH.2010.5507899.

[139] T. H. Kim, J. Ni, R. Srikant, and N. H. Vaidya. On the Achievable Throughput of CSMA under Imperfect Carrier Sensing. In *INFOCOM*, 2011.

[140] L. Kleinrock and F. Tobagi. Packet Switching in Radio Channels: Part I–Carrier Sense Multiple-Access Modes and Their Throughput-Delay Characteristics. *IEEE Transactions on Communications*, 23(12), 1975. ISSN 0096-2244. doi: 10.1109/TCOM.1975.1092768.

[141] R. Knopp and P. Humblet. Information capacity and power control in single-cell multiuser communications. In *Proceedings IEEE International Conference on Communications ICC '95*, volume 1. IEEE, 1995. ISBN 0-7803-2486-2. doi: 10.1109/ICC.1995.525188.

[142] A. Köpke, M. Swigulski, K. Wessel, D. Willkomm, P. T. Klein Haneveld, T. E. V. Parker, O. W. Visser, H. S. Lichte, and S. Valentin. Simulating Wireless and Mobile Networks in OMNeT++ The MiXiM Vision. In *Simulation tools and techniques for communications, networks and systems & workshops (SIMUTools)*, Marseille, France, 2008. Icst. doi: 10.4108/ICST.SIMUTOOLS2008.3031.

[143] K. Kosek-Szott, M. Natkaniec, and A. R. Pach. BusySiMOn - A New Protocol for IEEE 802.11 EDCA-Based Ad-Hoc Networks with Hidden Nodes. In *2010 IEEE Global Telecommunications Conference GLOBECOM 2010*, Miami, FL, 2010. IEEE. ISBN 978-1-4244-5636-9. doi: 10.1109/GLOCOM.2010.5684277.

[144] M. Kurth. Carrier sensing and receiver performance in indoor IEEE 802.11b mesh networks. Technical Report SAR-PR-2008-22, Systems Architecture Group, Computer Science Department, Humboldt University Berlin, DE, 2009.

[145] M. Kurth and J.-P. Redlich. Carrier sensing and receiver performance in indoor IEEE 802.11b mesh networks. In *Proceedings of the 2009 International Conference on Wireless Communications and Mobile Computing Connecting the World Wirelessly - IWCMC '09*. ACM Press, 2009. ISBN 9781605585697. doi: 10.1145/1582379.1582537.

[146] M. Kurth and J.-P. Redlich. Delay properties of opportunistic back-pressure routing in CSMA-based wireless mesh networks. In *2010 IEEE 21st International Symposium on Personal, Indoor and Mobile Radio Communications Workshops*, 2010. ISBN 978-1-4244-9117-9. doi: 10.1109/PIMRCW.2010.5670525.

[147] M. Kurth and J.-P. Redlich. Opportunistic Routing with Adaptive CSMA/CA in Wireless Mesh Networks. In *2010 IEEE Global Telecommunications Conference GLOBECOM 2010*, 2010. ISBN 978-1-4244-5636-9. doi: 10.1109/GLOCOM.2010.5683520.

[148] M. Kurth and J.-P. Redlich. The Efficiency-Collision Tradeoff with Adaptive CSMA/CA in Wireless Mesh Networks. In *Proceedings of the 2011 International Conference on Wireless Communications and Mobile Computing Connecting the World Wirelessly - IWCMC '11*, 2011.

[149] M. Kurth, A. Zubow, and J.-P. Redlich. Cooperative Opportunistic Routing Using Transmit Diversity in Wireless Mesh Networks. In *2008 IEEE INFOCOM - The 27th Conference on Computer Communications*. IEEE, 2008. ISBN 978-1-4244-2026-1. doi: 10.1109/INFOCOM.2008.188.

[150] M. Kurth, U. Hermann, A. Zubow, and J.-P. Redlich. Network Coding for Bit Error Recovery in IEEE 802.11 Mesh Networks. In *2009 IEEE International Conference on Communications*, Dresden, Germany, 2009. IEEE. doi: 10.1109/ICC.2009.5199218.

[151] P. Kyasanur, J. Padhye, and P. Bahl. On the efficacy of separating control and data into different frequency bands. In *2nd International Conference on Broadband Networks, 2005.* IEEE, 2005. ISBN 0-7803-9276-0. doi: 10.1109/ICBN.2005.1589665.

[152] M. Lacage and T. R. Henderson. Yet another network simulator. In *Proceeding from the 2006 workshop on ns-2: the IP network simulator - WNS2 '06*. ACM Press, 2006. ISBN 1595935088. doi: 10.1145/1190455.1190467.

[153] M. Lacage, M. H. Manshaei, and T. Turletti. IEEE 802.11 rate adaptation. In *Proceedings of the 7th ACM international symposium on Modeling, analysis and simulation of wireless and mobile systems - MSWiM '04*. ACM Press, 2004. ISBN 1581139535. doi: 10.1145/1023663.1023687.

[154] A. Laourine and L. Tong. Betting on Gilbert-Elliot channels. *IEEE Transactions on Wireless Communications*, 9(2), 2010. ISSN 1536-1276. doi: 10.1109/TWC.2010.02.090055.

[155] P. Larsson. Selection diversity forwarding in a multihop packet radio network with fading channel and capture. *ACM SIGMOBILE Mobile Computing and Communications Review*, 5(4), 2001. ISSN 15591662. doi: 10.1145/509506.509517.

[156] P. Larsson and N. Johansson. Multiuser diversity forwarding in multihop packet radio networks. In *IEEE Wireless Communications and Networking Conference, 2005*, volume 4. IEEE, 2005. ISBN 0-7803-8966-2. doi: 10.1109/WCNC.2005.1424856.

[157] R. Laufer, H. Dubois-Ferriere, and L. Kleinrock. Multirate Anypath Routing in Wireless Mesh Networks. In *IEEE INFOCOM 2009 - The 28th Conference on Computer Communications*. IEEE, 2009. ISBN 978-1-4244-3512-8. doi: 10.1109/INFCOM.2009.5061904.

[158] L. B. Le, E. Modiano, and N. B. Shroff. Optimal Control of Wireless Networks with Finite Buffers. In *2010 Proceedings IEEE INFOCOM*. IEEE, 2010. ISBN 978-1-4244-5836-3. doi: 10.1109/INFCOM.2010.5462026.

[159] M. Leconte, J. Ni, and R. Srikant. Mixing Time of Glauber Dynamics with Parallel Updates and Heterogeneous Fugacities. *Workshop on Frontiers of Controls, Games, and Network Science with Civilian and Military Applications*, 2010.

[160] J. Lee, J. Lee, Y. Yi, S. Chong, A. Proutière, and M. Chiang. Implementing utility-optimal CSMA. In *2009 47th Annual Allerton Conference on Communication, Control, and Computing (Allerton)*. IEEE, 2009. ISBN 978-1-4244-5870-7. doi: 10.1109/ALLERTON.2009.5394849.

[161] J. Lee, S.-J. Lee, W. Kim, D. Jo, T. Kwon, and Y. Choi. Understanding interference and carrier sensing in wireless mesh networks. *IEEE Communications Magazine*, 47(7), 2009. ISSN 0163-6804. doi: 10.1109/MCOM.2009.5183479.

[162] J.-W. Lee, M. Chiang, and A. Calderbank. Utility-Optimal Random-Access Control. *IEEE Transactions on Wireless Communications*, 6(7), 2007. ISSN 1536-1276. doi: 10.1109/TWC.2007.05991.

[163] C.-P. Li and M. J. Neely. Exploiting channel memory for multi-user wireless scheduling without channel measurement: Capacity regions and algorithms. In *Modeling and Optimization in Mobile, Ad Hoc and Wireless Networks (WiOpt), 2010 Proceedings of the 8th International Symposium on*, volume 8, Avignon, France, 2010.

[164] C.-P. Li and M. J. Neely. Network Utility Maximization over Partially Observable Markovian Channels, 2010. arXiv:1008.3421.

[165] C.-P. Li and M. J. Neely. Exploiting channel memory for multiuser wireless scheduling without channel measurement: Capacity regions and algorithms. *Performance Evaluation*, 2011. ISSN 01665316. doi: 10.1016/j.peva.2011.01.007.

[166] S. C. Liew, C. Kai, J. Leung, and B. Wong. Back-of-the-Envelope Computation of Throughput Distributions in CSMA Wireless Networks. In *2009 IEEE International Conference on Communications*. IEEE, 2009. doi: 10.1109/ICC.2009.5198774.

[167] S. C. Liew, C. H. Kai, H. Ching, J. Leung, and P. B. Wong. Back-of-the-Envelope Computation of Throughput Distributions in CSMA Wireless Networks. *IEEE Transactions on Mobile Computing*, 9(9), 2010. ISSN 1536-1233. doi: 10.1109/TMC.2010.89.

[168] S. C. Liew, J. Zhang, C.-k. Chau, and M. Chen. Analysis of Frequency-Agile CSMA Wireless Networks, 2010. arXiv:1007.5255.

[169] K. C.-J. Lin, N. Kushman, and D. Katabi. ZipTx. In *Proceedings of the 14th ACM international conference on Mobile computing and networking - MobiCom '08*. ACM Press, 2008. ISBN 9781605580968. doi: 10.1145/1409944.1409984.

[170] X. Lin and N. B. Shroff. The impact of imperfect scheduling on cross-Layer congestion control in wireless networks. *IEEE/ACM Transactions on Networking*, 14 (2), 2006. ISSN 1063-6692. doi: 10.1109/TNET.2006.872546.

[171] E. Liu, Q. Zhang, and K. K. Leung. Resource Allocation for Frequency-Selective Fading, Multi-Carrier Systems with Fairness Constraints. In *2009 IEEE International Conference on Communications*. IEEE, 2009. doi: 10.1109/ICC.2009.5199411.

[172] J. Liu and A. L. Stolyar. Distributed Queue-Length based Algorithms for Optimal End-to-End Throughput Allocation and Stability in Multi-hop Random Access Networks. In *Forty-Fifth Annual Allerton Conference On Communication, Control, and Computing*, Monticello, IL, 2007.

[173] J. Liu, Y. Yi, A. Proutière, M. Chiang, and H. V. Poor. Maximizing Utility via Random Access without Message Passing. Technical Report MSR-TR-2008-128, Microsoft Research, Cambridge, UK, 2008.

[174] J. Liu, Y. Yi, A. Proutière, M. Chiang, and H. V. Poor. Convergence and Tradeoff of Utility-Optimal CSMA, 2009. arXiv:0902.1996.

[175] J. Liu, Y. Yi, A. Proutière, M. Chiang, and H. V. Poor. Towards utility-optimal random access without message passing. *Wireless Communications and Mobile Computing*, 10(1), 2010. ISSN 15308669. doi: 10.1002/wcm.897.

[176] S. Liu, L. Ying, and R. Srikant. Throughput-Optimal Opportunistic Scheduling in the Presence of Flow-Level Dynamics. In *2010 Proceedings IEEE INFOCOM*, San Diego, CA, 2010. IEEE. ISBN 978-1-4244-5836-3. doi: 10.1109/INFCOM.2010.5462121.

[177] M. Lotfinezhad and P. Marbach. Throughput-Optimal Random Access with Order-Optimal Delay. In *4th Workshop on Network Control and Optimization NET-COOP*, Ghent, Belgium, 2010.

[178] M. Lotfinezhad and P. Marbach. Delay Performance of CSMA policies in Multi-hop Wireless Networks: A New Perspective. In *Workshop on Frontiers of Controls, Games, and Network Science with Civilian and Military Applications*, 2010.

[179] H. Ma and S. Roy. Contention Window and Transmission Opportunity Adaptation for Dense IEEE 802.11 WLAN Based on Loss Differentiation. In *2008 IEEE International Conference on Communications*. IEEE, 2008. ISBN 978-1-4244-2075-9. doi: 10.1109/ICC.2008.484.

[180] P. Marbach, A. Eryilmaz, and A. Ozdaglar. On the Throughput-Optimality of CSMA Policies in Multihop Wireless Networks. Technical Report CNRL-08, Computer Networks Research Lab, University of Toronto, Canada, 2008.

[181] A. Mei and J. Stefa. Routing in Outer Space. In *2008 IEEE INFOCOM - The 27th Conference on Computer Communications*. IEEE, 2008. ISBN 978-1-4244-2026-1. doi: 10.1109/INFOCOM.2008.291.

[182] T. Meng, B. McFarland, D. Su, and J. Thomson. Design and implementation of an all-CMOS 802.11a wireless LAN chipset. *IEEE Communications Magazine*, 41 (8), 2003. ISSN 0163-6804. doi: 10.1109/MCOM.2003.1222734.

[183] S. P. Meyn. *Control techniques for complex networks*. Cambridge University Press, 2007. ISBN 0521884411.

[184] S. Misra, S. C. Misra, and I. Woungang. *Guide to Wireless Mesh Networks*. Springer, 2010. ISBN 1849968047.

[185] J. Mo and J. Walrand. Fair end-to-end window-based congestion control. *IEEE/ACM Transactions on Networking*, 8(5), 2000. ISSN 10636692. doi: 10.1109/90.879343.

[186] S. Moeller, A. Sridharan, B. Krishnamachari, and O. Gnawali. Routing without routes. In *Proceedings of the 9th ACM/IEEE International Conference on Information Processing in Sensor Networks - IPSN '10*. ACM Press, 2010. ISBN 9781605589886. doi: 10.1145/1791212.1791246.

[187] M. Naghshvar and T. Javidi. Opportunistic Routing with Congestion Diversity in Wireless Multi-hop Networks. In *2010 Proceedings IEEE INFOCOM*. IEEE, 2010. ISBN 978-1-4244-5836-3. doi: 10.1109/INFCOM.2010.5462183.

[188] M. Naghshvar, H. Zhuang, and T. Javidi. A general class of throughput optimal routing policies in multi-hop wireless networks. In *2009 47th Annual Allerton Conference on Communication, Control, and Computing (Allerton)*. IEEE, 2009. ISBN 978-1-4244-5870-7. doi: 10.1109/ALLERTON.2009.5394513.

[189] M. Neely. Optimal Backpressure Routing for Wireless Networks with Multi-Receiver Diversity. In *2006 40th Annual Conference on Information Sciences and Systems*. IEEE, 2006. ISBN 1-4244-0350-2. doi: 10.1109/CISS.2006.286424.

[190] M. Neely. Super-fast delay tradeoffs for utility optimal fair scheduling in wireless networks. *IEEE Journal on Selected Areas in Communications*, 24(8), 2006. ISSN 0733-8716. doi: 10.1109/JSAC.2006.879357.

[191] M. Neely, E. Modiano, and C. Rohrs. Dynamic power allocation and routing for time varying wireless networks. In *IEEE INFOCOM 2003. Twenty-second Annual Joint Conference of the IEEE Computer and Communications Societies (IEEE Cat. No.03CH37428)*, volume vol. IEEE, 2003. ISBN 0-7803-7752-4. doi: 10.1109/INFCOM.2003.1208724.

[192] M. Neely, E. Modiano, and C.-P. Li. Fairness and Optimal Stochastic Control for Heterogeneous Networks. *IEEE/ACM Transactions on Networking*, 16(2), 2008. ISSN 1063-6692. doi: 10.1109/TNET.2007.900405.

[193] M. J. Neely. Stability and Capacity Regions for Discrete Time Queueing Networks, 2010. arXiv:1003.3396.

[194] M. J. Neely and R. Urgaonkar. Opportunism, backpressure, and stochastic optimization with the wireless broadcast advantage. In *2008 42nd Asilomar Conference on Signals, Systems and Computers*. IEEE, 2008. ISBN 978-1-4244-2940-0. doi: 10.1109/ACSSC.2008.5074815.

[195] J. Ni, B. Tan, and R. Srikant. Q-CSMA: Queue-Length Based CSMA/CA Algorithms for Achieving Maximum Throughput and Low Delay in Wireless Networks, 2009. arXiv:0901.2333.

[196] J. Ni, B. Tan, and R. Srikant. Q-CSMA: Queue-Length Based CSMA/CA Algorithms for Achieving Maximum Throughput and Low Delay in Wireless Networks. In *2010 Proceedings IEEE INFOCOM*. IEEE, 2010. ISBN 978-1-4244-5836-3. doi: 10.1109/INFCOM.2010.5462229.

[197] W. Ouyang, S. Murugesan, A. Eryilmaz, and N. B. Shroff. Scheduling with Rate Adaptation under Incomplete Knowledge of Channel/Estimator Statistics, 2010. arXiv:1008.1828.

[198] W. Ouyang, S. Murugesan, A. Eryilmaz, and N. B. Shroff. Exploiting Channel Memory for Joint Estimation and Scheduling in Downlink Networks, 2010. arXiv:1009.3959.

[199] E. Perahia, A. Sheth, T. Kenney, R. Stacey, and D. Halperin. Investigation into the Doppler Component of the IEEE 802.11n Channel Model. In *2010 IEEE Global Telecommunications Conference GLOBECOM 2010*, Miami, FL, 2010. IEEE. ISBN 978-1-4244-5636-9. doi: 10.1109/GLOCOM.2010.5684207.

[200] C. Perkins and E. Royer. Ad-hoc on-demand distance vector routing. In *Proceedings WMCSA'99. Second IEEE Workshop on Mobile Computing Systems and Applications*. IEEE, 1999. ISBN 0-7695-0025-0. doi: 10.1109/MCSA.1999.749281.

[201] C. Perkins, E. Belding-Royer, and S. Das. Ad hoc On-Demand Distance Vector (AODV) Routing. RFC 3561 (Experimental), 2003.

[202] C. E. Perkins and P. Bhagwat. Highly dynamic Destination-Sequenced Distance-Vector routing (DSDV) for mobile computers. *ACM SIGCOMM Computer Communication Review*, 24(4), 1994. ISSN 01464833. doi: 10.1145/190809.190336.

[203] D. Perkins and M. Bayoumi. MAC-SCC: medium access control with a separate control channel for multihop wireless networks. In *23rd International Conference on Distributed Computing Systems Workshops*, volume 1. IEEE, 2003. ISBN 0-7695-1921-0. doi: 10.1109/ICDCSW.2003.1203644.

[204] J. Postel. User Datagram Protocol. RFC 768 (Standard), 1980.

[205] J. Postel. Internet Protocol. RFC 791 (Standard), 1981. Updated by RFC 1349.

[206] J. Postel. Transmission Control Protocol. RFC 793 (Standard), 1981. Updated by RFCs 1122, 3168, 6093.

[207] A. Proutière, Y. Yi, and M. Chiang. Throughput of random access without message passing. In *2008 42nd Annual Conference on Information Sciences and Systems*. IEEE, 2008. ISBN 978-1-4244-2246-3. doi: 10.1109/CISS.2008.4558579.

[208] A. Proutière, Y. Yi, T. Lan, and M. Chiang. Resource Allocation over Network Dynamics without Timescale Separation. In *2010 Proceedings IEEE INFOCOM*. IEEE, 2010. ISBN 978-1-4244-5836-3. doi: 10.1109/INFCOM.2010.5462201.

[209] M. O. Pun, W. Ge, D. Zheng, J. Zhang, and H. V. Poor. Distributed Opportunistic Scheduling for MIMO Ad-Hoc Networks. In *2008 IEEE International Conference on Communications*. IEEE, 2008. ISBN 978-1-4244-2075-9. doi: 10.1109/ICC.2008.694.

[210] R. Punnoose, P. Nikitin, and D. Stancil. Efficient simulation of Ricean fading within a packet simulator. In *Vehicular Technology Conference Fall 2000. IEEE VTS Fall VTC2000. 52nd Vehicular Technology Conference (Cat. No.00CH37152)*, volume 2. IEEE, 2000. ISBN 0-7803-6507-0. doi: 10.1109/VETECF.2000.887108.

[211] D. Qian, D. Zheng, J. Zhang, and N. Shroff. CSMA-Based Distributed Scheduling in Multi-hop MIMO Networks under SINR Model. In *2010 Proceedings IEEE INFOCOM*. IEEE, 2010. ISBN 978-1-4244-5836-3. doi: 10.1109/INFCOM.2010.5462119.

[212] D. Qiao, S. Choi, and K. Shin. Goodput analysis and link adaptation for IEEE 802.11a wireless LANs. *IEEE Transactions on Mobile Computing*, 1(4), 2002. ISSN 1536-1233. doi: 10.1109/TMC.2002.1175541.

[213] X. Qin and R. Berry. Exploiting multiuser diversity for medium access control in wireless networks. In *IEEE INFOCOM 2003. Twenty-second Annual Joint Conference of the IEEE Computer and Communications Societies (IEEE Cat. No.03CH37428)*, volume 03. IEEE, 2003. ISBN 0-7803-7752-4. doi: 10.1109/INFCOM.2003.1208945.

[214] X. Qin and R. Berry. Distributed approaches for exploiting multiuser diversity in wireless networks. *IEEE Transactions on Information Theory*, 52(2), 2006. ISSN 0018-9448. doi: 10.1109/TIT.2005.862103.

[215] B. Radunović and J. Le Boudec. Rate performance objectives of multihop wireless networks. *IEEE Transactions on Mobile Computing*, 3(4), 2004. ISSN 1536-1233. doi: 10.1109/TMC.2004.45.

[216] B. Radunović and J.-Y. Le Boudec. Rate performance objectives of multi-hop wireless networks. In *IEEE INFOCOM 2004*, volume 3. IEEE, 2004. ISBN 0-7803-8355-9. doi: 10.1109/INFCOM.2004.1354601.

[217] B. Radunović, C. Gkantsidis, P. Key, P. Rodriguez, and W. Hu. An optimization framework for practical multipath routing in wireless mesh networks. Technical Report MSR-TR-2007-83, Microsoft Research, Cambridge, UK, 2007.

[218] B. Radunović, C. Gkantsidis, D. Gunawardena, and P. Key. Horizon: Balancing TCP over Multiple Paths in Wireless Mesh Network. In *Proceedings of the 14th ACM international conference on Mobile computing and networking - MobiCom '08*. ACM Press, 2008. ISBN 9781605580968. doi: 10.1145/1409944.1409973.

[219] B. Radunović, D. Gunawardena, A. Proutière, N. Singh, V. Balan, and P. Key. Efficiency and Fairness in Distributed Wireless Networks through Self-interference Cancellation and Scheduling. Technical Report MSR-TR-2009-27, Microsoft Research, Cambridge, UK, 2009.

[220] B. Radunović, C. Gkantsidis, P. Key, and P. Rodriguez. Toward Practical Opportunistic Routing with Intra-Session Network Coding for Mesh Networks. *IEEE/ACM Transactions on Networking*, 18(2), 2010. ISSN 1063-6692. doi: 10.1109/TNET.2009.2030682.

[221] B. Radunović, D. Gunawardena, P. Key, A. Proutière, N. Singh, V. Balan, and G. Dejean. Rethinking Indoor Wireless Mesh Design: Low Power, Low Frequency, Full-Duplex. In *2010 Fifth IEEE Workshop on Wireless Mesh Networks*. IEEE, 2010. ISBN 978-1-4244-7975-7. doi: 10.1109/WIMESH.2010.5507905.

[222] H. Rahul, F. Edalat, D. Katabi, and C. G. Sodini. Frequency-aware rate adaptation and MAC protocols. In *Proceedings of the 15th annual international conference on Mobile computing and networking - MobiCom '09*. ACM Press, 2009. ISBN 9781605587028. doi: 10.1145/1614320.1614342.

[223] H. Rahul, H. Hassanieh, and D. Katabi. SourceSync. In *Proceedings of the ACM SIGCOMM 2010 conference on SIGCOMM - SIGCOMM '10*. ACM Press, 2010. ISBN 9781450302012. doi: 10.1145/1851182.1851204.

[224] S. Rajagopalan and D. Shah. Distributed algorithm and reversible network. In *2008 42nd Annual Conference on Information Sciences and Systems*. IEEE, 2008. ISBN 978-1-4244-2246-3. doi: 10.1109/CISS.2008.4558577.

[225] S. Rajagopalan, D. Shah, and J. Shin. Network adiabatic theorem. In *Proceedings of the eleventh international joint conference on Measurement and modeling of computer systems - SIGMETRICS '09*. ACM Press, 2009. ISBN 9781605585116. doi: 10.1145/1555349.1555365.

[226] J. Rajahalme, A. Conta, B. Carpenter, and S. Deering. IPv6 Flow Label Specification. RFC 3697 (Proposed Standard), 2004.

[227] A. Rajanna and N. Jindal. Multiuser Diversity in Downlink Channels: When does the Feedback Cost Outweigh the Spectral Efficiency Gain?, 2011. arXiv:1102.1552.

[228] T. S. Rappaport. *Wireless Communications: Principles and Practice (2nd Edition)*. Prentice Hall PTR, 2001. ISBN 0130422320.

[229] B. Roman, F. Stajano, I. Wassell, and D. Cottingham. Multi-Carrier Burst Contention (MCBC): Scalable Medium Access Control for Wireless Networks. In *2008 IEEE Wireless Communications and Networking Conference*. IEEE, 2008. ISBN 978-1-4244-1997-5. doi: 10.1109/WCNC.2008.298.

[230] B. Roman, I. Chatzigeorgiou, I. J. Wassell, and F. Stajano. Evaluation of Multi-Carrier Burst Contention and IEEE 802.11 with fading during channel sensing. In *2009 IEEE 20th International Symposium on Personal, Indoor and Mobile Radio Communications*. IEEE, 2009. ISBN 978-1-4244-5122-7. doi: 10.1109/PIMRC.2009.5450007.

[231] B. Roman, I. Wassell, and I. Chatzigeorgiou. Scalable Cross-Layer Wireless Access Control Using Multi-Carrier Burst Contention. *IEEE Journal on Selected Areas in Communications*, 29(1), 2011. ISSN 0733-8716. doi: 10.1109/JSAC.2011.110112.

[232] E. Rozner, J. Seshadri, Y. Mehta, and L. Qiu. SOAR: Simple Opportunistic Adaptive Routing Protocol for Wireless Mesh Networks. *IEEE Transactions on Mobile Computing*, 8(12), 2009. ISSN 1536-1233. doi: 10.1109/TMC.2009.82.

[233] J. Ryu, J. Lee, S.-J. Lee, and T. Kwon. Revamping the IEEE 802.11a PHY simulation models. In *Proceedings of the 11th international symposium on Modeling, analysis and simulation of wireless and mobile systems - MSWiM '08*. ACM Press, 2008. ISBN 9781605582351. doi: 10.1145/1454503.1454513.

[234] A. Sabharwal, A. Khoshnevis, and E. Knightly. Opportunistic Spectral Usage: Bounds and a Multi-Band CSMA/CA Protocol. *IEEE/ACM Transactions on Networking*, 15(3), 2007. ISSN 1063-6692. doi: 10.1109/TNET.2007.893230.

[235] B. Sadeghi, V. Kanodia, A. Sabharwal, and E. Knightly. Opportunistic media access for multirate ad hoc networks. In *Proceedings of the 8th annual international conference on Mobile computing and networking - MobiCom '02*. ACM Press, 2002. ISBN 158113486X. doi: 10.1145/570645.570650.

[236] B. Sadiq, S. J. Baek, and G. de Veciana. Delay-Optimal Opportunistic Scheduling and Approximations: The Log Rule. In *IEEE INFOCOM 2009 - The 28th Conference on Computer Communications*. IEEE, 2009. ISBN 978-1-4244-3512-8. doi: 10.1109/INFCOM.2009.5062088.

[237] B. Sadiq, S. J. Baek, and G. de Veciana. Delay-optimal opportunistic scheduling and approximations: The log rule. *Networking, IEEE/ACM Transactions on*, 19(2), 2011. ISSN 1063-6692. doi: 10.1109/TNET.2010.2068308.

[238] L. Scalia, I. Tinnirello, and D. Giustiniano. Side Effects of Ambient Noise Immunity Techniques on Outdoor IEEE 802.11 Deployments. In *IEEE GLOBECOM 2008 - 2008 IEEE Global Telecommunications Conference*. IEEE, 2008. ISBN 978-1-4244-2324-8. doi: 10.1109/GLOCOM.2008.ECP.941.

[239] S. Sen, R. R. Choudhury, and S. Nelakuditi. Listen (on the frequency domain) before you talk. In *Proceedings of the Ninth ACM SIGCOMM Workshop on Hot Topics in Networks - Hotnets '10*. ACM Press, 2010. ISBN 9781450304092. doi: 10.1145/1868447.1868463.

[240] S. Sen, R. Roy Choudhury, and S. Nelakuditi. CSMA/CN. In *Proceedings of the sixteenth annual international conference on Mobile computing and networking - MobiCom '10*. ACM Press, 2010. ISBN 9781450301817. doi: 10.1145/1859995.1859999.

[241] D. Shah and J. Shin. Randomized Scheduling Algorithm for Queueing Networks, 2009. arXiv:0908.3670.

[242] D. Shah and J. Shin. Efficient Queue-based CSMA with Collisions, 2010. arXiv:1003.2749.

[243] D. Shah and J. Shin. Delay optimal queue-based CSMA. In *Proceedings of the ACM SIGMETRICS international conference on Measurement and modeling of computer systems - SIGMETRICS '10*, number 1 in 38. ACM Press, 2010. ISBN 9781450300384. doi: 10.1145/1811039.1811093.

[244] S. Shakkottai and R. Srikant. Network Optimization and Control. *Foundations and Trends in Networking*, 2(3), 2007. ISSN 1554-057X. doi: 10.1561/1300000007.

[245] Z. Shao, M. Chen, S. Avestimehr, and S.-y. R. Li. Cross-layer Optimization for Wireless Networks with Deterministic Channel Models. In *2010 Proceedings IEEE INFOCOM*. IEEE, 2010. ISBN 978-1-4244-5836-3. doi: 10.1109/INFCOM.2010.5462247.

[246] B. Sklar. *Digital Communications: Fundamentals and Applications*. Prentice Hall PTR, 2001. ISBN 9780130847881.

[247] D. Soldani and S. Dixit. Wireless relays for broadband access [radio communications series]. *IEEE Communications Magazine*, 46(3), 2008. ISSN 0163-6804. doi: 10.1109/MCOM.2008.4463772.

[248] R. Sombrutzki, A. Zubow, M. Kurth, and J.-P. Redlich. Self-Organization in Community Mesh Networks The Berlin RoofNet. In *2006 1st Workshop on Operator-Assisted (Wireless Mesh) Community Networks*. IEEE, 2006. ISBN 1-4244-0691-9. doi: 10.1109/WOACN.2006.337188.

[249] B. Soret, M. C. Aguayo Torres, and J. T. Entrambasaguas. Analysis of the Tradeoff between Delay and Source Rate in Multiuser Wireless Systems. *EURASIP Journal on Wireless Communications and Networking*, 2010, 2010. ISSN 1687-1472. doi: 10.1155/2010/726750.

[250] A. Sridharan, S. Moeller, and B. Krishnamachari. Investigating Backpressure-based Rate Control Protocols for Wireless Sensor Networks. In *ITA workshop*, 2009.

[251] K. Srinivasan, M. Jain, J. I. Choi, T. Azim, E. S. Kim, P. Levis, and B. Krishnamachari. The κ factor: inferring protocol performance using inter-link reception correlation. In *Proceedings of the sixteenth annual international conference on Mobile computing and networking - MobiCom '10*. ACM Press, 2010. ISBN 9781450301817. doi: 10.1145/1859995.1860032.

[252] V. G. Subramanian and D. J. Leith. Draining time based scheduling algorithm. In *2007 46th IEEE Conference on Decision and Control*. IEEE, 2007. ISBN 978-1-4244-1497-0. doi: 10.1109/CDC.2007.4434661.

[253] I. Sutskover and D. Ben-Eli. Transmitter operations for interference mitigation, 2003. United States Patent 7702023.

[254] K. Tan, J. Fang, Y. Zhang, S. Chen, L. Shi, J. Zhang, and Y. Zhang. Fine-grained channel access in wireless LAN. In *Proceedings of the ACM SIGCOMM 2010 conference on SIGCOMM - SIGCOMM '10*. ACM Press, 2010. ISBN 9781450302012. doi: 10.1145/1851182.1851202.

[255] S.-s. Tan, D. Zheng, J. Zhang, and J. Zeidler. Distributed Opportunistic Scheduling for Ad-Hoc Communications Under Delay Constraints. In *2010 Proceedings IEEE INFOCOM*. IEEE, 2010. ISBN 978-1-4244-5836-3. doi: 10.1109/INFCOM.2010.5462120.

[256] A. S. Tanenbaum. *Computer Networks, Fourth Edition*. Prentice Hall PTR, 2002. ISBN 0130661023.

[257] A. Tang, L. L. H. Andrew, K. Jacobsson, K. H. Johansson, H. k. Hjalmarsson, and S. H. Low. Queue Dynamics with Window Flow Control. *IEEE/ACM Transactions on Networking*, 18(5), 2010. ISSN 1063-6692. doi: 10.1109/TNET.2010.2047951.

[258] L. Tassiulas and A. Ephremides. Stability properties of constrained queueing systems and scheduling policies for maximum throughput in multihop radio networks. *IEEE Transactions on Automatic Control*, 37(12), 1992. ISSN 00189286. doi: 10.1109/9.182479.

[259] C. Thejaswi, J. Zhang, M.-O. Pun, and V. H. Poor. Distributed Opportunistic Scheduling with Two-Level Channel Probing. In *IEEE INFOCOM 2009 - The 28th Conference on Computer Communications*, volume 85287. IEEE, 2009. ISBN 978-1-4244-3512-8. doi: 10.1109/INFCOM.2009.5062087.

[260] C. Thejaswi P. S., J. Zhang, M.-O. Pun, H. V. Poor, and D. Zheng. Distributed Opportunistic Scheduling with Two-Level Probing. *IEEE/ACM Transactions on Networking*, 18(5), 2010. ISSN 1063-6692. doi: 10.1109/TNET.2010.2042610.

[261] J. Thomson, B. Baas, E. Cooper, J. Gilbert, G. Hsieh, P. Husted, A. Lokanathan, J. Kuskin, D. McCracken, B. McFarland, T. Meng, D. Nakahira, S. Ng, M. Rattehalli, J. Smith, R. Subramanian, L. Than, and R. Yu. An integrated 802.11a baseband and MAC processor. In *2002 IEEE International Solid-State Circuits Conference. Digest of Technical Papers (Cat. No.02CH37315)*. IEEE, 2002. ISBN 0-7803-7335-9. doi: 10.1109/ISSCC.2002.992137.

[262] I. Tinnirello, D. Giustiniano, L. Scalia, and G. Bianchi. On the side-effects of proprietary solutions for fading and interference mitigation in IEEE 802.11b/g outdoor links. *Computer Networks*, 53(2), 2009. ISSN 13891286. doi: 10.1016/j.comnet.2008.10.006.

[263] F. Tobagi and L. Kleinrock. Packet Switching in Radio Channels: Part II–The Hidden Terminal Problem in Carrier Sense Multiple-Access and the Busy-Tone Solution. *IEEE Transactions on Communications*, 23(12), 1975. ISSN 0096-2244. doi: 10.1109/TCOM.1975.1092767.

[264] D. Tse and P. Viswanath. *Fundamentals of Wireless Communication*. Cambridge University Press, 1 edition, 2005. ISBN 0521845270.

[265] D. Tse, P. Viswanath, and R. Laroia. Opportunistic beamforming using dumb antennas. *IEEE Transactions on Information Theory*, 48(6), 2002. ISSN 0018-9448. doi: 10.1109/TIT.2002.1003822.

[266] M. Valenti and N. Correal. Exploiting macrodiversity in dense multihop networks and relay channels. In *2003 IEEE Wireless Communications and Networking, WCNC*, New Orleans, LA, 2003. IEEE. ISBN 0-7803-7700-1. doi: 10.1109/WCNC.2003.1200673.

[267] P. M. van de Ven, A. J. Janssen, and J. S. van Leeuwaarden. Optimal tradeoff between exposed and hidden nodes in large wireless networks. In *Proceedings of the ACM SIGMETRICS international conference on Measurement and modeling of computer systems - SIGMETRICS '10*. ACM Press, 2010. ISBN 9781450300384. doi: 10.1145/1811039.1811060.

[268] P. M. van de Ven, J. S. H. van Leeuwaarden, D. Denteneer, and A. J. E. M. Janssen. Spatial fairness in linear wireless multi-access networks, 2010. arXiv:1004.1042.

[269] V. J. Venkataramanan, X. Lin, L. Ying, and S. Shakkottai. On Scheduling for Minimizing End-to-End Buffer Usage over Multihop Wireless Networks. In *2010*

Proceedings IEEE INFOCOM, West Lafayette, IN, 2010. School of Electrical and Computer Engineering, Purdue University, IEEE. ISBN 978-1-4244-5836-3. doi: 10.1109/INFCOM.2010.5462117.

[270] M. Vutukuru, H. Balakrishnan, and K. Jamieson. Cross-layer wireless bit rate adaptation. *ACM SIGCOMM Computer Communication Review*, 39(4), 2009. ISSN 01464833. doi: 10.1145/1594977.1592571.

[271] B. H. Walke, S. Mangold, and L. Berlemann. *IEEE 802 Wireless Systems: Protocols, Multi-Hop Mesh/Relaying, Performance and Spectrum Coexistence*. Wiley & Sons, 1. edition, 2007. ISBN 0470014393.

[272] H. S. Wang and N. Moayeri. Finite-state Markov channel-a useful model for radio communication channels. *IEEE Transactions on Vehicular Technology*, 44(1), 1995. ISSN 00189545. doi: 10.1109/25.350282.

[273] J. Wang, H. Zhai, and Y. Fang. Opportunistic packet Scheduling and Media Access control for wireless LANs and multi-hop ad hoc networks. In *2004 IEEE Wireless Communications and Networking Conference (IEEE Cat. No.04TH8733)*. IEEE, 2004. ISBN 0-7803-8344-3. doi: 10.1109/WCNC.2004.1311365.

[274] J. Wang, H. Zhai, Y. Fang, J. M. Shea, and D. Wu. OMAR: Utilizing Multiuser Diversity in Wireless Ad Hoc Networks. *IEEE Transactions on Mobile Computing*, 5(12), 2006. ISSN 1536-1233. doi: 10.1109/TMC.2006.186.

[275] X. Wang and K. Kar. Throughput modelling and fairness issues in CSMA/CA based ad-hoc networks. In *Proceedings IEEE 24th Annual Joint Conference of the IEEE Computer and Communications Societies.*, volume 1. IEEE, 2005. ISBN 0-7803-8968-9. doi: 10.1109/INFCOM.2005.1497875.

[276] A. Warrier, S. Janakiraman, S. Ha, and I. Rhee. DiffQ: Practical Differential Backlog Congestion Control for Wireless Networks. In *IEEE INFOCOM 2009 - The 28th Conference on Computer Communications*. IEEE, 2009. ISBN 978-1-4244-3512-8. doi: 10.1109/INFCOM.2009.5061929.

[277] M. Welzl. *Network congestion control: managing Internet traffic*. John Wiley & Sons, 2005. ISBN 978-0-470-02528-4.

[278] K. Wu, H. Tan, Y. Liu, J. Zhang, Q. Zhang, and L. Ni. Side channel. In *Proceedings of the sixteenth annual international conference on Mobile computing and networking - MobiCom '10*. ACM Press, 2010. ISBN 9781450301817. doi: 10.1145/1859995.1859998.

[279] S. Wu and H. Wang. Measurement Based Investigation of Indoor IEEE 802.11g Channel Dynamics. In *2010 IEEE Global Telecommunications Conference GLOBECOM 2010*, Miami, FL, 2010. IEEE. ISBN 978-1-4244-5636-9. doi: 10.1109/GLOCOM.2010.5683233.

[280] K. Xu, O. Dousse, and P. Thiran. Self-synchronizing properties of CSMA wireless multi-hop networks. *ACM SIGMETRICS Performance Evaluation Review*, 38(1), 2010. ISSN 01635999. doi: 10.1145/1811099.1811048.

[281] D. Xue and E. Ekici. Delay-Guaranteed Cross-Layer Scheduling in Multi-Hop Wireless Networks, 2010. arXiv:1009.4954.

[282] F. Xue and P. Kumar. Scaling Laws for Ad Hoc Wireless Networks: An Information Theoretic Approach. *Foundations and Trends in Networking*, 1(2), 2006. ISSN 1554-057X. doi: 10.1561/1300000002.

[283] Y. Yang, F. Huang, X. Gu, M. Guizani, and H.-H. Chen. Double sense multiple access for wireless ad hoc networks. In *Proceedings of the 3rd international conference on Quality of service in heterogeneous wired/wireless networks - QShine '06*. ACM Press, 2006. ISBN 1595935371. doi: 10.1145/1185373.1185386.

[284] Z. Yang, K. Zeng, and W. Lou. FSA: A Fast Coordination Scheme for Opportunistic Routing. In *2009 IEEE International Conference on Communications*. IEEE, 2009. doi: 10.1109/ICC.2009.5199042.

[285] Y. Yi and M. Chiang. *Stochastic Network Utility Maximization and Wireless Scheduling*, chapter 1. Cambridge University Press, 2010. ISBN 9780521113687.

[286] Y. Yi and S. Shakkottai. Hop-by-Hop Congestion Control Over a Wireless Multi-Hop Network. *IEEE/ACM Transactions on Networking*, 15(1), 2007. ISSN 1063-6692. doi: 10.1109/TNET.2006.890121.

[287] Y. Yi, A. Proutière, and M. Chiang. Complexity in wireless scheduling. In *Proceedings of the 9th ACM international symposium on Mobile ad hoc networking and computing - MobiHoc '08*. ACM Press, 2008. ISBN 9781605580739. doi: 10.1145/1374618.1374624.

[288] Y. Yi, J. Lee, S. Chong, M. Chiang, and A. Proutière. Towards optimal MAC without message passing in wireless networks. In *Proceedings of the 4th International Conference on Future Internet Technologies - CFI '09*. ACM Press, 2009. ISBN 9781605586861. doi: 10.1145/1555697.1555719.

[289] Y. Yi, J. Zhang, and M. Chiang. Delay and effective throughput of wireless scheduling in heavy traffic regimes. In *Proceedings of the tenth ACM international symposium on Mobile ad hoc networking and computing - MobiHoc '09*. ACM Press, 2009. ISBN 9781605585314. doi: 10.1145/1530748.1530757.

[290] L. Ying and S. Shakkottai. Scheduling in Mobile Ad Hoc Networks with Topology and Channel-State Uncertainty. In *IEEE INFOCOM 2009 - The 28th Conference on Computer Communications*. IEEE, 2009. ISBN 978-1-4244-3512-8. doi: 10.1109/INFCOM.2009.5062161.

[291] L. Ying, S. Shakkottai, and A. Reddy. On Combining Shortest-Path and Back-Pressure Routing Over Multihop Wireless Networks. In *IEEE INFOCOM 2009 - The 28th Conference on Computer Communications*, Rio de Janeiro, Brazil, 2009. IEEE. ISBN 978-1-4244-3512-8. doi: 10.1109/INFCOM.2009.5062086.

[292] Y. Yuan, H. Yang, S. H. Y. Wong, S. Lu, and W. Arbaug. ROMER: Resilient Opportunistic Mesh Routing for Wireless Mesh Networks. In *IEEE Workshop on Wireless Mesh Networks (WiMesh)*, Santa Clara, CA, 2005.

[293] M. Zargari, D. Su, C. Yue, S. Rabii, D. Weber, B. Kaczynski, S. Mehta, K. Singh, S. Mendis, and B. Wooley. A 5-GHz CMOS transceiver for IEEE 802.11a wireless LAN systems. *IEEE Journal of Solid-State Circuits*, 37(12), 2002. ISSN 0018-9200. doi: 10.1109/JSSC.2002.804353.

[294] M. Zargari, M. Terrovitis, S.-M. Jen, B. Kaczynski, M. Mack, S. Mehta, S. Mendis, K. Onodera, H. Samavati, W. Si, K. Singh, A. Tabatabaei, D. Weber, D. Su, and B. Wooley. A single-chip dual-band tri-mode CMOS transceiver for IEEE 802.11a/b/g wireless LAN. *IEEE Journal of Solid-State Circuits*, 39(12), 2004. ISSN 0018-9200. doi: 10.1109/JSSC.2004.836349.

[295] K. Zeng, W. Lou, and H. Zhai. On End-to-End Throughput of Opportunistic Routing in Multirate and Multihop Wireless Networks. In *2008 IEEE INFOCOM - The 27th Conference on Computer Communications*. IEEE, 2008. ISBN 978-1-4244-2026-1. doi: 10.1109/INFOCOM.2008.133.

[296] K. Zeng, Z. Yang, and W. Lou. Opportunistic Routing in Multi-radio Multi-channel Multi-hop Wireless Networks. In *2010 Proceedings IEEE INFOCOM*. IEEE, 2010. ISBN 978-1-4244-5836-3. doi: 10.1109/INFCOM.2010.5462187.

[297] H. Zhai, J. Wang, and Y. Fang. DUCHA: A New Dual-Channel MAC Protocol for Multihop Ad Hoc Networks. *IEEE Transactions on Wireless Communications*, 5 (10), 2006. ISSN 1536-1276. doi: 10.1109/TWC.2006.04869.

[298] J. Zhang, K. Tan, J. Zhao, H. Wu, and Y. Zhang. A Practical SNR-Guided Rate Adaptation. In *2008 IEEE INFOCOM - The 27th Conference on Computer Communications*. IEEE, 2008. ISBN 978-1-4244-2026-1. doi: 10.1109/INFOCOM.2008.274.

[299] Q. Zhang, L. Benmohamed, and I.-J. Wang. Exploiting Time and User Diversity in Distributed Medium Access Control for Mobile Ad-Hoc Networks. In *Proceedings of the Fifth International ICST Conference on Heterogeneous Networking for Quality, Reliability, Security and Robustness*, Gent, Belgium, 2008. ICST. doi: 10.4108/ICST.QSHINE2008.3968.

[300] X. Zhang and B. Li. Dice. In *Proceedings of the 9th ACM international symposium on Mobile ad hoc networking and computing - MobiHoc '08*. ACM Press, 2008. ISBN 9781605580739. doi: 10.1145/1374618.1374658.

[301] Y. Zhang, J. Luo, and H. Hu. *Wireless Mesh Networking: Architectures, Protocols and Standards*. Auerbach Publications, 2006. ISBN 0849373999.

[302] Z. Zhang and H. Jiang. Distributed Opportunistic Channel Access in Wireless Relay Networks, 2011. arXiv:1102.5461.

[303] Y. Zhao, Y. Xiang, L. Xu, and M. Shi. A multi-channel medium access control protocol for multicast in mobile ad-hoc network. In *14th IEEE Proceedings on Personal, Indoor and Mobile Radio Communications, 2003. PIMRC 2003.* IEEE, 2003. ISBN 0-7803-7822-9. doi: 10.1109/PIMRC.2003.1260392.

[304] D. Zheng, W. Ge, and J. Zhang. Distributed opportunistic scheduling for ad-hoc communications. In *Proceedings of the 8th ACM international symposium on Mobile ad hoc networking and computing - MobiHoc '07*. ACM Press, 2007. ISBN 9781595936844. doi: 10.1145/1288107.1288109.

[305] D. Zheng, M. Cao, J. Zhang, and P. R. Kumar. Channel Aware Distributed Scheduling for Exploiting Multi-Receiver Diversity and Multiuser Diversity in Ad-Hoc Networks: A Unified PHY/MAC Approach. In *2008 IEEE INFOCOM - The 27th Conference on Computer Communications*. IEEE, 2008. ISBN 978-1-4244-2026-1. doi: 10.1109/INFOCOM.2008.204.

[306] D. Zheng, M.-O. Pun, W. Ge, J. Zhang, and H. Poor. Distributed opportunistic scheduling for ad hoc communications with imperfect channel information. *IEEE Transactions on Wireless Communications*, 7(12), 2008. ISSN 1536-1276. doi: 10.1109/T-WC.2008.071368.

[307] D. Zheng, M. O. Pun, W. Ge, J. Zhang, and H. V. Poor. Distributed Opportunistic Scheduling For Ad-Hoc Communications under Noisy Channel Estimation. In *2008 IEEE International Conference on Communications*, volume 1. IEEE, 2008. ISBN 978-1-4244-2075-9. doi: 10.1109/ICC.2008.698.

[308] D. Zheng, W. Ge, and J. Zhang. Distributed Opportunistic Scheduling for Ad Hoc Networks with Random Access: An Optimal Stopping Approach. *IEEE Transactions on Information Theory*, 55(1), 2009. ISSN 0018-9448. doi: 10.1109/TIT.2008.2008137.

[309] Z. Zhong and S. Nelakuditi. On the Efficacy of Opportunistic Routing. In *2007 4th Annual IEEE Communications Society Conference on Sensor, Mesh and Ad Hoc Communications and Networks*. IEEE, 2007. ISBN 1-4244-1268-4. doi: 10.1109/SAHCN.2007.4292856.

[310] H. Zhou, P. Fan, and D. Guo. Joint Channel Probing and Proportional Fair Scheduling in Wireless Networks, 2010. arXiv:1009.2602.

[311] H. Zimmermann. OSI Reference Model–The ISO Model of Architecture for Open Systems Interconnection. *IEEE Transactions on Communications*, 28(4), 1980. ISSN 0096-2244. doi: 10.1109/TCOM.1980.1094702.

[312] M. Zorzi and R. Rao. Geographic Random Forwarding (GeRaF) for Ad Hoc and Sensor Networks: Energy and Latency Performance. *IEEE Transactions on Mobile Computing*, 2(4), 2003. ISSN 1536-1233. doi: 10.1109/TMC.2003.1255650.

[313] M. Zorzi and R. Rao. Geographic Random Forwarding (GeRaF) for Ad Hoc and Sensor Networks: Multihop Performance. *IEEE Transactions on Mobile Computing*, 2(4), 2003. ISSN 1536-1233. doi: 10.1109/TMC.2003.1255648.

[314] R. Zorzi, A. Chockalingam, and R. Rao. Throughput analysis of TCP on channels with memory. *IEEE Journal on Selected Areas in Communications*, 18(7), 2000. ISSN 07338716. doi: 10.1109/49.857929.

[315] A. Zubow. *Kooperatives Forwarding in drahtlosen Maschennetzen*. PhD thesis, Humboldt-Universität zu Berlin, 2009.

[316] A. Zubow, M. Kurth, and J.-P. Redlich. Multi-Channel Opportunistic Routing. In *2007 13th European Wireless Conference*, 2007.

[317] A. Zubow, M. Kurth, and J.-P. Redlich. An Opportunistic Cross-Layer Protocol for Multi-Channel Wireless Networks. In *2007 IEEE 18th International Symposium on Personal, Indoor and Mobile Radio Communications*. IEEE, 2007. ISBN 978-1-4244-1143-6. doi: 10.1109/PIMRC.2007.4394509.

[318] A. Zubow, M. Kurth, and J.-P. Redlich. Considerations on forwarder selection for opportunistic protocols in wireless networks. In *2008 14th European Wireless Conference*. IEEE, 2008. ISBN 978-3-8007-3102-2. doi: 10.1109/EW.2008.4623904.

[319] A. Zubow, M. Kurth, and J.-P. Redlich. Opportunistic Protocols in Multi-rate Environments. In *Sensor Technologies and Applications, 2008. SENSORCOMM '08. Second International Conference on*. IEEE, 2008. doi: 10.1109/SENSORCOMM.2008.24.

List of Figures

List of Tables

Acronyms

AARF adaptive auto rate fallback. 23, 164

ACK acknowledgement. 26, 27, 31, 42, 50, 51, 69, 71–73, 82, 94, 107, 154, 158, 184

ADC analog-to-digital converter. 218

AFD average fade duration. 16, 175

AMC adaptive modulation and coding. 23, 24, 77, 133–135, 138, 142, 164, 187, 189, 198, 201, 209–211, 219

ANFD average non-fade duration. 16, 175

AODV ad-hoc on-demand distance vector. 29, 31, 32

AP access point. 18, 31, 41, 189–194, 219

API application programming interface. 32

ARF auto rate fallback. 23

ARQ automatic repeat request. 26, 136, 140, 149, 206

AWGN additive white Gaussian noise. 15, 20–23, 34, 55, 57, 58, 94, 112, 117, 162, 182, 196, 198, 202

BEB binary exponential backoff. 26, 31

BER bit error rate. 21, 24, 32, 55, 57, 94, 116, 162, 202

BPSK binary phase shift keying. 20–22, 57, 221

BT busy tone. 50, 51, 53, 58, 61, 129, 161, 212

BTC contention busy tone. 50–52, 54

BTD data busy tone. 50–52, 118, 121

BTMA busy-tone multiple-access. 27, 217

BTS synchronization busy tone. 51–53

C node credit. 66–69, 72, 75, 151

CA collision avoidance. 6, 25, 34, 39, 45, 46, 128, 149

CAN controller area network. 218

CBR constant bit-rate. 138

CCA clear channel assessment. 19, 20, 55, 58–61, 72, 112, 113, 116, 129, 161, 162, 198, 202, 217

CCDF complementary cumulative distribution function. 55, 56

CDF cumulative distribution function. 117, 118

CDMA code-division multiple access. 24

CQI channel quality information. 134, 135, 138–141, 144, 149, 150, 153, 154, 168, 178, 188, 193, 198, 199, 201, 210–212

CS carrier sensing. 2, 3, 6, 25, 27, 34, 35, 37, 38, 42, 44–46, 50, 58, 113, 128, 129, 134, 149, 161, 164, 168, 188, 192, 198, 212, 216–218

CSI channel state information. 23, 168, 173

CSMA carrier sense multiple access. iii, v, 2–6, 8, 18, 24–26, 34, 35, 37–41, 44–49, 51, 53, 54, 56, 57, 61, 63, 69, 70, 72–74, 76, 78, 79, 83, 84, 87, 88, 94, 96, 106, 107, 112, 128–130, 134, 135, 141, 143–147, 149–153, 155, 156, 159, 163, 164, 168, 169, 173, 174, 176–181, 188, 197, 201, 203, 206, 210, 212, 213, 215–217, 221, 222, 225

CSMA/BA carrier sense multiple access/bitwise arbitration. 217

CSMA/HBT CSMA/CA with hierarchical busy tones. 6, 49, 50, 52, 53, 55, 57, 59, 71, 94, 116, 128, 129, 153, 154, 161, 164, 201, 202, 217

CTS clear to send. 25–27, 39, 48, 50, 51, 55, 71, 84, 93, 94, 101, 107, 129, 153, 154, 156, 158, 160, 162, 216

DART dynamic address routing. 28

DBTMA dual busy tone multiple access. 27, 34, 50, 128

DCF distributed coordination function. iii, v, 25, 27, 49, 50, 202, 218, 219

DIFS distributed interframe space. 25, 26

DOS distributed opportunistic scheduling. 7, 134, 135, 141, 143, 182–184, 186–188, 210, 211, 213, 214

DSDV destination-sequenced distance-vector routing. 29

DSR dynamic source routing. iii, v, 29, 32, 93–96, 101, 107, 109, 117, 118, 124, 164, 165, 201, 203, 206, 209

DSSS direct-sequence spread spectrum. 18, 19, 32

EDCA enhanced distributed channel access. 25, 26, 153

EM electromagnetic. 11, 13

ETT expected transmission time. iii, v, 23, 30–32, 91, 112, 113, 122, 198, 201, 202

ETX expected transmission count. 30–32, 42, 91

EU European Union. 10, 11

EWMA exponentially weighted moving average. 74, 76, 84, 162, 192, 202

ExOR extremely opportunistic routing. iii, v, 33, 107, 109, 118, 121, 122, 124, 201, 203, 206, 209

FAMA floor acquisition multiple access. 27

FCFS first-come, first-served. 136, 137, 209

FDM frequency-division multiplexing. 19

FDMA frequency-division multiple access. 24

FEC forward error correction. 20

FER frame error rate. 112, 162, 202

FHSS frequency-hopping spread spectrum. 19

FIFO first in, first out. 25, 155

FSMC finite-state Markov channel. 143, 175, 182, 185

FTP file transfer protocol. 32, 34, 79, 134, 197

GeRaF geographic random forwarding. 28

GPS Global Positioning System. 28, 217

GPSR greedy perimeter stateless routing. 28

HCCA HCF controlled channel access. 25

HFD hidden node free design. 27, 44, 45, 48

HOL head of line. 143

HWMP hybrid wireless mesh protocol. 31

i.i.d. independent and identically distributed. 20, 22, 34, 57, 59, 61, 105, 111, 112, 116, 123, 129, 138–140, 182, 189–191, 194, 195, 198

IEEE Institute of Electrical and Electronics Engineers. iii, v, 1, 5, 9–11, 17–27, 31, 32, 34, 38, 41–46, 49, 54, 55, 57, 76, 94, 107, 112, 122, 128, 129, 133–135, 141, 142, 153, 162, 164, 168, 176, 197, 201–203, 209, 211, 215–220

IMT-Advanced International Mobile Telecommunications Advanced. 211

IP Internet protocol. 1, 18, 28, 32, 196, 209, 216

IQR interquartile range. 80, 97, 99

IR infrared. 19

ISM industrial, scientific and medical. 17, 18

ISO International Organization for Standardization. 1, 18

ITU International Telecommunication Union. 211

JiST Java in Simulation Time. 32, 93, 161

KKT Karush-Kuhn-Tucker. 67, 223, 226

KL Kullback-Leibler. 146, 147

LAD layering as optimization decomposition. 5, 36, 37, 134, 215

LAN local area network. 18, 218

LCG link conflict graph. 37, 38, 46, 47, 61, 63, 93, 105, 110, 113, 116, 129, 144, 149, 150, 164, 174, 175, 198, 212

LCR level crossing rate. 16, 17, 176

LHS left-hand side. 223–226

LIFO last in, first out. 41

LLC logical link control. 18

LOS line of sight. 11, 13, 14, 16, 17, 177

LQI link quality indicator. 122

LTE Long Term Evolution. 211

MAC medium access control. 3–6, 18, 20, 24–28, 30–33, 36, 40, 42–45, 49, 51, 54, 68, 71, 73, 76, 77, 87, 88, 106, 107, 111, 116–118, 122, 128, 129, 140, 141, 145, 153–155, 157–159, 161, 168, 184, 187, 188, 201, 202, 206, 216, 217, 219, 220

MACA multiple access with collision avoidance. 27, 217

MAD medium access diversity. 142

MAN metropolitan area network. 10

MANET mobile ad-hoc network. 28, 30, 141

MCBC multi-carrier burst contention. 218

MCS modulation and coding scheme. 3, 20, 21, 23, 37, 144, 221

MDP Markov decision process. 138, 139

MIMO multiple-input multiple-output. 1, 18, 19, 37, 141, 215, 217, 219, 220

MIS maximal independent set. 38, 40

MISO multiple-input single-output. 43

ML maximum likelihood. 49, 222

MOAR multi-channel opportunistic auto-rate. 141

MRF Markov random field. 37, 38, 46, 48, 143, 221, 222

MTU maximum transmission unit. 219

MUD multi-user diversity. iii, 1, 3, 33, 35, 42, 44, 91, 105–107, 110, 111, 113, 116, 117, 121, 122, 130, 133, 135, 138, 139, 141, 142, 188, 189, 193, 196, 211

MWS maximum-weight scheduling. 1, 36, 37, 39–42, 44, 52, 78, 83, 112, 134, 139, 140, 142, 143, 168–170, 172

NAV network allocation vector. 25, 27

NHDP MANET neighborhood discovery protocol. 29

NIC network interface controller. 24, 28

NLOS non line of sight. 11, 13, 14, 16, 17, 177, 201

NP nondeterministic polynomial time. 2, 36, 39, 44, 134, 140

NUM network utility maximization. 2, 5, 6, 35–37, 83, 134, 135, 138, 210, 213, 215

OAR opportunistic auto-rate. 23

OFDM orthogonal frequency-division multiplexing. 15, 18, 19, 23, 219

OFDMA orthogonal frequency-division multiple access. 1, 51, 218, 220

OLSR optimized link state routing. 29, 31, 32, 92

OR opportunistic routing. iii, v, 3, 4, 6, 33–35, 42–45, 61, 63, 67, 93, 103, 111, 117, 122, 128–131, 133, 202, 212, 215

OS opportunistic scheduling. iii, v, 4, 6, 7, 34, 61, 129, 133–135, 137–139, 142, 147, 148, 150–152, 155, 162–164, 168, 173, 182, 188, 192, 193, 197, 199, 201, 203, 209, 211, 215, 219

OSI Open System Interconnection. 1, 18

PCF point coordination function. 25

PDF probability density function. 16, 17, 59

PDR packet delivery ratio. 30, 31

PER packet error rate. 8, 22–24, 33, 34, 55, 112

PF proportional fairness. 36, 66, 70, 73–75, 77, 78, 87, 96, 124, 127, 139, 151, 153, 157, 159, 161, 166

PHY physical layer. iii, v, 1, 2, 4, 10, 18–20, 24, 30, 32, 43, 53, 55, 57, 76, 94, 112, 162, 193, 194, 196, 198, 202, 215, 217, 219, 221

PLCP physical layer convergence protocol. 19, 20

POMDP partially observable Markov decision process. 138, 140

PSR packet success rate. 22, 55, 57–63, 71, 94, 103–107, 109, 111, 116, 117, 119, 129, 151, 193, 223, 225

QAM quadrature amplitude modulation. 20–22, 221

QoS quality of service. 18, 25, 30, 143

QPSK quadrature phase-shift keying. 20, 21, 221

RBAR receiver-based auto-rate. iii, v, 23, 154, 162–166, 184, 187–190, 192, 195, 196, 199, 201, 203, 206, 209

RF radio frequency. 3, 19, 31, 37, 141, 215, 219

RFC Request for Comments. 3, 202

RHS right-hand side. 40, 224–226

RPC randomized pick-and-compare. 41

RSS received signal strength. 23

RSSI received signal strength indication. 23, 24

RTS request to send. 25–27, 39, 45, 50–52, 55, 71, 84, 93, 94, 101, 107, 118, 124, 153, 154, 156, 158, 160, 162, 167, 203, 206, 216

RTT round trip time. 136, 137

SDF selection diversity forwarding. 42

SIFS short interframe space. 26

SINR signal to interference and noise ratio. 21, 23, 55, 57, 58, 118, 121, 141, 162, 202, 217, 219

SNR signal to noise ratio. 21–24, 27, 32, 44, 77, 112, 116, 117, 138, 141, 144, 151, 162, 182, 184, 189–194, 198, 202

SSR scalable source routing. 29

STA station. 18, 31, 41

STC space-time coding. 1, 43

SWANS Scalable Wireless Ad hoc Network Simulator. 32, 93, 161

TA transmission aggressiveness. 8, 48–50, 55, 56, 69, 70, 72–75, 78, 80, 84, 87–90, 93–99, 101, 103–111, 116, 129, 145–148, 150, 152, 153, 156, 157, 159–167, 175–177, 180, 184, 188, 192, 193, 201, 202, 209, 210, 212–214, 223

TC transmission credit. 8, 66–69, 72, 75, 81, 88–90, 104, 105, 107, 225, 227

TCP transmission control protocol. 32, 36, 87, 93–96, 101, 107, 118, 124, 136, 137, 142, 155, 157, 164–166, 168, 173, 187, 188, 196, 202, 206, 216

TDiCOR Transmit Diversity based Cooperative Opportunistic Routing. 220

TDMA time-division multiple access. 24, 36, 43, 140, 220

TX transmission. 57, 112, 162, 198, 202

TXOP transmission opportunity. 23, 26, 51, 53, 56, 84, 85, 94, 107, 109, 116, 118, 153, 154, 156, 162, 169–173, 177, 180, 182, 184, 185, 187–189, 196, 202, 203, 211, 212, 214, 216, 217, 219, 220

UDP user datagram protocol. 32, 93–96, 101, 107, 117, 122, 124, 164–166, 202, 203, 206, 209

UO-CSMA utility-optimal CSMA. 35, 37–39, 41, 42, 44, 53, 56, 61, 64, 70, 73, 75, 82, 83, 87, 101, 107, 111, 112, 116, 117, 121, 122, 124, 127–131, 135, 137, 159, 217, 222, 223

WAHN wireless ad-hoc network. 140, 141

WCC windowed congestion control. 135, 136, 155, 168, 169, 188, 196

WiMAX Worldwide Interoperability for Microwave Access. 11, 211

WLAN wireless local area network. 11, 31

WLOG without loss of generality. 67, 225, 226

WMAN wireless metropolitan area network. 11

WMN wireless mesh network. iii, v, 1–7, 9–11, 24, 27, 28, 30, 31, 33–37, 42–46, 61, 63, 75, 87, 92, 93, 111, 112, 117, 122, 128, 133–135, 137, 140, 142, 143, 151–153, 155, 189, 196, 197, 210, 211, 214–220

WPAN wireless personal area network. 11

WSN wireless sensor network. 42

ZRP zone routing protocol. 32

Selbständigkeitserklärung

Ich erkläre hiermit, dass

1. ich die vorliegende Dissertationsschrift *Contention Techniques for Opportunistic Communication in Wireless Mesh Networks* selbständig und ohne unerlaubte Hilfe angefertigt habe;
2. ich mich weder bereits anderwärts um einen Doktorgrad im Promotionsfach Informatik beworben habe noch einen solchen besitze;
3. mir die Promotionsordnung der Mathematisch-Naturwissenschaftlichen Fakultät II der Humboldt-Universität zu Berlin (Amtliches Mitteilungsblatt der Humboldt-Universität, Nr. 34/2006) bekannt ist.

Berlin, den 26. Januar 2012 Mathias Kurth